FREIE UNIVERSITÄT BERLIN
DEPARTMENT OF PHYSICS

# On the controllability and quantum speed limit of qubit arrays

DISSERTATION

zur Erlangung des akademischen Grades

DOCTOR RERUM NATURALIUM

(Dr. rer. nat.)

am Fachbereich Physik
der Freien Universität Berlin
vorgelegt von

**FERNANDO GAGO ENCINAS**

Berlin, 21. August 2024

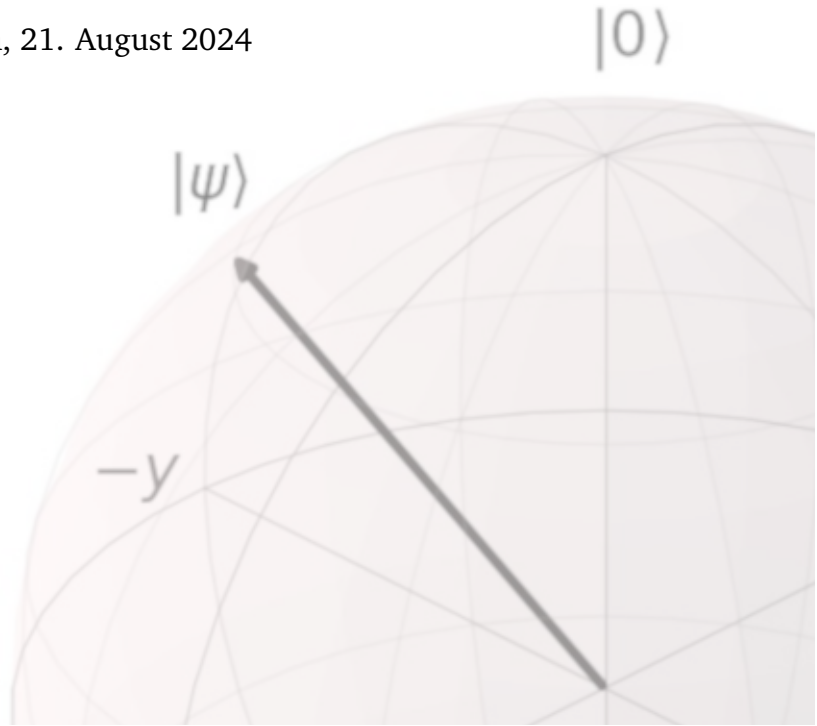

**Erstgutachterin:** PROF. DR. CHRISTIANE KOCH
Freie Universität Berlin
Fachbereich Physik
Berlin, Deutschland

**Zweitgutachter:** PROF. DR. KARL JANSEN
Center for Quantum Technology and Applications (CQTA)
Deutsches Elektronen-Synchrotron (DESY)
Zeuthen, Deutschland

**Tag der Disputation:** 6. Dezember 2024

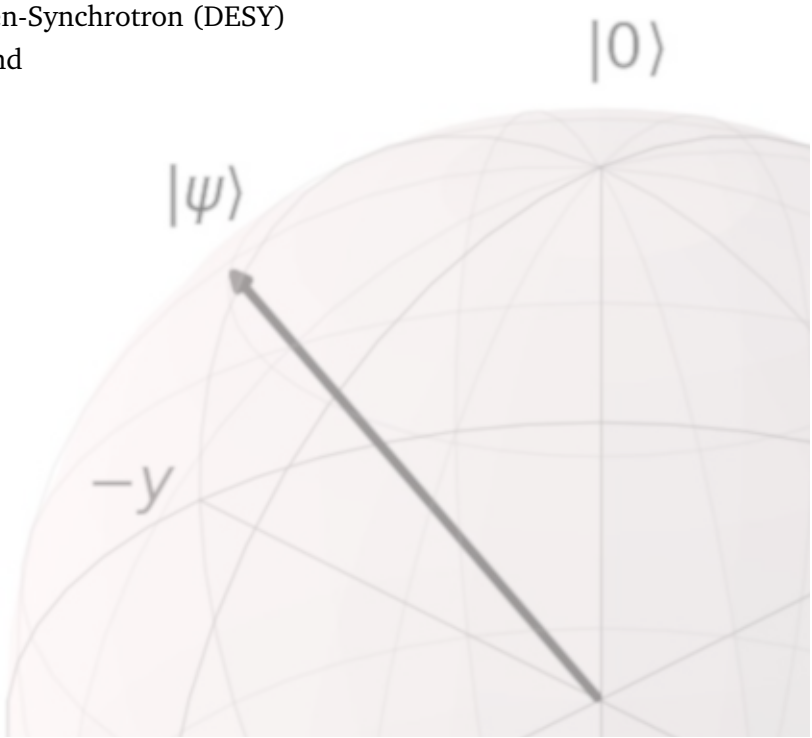

# Acknowledgements

There are many, many people who have stood by my side during the writing of this thesis and the years that have gone before. It is impossible to name them all, but I would like to mention some of the people who have helped me in one way or another. First of all, I would like to thank my supervisor, Christiane Koch, for giving me the wonderful opportunity to join her group as a PhD student. This experience has fundamentally changed my life and given me the chance to immerse myself in the fascinating world of quantum physics. I could not have done it without her. She provided me with many useful insights and enabled several collaborations that would pave the way for lasting connections. Thank you for your motivation and patience.

Having spent a lot of time discussing with many brilliant scientists, I have to say that it is always a pleasure to find someone who can share their passion for science with other researchers. I would therefore like to thank my second reviewer, Karl Jansen, for his advice and enthusiasm. Thank you for giving me a new perspective on science and for rekindling my spark of curiosity. I look forward to many new projects in our future.

A big thank you to my science outreach mentors, Shaeema Zaman and Sabrina Patsch, for the joy of science communication. They will always be my role models and I will never forget the good times we had sharing our love of science with astonished audiences. It is easy to forget the wonders of science when you are so close to it, but you have always made it refreshing and unique.

None of this would have been possible without the innovative training network QuSCo (funded by the Marie Skłodowska-Curie Actions of the European Commission) and the Einstein Research Unit on Near-Term Quantum Devices (funded by the Einstein Foundation from the Berlin University Alliance).Thank you for the financial support that made all this research possible.Thank you for the formative years and the wonderful people I met there.

Knowing that I could always count on my colleagues gave me a real sense of security. I would like to thank all former and current members of AG Koch. From my old office mate, Daniel Basilewitsch, to the new one, Matthias Krauß. To my group seminar colleague, Karl Horn, who took so much work off my shoulders. To each and every one of you. Thank you for sharing your knowledge, your experience and your jokes.

Years in a foreign country can seem daunting at first. I must thank everyone who welcomed me with open arms and made my days full of joy and fun. Whether it was with a thunderous melody, the tap of dancing feet or the sound of rolling dice, you broke the silence in my life. Thank you for keeping both my sanity and my insanity in check.

Only true friendship would survive such a long distance. And let's face it, keeping in touch has been a real odyssey. But to those who are still there, thank you for your kindness and forgiveness. To those who are still waiting for me in Madrid and to those who knew I would come here to stay (and still encouraged me to take the step). To my mother and my brother. To my family; to my friends; to the friends who are family.

Ultimately, there is one person to whom I owe my eternal gratitude: My partner. The one with whom I have always navigated through stormy weather and then sat down to contemplate the clear, sunny skies. I hope I have many years to repay you for the understanding and courage you have given me. To the one who has always been my number one fan.

# Abstract

Universal quantum computing is a coveted goal in the current technological landscape. Due to the unique laws of quantum mechanics, quantum computers would be able to run more efficient algorithms than their classical counterparts. Universality simply implies that said computer is capable of performing any quantum operation. This thesis presents a theoretical study of qubit arrays, the basic system for processing quantum information, tackling three important problems using results from Lie groups and algebras.

Since every real system is subject to decoherence due to interaction with its environment, it is crucial to find quantum devices capable of fast dynamics. The quantum speed limit of a system serves as a measure of the minimum time in which a given unitary evolution can be performed, depending on its controls and qubit couplings. A new method for its estimation is introduced in this thesis. Furthermore, the estimator is extended to determine the quantum speed limit of state-to-state transfers and quantum gates acting on a logical subspace of the total Hilbert space.

The number and type of controls and qubit couplings in the system also determine whether all operations in the system are feasible, i.e. whether the system is controllable. Controllability is a necessary property for universality. However, determining a system's controllability is generally a difficult task. Here, two controllability tests are presented, particularly tailored to the case of qubit arrays: A classical test based on notions from graph theory and a hybrid quantum-classical algorithm that employs parametric quantum circuits. While the complexity of these tests also scales exponentially with the number of qubits, they greatly expand the number of cases that can be studied.

Finally, a method for designing arbitrarily large controllable qubit arrays is presented. This is achieved by juxtaposing smaller controllable arrays and connecting them via tunable couplings. The modular architecture allows the construction of larger devices that are in principle suitable for universal quantum computing, even if the controllability of the overall system cannot be directly analysed by any of the previous tests.

The concepts shown here introduce an arsenal of tools that can provide valuable information for the study and development of systems with the aim of bringing quantum technologies closer to universal quantum computing.

# Zusammenfassung

Universelle Quantencomputer sind ein begehrtes Ziel in der aktuellen Technologielandschaft. Aufgrund der einzigartigen Gesetze der Quantenmechanik wären Quantencomputer in der Lage, effizientere Algorithmen auszuführen als ihre klassischen Gegenstücke. Universalität bedeutet einfach, dass der Computer jede beliebige Quantenoperation ausführen kann. In dieser Arbeit wird eine theoretische Untersuchung von Qubit-Arrays, dem grundlegenden System für die Verarbeitung von Quanteninformationen, vorgestellt. Dabei werden drei wichtige Probleme unter Verwendung von Ergebnissen aus Lie-Gruppen und Algebren angengangen.

Da jedes reale System aufgrund der Wechselwirkung mit seiner Umgebung der Dekohärenz unterliegt, ist es von entscheidender Bedeutung, Quantengeräte zu finden, die zu einer schnellen Dynamik fähig sind. Das Quantengeschwindigkeitslimit eines Systems dient als Maß für die minimale Zeit, in der eine gegebene einheitliche Entwicklung abhängig von seinen Kontrollen und Qubit-Kopplungen durchgeführt werden kann. In dieser Arbeit wird eine neue Methode zu ihrer Schätzung vorgestellt. Darüber hinaus wird dieser Schätzer erweitert, um die Quantengeschwindigkeitsgrenze von Zustand-zu-Zustand-Überführungen und Quantengattern zu bestimmen, die auf einen logischen Unterraum des gesamten Hilbert-Raums wirken.

Die Anzahl und Art der Steuerungen und Qubit-Kopplungen im System bestimmen auch, ob alle Operationen im System durchführbar sind, d. h. ob das System kontrollierbar ist. Kontrollierbarkeit ist eine notwendige Eigenschaft für Universalität. Die Bestimmung der Kontrollierbarkeit eines Systems ist jedoch im Allgemeinen eine schwierige Aufgabe. Hier werden zwei Kontrollierbarkeitstests vorgestellt, die speziell auf den Fall von Qubit-Arrays zugeschnitten sind: Ein klassischer Test, der auf Befunden aus der Graphentheorie basiert, und ein hybrider quantenklassischer Algorithmus, der parametrische Quantenschaltungen einsetzt. Trotz der ebenfalls exponenziell skalierenden Komplexitaet dieser Tests, kann die Anzahl der untersuchbaren Faelle erheblich erweitert werden.

Schließlich wird eine Methode zum Entwurf beliebig großer kontrollierbarer Qubit-Arrays vorgestellt. Dies wird durch die Aneinanderreihung kleinerer kontrollierbarer Arrays und deren Verbindung über abstimmbare Kopplungen erreicht. Die modulare Architektur erlaubt die Herstellung größerer Geräte, die prinzipiell für universelles Quantencomputing geeignet sind, ohne die Kontrollierbarkeit des Gesamtsystems durch Anwendung des bisherigen Tests direkt analysieren zu müssen.

Die bisher erwaehnten Konzepte stellen ein ganzes Arsenal an Werkzeugen dar, die wertvolle Informationen für die Untersuchung und Entwicklung von Systemen liefern können, die dem Ziel Quantentechnologien dem universellen Quantencomputing näher zu bringen unterstuetzen, indem sie wertvolle Informationen fuer dessen Untersuchung und Entwicklung liefern.

# List of publications

Two chapters are based on the following publications:

- Michael H. Goerz, Daniel Basilewitsch, **Fernando Gago-Encinas**, Matthias G. Krauss, Karl P. Horn, Daniel M. Reich, Christiane P. Koch.
  *Krotov: A Python implementation of Krotov's method for quantum optimal control.*
  *SciPost Phys.* 7, 080 (2019)
  DOI: 10.21468/SciPostPhys.7.6.080
  

  The contents of this publication are not part of the main chapters of the thesis.

- **Fernando Gago-Encinas**, Monika Leibscher and Christiane P. Koch.
  *Graph test of controllability in qubit arrays: a systematic way to determine the minimum number of external controls.*
  *Quantum Sci. Technol.* 8 045002 (2023)
  DOI: 10.1088/2058-9565/ace1a4
  

  Basis for Chapter 4. FGE wrote the code and performed the calculations. ML and CPK provided supervision and exchanged ideas with FGE. All authors contributed to the writing and edition of the manuscript.

- **Fernando Gago-Encinas**, Tobias Hartung, Daniel M. Reich, Karl Jansen, and Christiane P. Koch.
  *Determining the ability for universal quantum computing: Testing controllability via dimensional expressivity.*
  *Quantum* 7, 1214 (2023)
  DOI: 10.22331/q-2023-12-21-1214
  

  Basis for Chapter 5. FGE wrote the algorithm and performed the simulations. All authors contributed to developing the theory and to writing the manuscript.

The ideas presented in Chapter 3 were developed in collaboration with Christiane P. Koch and Thomas Chambrion[1]. The bachelor thesis [1] was written under my co-supervision and it is mentioned in Chapter 4. A manuscript for Chapter 6 is in preparation.

[1] Institut de Mathématiques de Bourgogne, Dijon, France

# Contents


**1 Introduction** **1**

**2 Theoretical background** **7**

2.1 Control of quantum systems . . . . . 7

2.2 Control of qubit arrays . . . . . 10

2.2.1 Model of a qubit . . . . . 10

2.2.2 Model of a qubit array . . . . . 11

2.2.3 Types of couplings and control . . . . . 13

2.2.4 Universal quantum computing . . . . . 14

2.3 Lie groups and Lie algebras in quantum systems . . . . . 16

2.3.1 Lie groups . . . . . 17

2.3.2 Lie algebras . . . . . 19

2.3.3 Relation between Lie algebras and Lie groups . . . . . 20

2.3.4 Generating a basis for a Lie algebra . . . . . 22

2.4 Controllability of closed quantum systems . . . . . 23

2.4.1 Types of controllability . . . . . 24

2.4.2 Dynamical Lie algebra and related controllability tests . . . . . 27

2.4.3 Controllability with connectedness chains . . . . . 30

2.5 Analysis of parametric quantum circuits . . . . . 32

2.5.1 Parametric quantum circuits . . . . . 33

2.5.2 Dimensional expressivity analysis . . . . . 36

2.6 Quantum speed limit . . . . . 39

2.6.1 Heisenberg's uncertainty principle . . . . . 40

2.6.2 The quantum speed limit: from orthogonal states to more general definitions . . . . . 41

**3 Quantum speed limit estimator** **43**

3.1 Quantum speed limit of controlled systems . . . . . 45

3.1.1 Quantum speed limit of quantum gates . . . . . 46

3.1.2 Quantum speed limit of state transfers and gates acting on subspaces . . . . . 47

3.2 Quantum-speed-limit estimator . . . . . 48

3.2.1 Partition of the dynamical Lie algebra . . . . . 49

3.2.2 The available velocity polytope . . . . . 52

3.2.3 Geometry and computation of convex sets . . . . . 55
3.2.4 Alternative approximations of the available velocity polytope . 58
3.2.5 Parametrization of unitary operators that meet the target conditions . . . . . 62
3.2.6 Algorithm outline . . . . . 66
3.3 Results . . . . . 72
3.3.1 Example A: Unitary gates . . . . . 73
3.3.2 Example B: State-to-state transfer . . . . . 75
3.3.3 Example C: Simultaneous state transfers . . . . . 77
3.3.4 Numerical complexity and applicability . . . . . 80
3.4 Summary . . . . . 82

**4 Graph test for controllability of qubit arrays 85**
4.1 Introduction . . . . . 85
4.2 Controllability analysis . . . . . 86
4.3 Graph test of controllability for coupled subsystems . . . . . 89
4.3.1 Resonant transitions and graphical commutators . . . . . 89
4.3.2 Algorithms for graph test of controllability for coupled subsystems with resonant transitions . . . . . 92
4.3.3 Illustrative examples . . . . . 100
4.4 Results . . . . . 103
4.4.1 Example A: five-qubit system similar to *ibmq_quito* . . . . . 104
4.4.2 Example B: five-qubit system with reduced number of controls . 105
4.4.3 Example C: five-qubit system with single local control . . . . . 106
4.5 Summary . . . . . 108

**5 Controllability of qubit arrays using parametric quantum circuits 111**
5.1 Introduction . . . . . 111
5.2 Theoretical background . . . . . 113
5.2.1 Controllability . . . . . 113
5.2.2 Dimensional expressivity . . . . . 113
5.3 Pure-state controllability test using dimensional expressivity . . . . . 115
5.3.1 Circuit expressivity and pure-state controllability . . . . . 115
5.3.2 Controllability test . . . . . 118
5.3.3 Examples . . . . . 120
5.4 Operator controllability test using dimensional expressivity analysis . . 123
5.4.1 Lifting pure-state to operator controllability via the Choi-Jamiołkowski isomorphism . . . . . 123
5.4.2 Controllability test . . . . . 127
5.4.3 Algorithm outline . . . . . 129
5.4.4 Examples . . . . . 132
5.5 Summary . . . . . 134

**6 Controllability condition for modular qubit arrays** **137**
6.1 Introduction . . . . . 137
6.2 Controllability of bipartite systems with an entangling control . . . . . 139
6.3 Mathematical derivation . . . . . 142
6.3.1 Notation and problem statement . . . . . 142
6.3.2 Operations with tensor products of Pauli matrices . . . . . 144
6.3.3 Preliminary lemmas . . . . . 146
6.3.4 Controllability of two controllable qubit arrays coupled via a two-qubit control . . . . . 149
6.4 Design of large qubit arrays . . . . . 151
6.5 Summary . . . . . 155

**7 Conclusions and outlook** **157**

**8 Bibliography** **161**

"*Science makes people reach selflessly for truth and objectivity; it teaches people to accept reality, with wonder and admiration, not to mention the deep awe and joy that the natural order of things brings to the true scientist.*"

Lise Meitner

# 1 Introduction

Since the dawn of history, people have sought to comprehend the laws of the universe. Mathematics and natural sciences are the very foundations on which we build our understanding of the reality in which we live. But to develop solid theories and make accurate predictions we need solid tools and accurate methods to perform increasingly complex calculations. From the early abacus to the first computers, the power of computation has always been at the heart of technological progress. Physics can help revolutionise the technological landscape. It did so in the 1950s with the invention of integrated circuits, which enabled the creation of personal computers. Today, quantum physics is once again on the cusp of new horizons.

In 1982 Richard Feynman first proposed to simulate nature using quantum systems [2]. In principle, the inherently unique laws of quantum mechanics allow its behaviour to be reproduced much more efficiently using other quantum systems rather than classical computers. The spark of quantum simulation and quantum computation had been lit. It ignited the idea of using quantum bits, or qubits, as the basic units for processing information. Unlike classical bits, qubits had access to two exciting properties: Superposition of states and quantum entanglement. This opened up a whole new world of calculations that were not possible in the contemporary machines. However, their physical implementation and the efficient mapping of the problems to be solved are still two major obstacles to overcome.

It was a decade later that algorithms were proposed to solve specific problems using quantum computing [3, 4]. Two important ones are worth mentioning: Grover's algorithm[5], which could efficiently search a database, and Shor's algorithm [6], whose fast integer factorization was a double-edged sword in the world of cryptogra-

phy. Suddenly the realisation of these quantum computers became a desirable goal. Following the equivalent idea of a classical universal Turing machine, in 2000 David P. DiVincenzo wrote the criteria that a quantum device would need to fulfill in order to be capable of performing every conceivable quantum algorithm [7]. The quest for universal quantum computing lingered on the horizon, waiting to be achieved.

There have been many approaches to the physical implementation of qubits. For starters, photons presented a natural two-level quantum system with their two different polarizations. The binary logical subspace could thus be directly encoded on them. This made them the first system to be turned into a qubit [8]. Since then, a wide variety of different platforms has been used to encode qubits, including trapped ions [9], semiconductors [10] and superconducting qubits [11]. The state of the quantum system contains the information that can be obtained by measuring. The underlying physics may vary, but all qubit implementations lead to a similar perspective from the point of view of information theory. A number of qubits are set up with some interaction between them. These interactions are the so-called qubit couplings that allow the qubits to become entangled. Since we need to change the dynamics of the system to perform computations, the system must include some variables that can be changed over time. These are the controls of the system and they are necessary to alter its state. Together, qubits, controls and couplings make up the description of a qubit array, the basic platform for quantum computing. This thesis aims at studying controlled qubit arrays based on their architecture, gauging whether the systems are a passing candidate for universal quantum computing.

Finding the right controls to produce certain dynamics on a controlled quantum system is in general a difficult task, which scales with the dimension of the system. Quantum optimal control presents solutions to many problems by using optimization algorithms [12]. But there is a question that is previous to the one that optimal control answers: Whether this task is possible at all. Indeed, a system may not have enough controls or the right type of couplings to perform some dynamics. Controllability is the study of this very question. A system can be deemed either controllable or not controllable depending on the available resources, i.e. the number and type of controls and couplings. If it can be proven that there are enough controls and couplings to produce the target evolutions, then the system is labelled as controllable. Testing controllability is an important goal to achieve universal quantum computing, as the latter one requires a controllable quantum system.

Multiple controllability tests have been developed for a generic quantum system in the past [13, 14, 15, 16]. Nevertheless, it is difficult to make them suitable for large systems in the general case, as the dimension of the Hilbert space of a qubit array scales exponentially with the number of qubits. From a theoretical point of view, the

dynamics of a qubit array can be described using the bilinear Schrödinger equation. Control theory is then used to analyse the differential equation and understand, using notions on Lie groups and Lie algebras, which dynamics are possible. The dimensions of these algebras scale with the Hilbert space dimension, making it a hard endeavor to tackle numerically using only classical computers. One of the goals of this thesis is to extend the applicability of previous tests. To this end, two new tests are defined to analyse the controllability of quantum systems and, more particularly, qubit arrays.

Chapter 4 presents a controllability test based on graph theory. For every quantum system, it generates a graph that contains the relevant information about the controllability of the system. Unlike previous methods that had to calculate the whole dynamical Lie algebra of the system, containing all the information about the possible evolutions of the system, the graph method avoids the complete calculation of the algebra while maintaining the relevant information of whether the system is controllable or not. Computing the complete algebra is very demanding, as small computational errors may add up quickly for higher dimensions and yield a false result. This effect comes from the so-called curse of dimensionality. This means than the graph method can study systems that are larger that the ones that can be studied by computing the entire Lie algebra numerically. The method had already been suggested for the study of quantum systems [15, 17], but it came with a big caveat. The method was not applicable if there were any degeneracies in the energy gaps of the quantum system, i.e. the differences between energy levels. This is a tough blow for multipartite systems like qubit arrays, as these types of degeneracies are bound to happen due to the tensor product structure of the Hilbert space. The main original result that is contributed to the method is the inclusion of some operations that allow to circumvent these degeneracies to obtain a meaningful result. This is extremely important for qubit arrays, as now they can also be studied using the method. Additionally, the related chapter also includes some five-qubit examples whose controllability has been determined. In particular, it is proven that the system in question can still be controlled even by removing some of the local controls present in the system. Reducing the number of local controls in a qubit array ensures that the architecture uses fewer resources that must be built in and calibrated, which in turn makes it easier for the system to be scaled up to a larger number of qubits.

All the aforementioned controllability tests rely on a good theoretical model of a physical system that is studied either analytically or using classical numerical computations. But the question still remained about whether it would be possible to determine the controllability of a system by measuring directly on the physical system. Chapter 5 introduces the idea of a hybrid quantum-classical algorithm that does exactly that. It is based on parametric quantum circuits, which constitute the foundation of variational quantum algorithms, a revolutionary optimization method based on

quantum systems [18]. These parametric quantum circuits are sequences of quantum logic gates, some of which depend on certain parameters. Understanding the different states that a parametric quantum circuit can produce when varying the parameters is key to determine whether a variational quantum algorithm can be successful. The dimensional expressivity of a parametric quantum circuit represents the number of independent parameters that are present on the circuit, which can help to identify which gates can be removed from the quantum circuit. To measure the expressivity, the dimensional expressivity analysis can be used as a hybrid algorithm on a real quantum circuit, combining quantum measurements and classical computations [19, 20]. The controllability test here presented bridges the gap between the controllability of quantum systems and the expressivity of parametric quantum circuits. For every quantum system, it is possible to define a parametric quantum circuit whose expressivity contains the relevant information to claim if a system is controllable or not controllable. This unique approach allows to obtain controllability information from a system itself or rather from a qubit array that can simulate the dynamics of the original system. Chapter 5 contains the description of this dimensional expressivity controllability test as well as examples of three- and four-qubit arrays that have been investigated through classical simulations of their respective parametric quantum circuits.

These two new controllability tests expand the horizons of the previous methods and can provide more information about qubit arrays. Nonetheless, the methods will eventually be unsuccessful for a sufficiently large number of qubits, where computations on the graph will be too demanding and the parametric quantum circuit will have an impossible depth. But there is still hope for the study of controllability in larger systems. The solution comes in the form of a modular architecture that uses smaller controllable systems as the basic building blocks. The cement that hold these pieces together are tunable couplings, i.e. couplings that can be modified over time and be understood as a control that is entangling between two or more qubits. Connecting controllable qubit arrays with tunable couplings results in a larger qubit array that is also controllable. In Chapter 6, this result is mathematically proven. Furthermore, the chapter studies the controllability of a 127-qubit system of one of IBM's systems based on superconducting qubits [21]—a giant leap when compared to the dimension of the previous examples. With this modular architecture it is possible to build larger systems ad infinitum by connecting new subsystems in a multipartite system. This structure may be beneficial when considering the subsystems in the partition as quantum processing units that can run some code in parallel to and then recombine all the information by entangling them with the rest of the quantum processing units.

But controllability is not the only problem to tackle in the landscape of quantum technologies. Every real quantum system is surrounded by an environment that can, to a greater or lesser extent, interact with it. Interaction with the environment may lead to dephasing or, in simpler terms, to the loss of the quantum properties of the system [22]. To use a quantum system effectively, one must implement the desired dynamics and measure before decoherence destroys the information. A quantum system must therefore not only be controllable, but capable of fast dynamics as well. The quantum speed limit serves as a measure of how quickly some evolution can be implemented on a quantum system. It is the minimal time in which one can find controls on the system such that the targets are achieved. To ensure that a qubit array is suitable for universal quantum computing it is also important to gauge how fast it can perform the quantum operations necessary for computing a quantum algorithm. Some bounds have been found for the quantum speed limit of particular dynamics, like state-to-state transfers [23, 24]. In Chapter 3, a quantum speed limit estimator is presented, which can estimate the minimum required time on a given system for three different targets: Unitary evolutions, simultaneous state transfers and quantum gates acting on a subspace of the total system. It does so by defining a partition in the dynamical Lie algebra of the system into fast and slow directions. The quantum speed limit is calculated depending on how long the system must evolve using only the drift, the time-independent part of the Hamiltonian. To showcase the estimator, the method is used on three illustrative two-qubit examples.

The thesis is structured as follows. Chapter 2 contains the theoretical background that serves as a basis for the following chapters. It formally introduces the dynamical study of quantum systems, control of qubit arrays, basic definitions of controllability, necessary results on Lie algebras and Lie groups, important concepts on parametric quantum circuits and a comprehensive history and definition of the quantum speed limit. The central body is composed by Chapters 3-6, which present the main research of the dissertation. They tackle the study of qubit arrays from three different angles: Quantum speed limit, controllability and scalable design of qubit arrays. They form a coherent and multifaceted analysis of qubit arrays, providing some answers to the questions that are relevant for universal quantum computing. Each central chapter includes a brief introduction and a summary with the most important results. Finally, Chapter 7 closes with the conclusions of the thesis and the outlook for the next problems to solve towards the goal of universal quantum computing.

# 2 Theoretical background

This chapter is an introduction to widely known concepts and some more obscure results that provide the basis for the rest of the material in this dissertation. As such, it does not contain any original material, although the physical explanations and insights have been tailored to serve as foundations for the following chapters.

The first two sections involve the definition and study of controlled quantum systems and, more specifically, qubit arrays. We then present basic notions of Lie groups and Lie algebras that are used for the study of controllability of quantum systems. Controllability is one of the core problems of this thesis, with Chapter 4, 5 and 6 presenting controllability tests for the study of qubit arrays and Chapter 3 heavily using notions of Lie algebras and controllability. Therefore, it is recommended to read in detail Sections 2.3 and 2.4. On the other hand, the last two sections present more specialized knowledge that will be relevant only for specific chapters. Section 2.5 introduces basic ideas of parametric quantum circuits, that will be necessary to understand the mathematical implementation and physical interpretation of Chapter 5. Finally, Section 2.6 explains the quantum speed limit of a quantum system and it is related to the last central chapter of this thesis, Chapter 6.

## 2.1 Control of quantum systems

The first postulate of quantum mechanics claims that the state of an isolated quantum system $\mathcal{S}$ can be represented as a vector $|\Psi\rangle$ in a complex Hilbert space $\mathcal{H}$ [25]. We call the space $\mathcal{H}$ the state space related to $\mathcal{S}$. The set of all normalized states of the system lies on the unit sphere of $\mathcal{H}$, $S_{\mathcal{H}}$. In quantum mechanics, however, not all of these states represent different physical states. Two normalized states $|\phi_1\rangle$ and $|\phi_2\rangle$ are physically equivalent if and only if $|\langle\phi_1||\phi_2\rangle| = 1$. In particular, this means that two states $|\phi\rangle$ and $e^{i\varphi}|\phi\rangle$ that are identical up to a phase $e^{i\varphi}$ represent the same physical state of a quantum system. Indeed, for any observable represented by a Hermitian operator $\hat{A}$, the expectation values that we obtain from both states are identical

$$\langle\hat{A}\rangle_{|\phi\rangle} = \langle\phi|\hat{A}|\phi\rangle = \langle\phi|e^{-i\varphi}\hat{A}e^{i\varphi}|\phi\rangle = \langle\hat{A}\rangle_{e^{i\varphi}|\phi\rangle}. \tag{2.1}$$

As the previous result is true for every observable $\hat{A}$, both states must represent the same physical states. The phase $e^{i\varphi}$ is called a *global phase*. This reasoning proves that, while the global phase is something that can be identified in theoretical definitions, it is simply a mathematical construct that cannot be measured in reality. The global phase will play an important role in some of the tools that will be used in the current chapter. In particular, it will be used extensively in the definition of different Lie algebras. For a complex Hilbert space with dimension $d$, the set of all physical states can be represented as the sphere $S_{\mathcal{H}}$ up to a global phase, i.e. as a real manifold with dimension $2(d-1)$.

Assuming units such that $\hbar = 1$, a closed quantum device subject to coherent dynamics can be described following the time-dependent Schrödinger equation [26]

$$i\frac{d}{dt}\left|\Psi(t)\right\rangle = \hat{H}(t)\left|\Psi(t)\right\rangle, \quad \left|\Psi(0)\right\rangle = \left|\Psi_0\right\rangle, \tag{2.2}$$

where $\hat{H}$ is the Hamiltonian of the system, $|\Psi(t)\rangle$ is the state that describes the system at time $t$ and $|\Psi_0\rangle$ is the so called initial state. Solving the differential equation leads to

$$\left|\psi(t)\right\rangle = \hat{U}(t)\left|\psi(0)\right\rangle, \qquad \text{where } \hat{U}(t) := \mathcal{T}\exp\left(-i\int_0^t \hat{H}(\tau)\,d\tau\right) \tag{2.3}$$

with $\mathcal{T}$ being the time-ordering operator. The operator $\hat{U}(t)$ is called the time evolution operator (or simply evolution operator). $\hat{U}(t)$ is always unitary for closed systems, i.e. those described by Hermitian Hamiltonians. For the case of time independent Hamiltonians, Equation (2.3) can be simplified into $\hat{U}(t) = \exp(-i\hat{H}t)$. This is an accurate description the dynamics if assuming that the system is perfectly isolated from the environment surrounding it. Of course, in reality, there will always be some interaction between the studied system and its environment up to a certain degree. Nevertheless, if the dynamics are performed much faster than the decoherence rate, this can be used as a first approximation to describe multiple physical systems. Among the systems can be described using Equation (2.2) we can find examples like atoms, molecules, photons in cavities and even superconducting circuits.

It is also possible to represent the case where the system is in a classical superposition of different possible states $|\psi_j\rangle$, i.e. a mixed state, through a density matrix $\hat{\rho} := \sum_j \lambda_j \left|\psi_j\right\rangle \left\langle\psi_j\right|$. The coefficients $\lambda_j$ are the probabilities of finding the system on the state $|\psi_j\rangle$. As classical probabilities they must obey the general rules $\sum_j \lambda_j = 1$ and $0 \leq \lambda_j \leq 1\,\forall j$. The evolution of the system is given by the von Neumann equation

$$i\frac{d}{dt}\hat{\rho}(t) = \left[\hat{H}, \hat{\rho}(t)\right], \quad \hat{\rho}(0) = \hat{\rho}_0, \tag{2.4}$$

where the square brackets represent the commutator. The case where the density matrix represents a pure state, i.e. $\hat{\rho} = \left|\psi\right\rangle\left\langle\psi\right|$ will be particularly relevant later on.

In Equation (2.2) we can see the evolution of the initial state $|\Psi_0\rangle$. This is relevant when we want to analyze what states we can generate on the system at different points in time. However, bluntly speaking, we are unaware of what happens to the rest of the Hilbert space under the same dynamics. For a system with Hilbert space dimension $\dim(\mathcal{H}) = d$, we can always find an orthonormal basis $\{|e_j\rangle\}_{j=0}^{d-1}$ such that $\langle e_i|e_j\rangle = \delta_{i,j}$ and $|e_0\rangle := |\Psi_0\rangle$. Then, Equation (2.2) represents the dynamics of the first state of the chosen basis. Similarly, we can generate another $d-1$ equations for the rest of the states $|e_j\rangle$. To group these equations, we can define the unitary matrix

$$\hat{V}_0 := \Big(|e_0\rangle \;\Big|\; |e_1\rangle \;\Big|\cdots\Big|\; |e_{d-1}\rangle\Big)\,. \tag{2.5}$$

Compacting all previous equations for the elements of the orthonormal basis $\{|e_j\rangle\}_j$, the dynamics of all states in the Hilbert space are captured in the equation

$$i\frac{d}{dt}\hat{V}(t) = \hat{H}\hat{V}(t), \quad \hat{V} = \hat{V}_0 \tag{2.6}$$

Note that $\hat{V}(t)$ is always a unitary matrix for every time $t$. Indeed, $\hat{V}_0$ is unitary by definition and $\hat{V}(t) = \hat{U}(t)\hat{V}_0$ for some unitary evolution operator $\hat{U}(t)$. Without loss of generality, we can choose $\{|e_j\rangle\}_{j=0}^{d-1}$ as the basis for our matrix representation, achieving the more canonical equation

$$i\frac{d}{dt}\hat{V}(t) = \hat{H}\hat{V}(t), \quad \hat{V}(0) = \mathbb{1}_d. \tag{2.7}$$

$\hat{V}_0 = \mathbb{1}_d$. In that case, the time-dependent orthonormal basis $\hat{V}(t)$ represents the unitary evolution of the system $\hat{U}(t)$. This makes Equation (2.7) extremely useful to study unitary matrices that can be generated in a quantum system at a time $t$. Furthermore, since it is a control equation over the set of unitary matrices, we can use different tools from Lie groups and Lie algebras, as will be shown in Section 2.3.

Whether we want to evolve the system to a certain state or generate a particular unitary matrix, it is useful to manipulate the Hamiltonian $\hat{H}(t)$ over time to achieve the desired target. A common approach to this goal is the inclusion of external controls that can be varied over time, such that the Hamiltonian from Equation (2.2) can be described as

$$\hat{H}(t) = H_0 + \sum_{j=1}^{m} u_j(t)\hat{H}_j. \tag{2.8}$$

The time-independent operator $\hat{H}_0$ is commonly referred to as the *drift*. The real-valued functions $u_j(t)$ represent the *controls* of the system, which are defined to be piece-wise constant. The operators $\hat{H}_j$ are their associated *control Hamiltonians*. Note that Equation (2.8) only explores systems where the controls and control Hamiltonians are linearly coupled in the total time-dependent Hamiltonian $\hat{H}(t)$. The controls $u_j(t)$

can represent different physical magnitudes, from electromagnetic fields [27, 28] to mechanical vibrations [29].

## 2.2 Control of qubit arrays

### 2.2.1 Model of a qubit

The theory of classical information and classical computing is built upon the concept of bits. A *bit* is the minimal unit of information and it can take two values: Either 0 or 1. A *quantum bit* or *qubit* acts as a two-level quantum system with two logic states commonly labeled $|0\rangle$ and $|1\rangle$. This qubit is also subject to the laws of quantum mechanics and is thus able to be in any superposition $\alpha|0\rangle + \beta|1\rangle$ with $\alpha, \beta \in \mathbb{C}$ and $|\alpha|^2 + |\beta|^2 = 1$. Qubits are the minimal unit in quantum information and as such they can be understood as the building blocks of a platform that is capable to processing quantum information or carrying out quantum computations.

In practice, a qubit can be physically implemented in multiple ways. For example, photons were one of the first systems to be used theoretically as qubits, due to the two possible polarizations [8]. Any spin-$\frac{1}{2}$ particle is also a natural candidate for a two-level quantum system. In reality, however, it is common to use many-level systems and then restrict the dynamics to a two-level subspace, the so-called "logical space". In this manner we can use the quantized modes of electromagnetic fields inside cavities as harmonic oscillators [30], the electronic state of ions trapped in a lattice [9], semiconductors [31, 10] or even superconducting circuits that can be modelled as anharmonic oscillators [11]. In the present work, I will restrict myself to speaking about theoretical qubits in the form of perfectly isolated two-level systems. With these assumptions the constant local Hamiltonian of a qubit can be easily described as

$$\hat{H}_{qubit} = -\frac{\omega}{2}\hat{\sigma}_z \tag{2.9}$$

where $\omega$ is the natural frequency between the two energy levels and $\hat{\sigma}_z$ is the Pauli z matrix. If we integrate Equation (2.2), the state of the system with initial state $|\Psi_0\rangle = \alpha|0\rangle + \beta|1\rangle$ at $t = 0$ under the Hamiltonian (2.9) can be described as

$$|\Psi(t)\rangle = e^{-i\frac{\omega}{2}\hat{\sigma}_z t}|\Psi_0\rangle = e^{-i\frac{\omega}{2}t}\alpha|0\rangle + e^{i\frac{\omega}{2}t}\beta|1\rangle . \tag{2.10}$$

We can visualize the evolution by plotting the state of the two-dimensional system onto a Bloch sphere (consult e.g. section 1.2 from [32]). Looking at the curve $\gamma(t)$ that $|\Psi(t)\rangle$ traces over the sphere we see that it is a horizontal circumference with constant polar angle $\theta = \arctan(\frac{|\beta|}{|\alpha|})$. This is to be expected, as it represents the precession of the initial state $|\Psi_0\rangle$ around the Z-axis, the direction established by $\hat{H}_{qubit}$. The evolution curve $\gamma(t)$ is, however, a closed line that does not cover the whole Bloch

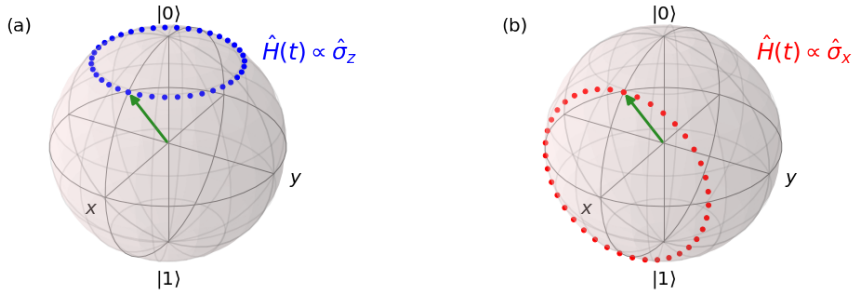


**Figure 2.1:** Bloch sphere representation of evolution of the state $|\psi\rangle = \frac{2\sqrt{2}}{3}|0\rangle + \frac{1}{3}|1\rangle$ under different Hamiltonians $\hat{H}$. (a) Evolution of $|\psi\rangle$ with $\hat{H}$ proportional to $\sigma_z$. (b) Evolution of $|\psi\rangle$ with $\hat{H}$ proportional to $\sigma_x$.

sphere. There are many states that the system will never take, no matter the chosen final time. To achieve states out of this circumference, it is necessary to change the Hamiltonian of the system, for example by adding an external control that we can modify over time.

Following Equation (2.8) we may add a control Hamiltonian $\hat{\sigma}_x$, leading to a total Hamiltonian

$$\hat{H}(t) = -\frac{\omega}{2}\hat{\sigma}_z + u(t)\hat{\sigma}_x \tag{2.11}$$

that would allow us to modify the polar angle $\theta$. This behaviour can be visualized in Figure 2.1. The $u(t)\hat{\sigma}_x$ term induces a rotation around the X axis. In the limit where $||u(t)\hat{\sigma}_x|| \gg ||\omega\hat{\sigma}_x||$ the Hamiltonian $\hat{H}(t)$ is approximately proportional to $\hat{\sigma}_x$. We can implement the evolution to a chosen polar angle and then set the control $u(t)$ to zero to continue with a precession around the Z axis. With this set up, it is trivial to see that for any state $|\Psi\rangle \in \mathcal{H}$ there exist a final time $t_f \geq 0$ and a real control $u(t)$ such that $|\psi(t_f)\rangle = |\psi\rangle$.

### 2.2.2 Model of a qubit array

We consider a qubit array to be any collection of qubits that can be connected via some physical interactions or couplings. Similarly as before, a qubit array may also include controls of the system that allow us to alter the dynamics in the system. A typical Hamiltonian for an $N$-qubit array with $m$ controls can be written as

$$\hat{H}_{array}(t) = \sum_{j=0}^{N-1} \hat{H}_{qubit}^{(j)} + \hat{H}_c + \sum_{k=1}^{m} u_k(t)\hat{H}_k \tag{2.12}$$

where $\hat{H}_{qubit}^{(j)}$ are the local Hamiltonians of the qubits, $\hat{H}_c$ are the qubit couplings and $u_k(t)$ are the controls coupled to the operators $\hat{H}_k$. This model includes the

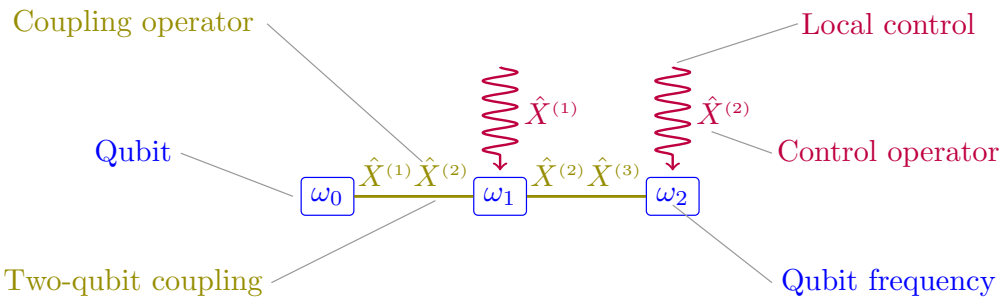


**Figure 2.2:** Example of a three-qubit array (cf. Equation (2.15) ).

Hamiltonians of the free qubits, which are decoupled from the rest of the operators. The couplings $\hat{H}_c$ contain any time-independent interaction between the qubits, which in many cases will be two-qubit couplings. The type of control operators $\hat{H}_k$ determines how the controls are coupled to the system. Relevant examples include local controls addressing a single qubit or dynamic couplings, whose amplitude can be varied over time, that affect multiple qubits. An example of a qubit array can be found in Figure 2.2.

The Hilbert space $\mathcal{H}_{array}$ of an $N$-qubit array has dimension $\dim(\mathcal{H}_{array}) = 2^N$ and can be decomposed as the tensor product $\mathcal{H}_{array} = \mathcal{H}_2^{\otimes N}$, with $\mathcal{H}_2$ a two-dimensional Hilbert space. To represent operators that act non-trivially in only one qubit we will use the following notation

$$\hat{A}^n := \mathbb{1}_2 \otimes ... \otimes \mathbb{1}_2 \otimes \underbrace{\hat{A}}_{n\text{-th position}} \otimes \mathbb{1}_2 \otimes ... \mathbb{1}_2. \tag{2.13}$$

Note that the number of qubits $N$ is not explicitly specified for $\hat{A}^n$ and should be determined from the context of the system on which the operator is used. Any operation acting non-trivially in a single qubit is called a *local* operation. By definition, every local operation is non-entangling. In some cases we will be simplifying the Pauli matrices nomenclature as

$$\hat{X} := \hat{\sigma}_x; \qquad \hat{Y} := \hat{\sigma}_y; \qquad \hat{Z} := \hat{\sigma}_z. \tag{2.14}$$

For example, the system displayed in Figure 2.2 has a related Hamiltonian

$$\hat{H}_{array}(t) = \sum_{j=0}^{2} -\frac{\omega_j}{2}\hat{Z}^{(j)} + \sum_{k=0,1} \hat{X}^{(k)}\hat{X}^{(k+1)} + \sum_{l=1,2} u_l(t)\hat{X}^{(l)}. \tag{2.15}$$

The terms in the right-hand side of the equation represent the local Hamiltonians, the qubit couplings and the controls, respectively.

### 2.2.3 Types of couplings and control

So far we have worked with a very general definition of the couplings and the controls in our system. Theoretically, there are no restrictions to the shape that these operators might take apart from the ones given by basic quantum mechanics. In practice, however, there are some configurations that are more common than others, and thus it makes sense to take them as common examples to study as quantum systems. In the following, we showcase some of the different types of couplings and controls that can be included in qubit arrays.

In principle, every qubit could interact with every other qubit in an array, which would lead to very complex interactions in the coupling operator $\hat{H}_c$, which are in reality hard to engineer. In many cases, however, some approximations might be taken to neglect the lesser contributions, which leads to nearest-neighbour interactions, i.e. two-qubit couplings that only affect adjacent qubits in a line or lattice. An example of this case can be seen in the one-dimensional Ising model for an array of spin-$\frac{1}{2}$ particles

$$\hat{H} = -\sum_j J_{j,j+1} \hat{Z}^{(j)} \hat{Z}^{(j+1)} - \mu \sum_k B_k \hat{Z}^{(k)}, \tag{2.16}$$

where $J_{j,j+1}$ are the qubit interactions, $\mu$ is the magnetic moment and $B_k$ is the magnetic field at the node $k$. If we neglect any other degree of freedom, each of these spins can be understood as a qubit that only couples with its neighbours. More distant interactions are neglected, leaving behind only nearest-neighbor couplings. Two-qubit couplings are one of the most common types of interaction in most models. Couplings of higher degree are still possible and even preferred in certain occasions. In fact, there exist some quantum algorithms that greatly benefit from having direct access to gates that simultaneously address more qubits, like three-qubit quantum gates [33, 34]. In practice, however, couplings of three qubits or more are more sophisticated and difficult to implement, and are usually associated with weaker interactions.

So far we have only shown examples where the qubit couplings were time-independent. It is also possible to include couplings that can be varied over time. These are the *tunable couplings* [35, 36, 37], which are useful for multiple reasons. First, if they can be set to zero and non-zero values, they can essentially be used to isolate a qubit from the the network or to connect it back to generate entanglement between it and the rest of the array. Second, if their amplitude can be modified over time, we can treat them as if they were a non-local control that is able to directly generate entanglement between two qubits.

Controls can also come in multiple shapes. For example, if we are able to modify the magnetic fields $B_k$ in Equation (2.16) over time, we could treat every $B_k(t)$ as a control with $\mu\hat{Z}^{(k)}$ as their related control Hamiltonian. Since they act in only one

qubit (spin) at a time, they would be classified as *local controls*. If all the controls are the same, i.e. $B_j(t) = B_k(t) =: B(t)$ for all $k$ and $j$, then we can rewrite Equation (2.16) with $B(t)$ as a control and $\sum_k \hat{Z}^{(k)}$ as its associated control Hamiltonian. Note that, similar to tunable couplings, the control operator $\sum_k \hat{Z}^{(k)}$ corresponds to a control that acts on multiple qubits simultaenously. Unlike tunable couplings, however, it is not able to generate entanglement between qubits.

In this dissertation we will mainly focus on qubit arrays with time-independent two-qubit couplings and local controls to showcase our results. However, most of the tools that have been developed could in principle either work directly or be expanded to the case of more general qubit couplings and controls.

### 2.2.4 Universal quantum computing

Quantum computing is the science in charge of studying, designing and implementing computations using some properties that are unique to quantum mechanics. Already theorized in the early 1980s [38, 39], quantum computing opens up the road for quantum algorithms that would be able to solve certain problems more efficiently. These include, among many others, Shor's factorization algorithm [6, 40] and Grover's search algorithm to scan databases [5]. Another noteworthy development is the more modern variational quantum eigensolver, a hybrid quantum-classical algorithm capable of simulating molecular electronic structures [41, 42]. Quantum technology has come a long way since quantum devices were used to perform computations. But it was only in 2019 when the first time quantum supremacy was claimed [43], i.e., the first time a problem was allegedly solved using a quantum computer more efficiently than a classical algorithm. While the validity of this so-called supremacy has been put under review in the light of recent results [44], other teams have kept showing possible quantum advantages using different systems [45, 46, 47].

To harness the true power of quantum computing, it is not sufficient to separate operations on the qubits. State superposition is a useful property to have in our system, but the effect that makes a real difference in the processing capability of a quantum computer is actually entanglement. We can classically store the information of a separable N-qubit state in $2^7 N$ (using double precision floats with $2^6$ bits per real number). Indeed, we only need 2 real parameters (the relative amplitude between the states $|0\rangle$ and $|1\rangle$ and the local phase) to contain the information of the state of a single qubit. For $N$ qubits, this results in $2N \cdot 2^6$. For a general N-qubit entangled state we would need to represent each and every state in the Hilbert space of the system, which is isomorphic to $\mathbb{C}^{2N}$. Therefore to encode a general entangled state we require an astounding $2^{7+N}$, a quite significant difference! It is quantum entanglement that

makes possible many quantum algorithms and that allows us to use qubits as an effective media for storing information.

Ideally, a quantum computer should be able to implement every possible operation and algorithm or, in other words, capable of performing *universal quantum computing* [39]. This is basically the equivalent of a quantum Turing machine [48], and a physical implementation would give researchers everywhere the possibility to perform much more complex simulations and computations. There are some conditions for universal quantum computing that were already compiled in 2000 by the American physicist David P. DiVincenzo [7].

**Definition 2.2.1** (DiVincenzo's criteria)**.** *The following points are required for the implementation of quantum computation:*

1. *A scalable physical system with well-characterized qubits*

2. *The ability to initialize the state of the qubits to a simple fiducial state, such as* $|000...\rangle$

3. *Long relevant decoherence times, much longer than the gate operation time*

4. *A "universal" set of quantum gates*

5. *A qubit-specific measurement capability*

Apart from these five requirements, there were two additional properties relevant only for quantum communication. Since quantum communication and its protocols are not the main focus of this dissertation, they have been left out from the previous definition. Here we will focus on three of the five listed bullet points. They are discussed in more detail in the current section, as they bring up important concepts that are the very foundation of the motivation of the upcoming chapters.

The first point involves two different aspects. First, the system should be scalable, i.e. its set-up should be suitable for a larger number of qubits too. If a design requires a lot of resources for just a few qubits, then it would not be possible to repeat a similar architecture for a large number of qubits. Second, it is necessary to use well-characterized qubits, i.e. the dynamics and interactions with every qubit should be known. This includes the local qubit Hamiltonians, every type of coupling with other qubits and the environment and the controls that are use to modify the system's state. While this is a very demanding task, in this work we will approach always from a

theoretical point of view, defining the Hamiltonians for every example from scratch and essentially avoiding this issue. To keep in touch with the applied side of physics, however, we always try to use models that are close to real devices.

The third criterion revolves around the relation between the system's decoherence times and the duration of the operation on the system. We know that, in reality, every quantum system has some sort of interaction with its environment. The system's dynamics can then no longer be defined using unitary operators, as the states will start to deteriorate due to the decoherence and information loss. However, if these effects happen at a time scale that is much larger than the operations we want to perform, it is still possible to treat the system as if it was closed. We can achieve this in two different ways. The first one is to find devices that are well shielded against decoherence, such that more operations can be implemented. For example, circular states of Rydberg atoms are one of the platforms being used as a quantum system because they are protected against electric field perturbations, allowing them to have longer decoherence times [49]. The second precaution we can take is to find fast operations that we can implement in our qubits. It is not useful for a system to have very long decoherence times if the only operations it can carry out are in the same time scale. Conversely, a noisy system with short decoherence times may still be used if the gates it can implement are much faster. The minimum time in which a certain state is reached or a unitary operation performed is the quantum speed limit that will be the main focus of Section 2.6. Finding the quantum speed limit of depending on the different type of couplings and controls is a valuable piece of information that will have an impact on the kind of algorithms and operations that can be used in the studied device.

Finally, the fourth point speaks about the gates that the system can run. Similar to the classical Boolean logic gates, the *quantum logic gates* or simply *quantum gates* are all the different unitary operations we can run on a qubit array. The term "universal" refers to a set of quantum gates that can approximate any other quantum gate by performing a finite sequence of the gates in the universal set (cf. Section 1.3 of [32]). From a more abstract level, this also implies that the qubit array should be able to perform any unitary gate. As we will see in Section 2.3, the gates generated by an universal set include all the possible entangling gates that can be thought of. This question is answered by controllability, a property that is presented in Section 2.4.

## 2.3 Lie groups and Lie algebras in quantum systems

In this section we present some of the basic algebra notions that are required for the study of controllability of qubit arrays. In particular, the structure of Lie groups

and Lie algebras are at the core of the mathematics that are necessary to describe the dynamics of a system evolving under Schrödinger's equation. The base mathematical concepts have been taken from Hall's textbook [50], while the controllability notions are presented in d'Alessandro's book [14].

### 2.3.1 Lie groups

Here we present the general definition of a Lie group, that will be useful to understand some of the properties that will be used in future arguments. First, it is necessary to remember what a manifold is, as it is a notion that will appear multiple times in different chapters.

**Definition 2.3.1** (Manifold)**.** *An $n$-dimensional manifold $\mathcal{M}$ is a topological space where each point has a neighborhood that is homeomorphic to an open set of the vector space $\mathbb{R}^n$.*

*A differentiable manifold is a manifold where, for every point $p$, the local homeomorphism $f_p : \mathcal{M} \to \mathbb{R}^n$ is differentiable.*

We have already mentioned that the set of normalized states on a Hilbert space of dimension $d$, $S_{\mathcal{H}}$, is a $2(d-1)$-dimensional manifold. Other relevant examples of manifolds include the $n$-dimensional torus $\mathbb{T}^n = \mathbb{R}^n/\mathbb{Z}^n$ and the group of unitary $n \times n$ matrices $U(n)$. We can equip the latter one with a useful stronger structure, which brings us to the next core concept of this subsection.

**Definition 2.3.2** (Lie group)**.** *A Lie group $\mathcal{G}$ is a smooth manifold (i.e. infinitely differentiable) equipped with a binary operation $f(a,b) \mapsto a \cdot b$ that follows the structure of a group:*

- *$\mathcal{G}$ is closed under $f$:* $a \cdot b \in \mathcal{G} \quad \forall a, b \in \mathcal{G}$.
- *$\mathcal{G}$ includes the identity element:* $\exists e \in \mathcal{G} \mid e \cdot a = a \cdot e = a \quad \forall a \in \mathcal{G}$.
- *$\mathcal{G}$ includes inverse elements:* $\forall a \in \mathcal{G}\, \exists a^{-1} \mid a \cdot a^{-1} = a^{-1} \cdot a = e$.
- *$f$ is associative:* $(a \cdot b) \cdot c = a \cdot (b \cdot c) \quad \forall a, b, c \in \mathcal{G}$.

There are many different Lie groups that are relevant for multiple ares of physics. For the topic at hand, however, we will restrict ourselves to only two Lie groups: the unitary group $U(n)$ and the special unitary group $SU(n)$ with matrix multiplication

as their group operation. Both $U(n)$ and $SU(n)$ are subgroups of general linear group $Gl(n, \mathbb{C})$, the group of complex invertible $n \times n$ matrices [50]. They are described as follows:

- $U(n)$: the group of all matrices $\mathcal{M}_{n\times n}$ that are unitary.
- $SU(n)$: the group of all matrices $\mathcal{M}_{n\times n}$ that are unitary and have determinant equal to 1.

The dimension of a Lie group can be determined by the number of real parameters needed to describe any element in the group. Let us take $U(n) \subsetneq Gl(n, \mathbb{C})$ as an example. A unitary matrix $\hat{U}$ of dimension $n \times n$ needs at most $n^2$ complex parameters, i.e. $2n^2$ real ones. To be unitary, it also needs to fulfill $\hat{U}\hat{U}^\dagger = \hat{I}$. From this condition we can write a total of $n^2$ constraints, which implies that the real dimension of $U(n)$ must be $\dim(U(n)) = 2n^2 - n^2 = n^2$. For the case of $SU(n)$ one ought to add the determinant constraint, $\det(\hat{U}) = 1$, which leads to $\dim(SU(n)) = n^2 - 1$.

Unitary matrices are extremely important in the description of quantum mechanics. Indeed, the solution of Equation (2.2) can be expressed in terms of a unitary evolution operator $\hat{U}(t, t_0)$ such that

$$|\Psi(t)\rangle = \hat{U}(t, t_0)\,|\Psi(t_0)\rangle\,. \tag{2.17}$$

The operator $\hat{U}(t, t_0)$ is also by definition the solution to Equation (2.7). By analyzing all the different possible evolution operators $\hat{U}(t, t_0)$, we can better understand the different dynamics that we can induce in the system. To study this set, it is necessary to introduce the notion of Lie subgroups.

**Definition 2.3.3** (Lie subgroup)**.** *Given a Lie group $\mathcal{G}$, a Lie subgroup $\mathcal{H}$ is an analytic submanifold of $\mathcal{G}$ (i.e. a differentiable manifold with analytic local homeomorphisms) that is also a subgroup of $\mathcal{G}$ with its inherited structure.*

For example, $U(n)$ is a Lie subgroup of $Gl(n, \mathbb{C})$, whereas $SU(n)$ is a Lie subgroup of both $U(n)$ and $Gl(n, \mathbb{C})$. Similarly, the set of all unitary evolutions $\hat{U}(t, t_0)$ that can be created for any finite time $t$ on a system form a Lie subgroup $\mathcal{G} \in U(n)$ [51]. In other words, the set of solutions of Equation (2.7) is a submanifold of $U(n)$ that contains the identity. To know which evolution operators are possible in our system (i.e. which $\hat{U}(t, t_0)$ are contained in the subgroup $\mathcal{G}$) we can study the different directions within the manifold $U(n)$ in which our system can evolve.

### 2.3.2 Lie algebras

Given a Lie group $\mathcal{A}$, we can define the set of infinitesimal transformations under $\mathcal{A}$, a vector space denoted as $\mathfrak{A}$. The set $\mathfrak{A}$ is a Lie algebra, the properties of which are as follows.

**Definition 2.3.4** (Lie algebra)**.** *A Lie algebra $\mathfrak{g}$ over a field $\mathcal{F}$ is a vector space over $F$ equipped with a binary operation $[\cdot,\cdot] : \mathfrak{g} \times \mathfrak{g} \to \mathfrak{g}$ called a Lie bracket such that the following conditions are satisfied:*

- *The Lie bracket it is bilinear*

$$[x+y,z] = [x,z] + [y,z], \quad [x,y+z] = [x,y] + [x,z], \tag{2.18}$$

$$[\alpha x, y] = [x, \alpha y] = \alpha[x,y], \quad \forall \alpha \in \mathcal{F}.$$

- *The Lie bracket is null over the same element*

$$[x,x] = 0, \quad \forall x \in \mathfrak{g} \tag{2.19}$$

- *It satisfies the Jacobi Identity*

$$[x,[y,z]] + [y,[z,x]] + [z,[x,y]] = 0 \tag{2.20}$$

The Lie algebras defined by the Lie groups $Gl(n,\mathbb{C})$, $U(n)$ and $SU(n)$ can be defined as sets of $n \times n$ matrices with commutators as their Lie bracket operations. It is a fact that for every Lie group there exists a related Lie algebra [50]. For the case of finite dimension, the converse is also true in virtue of Lie's third theorem [52]. Since Lie algebras are also vector spaces, their dimension is naturally defined as the maximum number of linearly independent elements that can be simultaneously found. The dimension of a Lie algebra corresponds to the dimension of their associated Lie group.

Similarly to Lie subgroups, one can define Lie subalgebras in the following manner:

**Definition 2.3.5** (Lie subalgebra)**.** *Given a Lie algebra $\mathfrak{g}$, a vector subspace $\mathfrak{a} \subseteq \mathfrak{g}$ that is also closed under Lie brackets is called a Lie subalgebra.*

| Name | Lie groups | | Associated Lie algebras | | dim |
|---|---|---|---|---|---|
| - | Notation | Definition | Notation | Definition | - |
| General linear group | $Gl(n, \mathbb{C})$ | $n \times n$ complex invertible matrices | $\mathfrak{gl}(n, \mathbb{C})$ | $n \times n$ complex matrices | $2n^2$ |
| Unitary group | $U(n)$ | $n \times n$ complex unitary matrices | $\mathfrak{u}(n)$ | $n \times n$ skew-Hermitian matrices | $n^2$ |
| Special unitary group | $SU(n)$ | $n \times n$ complex unitary matrices with determinant equal to 1 | $\mathfrak{su}(n)$ | $n \times n$ traceless skew-Hermitian matrices | $n^2 - 1$ |

**Table 2.1:** List of relevant Lie groups and their associated Lie algebras with their respective real dimensions.

Let $\mathcal{G}$ be a Lie group and $\mathfrak{g}$ its associated Lie algebra. Then, for every Lie subgroup $\mathcal{S} \subseteq \mathcal{G}$ there exists a Lie subalgebra $\mathfrak{s} \subseteq \mathfrak{g}$ such that $\mathfrak{s}$ is the associated Lie algebra of $\mathcal{S}$. Section 2.4 explains how to gather information about the subgroup of possible evolution operators of Equation (2.7) by studying the associated Lie subalgebra.

A different structure that we can define in Lie algebras is an ideal, which is defined as follows:

**Definition 2.3.6** (Ideal)**.** *Let $\mathfrak{g}$ be a Lie algebra. A vector subspace $\mathfrak{I} \subseteq \mathfrak{g}$ is called an ideal if*

$$[x, y] \in \mathfrak{I}, \quad \forall x \in \mathfrak{I}, \forall y \in \mathfrak{g}. \tag{2.21}$$

*A Lie algebra without any proper ideals is called simple.*

For example, the Lie algebra of $SU(n)$, $\mathfrak{su}(n)$, has only two ideals, $\{0_{n\times n}\}$ and itself [53]. Therefore $\mathfrak{su}(n)$ is simple for every positive integer $n$. Conversely, the Lie algebra of $U(n)$, $\mathfrak{u}(n)$, can be decomposed as $\mathfrak{u}(n) = span\{i\mathbb{1}_n\} \oplus \mathfrak{su}(n)$. So $\mathfrak{su}(n)$ is a proper ideal of $\mathfrak{u}(n)$, which implies that $\mathfrak{u}(n)$ is not simple. These concepts will play a major role in the proof of the main theorem in Chapter 6.

### 2.3.3 Relation between Lie algebras and Lie groups

Table 2.1 shows the relations of the groups and algebras that will be the core of this dissertation.

As the set of infinitesimal transformations, a Lie algebra can also be used to represent the tangent space of the Lie group at a given point. Figure 2.3 shows this relation for the tangent space around the identity $\hat{I}$. For the case of Lie groups and

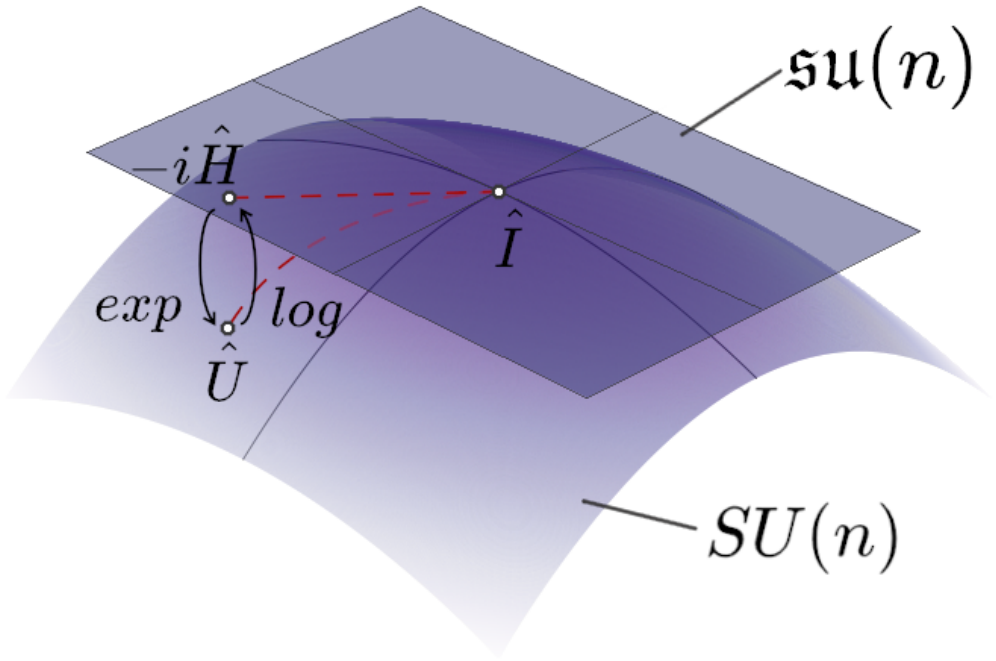


**Figure 2.3:** Visual relation between the Lie group $SU(n)$ and its tangent space, the Lie algebra $\mathfrak{su}(n)$. The exponentiation and logarithm operations can take one element from the tangent plane to the group manifold and vice versa, respectively. Figure adapted from [54].

algebras in a matrix representation the exponential map provides a method to link the elements in the algebra to the elements in the group.

As an example, if $i\hat{A}$ is a skew-Hermitian operator (i.e. contained in $\mathfrak{u}(\mathfrak{n})$), then it is easy to prove that $e^{i\hat{A}t}$ is a unitary operator for every t. The Lie algebra $\mathfrak{u}(\mathfrak{n})$ can therefore be seen as the space tangent to all the curves $\{e^{i\hat{A}t} \,|\, t \in \mathbb{R}\}$. For $t > 0$, we can understand these curves as the time evolution operators $\hat{U}(t)$ generated by a time-independent Hamiltonian $-\hat{A}$. The set of all tangent vectors of these curves $e^{i\hat{A}t}$ form the tangent space of $U(n)$, i.e. the Lie algebra $\mathfrak{u}(n)$.

Conversely, a Lie group $\mathcal{G}$ with a matrix representation can also be generated in terms of its Lie algebra $\mathfrak{g}$ as follows:

$$\mathcal{G} = e^{\mathfrak{g}} = \overline{\{e^{a_1}e^{a_2}\cdots e^{a_m} \,|\, \forall a_j \in \mathfrak{g},\, 0 \leq j \leq m,\, m \in \mathbb{Z}^*,\}}. \tag{2.22}$$

Therefore, the exponential map takes elements from the Lie algebra and converts them into elements of the Lie group. The set $e^{\mathfrak{g}}$ defined in Equation (2.22) is defined as the Lie group generated by the Lie algebra $\mathfrak{g}$. This is always well defined for Lie algebras $\mathfrak{g}$ of skew-Hermitian matrices, i.e. Lie subalgebras of $\mathfrak{u}(n)$. The logarithmic map can also be used to take an element $\hat{U}$ in the group manifold to an element

$-i\hat{B} := \log(\hat{U})$ in the tangent space. Analogously to the logarithm of complex numbers, the logarithmic map is in principle not uniquely defined, but we can always find a neighbourhood around any $\hat{V} \in U(n)$ in which the pair of the exponential and logarithmic maps are bijections. Here $-i\hat{B}$ represents the direction in the manifold of unitary operators that a curve $e^{-i\hat{B}t}$ would have to follow to achieve the unitary evolution $\hat{U}$ in exactly $t = 1$ units of time. Note that this method of reaching a certain point in the manifold is not unique, as one can write a sequence of finite curves with different directions, much like the expression found in Equation (2.22). For example, in the case of a single qubit, a rotation gate $\hat{R}_Y(\frac{\pi}{2}) := \exp(-i\frac{\pi}{4}\hat{\sigma}_y)$ can be reached by following the direction $-i\hat{\sigma}_y$ on the Lie algebra. But we can also decompose the gate into a product $\hat{R}_Y(\frac{\pi}{2}) = \hat{R}_X(-\frac{\pi}{2})\hat{R}_Z(\frac{\pi}{2})\hat{R}_X(\frac{\pi}{2})$, which means that one can obtain the same result of the gate $\hat{R}_Y(\frac{\pi}{2})$ by following the more convoluted path given by the directions $-i\hat{\sigma}_x$, $-i\hat{\sigma}_z$ and $i\hat{\sigma}_x$ in sequence.

### 2.3.4 Generating a basis for a Lie algebra

As previously mentioned, Lie algebras have the structure of a vector space. It is therefore useful to find a basis of the algebra $\mathfrak{A}$ generated by a set of elements $\{A_1, A_2, ...A_n\}$, which is denoted as

$$\mathfrak{A} = Lie\left(A_1, A_2, ...A_n\right). \tag{2.23}$$

While there is no unique basis, finding an arbitrary basis $\mathfrak{A}$ is a simple method for determining the algebra dimension $dim(\mathfrak{A})$, as the cardinality of every basis should be identical. One method to find an orthonormal basis is as follows [14]:

1. Orthonormalise the elements of the initial set $\{A_1, A_2, ...A_n\}$ into a maximal set of linearly independent orthonormal elements $\{\tilde{A}_1, \tilde{A}_2, ...\tilde{A}_m\}$ (e.g. by running the Gram-Schmidt algorithm).

2. Define $\{\tilde{A}_1, \tilde{A}_2, ...\tilde{A}_m\}$ as the elements of depth 0.

3. Set $p = 1$.

4. Iterate over the next steps:

    a) Compute the Lie brackets $C_{i,j} = [\tilde{B}_j, \tilde{A}_i]$ where $\tilde{A}_i$ are the elements of depth 0 and $\tilde{B}_j$ the elements of depth $p-1$. The vectors $C_{i,j}$ are potential candidates for elements of depth $p$.

    b) Orthonormalise the set of vectors $\{C_{i,j}\}$ with respect to the set of elements of depth less or equal than $p-1$.

c) The new orthonormal nonzero vectors $\tilde{B}_k$ obtained in the previous step are considered the elements of depth $p$ from now on.

d) Stop the algorithm if the set of elements of depth $p$ is empty (i.e. no new linearly independent vector was found through Lie brackets).

e) Set $p \leftarrow p + 1$

As shown in Table 2.1, $\mathfrak{u}(n)$ has a finite dimension for any positive integer $n$. This implies that any subalgebra $\mathfrak{A} \subseteq \mathfrak{u}(n)$ must also be finite and the method described above must end in a finite number of steps. In particular, for the case of matrices in $\mathfrak{u}(n)$ or $\mathfrak{su}(n)$ the method can be stopped if the dimension (i.e. the number of linearly independent vectors found) reaches $n^2$ or $n^2 - 1$. These two results imply that the generated algebras are $\mathfrak{u}(n)$ or $\mathfrak{su}(n)$, respectively.

## 2.4 Controllability of closed quantum systems

Given a quantum system with linearly coupled controls as defined in Equation (2.8), one may wonder what dynamics can be implemented. For example, is it possible to drive the population from a certain initial state to any final state? Or perhaps is it feasible to map an orthonormal basis of the Hilbert space into any other orthonormal basis of the Hilbert space at any point in time? This is the question that controllability answers in a dichotomous manner. The material covering types of controllability and their related tests described in this section has been extracted from chapter 3 in [14].

Depending on the types of dynamics, we can define multiple types of controllability. For example, if we are interested in the electronic state of an atom or molecule we might want to ensure that we have controllability over all the different electronic states that we can generate starting from the ground level. But if we are looking at a qubit array we might be more interested in studying which quantum logic gates our system can perform. These different types of controllability and their relevance in quantum physics are explained in detail in Subsection 2.4.1.

Taking Equation (2.8) as the model of a closed system, if we impose no restriction on the shapes of the $m$ controls $u_j(t)$ all the relevant information is contained in its Hamiltonian $\hat{H}(t)$ (cf. Eq. (2.8)). Since the controls $u_j(t)$ are dummy functions in the general case, this means that the controllability of a system can be determined simply by the time independent drift $\hat{H}_0$ and the control operators $\hat{H}_j$ (with $1 \leq j \leq m$).

### 2.4.1 Types of controllability

This section focuses exclusively on systems with a Hamiltonian defined by Equation (2.8) composed of a linear combination of a drift and some control operators linearly coupled to some controls. Previously, we have seen two different versions of the Schrödinger equation: one in Equation (2.2) which normalized vectors $|\psi(t)\rangle$ of the system's Hilbert space $\mathcal{H}$ and a second one in Equation (2.7) using the set of unitary operators $\hat{V}(t)$ as the domain of possible states.

Before we look into controllability it is an interesting question to ask which elements (either $|\psi(t)\rangle$ for Equation (2.7) or $\hat{V}(t)$ for Equation (2.7)) can be reached in the system before a certain time $T \geq 0$. Given a controlled system following Equation (2.7) starting in an initial state $|\psi(t=0)\rangle = |\phi_0\rangle$ we define the set of reachable states at time $T$, $\mathcal{R}_{|\psi\rangle}(T)$, as

$$\mathcal{R}_{|\psi\rangle}(T) = \left\{ |\chi\rangle \;\middle|\; \exists u_1, ...u_m \in \mathcal{U}_{\mathbb{R}},\, \exists t \leq T :\; |\psi(t)\rangle = |\chi\rangle \right\}. \tag{2.24}$$

Note that the previous definition depends implicitly on the description of our system, which includes both the Hamiltonian $\hat{H}(t)$ with its controls $u_j(t)$ and the initial state of the system $|\phi_0\rangle$. From a physical perspective, the set $\mathcal{R}_{|\psi\rangle}(t)$ simply represents all the states that the system can reach at times before or equal to $T$ when it is initialized in the state $|\phi_0\rangle$. In other words, this is the set of all states $\hat{U}(\tilde{t})\,|\phi_0\rangle$ that can be generated including all the different unitary evolutions $\hat{U}(\tilde{t})$ at a time $\tilde{t} \leq T$ that can be realized given the definition of the Hamiltonian $\hat{H}(t)$. For this reason, $\mathcal{R}_{|\psi\rangle}(T)$ is known as the manifold of reachable states at a time $T$. A state $|\chi\rangle$ is called reachable for a time $T$ if it belongs to the manifold $\mathcal{R}_{|\psi\rangle}(T)$.

Extending the definition to an arbitrarily large but finite time, we get $\mathcal{R}_{|\psi\rangle} := \bigcup_{T\geq 0} \mathcal{R}_{|\psi\rangle}(T)$, the so-called manifold of reachable states. This includes all the states that can be implemented in the system, without taking into account the required time. In a closed system, this manifold is evidently a subset of the set of normalized states, the unit sphere $S_{\mathcal{H}}$.

Alternatively, it is possible to use Equation (2.7) to define an analogous version of this reachable set for the case of unitary operations, $\mathcal{R}_{\hat{V}}(t)$. This set is defined as

$$\mathcal{R}_{\hat{V}}(T) = \left\{ \hat{W} \;\middle|\; \exists u_1, ...u_m \in \mathcal{U}_{\mathbb{R}},\, \exists \tilde{t} \leq T :\; \hat{V}(\tilde{t}) = \hat{W} \right\}. \tag{2.25}$$

$\mathcal{R}_{\hat{V}}(T)$ is also implicitly dependent on $\hat{H}(t)$ and the initial condition $\hat{V}_0$. If we understand $\hat{V}_0$ as an initial orthonormal basis, the set $\mathcal{R}_{\hat{V}}(T)$ represents all the different orthonormal bases into which we can transform the original one at a time $t \leq T$. In the particular case where $\hat{V}_0 = \mathbb{1}$, $\mathcal{R}_{\hat{V}}(T)$ is called the set of reachable

evolution operators, because it contains all the different operators $\hat{U}(t)$ that our system can implement for a certain $t \leq T$. This manifold $\mathcal{R}_{\hat{V}}(T)$ is a submanifold of the Lie group $U(d)$, where $d$ is the Hilbert space dimension of the system. Similarly, an evolution operator is reachable at a time $t \leq T$ if it belongs to $\mathcal{R}_{\hat{V}}(T)$. Taking the limit towards arbitrarily large time, we can once again reach the manifold of reachable evolution operators, $\mathcal{R}_{\hat{V}} := \bigcup_{T \geq 0} \mathcal{R}_{|\psi\rangle}(T)$. Alternatively, the elements of $\mathcal{R}_{\hat{V}}$ will also be referred to as the feasible or possible (unitary) evolutions of the system in question. In a closed system these evolutions are always unitary. Thus $\mathcal{R}_{\hat{V}}$ is a subset of the Lie group $U(n)$, with $n$ the Hilbert space dimension of the system. Furthermore, for every closed system it can be proven that $\mathcal{R}_{\hat{V}}$ is also a Lie subgroup of $U(n)$ [55, 56].

Now that the notions of reachable spaces have been introduced, we can ask if the sets $\mathcal{R}_{|\psi\rangle}$ and $\mathcal{R}_{\hat{V}}$ are maximal for a given system with Hamiltonian (2.8). Note that the reachable sets are defined in terms of the dynamics described by Equations (2.8) and (2.7), respectively, but the system's Hamiltonian remains the same in both cases. If $\mathcal{R}_{|\psi\rangle} = S_{\mathcal{H}}$, all pure states in the Hilbert space of the system can be reached at (possibly different) final times. Similarly, if $\mathcal{R}_{\hat{V}} = U(n)$, then all unitary operators can be implemented as evolution operators on the system at (possibly different) final times. Based on these two separate cases, there exist two different types of controllability, defined below.

**Definition 2.4.1** (Pure-state controllability)**.** *A quantum system with Hamiltonian (2.8) evolving under Equation (2.2) is pure-state controllable (PSC) if for any initial state $|\phi_0\rangle \in \mathcal{H}$ and any final state $|\phi_f\rangle \in \mathcal{H}$ there exist a series of controls $u_j(t)$ and a final time $t_f \leq 0$ such that the state of the system $|\psi(t)\rangle$ verifies*

$$|\psi(t=0)\rangle = |\phi_0\rangle \qquad \textit{and} \qquad |\psi(t=t_f)\rangle = |\phi_f\rangle\,.$$

Pure-state controllability is obviously linked to the aforementioned case of $\mathcal{R}_{|\psi\rangle} = S_{\mathcal{H}}$. Since the possible unitary evolutions in the system (i.e. elements of $\mathcal{R}_{\hat{V}}$) form a group for closed systems, it is sufficient to prove that given a single initial state $|\psi_a\rangle$ there exist different controls $u_j(t)$ to reach all the different states $|\psi_f\rangle$ in the Hilbert space. Indeed if we have two states $|\psi_f\rangle$ and $|\psi_b\rangle$ connected to the same initial state $|\psi_a\rangle$ by some available unitary evolutions in in the system, i.e. $|\psi_f\rangle = \hat{U}_{a,f}\,|\psi_a\rangle$ and $|\psi_b\rangle = \hat{U}_{a,b}\,|\psi_a\rangle$, then the states $|\psi_f\rangle$ and $|\psi_b\rangle$ are also connected by a unitary evolution $|\psi_f\rangle = \hat{U}_{b,f}\,|\psi_b\rangle := \hat{U}_{a,f}\hat{U}_{a,b}^{-1}\,|\psi_b\rangle$. The element $\hat{U}_{a,b}^{-1}$ must belong to the Lie group $\mathcal{R}_{\hat{V}}$, and thus the evolution $\hat{U}_{b,f} = \hat{U}_{a,f}\hat{U}_{a,b}^{-1}$ is one of the possible unitary evolutions of the system. Therefore, a system is pure-state controllable if and only if the manifold of reachable states is maximal, $\mathcal{R}_{|\psi\rangle} = S_{\mathcal{H}}$, a condition that is not dependent on the choice of the initial state of the system. Physically, a system with

pure-state controllability may be useful because, if the initial state is known, there are always controls that allow us to prepare the system into any chosen state. For example, we could decide to populate a certain level of the electronic state of an atom or initialize a qubit array in a certain state before performing some quantum logic gates. These operations are sometimes referred to as state transfers, since the population in the initial state is transferred or evolved into the selected final state.

A relevant question to pose is whether it makes a difference if we take into account global phases for the case of pure-state controllability or not. According to definition 2.4.1 a system is PSC if there exists a unitary evolution connecting any two states in the Hilbert space. However, one could ask if, for any pair of states $|\psi_0\rangle$ and $|\psi_f\rangle$, there exists an evolution $\hat{U}_{0,f}$ such that $e^{i\phi_{0,f}}|\psi_f\rangle = \hat{U}_{0,f}|\psi_0\rangle$ for some phase $\phi_{0,f}$, a condition that has been referred to as equivalent-state controllability. This would be sufficient in terms of quantum mechanics, as the term $e^{i\phi_{0,f}}$ is a global phase with no physical meaning. It is evident that pure-state controllability would imply equivalent-state controllability with trivial phases $\phi_{0,f} = 0$. But in fact, it has been proven that if a system is equivalent-state controllable, it is also pure-state controllable in general [14]. Thus both definitions are equivalent. Therefore the definition of pure-state controllability is still useful from a physical point of view, as the conditions required to reach all normalized vectors $|\chi\rangle$ in the Hilbert space are the same as the ones needed to reach all physical states $\{e^{i\phi}|\chi\rangle \mid \phi \in [0, 2\pi)\}$.

If we have a look at the reachable set of Equation (2.7), we can associate a new type of controllability to the case where $\mathcal{R}_{\hat{V}}(T)$ is maximal. In other words, it is useful to define a label for a system with certain controls that is able to implement every possible unitary operator. However, as previously discussed, two evolutions $\hat{U}$ and $e^{i\theta}\hat{U}$ are equivalent for every $\theta \in \mathbb{R}$. The next definition encompasses this property.

**Definition 2.4.2** (Operator controllability)**.** *A quantum system with Hamiltonian (2.8) and Hilbert space dimension $n$ evolving under Equation (2.7) is operator controllable if for any unitary operator $\hat{U}_{tgt} \in \mathcal{H}$ there exist a series of controls $u_j(t)$, a final time $t_f \leq 0$ and a phase angle $\theta \in [0, 2\pi]$ such that the state of the system $|\psi(t)\rangle$ verifies*

$$\hat{U}(t=0) = \mathbb{1}_n \qquad \textit{and} \qquad \hat{U}(t=t_f) = e^{i\theta}\,\hat{U}_{tgt}.$$

Unlike the previous case of state manifolds, we may have systems where we can reach any unitary evolution up to a global phase yet it may be impossible to implement certain unitary evolutions when their exact global phase is taken into account. This may not be as surprising as one may expect at first sight. Indeed, we have already mentioned that the reachable set $\mathcal{R}_{\hat{V}}(T)$ is always a Lie subgroup of $U(n)$ (with $n$ the

Hilbert space dimension). As $SU(n)$ is a proper Lie subgroup of $U(n)$, it may happen that $\mathcal{R}_{\hat{V}}(T) \cong SU(n) \subsetneq U(n)$. It is easy to see how $SU(n)$ describes every unitary evolution up to a global phase. Indeed, for any unitary evolution $\hat{U} \in U(n)$ the unitary operator $\hat{\tilde{U}} := \exp(-\frac{\det(\hat{U})}{n})\hat{U}$ is equivalent to $\hat{U}$ up to a phase. $\hat{\tilde{U}}$ has determinant $\det(\hat{\tilde{U}}) = 1$ and thus $\hat{\tilde{U}} \in SU(n)$.

### 2.4.2 Dynamical Lie algebra and related controllability tests

Now that the main notions of controllability have been introduced, we still have to identify which ones apply to a given a quantum system with controls following Equation (2.8). Assuming that the $m$ controls $u_j$ can be taken from any piece-wise continuous functions, all the information about the possible dynamics that can be implemented on the system has to be contained in its Hamiltonian drift $\hat{H}_0$ and the control operators $\hat{H}_j$ (with $1 \leq j \leq m$). Note that no matter whether we are looking at the set of reachable states $\mathcal{R}_{|\psi\rangle}$ using Equation (2.2) or at the set of reachable unitary operations $\mathcal{R}_{\hat{V}}$ via Equation (2.7), the system Hamiltonian $\hat{H}(t)$ remains identical. Thus, both types of controllability can be analysed by studying the different drift and control operators.

**Definition 2.4.3** (Dynamical Lie algebra)**.** *Given a quantum system with a controlled Hamiltonian as described by Equation (2.8), the Lie algebra $\mathcal{L}$ generated by the drift and the control operators,*

$$\mathcal{L} := Lie\left(i\hat{H}_0, i\hat{H}_1, ..., i\hat{H}_m\right), \tag{2.26}$$

*is called the dynamical Lie algebra of the system.*

The addition of the imaginary unit in Equation (2.26) turns the Hermitian Hamiltonian operators into skew-Hermitian elements that are suitable for generating a Lie algebra with the usual commutator as Lie bracket. To fully understand the physical meaning of the dynamical Lie algebra we can go back to the visualization of Figure 2.3. If the manifold at the bottom of the picture represents the group of unitary evolutions that can be achieved in the system, the tangent space at the identity is given by the dynamical Lie algebra. In other words, the dynamical Lie algebra is the collection of the tangent vectors of all the different curves in which the system can evolve over time. By using Equation (2.8) to describe the system's Hamiltonian it is implicitly assumed that the drift $\hat{H}_0$, the control operators $\hat{H}_j$ (with $1 \leq j \leq m$) and their nested commutators are always constant (but not the controls $u_j$ themselves). Therefore, the tangent space defined at any point $\hat{U}_1$ of the manifold of reachable unitary evolutions $\mathcal{R}_{\hat{V}}$ is isomorphic to any other tangent space defined at a different point $\hat{U}_2$. Following this logic, by studying the dynamical Lie algebra, i.e. by obtaining information at a local level in the form of the tangent space, we can make claims about the manifold

of reachable unitary evolutions $\mathcal{R}_{\hat{V}}$, i.e. make statements that are globally true. This leads to the following conditions that help to determine whether a system is operator controllable [14].

**Theorem 2.4.1** (Operator controllability test)**.** *Given a quantum system $\mathcal{S}$ with Hilbert space dimension $\dim(\mathcal{H}) = n$ and dynamical Lie algebra $\mathcal{L}$, the system is operator controllable if and only if $\dim(\mathcal{L}) = n^2$ or $\dim(\mathcal{L}) = n^2 - 1$.*

Essentially, the previous test specifies that every unitary can be implemented in the system (up to a global phase) only in the cases where $\mathcal{L} \cong \mathfrak{su}(n)$ or $\mathcal{L} \cong \mathfrak{u}(n)$. The latter case leads to $\mathcal{R}_{\hat{V}} \cong U(n)$, where every unitary operation is reachable including any global phase. The former one represents the case $\mathcal{R}_{\hat{V}} \cong SU(n)$, where global phases cannot be adjusted at will, although physically they make no difference. As a remark, this is the only possibility for operator controllability on systems with traceless Hamiltonians, e.g. those described in terms of tensor products of Pauli matrices.

As a last addition to this section, it is necessary to add a different test for pure-state controllability, which may be described in the following form [57, 14]:

**Theorem 2.4.2** (Pure-state controllability test)**.** *Let $\mathcal{L}$ be the dynamical Lie algebra of a controlled quantum system with Hilbert space dimension $\dim(\mathcal{H}) = n$. Let $|\phi\rangle \in \mathcal{H}$ be an arbitrary pure state in the Hilbert space. Then the system is pure-state controllable if and only if*

$$\dim\Big(\Big[\,\mathcal{L}, i\,|\phi\rangle\langle\phi|\,\Big]\Big) = 2(n-1). \tag{2.27}$$

To explain the previous result, we first remember that $\mathcal{R}_{|\psi\rangle} \subseteq \mathcal{S}_{\mathcal{H}}$ and $\dim(\mathcal{S}_{\mathcal{H}}) = 2(n-1)$. On the left hand side of Equation (2.27), the term $[\,\mathcal{L}, i\,|\phi\rangle\langle\phi|\,]$ appears. Looking back to the von Neumann equation (2.1) we see a similar term in the form of $\Big[\hat{H}, \hat{\rho}\Big]$, which it represents the change of $\hat{\rho}$ due to the Hamiltonian $\hat{H}$. In other words, it defines a tangent vector along the curve given by $\hat{\rho}(t) \subset \mathcal{S}_{\mathcal{H}}$. We can connect both equations by identifying the initial density matrix $\hat{\rho}_0$ with a pure state $\hat{\rho}_0 = |\phi\rangle\langle\phi|$. Then, $-[\,\mathcal{L}, i\,|\phi\rangle\langle\phi|\,]$ gives the set of all the possible tangent vectors for the curve described by a pure state $|\psi(t)\rangle$ at $t = 0$ with $|\psi(t)\rangle = |\psi(t)\rangle$. The dynamical Lie algebra $\mathcal{L}$ is included in the commutator to take into account all possible effective Hamiltonians that can be implemented in the system. Calculating the dimension of this set yields the local dimension of the tangent space of all the possible curves $|\psi(t)\rangle$ at $t = 0$. To summarize, Equation (2.27) simply states that a system is pure-state controllable if and only if the dimension of the space tangent to $|\psi(t)\rangle$ at $t = 0$ is maximal, i.e. it is exactly $2(n-1)$.

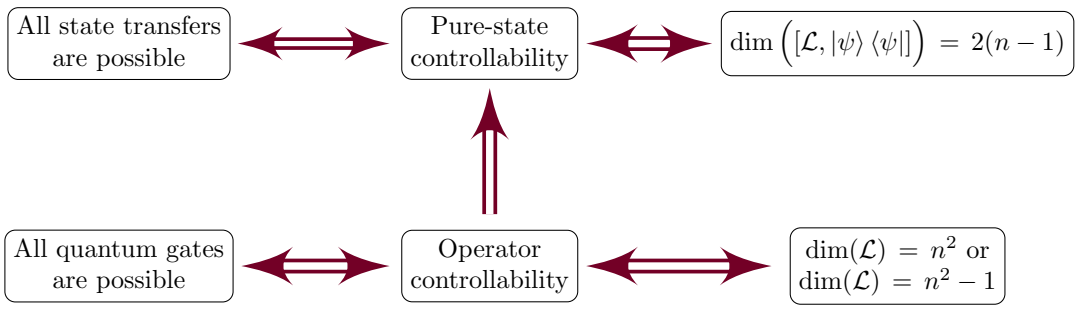


**Figure 2.4:** Relation between pure-state controllability and operator controllability. The diagram also shows the Lie rank conditions for each type of controllability for a system with Hilbert space dimension $n$ and dynamical Lie algebra $\mathcal{L}$.

Note that the pure-state controllability test does not depend on the chosen state $|\phi\rangle$. We can link this back to the fact that pure-state controllability does not depend on the initial state of the system for coherent dynamics. Since the dynamical Lie algebra is not dependent on the initial state, any state can be used for the test, e.g. $|\phi\rangle = (1, 0, ..., 0)$ for any given basis. To compute the dimension of $[\,\mathcal{L}, i\,|\phi\rangle\langle\phi|\,]$ it is sufficient to take into account only a vector basis of $\mathcal{L}$ to compute the different commutators and check the maximal amount of linearly independent elements that can be found.

Therefore, once the dynamical Lie algebra has been calculated we have access to two different tests (for both operator and pure-state controllability). These correspond to the so-called Lie rank method. They can be used to determine whether the system is capable of performing every state-to-state transfer and whether every quantum logic gate can be implemented, respectively. A brief overview of the tests' conditions and the different relations with the types of controllability is shown in Figure 2.4. The only piece of information needed for them is the exact system's Hamiltonian (2.8).

The tests can be computed either algebraically or numerically. However, an important aspect to be mentioned is the scalability of the procedure. The dimension of the Lie algebra scales quadratically with respect to the Hilbert space dimension, which in turn scales exponentially in the number of qubits in a qubit array. For an array of $Q$ qubits, the dynamical Lie algebra can have a maximum dimension of $2^{2Q}$. This leads to some serious issues in terms of computability. In some cases the dynamical Lie algebra can be calculated by induction independently of the dimension of the system [58]. If the Lie algebra has to be calculated numerically, the Lie rank method starts to be unstable for a low number of qubits. The most straightforward way of implementing the Lie rank method is to generate a basis of the Lie algebra and then counting its dimension. To do this, it is necessary to check whether the commutators of higher depth of the control Hamiltonians and the drift are linearly independent or not with the previous elements of the basis. In other words, it is necessary to perform

a matrix rank calculation or an orthonormalization procedure, e.g. Gram-Schmidt. Both operations incur in the so-called curse of dimensionality, where small errors start to pile up in very high-dimensional vector spaces. The large dimension makes very difficult to accurately determine whether a set of vectors is linearly independent or not, leading to inaccurate results in the dimension of the dynamical Lie algebra and, possibly, yielding false positive results for the controllability of a system. This is the reason why alternative tests are needed and can help us expand the size of the arrays that we can study.

### 2.4.3 Controllability with connectedness chains

The Lie rank condition is not the only test that can be used to determine controllability in a quantum system. Here we present an already known test that does not require full calculation of the dynamical Lie algebra to give a positive result on the controllability. The theory behind this subsection can be found in [15], including a mathematical proof of the result. It has previously been used in other systems, like rotational states of molecules [17, 59]. This method is the foundation on which the graph test presented in Chapter 4 is built.

To fully understand the test, we must introduce two new concepts. Let $\hat{H}_0$ and $\hat{H}_1$ be the drift and the control operator as described by Equation (2.8) for an $n$-dimensional Hilbert space. We represent these two operators in the eigenbasis of $\hat{H}_0$. A subset $S$ of the double set of eigenstates indices $\mathcal{I}_{\mathcal{H}}^{\otimes 2} := \{0, 1, \cdots n-1\}^{\otimes 2}$ is said to *couple* two levels $j, k$ in $\{0, 1, \cdots n-1\}^{\otimes 2}$, if there exists a finite sequence $((s_1^1, s_2^1), ..., (s_1^p, s_2^p))$ in $S \subset \mathcal{I}_{\mathcal{H}}^{\otimes 2}$ such that

1. $s_1^1 = j$ and $s_2^p = k$ (i.e. the sequence starts with one index of the two coupled levels and ends with the other one);

2. $s_2^j = s_1^{j+1}$ for every $1 \leq j \leq p-1$ (i.e. the sequence has the structure $((\alpha, \beta), (\beta, \gamma), (\gamma, \delta), (\delta, \epsilon), \cdots)$);

3. $\langle \phi_{s_2^j} | \hat{H}_1 | \phi_{s_1^{j+1}} \rangle \neq 0 \, for \, 1 \leq j \leq p$ and $\phi_i$ the $\hat{H}_0$ eigenstates (i.e. the matrix element $\hat{H}_{1,(j,k)}$ in the eigenbasis of $\hat{H}_0$ is nonzero).

The set $S$ is called a *connectedness chain* if $S$ couples every pair of levels in $\mathcal{I}_{\mathcal{H}}^{\otimes 2}$, i.e. if for every pair of levels $(j, k)$ we can define a sequence following the three aforementioned requirements. From a physical point of view, this ensures that we can transfer population from the level $j$ to the level $k$ using $\hat{H}_1$ as a control. This, however, is not enough to ensure controllability in the system if there exist symmetries

or degeneracies in the spectrum. Therefore, it makes sense to include a new definition for the case where resonances are present.

A connectedness chain $S$ is said to be *non-resonant* if for every tuple $(a, b) \in S$, the energy gap $\Delta E_{a,b} := |E_a - E_b|$ is different from any other energy gap $\Delta E_{c,d}$ of any other pair $(c, d) \in S$ and $(c, d) \in \mathcal{I}_{\mathcal{H}}^{\otimes 2} \setminus \{(a, b), (b, a)\}$.

The controllability test can be summarized as follows: If there is a non-resonant connectedness chain for such a system, then it is approximately controllable, i.e. every unitary gate on the system can be approximated by an arbitrarily small error [15]. For the intents and purposes of this thesis, this is equivalent to operator controllability. In other words, if a system has a connectedness chain given by the drift and a control operator, then the system is operator controllable.

The definitions and results can be better understood through an illustrative example (obtained from [15]). Let $\hat{H}_0$ and $\hat{H}_1$ be defined by

$$\hat{H}_0 = \begin{pmatrix} 1 & 0 & 0 & 0 \\ 0 & 2 & 0 & 0 \\ 0 & 0 & 4 & 0 \\ 0 & 0 & 0 & 4 \end{pmatrix}, \qquad \hat{H}_1 = \begin{pmatrix} 0 & i & 3 & 0 \\ -i & 0 & 0 & \frac{i}{2} \\ 3 & 0 & 0 & 0 \\ 0 & -\frac{i}{2} & 0 & 0 \end{pmatrix}.$$

The set of indices is $\mathcal{I}_{\mathcal{H}}^{\otimes 2} = \{0, 1, 2, 3\}^{\otimes 2}$. We can try to define a connectedness chain by looking at the off-diagonal nonzero matrix elements in $\hat{H}_1$. It is easy to prove that a connectedness chain is given by $S = \{(0, 1), (1, 0), (0, 2), (2, 0), (1, 3), (3, 1)\}$. For example, the chain $S$ connects the pair $(0, 3)$ with the sequence $((0, 1), (1, 3))$. The same idea can be used for any pair $(j, k) \in \mathcal{I}_{\mathcal{H}}^{\otimes 2}$. The energy gaps of tuples present in the chain are $\Delta E_{1,0} = 1$, $\Delta E_{2,0} = 3$ and $\Delta E_{3,1} = 2$. Therefore, the chain of connectedness $S$ is non-resonant and the system is operator controllable. Notice that, even though $\Delta E_{3,1} = \Delta E_{2,1} = 2$, it does not matter as the elements (1,2) and (2,1) do not appear in the chain. Similarly, it is irrelevant that the spectrum of $\hat{H}_0$ is degenerate. The non-resonant connectedness chain is sufficient to prove controllability of the system.

If we take every level $j$ of the system as node, then the tuples $(j, k)$ can be understood as edges on a graph. This is the reason why this method has sometimes been described using graph theory. The energy gaps $\Delta E_{j,k}$ can be added as the weight of the different edges. Finding a non-resonant chain of connectedness equates to finding a subgraph that where, for every pair of nodes $j$ and $k$, there is a path that connects them without using the same weight for two different edges. This connection will be further developed in the graph controllability test presented in Chapter 4.

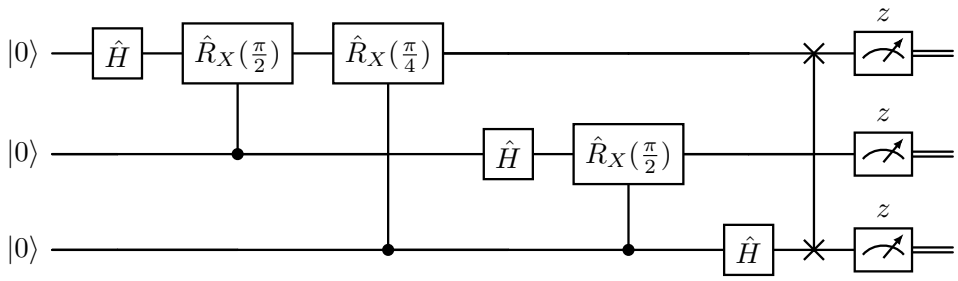


**Figure 2.5:** Implementation of the quantum Fourier transform for the case of three qubits [32]. Rectangular boxes, circles and vertical lines represent quantum logic gates [61] whereas horizontal lines represent the wires in the logic circuit. States are measured at the end of the system on the logical basis of each qubit.

## 2.5 Analysis of parametric quantum circuits

Qubit arrays are the hardware on which we can perform quantum computing and run quantum algorithms. Quite often, quantum circuits are used to represent the change of the qubit's state along the different calculations. *Quantum circuits* are models composed of a set of qubits, initialized on a specific state, upon which we apply a series of operations called *quantum gates* [32]. At the end of the circuit, it is necessary to measure the qubits in order to extract information from the final state of the system. Relative phases between the eigenstates of the measuring operator are lost at this final step. Therefore, the relevant information of a quantum algorithm has to be encoded in the population of the different states that can be measured at the end of the circuit. If we use only coherent dynamics, quantum gates must be unitary operations. At first glance, it looks like this condition actually leaves out many of the classical logic gates that could be used as bits operations. However, it is possible to encode a non-unitary operation of $N$ qubits with the help of an extra auxiliary qubit, turning them into $N+1$-qubit unitary gates [60].

An example of a quantum circuit is shown in Figure 2.5. Following their classical counterpart, quantum circuits are read left to right, with leftmost gates acting first on the qubits. They include wires in the form of straight lines that represent the flow of information and help to determine which qubits are affected by which operations. Contrary to classical Boolean circuits, each qubit starts with a single wire that will remain until measured. Multiple quantum wires cannot be merged into a single qubit using quantum gates. Analogously, operations that would split one input wire into multiple output wires, e.g. duplicating a qubit, are not allowed according to the rules of quantum mechanics.

Quantum circuits will be relevant for the material in Chapter 5 or, more precisely, the study of parametric quantum circuits. Thus, the current section contains all the introductory material needed to make this dissertation and a coherent self-contained reading when it comes to controllability tests based on parametric quantum circuits. The reader is encouraged to skip this section if this topic is not included among their interests.

### 2.5.1 Parametric quantum circuits

A *parametric quantum circuit* (PQCs) is a type of quantum circuit in which some of the quantum logic gates depend on one or more parameters $\vartheta_j$ [62]. These parameters can be modified before the circuit is implemented, leading to different results. Every PQC is therefore a class of quantum circuits that share the same operation structure with certain modifications on the circuit output depending on the chosen parameters $\vec{\vartheta}$. Other names for this kind of circuits include parameterized quantum circuit, parametrized quantum circuit or variational circuit. The latter name arises from their relation with variational quantum algorithms, a type of algorithm that was first introduced for quantum chemistry [18]. Variational quantum algorithms have become particularly relevant for systems in the noisy-intermediate quantum computing (NISQ) era [63], where they are used to leverage the quantum nature of the systems to solve problems that are classicaly hard to work out [64, 65]. Variational algorithms link an optimization problem into a cost function that is measured via the state of the quantum circuit. The iterative process relies on alternating between running the parametric quantum circuit with a given set of parameters to calculate the cost function and then updating the parameters for the next run if the minimum has not been reached.

It is therefore important to know whether a parametric quantum circuit can explore the whole Hilbert space, i.e., what the set of possible final states is at the end of the PQC. In the literature, the term *expressivity* (sometimes also expressibility or expressiveness) is used to speak about the ability of a PQC to produce states that are representative of the full Hilbert space of the system [66, 67]. This definition, far from being a mathematical one, is an umbrella term that encompasses a broad group of measures that try to quantify the possible output of a given PQC. Not all of the different types of expressivity are equivalent, a reason why it is necessary to be rigorous when choosing and discussing a certain expressivity.

Here, we focus on the dimensional expressivity $expr_{dim}$. This expressivity, as we will see, contains information about the dimension of the circuit as a real differentiable manifold [19]. Maximal dimensional expressivity means that the parametric quantum circuit is able to explore a manifold of reachable states that has the same dimension as

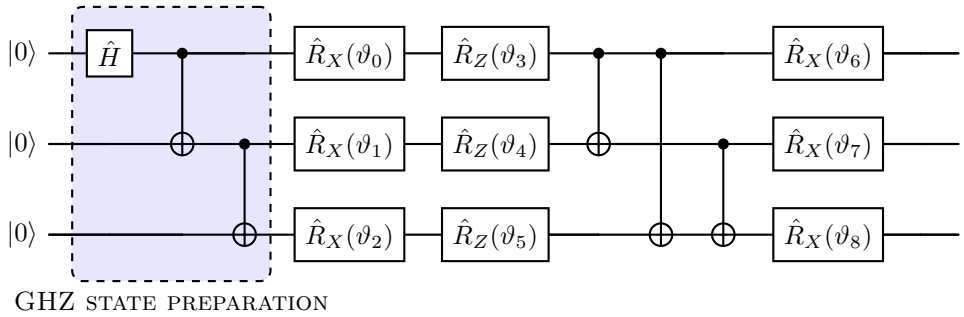


**Figure 2.6:** Example of a parametric quantum circuit. In this case, the parameters $\vartheta_j$ represent the angle of the rotation gates $\hat{R}_G\vartheta_j$ around the $G$ axis. Note that not all gates are parametric, like the initial layer that prepares the system into the Greenberger–Horne–Zeilinger state $(|000\rangle + |111\rangle)/\sqrt{2}$ (cf. [68]).

the Hilbert space. To define this concept properly, we need to mathematically define the map of a parametric quantum circuit.

We can understand a parametric quantum circuit as a protocol implemented on a set of qubits that are initialized in a state $|\psi_0\rangle$. It consists of a sequence of logic gates $\hat{G}_j$, some of which depend on real parameters $\vartheta_k$. We consider a parametric quantum circuit as the map $C(\vec{\vartheta})$ that identifies an array of parameters $\vec{\vartheta}$ in the parameter space $\mathcal{P} \ni \vec{\vartheta}$ with

$$C(\vec{\vartheta}) = \hat{G}_m(\vec{\vartheta})...\hat{G}_0(\vec{\vartheta})\,|\psi_0\rangle\,. \tag{2.28}$$

$C(\vec{\vartheta})$ implicitly depends on the circuit's initial state $|\psi_0\rangle$[1]. An example of a parametric quantum circuit is found in Figure 5.1. Note that the amount of parameters on which each gate $\hat{G}_j(\vec{\vartheta})$ depends may vary from zero to the total number of parameters, e.g.

$$\hat{G}_0(\vartheta_1, \vartheta_2) = \hat{P}(\vartheta_1)\exp\left(-i\frac{\vartheta_2}{2}\hat{X}\right)\hat{H}\hat{P}(-\vartheta_1), \tag{2.29}$$

with the phase gate $\hat{P}$ and the Hadamard gate $\hat{H}$.

Since PQCs are the main object of the optimizations in variational quantum algorithms, it is relevant to also speak about over-parametrization. Having more parameters than strictly necessary can be beneficial for some algorithms, making them more efficient for optimization [69] or more resilient against noise [70, 71]. However, adding more parametric gates also increases the depth of the algorithm, which in turn raises the error produced e.g. by NISQ devices. Finding the sweet spot between both approaches is required to obtain the best of both worlds. For this reason, quantifying and identifying the number of independent parameters in a PQC is a crucial goal for the purposes of variational quantum algorithm.

[1] This is in contrast to many commonly used definitions of a circuit that only consider the gate sequence and not the device initialization.

A parameter $\vartheta_j$ of a PQC is deemed *redundant* if the changes that can be achieved in the final state of the circuit by varying $\vartheta_j$ infinitesimally can also be achieved by keeping $\vartheta_j$ constant and varying other parameters $\vartheta_k$ with $k \neq j$. A nonredundant parameter is called *independent*. If a parameter $\vartheta_j$ is determined to be redundant with respect to a set of different parameters $\{\vartheta_k\}_k$ (with $k \neq j$), then $\vartheta_j$ can be kept at a fixed value without impacting the set of reachable states at the end of the circuit.

If we define a PQC as a map $C(\vec{\vartheta})$ from the parameter space $\mathcal{P}$ to the state space $\mathcal{H}$, $C : \mathcal{P} \to \mathcal{H}$, then the previous definition can be restated in more mathematical terms. If we take into account all the possible parameters $\vec{\vartheta} \in \mathcal{P}$, we can understand the set $C(\mathcal{P})$ as the manifold containing all the reachable states at the end of the circuit. To include this function in the definition of the redundant parameters, we first define the real Jacobian $J_C(\vec{\vartheta})$ of the PQC as

$$J_C(\vec{\vartheta}) = \begin{pmatrix} | & & | \\ \mathfrak{Re}\left(\partial_1 C(\vec{\vartheta})\right) & \cdots & \mathfrak{Re}\left(\partial_N C(\vec{\vartheta})\right) \\ | & & | \\ & & \\ | & & | \\ \mathfrak{Im}\left(\partial_1 C(\vec{\vartheta})\right) & \cdots & \mathfrak{Im}\left(\partial_N C(\vec{\vartheta})\right) \\ | & & | \end{pmatrix}, \tag{2.30}$$

where $\partial_k C(\vec{\vartheta})$ represents the derivative of the map $C(\vec{\vartheta})$ with respect to $\vartheta_k$. Note that, for a $d$-dimensional Hilbert space $\mathcal{H}$, both $\mathfrak{Re}\left(\partial_k C(\vec{\vartheta})\right)$ and $\mathfrak{Re}\left(\partial_k C(\vec{\vartheta})\right)$ are $d$-dimensional column vectors for every index $k$. We define the partial real Jacobian $J_C^{(k)}(\vec{\vartheta})$ with respect to the parameter $\vartheta_k$ as the $k$-th column of $J_C(\vec{\vartheta})$ as defined in Equation (2.30).

With the previous information, let us assume a set of parameters $\{\vartheta_k\}_{k=k_1}^{k_m}$ and a different parameter $\vartheta_j$. Then $\vartheta_j$ is independent with respect to $\{\vartheta_k\}_k$ if and only if

$$rank\left(J_C^{(k_1)}(\vec{\vartheta}), ..., J_C^{(k_m)}(\vec{\vartheta})\right) = rank\left(J_C^{(k_1)}(\vec{\vartheta}), ..., J_C^{(k_m)}(\vec{\vartheta}), J_C^{(j)}(\vec{\vartheta})\right), \tag{2.31}$$

i.e. if the vector $J_C^{(j)}(\vec{\vartheta})$ is linearly dependent with respect to the set of vectors $J_C^{(k)}(\vec{\vartheta})$. We can bring this idea back to the manifold of reachable states $C(\mathcal{P})$. The real partial derivatives $J_C^{(k)}(\vec{\vartheta})$ represent vectors of the tangent space at the point $C(\vec{\vartheta}) \in C(\mathcal{P})$. A parameter $\vartheta_j$ is redundant with respect to a parameter set $\{\vartheta_k\}_{k=k_1}^{k_m}$ if the direction generated by $\vartheta_j$ in the tangent space is linearly dependent with respects to the directions already generated by $\{\vartheta_k\}_{k=k_1}^{k_m}$.

To quantify the number of states that can be obtained as a final state in a PQC, we can use the concept of dimensional expressivity [19, 20].

**Definition 2.5.1** (Dimensional expressivity)**.** *Given a parametric quantum circuit $C(\vec{\vartheta}) : \mathcal{P} \rightarrow \mathcal{H}$, the dimensional expressivity of the circuit $expr_{dim}$ is the maximum number of independent parameters $\vartheta_j$ in the circuit.*
*Additionally, $expr_{dim}$ also represents the local dimension of the manifold of possible final states $C(\mathcal{P})$.*

The last part of the definition gives further meaning to the mathematical description of independent parameters shown in Equation (2.31). If we have a maximal set of independent parameters $\{\vartheta_{k_j}\}_{j=1}^{expr_dim}$ then, by definition, the set $\{J_C^{(k_j)}(\vec{\vartheta})\}_{j=1}^{expr_dim}$ is a maximal linearly independent set of vectors in the tangent space $T_{\vartheta}$. Therefore, the parameter set $\{\vartheta_{k_j}\}_{j=1}^{expr_dim}$ can be locally used as a full coordinate set of the manifold of final states $C(\mathcal{P})$. From a physical perspective, all final states in a neighborhood around $C(\vartheta) =: |\psi_{\vec{\vartheta}}\rangle \in \mathcal{H}$ can be navigated by varying $\{\vartheta_{k_j}\}_{j=1}^{expr_dim}$ and leaving all the other parameters in the PQC fixed. As the set of reachable states is contained in the unit sphere of the Hilbert space $\mathcal{H}$, the maximal real dimension of this manifold is $2d-1$, with $d = \dim()$. In other words, the dimensional expressivity always has an integer value with an upper bound of $2d-1$.

Note that the definition of dimensional expressivity speaks about the maximum number of independent parameters $\theta_j$. There is, however, an important clarification to be made. While the maximum number of independent parameters is fixed, there may not be a unique maximal set of parameters. Indeed, if two parameters $\vartheta_1$ and $\vartheta_2$ are redundant with respect to each other, then there is a choice to be made about whether to label the former or the latter as independent.

In Chapter 5 we will see how the concept of dimensional expressivity of parametric quantum circuits can be linked to the controllability of qubit arrays. The following subsection presents one of the possible methods to find a maximal set of independent parameters. This will also be useful for finding the connection between expressivity and and controllability.

### 2.5.2 Dimensional expressivity analysis

Identifying a maximal set of independent parameters in a systematic process is a valuable tool to use when studying parametric circuits and their capabilities. As previously mentioned, it is true that adding more parameters can be beneficial in some cases, reducing the required time for certain algorithms. Nevertheless, verifying that the initial circuit has maximal dimensional expressivity is crucial to determine whether the solution can even be reached. Furthermore, labeling a set of independent parameters may give information about which operations are strictly necessary and which are effectively duplicating dynamics that can be achieved with others.

Dimensional expressivity analysis is a method to both determine the dimensional expressivity of a parametric quantum circuit and identify a maximal set of independent parameters [19, 20]. It is devised as a hybrid quantum-classical algorithm that obtains its information through some measurements on a quantum device and some simple numerical calculations in a classical computer.

The main idea of the dimensional expressivity analysis is to measure the rank of the real Jacobians $J_C(\vec{\vartheta})$ (cf. Equation (2.30)) for a given set of parameters $\vec{\vartheta}$ in order to determine the exact number of independent parameters. To determine which parameters are independent and which ones are redundant in a systematic manner, we define the partial matrices

$$J_{C,n}(\vec{\vartheta}) = \begin{pmatrix} | & & | \\ \mathfrak{Re}\partial_1 C(\vec{\vartheta}) & \cdots & \mathfrak{Re}\partial_n C(\vec{\vartheta}) \\ | & & | \\ & & \\ | & & | \\ \mathfrak{Im}\partial_1 C(\vec{\vartheta}) & \cdots & \mathfrak{Im}\partial_n C(\vec{\vartheta}) \\ | & & | \end{pmatrix}, \tag{2.32}$$

composed of the first $n$ columns of the real Jacobian $J_C(\vec{\vartheta})$. If the first parameter $\vartheta_1$ has a non-negligible effect on the circuit, i.e. $J_{C,1} \neq \vec{0}$, then we can interpret it as an independent parameter. If $rank(J_{C,n-1}) < rank(J_{C,n})$, then the parameter $\vartheta_n$ can be labelled as independent. Conversely, if the two ranks are equal then $\vartheta_n$ is redundant with respect to the previous parameters. This sets the basis for an iterative test that separates every parameter into one of the two categories. The exact parameter partition only depends on the order of parameters that have been checked. Different parameter sortings may result in different partitions, but the total number of independent parameters remains constant. To make these calculations more efficient, the method uses instead the matrices

$$S_{C,n}(\vec{\vartheta}) = J_{C,n}^T(\vec{\vartheta}) J_{C,n}(\vec{\vartheta}), \tag{2.33}$$

which have by construction the same rank as $J_{C,n}$.

So far we have only talked about classical computations of the ranks of some matrices. The last piece of the puzzle is obtaining the information of each $S_{C,n}$ matrix. The $(i,j)$ element of $S_{C,n}$, $S_{C,n}^{(i,j)}$, is given by $\mathfrak{Re}(\langle \partial_i C(\vec{(}\vartheta)), \partial_j C(\vec{(}\vartheta))\rangle)$. Let us denote the initial state of the circuit $C(\vec{\vartheta})$ as $|\psi_0\rangle$. Assuming we only include rotation gates $\hat{R}_{\hat{A}}(\varphi) := \exp(-i\frac{\varphi}{2}\hat{A})$ depending on a single parameter $\varphi$, the circuit is represented by

$$C(\vec{\vartheta}) = \hat{R}_{\hat{A}_1}(\vartheta_1)\hat{R}_{\hat{A}_2}(\vartheta_2)\cdots\hat{R}_{\hat{A}_n}(\vartheta_n)\,|\psi_0\rangle\,. \tag{2.34}$$

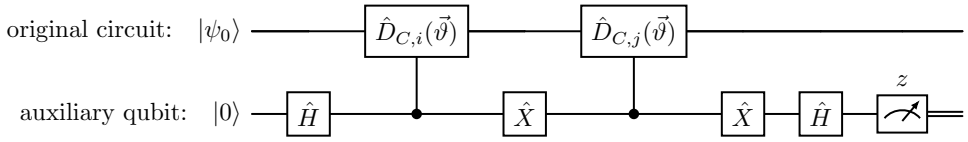


**Figure 2.7:** Implementation of the circuit required to perform the dimensional expressivity analysis of a parametric quantum circuit with quantum measurements. The top quantum wire encompasses the $N$ qubits of the PQC $C(\vec{\vartheta})$ that is meant to be studied and is initialized in the state $|\psi_0\rangle$ (cf. Equation (2.34)). The circuit is composed of the Hadamard gate $\hat{H}$ (not related to a Hamiltonian), the NOT gate $\hat{X}$ and the controlled gates $\hat{D}_{C,k}$ (cf. Equation (2.36)). Initial state of the first qubits Image adapted from [20].

In this particular case, the partial derivatives $\partial_k C(\vec{\vartheta})$ are simply given by

$$\partial_k C(\vec{\vartheta}) = \hat{R}_{\hat{A}_1}(\vartheta_1)\cdots\hat{R}_{\hat{A}_{k-1}}(\vartheta_{k-1})\left(\frac{-i}{2}\hat{A}_k\right)\hat{R}_{\hat{A}_k}(\vartheta_k)\cdots\hat{R}_{\hat{A}_n}(\vartheta_n)\,|\psi_0\rangle\,, \tag{2.35}$$

which represents a vector in the Hilbert space of the system $\mathcal{H}$. If the operator $\hat{A}_k$ is unitary, then $\partial_k C(\vec{\vartheta})$ represents a different parametric quantum circuit identical to $C(\vec{\vartheta})$ with the exception that it contains a $\hat{A}_k$ gate between the rotations $\hat{R}_{\hat{A}_{k-1}}(\vartheta_{k-1})$ and $\hat{R}_{\hat{A}_k}(\vartheta_k)$. If it is not unitary, a possibility for non-local operators, then it can be implemented as a unitary gate by including an additional auxiliary qubit [60]. The operation related to the derivative of the circuit can be defined as

$$\hat{D}_{C,k}(\vec{\vartheta}) := \hat{R}_{\hat{A}_1}(\vartheta_1)\cdots\hat{R}_{\hat{A}_{k-1}}(\vartheta_{k-1})\hat{A}_k\hat{R}_{\hat{A}_k}(\vartheta_k)\cdots\hat{R}_{\hat{A}_n}(\vartheta_n). \tag{2.36}$$

Note that, when comparing Equations (2.35) and (2.36), the latter one has the $\frac{-i}{2}$ factor removed for the definition of $\hat{D}_{C,k}$. Using the new notation, the $S_{C,n}^{(i,j)}$ elements can be rewritten as $\frac{1}{4}\mathfrak{Re}(\langle\langle\psi_0|\,\hat{D}_{C,i}^{\dagger}\hat{D}_{C,j}\,|\psi_0\rangle\rangle)$. To compute the different entries of $S_{C,n}$ on the quantum device we can use the state

$$|\psi_{i,j}\rangle = \frac{|0\rangle\otimes\left(\hat{D}_{C,i}\,|\psi_0\rangle + \hat{D}_{C,j}\,|\psi_0\rangle\right) + |1\rangle\otimes\left(\hat{D}_{C,i}\,|\psi_0\rangle - \hat{D}_{C,j}\,|\psi_0\rangle\right)}{2}. \tag{2.37}$$

Measuring the auxiliary qubit of the state $|\psi_{i,j}\rangle$ in the canonical basis we obtain a probability for the qubit to be in $|0\rangle$ of

$$P(\text{aux} = |0\rangle \mid |\psi_{i,j}\rangle) = \frac{1 + \mathfrak{Re}(\langle\langle\psi_0|\,\hat{D}_{C,i}^{\dagger}\hat{D}_{C,j}\,|\psi_0\rangle\rangle)}{2}. \tag{2.38}$$

Therefore, repeated measurements of the $|\psi_{i,j}\rangle$ state can be used to determine the entries $S_{C,n}^{(i,j)} = 2P(\text{aux} = |0\rangle \mid |\psi_{i,j}\rangle) - 1$. To obtain accurate statistics, the measurement of $|\psi_{i,j}\rangle$ has to be performed a sufficiently large number of times. This procedure must then be repeated for each pair of indices $(i, j)$. Finally, to construct the states $|\psi_{i,j}\rangle$ we can simply use the circuit described in Figure 2.7.

With this hardware implementation we can obtain the required $S_{C,k}$ matrices via measurements on the quantum device. Their rank can be calculated using a classical computer, which would determine the amount of independent parameters in the circuit and their location.

## 2.6 Quantum speed limit

In previous sections we have talked about controllability in quantum systems, which answers to the question of whether it is possible to implement certain dynamics on a device. This is a very interesting subject on a fundamental level. But it lacks insight on some of the more applied problems that are attached to the actual implementation of the operation. These practical issues include, for example, computing a set of pulses to produce some target dynamics, decomposing a desired gate into a sequence of well-calibrated gates on a qubit array or knowing how fast certain operations can be performed in the system. The latter is the main focal point of the current section and of Chapter 3.

In the current landscape of quantum technologies, generating fast evolutions on quantum devices is key to achieve efficient protocols in quantum simulation and quantum computing. This is intrinsically related to the quantum speed limit of a system, the minimum time in which some dynamics can be implemented in a given quantum system. Finding the quantum speed limit is fundamentally a theoretical question that still bears important applications at an experimental level. For example, it defines how fast quantum information can be processed and exchanged between systems [72, 73]. Whether trying to prepare a system in a certain state [74] or to implement unitary gates on a quantum device [75], the quantum speed limit provides valuable information about the feasible dynamics.

The problem of the quantum speed limit has been presented and extensively discussed in many reviews during the last decades [76, 77, 78, 79, 23]. The concept is usually understood as a lower bound on the time that it takes to transform a quantum system in some desired manner. This counterintuitive definition poses the first issue: The quantum speed limit is actually a measure of time and not of speed. A higher quantum speed limit means that the system will take longer to produce some target dynamics (i.e. the evolution will be slower) and vice versa. This section builds upon some of the historical definitions, from its natural appearance in quantum mechanics to the different definitions and exact formulas that were derived.

### 2.6.1 Heisenberg's uncertainty principle

Non-commuting observables are one of the defining features of quantum mechanics. Heisenberg's uncertainty principle can be derived from this property [80], leading to the well known inequalities

$$\Delta\hat{p}\Delta\hat{x} \geq \frac{\hbar}{2} \quad \text{and} \quad \Delta E\Delta t \geq \frac{\hbar}{2} \tag{2.39}$$

where $\Delta\hat{A}$ represents the variance of an operator $\hat{A}$ for an implicit state $|\psi\rangle$. The principle showcases the relation between the operators position $\hat{x}$ and momentum $\hat{p}$ and the variables energy $E$ and time $t$. This was also quickly generalized for other non-commuting operators as [81]

$$\Delta\hat{A}\Delta\hat{B} \geq \frac{\left|\langle[\hat{A},\hat{B}]\rangle\right|}{2}. \tag{2.40}$$

The physical meaning of the position and momentum relation in Equation (2.39) can easily be put into context for the wavefunction of a particle: The less spread the probability density is for the position operator $\hat{x}$, more variance for the momentum $\hat{p}$ of the particle. This also leads to the conclusion that no observer can have perfect knowledge of the position and momentum of a particle. According to Equation (2.40) this is also true for any two conjugated operators $\hat{A}, \hat{B}$, since they must satisfy the canonical commutation relation

$$\left[\hat{A},\hat{B}\right] = i\hbar. \tag{2.41}$$

The second relation appearing in Equation (2.39), however, is fundamentally different. Energy $E$ is represented in quantum mechanics by the Hamiltonian operator $\hat{H}$, which we can substitute by $\hat{H} = -i\hbar\partial_t$ according to the Schrödinger equation. Therefore, $\Delta E = \Delta\hat{H}$. Unfortunately, an analogous treatment is not possible for $\Delta t$. Time is not a well-defined operator in non-relativistic quantum mechanics [82]. Thus it would seem that there is no immediate physical explanation for the second inequality of Equation (2.39). In particular, other relations derived from Heisenberg's uncertainty principle given by Equation (2.40) show the connection between the variances of two operators for a given state $|\psi(t)\rangle$ at a fixed given time $t$. In other words, they are relations regarding simultaneous effects. Even if an operator for time existed, its variance would be null for a fixed moment of time.

The solution to this conundrum came decades later, with the idea that $\Delta E$ should not be understood as the variance in a fixed moment in time, but as the change over time of the system's energy, i.e. the change in the expectation value of the energy of the system over time.

### 2.6.2 The quantum speed limit: from orthogonal states to more general definitions

In 1945 Mandelstam and Tamm used the Heisenberg uncertainty principle to establish a connection between the energy variance in a finite quantum system with time-independent Hamiltonian $\hat{H}$ and the time $\tilde{t}$ required for one state to evolve to an orthogonal state depending on their energy distribution [83],

$$\tilde{t} \geq \tau_{QSL} = \frac{\pi\hbar}{2\,\Delta\hat{H}}. \tag{2.42}$$

Years later, a contending quantum speed limit between orthogonal states was also derived by Margolus and Levitin as [84]

$$\tilde{t} \geq \tau_{QSL} = \frac{\pi\hbar}{2\,\langle\hat{H}\rangle}, \tag{2.43}$$

where $\langle\hat{H}\rangle$ is the expected value for the energy assuming that the ground level is $E_0 = 0$. The two different expressions given by the Mandelstam-Tamm bound and the Margolus-Levitin bound were unified for orthogonal pure states in 2009 as

$$\tau_{QSL} = \max\left\{\frac{\pi\hbar}{2\,\Delta\hat{H}}, \frac{\pi\hbar}{2\,\langle\hat{H}\rangle}\right\}, \tag{2.44}$$

proving that the exact bound is achieved in some cases [24].

The unified bound in Equation (2.44) presented one of the first physical meanings for the quantum speed limit of a system. As previously stated, it holds information about the maximum rate at which a system's state can evolve over time. The definition, however was restricted to time-independent Hamiltonians and orthogonal states.

With time, different quantum speed limits were derived for states separated by arbitrary angles [85]. More importantly, other limits were studied for the case of driven dynamics [86]. These set the foundations to define quantum speed limits for a given unitary evolution. Naturally, a minimum time in which a quantum logic gate can be implemented provides a very useful piece of information for quantum computation. The time estimation of a certain quantum algorithm is upper bounded by the sum of all the quantum speed limits of the gates that it is composed of. Making these estimates is essential to knowing which physical platforms are suitable for which algorithms. The problem is that finding exact bounds for large systems is an arduous task that not always yields a solution. A close estimation of the quantum speed limit for some given dynamics is in principle enough to understand the time scale at which a system operates and the order of magnitude of the number of quantum operations that can be performed. As a final note, it is worth mentioning that it is not always guaranteed that the quantum speed limits can be saturated in reality. Physical setups

usually have restrictions like the maximum amplitude on a control or having a limited range of frequencies. These limitations may result in a higher minimal control time than the theoretical quantum speed limit that does not assume such limitations [87]. Nevertheless, the better understanding of the quantum speed limits of a system may provide valuable information regarding which dynamics are more easily implemented on the system.

These concepts will be expanded in Chapter 3, which focuses on the estimation of the quantum speed limit of three different types of dynamics: fixed unitary evolutions on the whole Hilbert space, simultaneous state transfers in a system (with arbitrary relative phases between them) and logic gates in a subspace of the total Hilbert space (with their respective fixed relative phases).

# 3 Quantum speed limit estimator

Closed quantum systems are the first approach for many numerical simulations of quantum physics. Nonetheless, it is no secret that there does not exist any perfect closed system in reality. Every device is subject to some form of decoherence or relaxation time scale in which the quantum nature of the system can no longer be described using coherent dynamics [22, 88]. This is the case, for example, in spontaneous emissions of atoms [89] or the dephasing of superconducting circuits [90]. Performing operations as fast as possible is crucial to tackle this issue. Therefore, finding systems where the desired dynamics can be implemented swiftly has become a relevant task in the last decades [91]. However, in quantum mechanics there is a fundamental bound to the speed at which certain dynamics can be performed: The quantum speed limit [92].

The first quantum speed limit arises from Heisenberg's uncertainty principle and the connection between energy and time. This relation lead to the idea that there is a limit at which the energy of a quantum system can change over time depending on the Hamiltonian of the system. The quantum speed limit was defined as the minimum possible time in which an initial state in the system can evolve to an orthogonal final state in the Hilbert space. This notion was first developed in the Mandelstam-Tamm bound [83] and later through the Levitin-Margolus bound [84]. Both of them were later combined to create a tight bound [24] to study the evolution of a single state in a system. With time, the term of "quantum speed limit" became broader, being applied not only to state-to-state transfers in closed systems but also to unitary operations [93, 94, 95] and even extended to open quantum systems [96, 97, 98]. Given a quantum system with some controls and a set of desired dynamics, determining the quantum speed limit may be useful to assess whether the system is suitable to conduct a certain experiment or protocol.

Over the years, there have been multiple approaches to determining the quantum speed limit of a system. These include geodesic curves and measurement theory in differential geometry and Lie groups [99, 100, 101], optimal control theory to determine the minimal time at which an evolution is feasible [102, 103], classical numerical estimations dependent on the norm of the Hamiltonian [104] and even

hybrid quantum-classical algorithms [105]. While analytical results derived from the underlying geometry of the system provide tight bounds to a small group of low-dimensional examples, numerical calculations can be used to determine bounds that are close enough to give relevant information about larger systems.

The goal of this chapter is to present a numerical method to estimate the quantum speed limit of either a unitary evolution on the total Hilbert space, a quantum gate on a subspace or a set of simultaneous state transfers. The algorithm takes into account local and global phases, either fixing them or leaving them as arbitrary parameters that can be changed to accommodate for the different dynamics. To compute the estimation we define the concept of the available velocity polytope of a quantum system. In a nutshell, the available velocity encompasses the information of how fast the system can evolve in every direction in the Lie algebra, the tangent space of the Lie group containing all possible unitary operations [14]. This polytope is computed numerically but it derives from the analytical study of adjoint orbits of operators acting on a Hilbert space [106]. The available velocity induces a natural partition of the Lie algebra as a vector space into the subspaces of fast, slow and very slow directions. Given a unitary evolution, we can associate a direction on the Lie algebra to it and give an estimation on the minimal time that the system requires to evolve. For the case of multiple simultaneous state transfers, the algorithm repeats the procedure for all the different unitaries that satisfy the conditions, finding the minimal quantum speed limit among them.

The chapter is structured as follows. Section 3.1 introduces the necessary notions of the quantum speed limit in quantum systems with linearly coupled controls. In particular, it details the differences between the limits when they are defined for unitary operations and for a set of simultaneous state transfers. The newly developed concepts and used tools are explained in Section 3.2, with a special focus on the available velocity polytope (cf. Section 3.2.2) and the partition that it naturally produces on the Lie algebra of the system (cf. Section 3.2.1). The section also includes the exact method for computing the available velocity polytope using the quickhull algorithm as well as methods that provide possible alternatives through looser, but less numerically demanding, approximations. The section closes with a detailed description of the quantum speed limit estimator for any desired target conditions. Section 3.3 showcases the algorithm applied to different examples and compares the results to bounds for the global quantum speed limit that were previously known. It also includes a brief discussion of the problems and complications inherent in the algorithm. Finally, Section 3.4 concludes.

## 3.1 Quantum speed limit of controlled systems

We have previously seen that the Hamiltonians of closed systems with linearly coupled controls are described by Equation (2.8). For this chapter, however, we will study the case where there is only one control, such that Equation (2.8) can be rewritten as

$$\frac{d}{dt}|\psi(t)\rangle = -i\left(\hat{H}_0 + u(t)\hat{H}_1\right)|\psi(t)\rangle\,. \tag{3.1}$$

Here we have a drift $\hat{H}_0$, a time-dependent control $u(t)$ and the associated control operator $\hat{H}_1$. The ideas here presented may in principle be extended to the case with more controls. This extension is briefly covered in the summary of the chapter. For the case of a single control, the dynamical Lie algebra is given by

$$\mathcal{L} = Lie\left(\{\hat{H}_0, \hat{H}_1\}\right). \tag{3.2}$$

To start with a toy model, we assume that $\mathcal{L} = \mathfrak{su}(n)$, which implies that the system is operator controllable according to Theorem 2.4.1. In other words, we ensure that all unitary operations (and by extension all state-to-state transfers) are possible for some final times. This is physically a severe constraint, although a necessary one to ensure that the system can produce any target gate or target state transfers that we may want to study. As a mathematical aside, however, this is feasible in a lot of theoretical examples. Indeed, if we randomly choose two Hermitian operators $\hat{H}_0$ and $\hat{H}_1$, they generate the whole $\mathfrak{su}(n)$ algebra almost always, with probability equal to one [107]. Randomly chosen bounded Hermitian operators will tend to not be degenerate and to have nonzero entries with different irrational values. This property ensures that their nested commutators are linearly independent, eventually generating a complete dynamical Lie algebra.

As usual, we assume no physical bound or maximal frequency on the control $u(t)$. In that case, we can choose a high amplitude for $u(\tilde{t})$ at a certain time $\tilde{t}$ such that $||\hat{H}_0 + u(t)\hat{H}_1|| \simeq ||u(t)\hat{H}_1|| \gg 1$. The implications of this result can be explained in two steps. First of all, both $i\hat{H}_0$ and $i\hat{H}_1$ belong to the Lie algebra, i.e. they are directions in the tangent space alongside which we can evolve. Second, all of the unitary matrices in the curve

$$\gamma_{\hat{H}_1}(\alpha) := \{e^{\hat{H}_1\alpha}\,|\,\alpha \in \mathbb{R}\} \quad \subset SU(n) \tag{3.3}$$

can be approximated arbitrarily fast for any error $\epsilon > 0$. That means that for any gate $e^{\hat{H}_1\alpha}$ and any final time $t_f > 0$ there exists a solution $u_{\alpha,t_f}(t)$ such that the evolution operator $\hat{U}(t_f)$ given by integrating Equation (3.1) fulfils the condition $||\hat{U}(t_f) - e^{\hat{H}_1\alpha}||_F \leq \epsilon$, where $||\cdot||_F$ represents the Frobenius norm [108]. On the other hand, the converse is not necessarily true for gates outside of the curve. Indeed,

to generate unitary evolutions not contained in $\gamma_{\hat{H}_1}$ we have to make use of the $\hat{H}_0$ contribution, which cannot be sped up. If the drift has to be used to access some operation, then there is no alternative to letting the system evolve a set amount of time $\tau$. Out of all the possible procedures and their respective times $\tau$, their minimum $\tau_{QSL} := \min(\tau)$ will be used as an estimator of the quantum speed limit, which is presented in Section 3.2.

The main goal of this project is to define an algorithm that is capable of numerically estimating the quantum speed limit $\tau_{QSL}$, given a system as defined in Equation (3.1) and a certain unitary gate or some desired state transfers. Evidently, $\tau_{QSL}$ implicitly depends on the system operators $\hat{H}_0$, $\hat{H}_1$ and the desired gate $\hat{U}$. Additionally, less restrictive conditions have also been included among the capabilities of this algorithm, allowing us to also explore single state transfers $|\psi_0\rangle \to |\psi_f\rangle$ and simultaneous state transfers defined as a set $\{|\psi_0^{(j)}\rangle \to |\psi_f^{(j)}\rangle\}_j$.

We must understand the fact that some directions in the tangent space are quasi instantaneous while other contributions are crucial to the estimation $\tau_{QSL}$. Subsection 3.2.1 expands on this notion and categorizes the different types of directions in the vector space of the Lie algebra based on their effect on the quantum speed limit $\tau_{QSL}$.

To maintain a structured analysis, we still must include the exact definitions for the quantum speed limit that will be used in the remainder of the chapter.

### 3.1.1 Quantum speed limit of quantum gates

In Chapter 2 we extended the Schrödinger equation (2.2) from one state to a complete orthonormal basis of the Hilbert space (cf. Equation (2.7). This lifted the control equation from normalized vectors in the Hilbert space to dynamical evolutions of closed systems in the Lie group of unitary operators. Analogously, we can rewrite Equation (3.1) as

$$\frac{d}{dt}\hat{U}(t) = -i\left(\hat{H}_0 + u(t)\hat{H}_1\right)\hat{U}(t), \quad \hat{U}(0) = \mathbb{1}_d. \tag{3.4}$$

In the equation above, $\hat{U}$ represents the evolution of an orthonormal basis that coincides with the canonical basis at $t = 0$. Solving an equation analogous to Equation (3.1), it is possible to explore all the unitary operations that are achievable in the system.

From an analytical point of view, we can restrict ourselves to the case of the special unitary group $SU(n)$. Global phases of unitary evolutions carry no physical meaning and can therefore be neglected, which reduces the group $U(n)$ to $SU(n)$.

Therefore we assume that the target unitary matrices $\hat{U}_{tgt}$ whose quantum speed limit we want to estimate are always included in the special unitary group. Nevertheless, from a numerical point of view, it is useful to include an equivalence class of unitary matrices, since any two evolutions $\hat{U}$ and $e^{i\varphi}\hat{U}$ (with $\varphi \in \mathbb{R}$) represent physically the same dynamics on a system. This expands the number of possible solutions that the algorithm could in principle find to satisfy the target conditions. Given a target evolution $\hat{U}_{tgt}$, we want to compute the quantum speed limit for the equivalence class $\{e^{i\varphi}\hat{U}_{tgt}\}_{\varphi\in\mathbb{R}}$. If two gates $\hat{U}_A$ and $\hat{U}_B$ belong to the same equivalence class (i.e. $\hat{U}_A = e^{i\varphi}\hat{U}_B$ for some real $\varphi$), then we say that $\hat{U}_A$ and $\hat{U}_B$ are *phase equivalent*.

The *quantum speed limit $\tau_{QSL}$ for a certain target unitary evolution $\hat{U}_{tgt}$* is the shortest final time $t_f$ for which there exists a control $\tilde{u}$ such that $\hat{U}_{\tilde{u}}(t_f)$ and $\hat{U}_{tgt}$ are phase equivalent. Here we have used $\hat{U}_{\tilde{u}}(t_f)$ as the unitary evolution generated by a control $\tilde{u}(t)$ at a final time $t_f$.

Since in this work the quantum speed limit is studied using numerical tools, which always have finite precision, the limit is an approximate estimate. Therefore, all controls $u(t)$ and final times $t_f$ that fulfill $||\hat{U}(t_f) - \hat{U}_{tgt}||_F \leq \epsilon$ for a chosen error tolerance $\epsilon$ are taken into account for the quantum speed limit calculation. Note that for the given question of the speed limit, calculating the exact control $\tilde{u}$ that approximates the quantum speed limit of the desired evolution is not the goal of the described estimator. Once the final time is known, one can use quantum optimal control to solve the problem of finding the right control pulse to obtain the target evolution $\hat{U}_{tgt}$ up to a global variable. Possible choices for the optimization method include Krotov's algorithm [109, 110], CRAB [111] and GRAPE [112].

### 3.1.2 Quantum speed limit of state transfers and gates acting on subspaces

Instead of choosing a unitary evolution as the necessary condition to calculate the quantum speed limit, it is possible to select different targets. One of the potential goals is to focus on state-to-state transfers defined by a set $\{|\psi_0^{(j)}\rangle \rightarrow |\psi_f^{(j)}\rangle\}_{j=0}^{n_s-1}$ containing pairs of initial and final states ($|\psi_0^{(j)}\rangle$ and $|\psi_f^{(j)}\rangle$ respectively. Without loss of generality we can assume that the states $\{|\psi_0^{(j)}\rangle\}$ (respectively $\{|\psi_f^{(j)}\rangle\}$) form a set of orthonormal states.

By choosing $n_s \leq \dim(\mathcal{H})$ and fixing the local phases of all the transitions in the test, one simply goes back to defining a single unitary operator up to a global phase, i.e. the target from the previous subsection. The more interesting case occurs when $n_s < \dim(\mathcal{H})$, as it expands the possibilities that we can explore. Given the

aforementioned set of state-to-state transfers, we say that a unitary operation $\hat{U}$ *meets the target conditions* if $\hat{U}\,|\psi_0^{(j)}\rangle = |\psi_f^{(j)}\rangle$ for every $j = 0, ..., n_s - 1$.

It is common in state transfers to overlook the local phases between (eigen)states and only care about the probability of finding the system in a certain eigenstate. To make this evident we use the notation $\{|\psi_0^{(j)}\rangle \to e^{i\varphi_j}\,|\psi_f^{(j)}\rangle\}_{j=0}^{n_s-1}$ for arbitrary phase angles $\varphi_j \in \mathbb{R}$ for every $0 \leq j \leq n_s - 1$. Analogously, we claim that a unitary evolution meets the target conditions $\{|\psi_0^{(j)}\rangle \to e^{i\varphi_j}\,|\psi_f^{(j)}\rangle\}_{j=0}^{n_s-1}$ if there exist phase angles $\varphi_j$ such that $\hat{U}\,|\psi_0^{(j)}\rangle = e^{i\varphi_j}\,|\psi_f^{(j)}\rangle$ for every $j = 0, ..., n_s - 1$. On the contrary, to define a set of $n_s$ conditions with fixed phases we will use the notation $\{|\psi_0^{(j)}\rangle \to |\psi_f^{(j)}\rangle\}_{j=0}^{n_s-1}$. This, while not common when talking about state-to-state transfers, essentially defines a quantum gate on a $n_s$-dimensional logical space. In both cases we will name $n_s$ as the number of given conditions.

Given a specific quantum system, we define the quantum speed limit $\tau_{QSL}$ for a number of conditions as the minimum final time $t_f$ for which there exists a control $\tilde{u}$ such that the evolution operator $\hat{U}_{\tilde{u}}(t_f)$ meets the target conditions. For a numerical approximation of the quantum speed limit with a maximum error of $\epsilon$ we must consider possible evolutions $\hat{U}(t_f)$ for arbitrary final times $t_f$ such that $||\hat{U}(t_f) - \hat{U}_{tgt}||_F \leq \epsilon$. Obtaining the minimum quantum speed limit among all feasible unitary operators that meet the target conditions is the main task of the quantum speed limit estimator for a set of $n_s < N$ target conditions.

## 3.2 Quantum-speed-limit estimator

The current section focuses on describing the method to find the minimal time at which the system's evolution can be implemented for a system with a single control as described by Equation (3.1). Note that in Section 3.1 the quantum speed limits were defined in terms of the shortest time for which a control $u(t)$ could be found such that certain conditions are met. However, the methods here described avoid the explicit calculation of any control function. Instead, combined efforts from numerical computation and algebra analysis provide enough data to compute a value to approximate the quantum speed limit $\tau_{QSL}$.

The main idea behind this estimator is at first glance quite simple. Assume there is a system with a drift $\hat{H}_0$ and a unitary evolution $\hat{U} := \exp(-i\hat{H}_{eff}t_1)$ whose quantum speed limit has to be determined. Here $t_1$ represents a unit of time in the chosen arbitrary units. Let $i\hat{H}_0$ and the implicitly defined effective Hamiltonian $i\hat{H}_{eff}$ be parallel vectors in the vector space of the Lie algebra $\mathfrak{u}(n)$. Then the evolution $\hat{U}$

can also be implemented as the rotation $\exp(-it_r\hat{H}_0)$ where $t_r$ is defined as the ratio between the two vector norms

$$t_r := \frac{\|\hat{H}_{eff}\|}{\|\hat{H}_0\|}t_1. \tag{3.5}$$

The coefficient $t_r$ is not only related to the angle of the rotation, but it also represents the time estimation that the system would have to evolve around its natural drift to produce the evolution $\hat{U}$. Similar to $\hbar$, $t_1$ will be omitted and implied henceforth.

Given any unitary matrix, the effective Hamiltonian can be calculated as $i\hat{H}_{eff} = -\log(\hat{U})$. The matrix logarithm is always well defined for unitary operators since they have a bounded, nonzero spectrum [50]. While the logarithm function is in general not uniquely defined, an injective function can be defined by choosing the principal branch of the logarithm [113]. This technique is used in different computational packages, including the *scipy* Python package [114] that will be used throughout this chapter.

The main problem, however, is that the hypothesis of having $i\hat{H}_{eff}$ parallel to the vector $i\hat{H}_0$ is not true in the general case. The following subsection explores how to get a vector from the dynamical Lie algebra that is parallel to the desired matrix logarithm $i\hat{H}_{eff}$ and whose norm carries the physical meaning of the quantum speed limit.

### 3.2.1 Partition of the dynamical Lie algebra

In Chapter 2 we have seen how it is sufficient for the dynamical Lie algebra to span $\mathfrak{su}(n)$ for the system to be operator controllable. Here, we make a qualitative categorization of all different dimensions of the vector space of the Lie algebra depending on how quickly the system can evolve along them. Indeed, in the general case not all directions in $\mathfrak{su}(n)$ can be followed with the same speed. It is vastly different to produce an evolution that is mostly generated by the control of a quantum system than implementing an operation that requires the system to evolve using the time-independent drift for a set amount of time. This subsection presents a Lie algebra partition split into three different vector subspaces: fast directions, slow directions and very slow directions.

We start with the system described in Equation (3.1) using traceless operators $\hat{H}_0$ and $\hat{H}_1$, which is assumed to have Hilbert space dimension $\dim(\mathcal{H}) = n$ and to be operator controllable. Without loss of generality one can also assume that $\hat{H}_0$ is

orthogonal to $\hat{H}_1$[1]. Evidently, evolutions along the $-i\hat{H}_1$ direction in the Lie algebra can be implemented in arbitrarily short times, as previously discussed. We call this a *fast direction* and we denote the corresponding subspace as $\mathcal{F}$.

On the other hand, evolutions $\exp(-i\hat{H}_0 t)$ following the direction given by the drift $-i\hat{H}_0$ cannot be sped up. They are subject to the natural speed at which the drift evolves the system. Equation (3.5) has already shown how the norm of the drift $\|\hat{H}_0\|$ can be linked to how fast these directions can be followed. The minimal time that the system must evolve using the drift imposes the quantum speed limit associated to given unitary operation. Similarly any evolution that can be decomposed into a sequence $e^{-i\hat{H}_1 t_1} e^{-i\hat{H}_0 t_2} e^{+i\hat{H}_0 t_1}$ only has the central evolution $e^{-i\hat{H}_0 t_2}$ as a real contribution to the quantum speed limit. This sequence follows $e^{-i\hat{H}_1 t_1}(-i\hat{H}_0)e^{+i\hat{H}_1 t_1}$ as a direction in the Lie algebra at the same speed. Coincidentally, $\|\hat{H}_0\| = \|e^{-i\hat{H}_1 t_1}(-i\hat{H}_0)e^{+i\hat{H}_1 t_1}\|$. From a physical point of view, the sequence implements an arbitrarily fast pulse using the control, an evolution along the drift for a certain amount of time $t_2$ and the opposite to the first implemented pulse. This opens up a new set of directions that evolve with the same speed as $\hat{H}_0$. The directions encompassed in the set $\{e^{-i\hat{H}_0 v}(-i\hat{H}_0)e^{+i\hat{H}_0 v}\}_{v\in\mathbb{R}}$ are named *slow directions* with a corresponding spanned subspace $\mathcal{S}$. Note that the evolutions that are defined by the set of slow directions are reminiscent of the bang-off-bang pulses that have been used in certain cases to obtain the quantum speed limit [115]. Indeed the evolutions in the sequence $e^{-i\hat{H}_1 t_1} e^{-i\hat{H}_0 t_2} e^{+i\hat{H}_0 t_1}$ represent a first and a final step $e^{\pm i\hat{H}_0 t_1}$ where the control is turned on for a certain amount of time (depending on the maximum available amplitude) and a middle evolution $e^{-i\hat{H}_0}$ where the control is turned off. This is a useful piece of information, as it connects evolutions along the slow directions in the Lie algebra to the exact control pulses that can implement them.

Without loss of generality, we assume any single control operator $\hat{H}_1$ in a finite-dimensional system to be diagonal in virtue of the spectral theorem [116]. As a second hypothesis, we assume the drift $\hat{H}_0$ to be completely off-diagonal, i.e. with all elements in the main diagonal equal to zero. The use of this convention will be useful both for visualising the geometric picture presented below and for comparing results with previous work. The latter assumption is not true in the general case. Nevertheless, it serves as a starting point for the study that simplifies calculations. The results here presented could in principle be extended to the case where $\hat{H}_0$ is

[1]Indeed if that was not the case, one can use the decomposition $\hat{H}_0 = \hat{H}_0^{\perp} + \hat{H}_0^{\parallel}$, where $\hat{H}_0^{\perp}$ (respectively $\hat{H}_0^{\parallel}$) is the contribution that is perpendicular (respectively proportional) to $\hat{H}_1$. Any dynamical contribution by the $\hat{H}_0^{\parallel}$ term can be effectively countered by the control operator $\hat{H}_1$. Thus, if $\hat{H}_0 \not\perp \hat{H}_1$ we can redefine the system as having a Hamiltonian

$$\hat{H}(t) = \hat{H}_0^{\perp} + u'(t)\hat{H}_1, \qquad \text{with } u'(t) := u(t) + \frac{Tr\left(\hat{H}_0\hat{H}_1\right)}{Tr\left(\hat{H}_1^2\right)}. \tag{3.6}$$

not off-diagonal, accounting for the overlap between $\hat{H}_0$ and $\hat{H}_1$. The off-diagonal hypothesis, however, also ensures that the operators $i\hat{H}_0$ and $i\hat{H}_1$ are orthogonal vectors in the Lie algebra space.

A simple example to showcase the partition of the generated Lie algebra is the one-qubit system described by the Hamiltonian

$$\hat{H}_{1q}(t) = \frac{\omega}{2}\hat{\sigma}_x + u(t)\hat{\sigma}_z. \tag{3.7}$$

Note that the control is a diagonal contribution whereas the drift is an off-diagonal operator. Here the space of fast directions is $\mathcal{F}_{1q} = span\{i\hat{\sigma}_z\}$. It contains all diagonal operators of $\mathfrak{su}(2)$ and gives control over all local phases on the system. The space of slow directions is given by

$$\mathcal{S}_{1q} = \textit{span}\left(\left\{-i\frac{\omega}{2}\left(\cos(\theta)\hat{\sigma}_x + \sin(\theta)\hat{\sigma}_y\right) \mid \theta \in [0, 2\pi]\right\}\right) = \textit{span}\left(i\hat{\sigma}_x, i\hat{\sigma}_y\right). \tag{3.8}$$

Therefore, in this case $\mathfrak{su}(2) = \mathcal{F}_{1q} \oplus \mathcal{S}_{1q}$. This implies that we can decompose the effective Hamiltonian $i\hat{H}_{eff}$ of any single-qubit unitary operation into diagonal contributions (fast directions) and off-diagonal contributions (slow directions) that dictate the quantum speed limit of the system.

Depending on the system, this decomposition into just fast and slow directions is not always possible. There are certain scenarios where the system is operator controllable, yet $\mathcal{F} \oplus \mathcal{S} \subsetneq \mathfrak{su}(n)$. What happens to the dimensions that do not belong to either $\mathcal{F}$ or $\mathcal{S}$? Operator controllability ensures that the remaining terms in the algebra will be generated via commutators (or linear combinations thereof). Physically, there may be unitary gates that cannot be implemented solely by doing a fast rotation around the control operator $\hat{R}_{\hat{H}_1}(\theta)$, letting the system evolve along its natural drift ($\exp(-i\hat{H}_0\, t)$) and implementing the opposite fast rotation around the control operator $\hat{R}_{\hat{H}_1}(-\theta)$. The elements not contained in the slow and fast directions have to be generated with commutators of depth greater or equal than 2. It is still necessary to understand how fast the system can follow any direction related to the projection of $-i\hat{H}_{eff}$ onto the subspace $\mathcal{V} := \mathfrak{su}(n)$
$(\mathcal{F} \oplus \mathcal{S})$. However, implementing a unitary evolution $\exp(-i\hat{V}t)$ with $-i\hat{V} \in \mathcal{V}$ for a time $0 \leq t \leq t_f$ is extremely demanding, as it requires alternating infinitesimal rotations $\exp(-i\hat{H}^{\mathcal{F}}_{eff,j})$ and $\exp(-i\hat{H}^{\mathcal{S}}_{eff,j})$ around directions $-i\hat{H}^{\mathcal{F}}_{eff,j}$ and $-i\hat{H}^{\mathcal{S}}_{eff,j}$ included in the subspaces of fast and slow directions, respectively. This is experimentally very costly to be feasible. For this reason, the directions included in the newly defined subspace $\mathcal{V}$ are called *very slow directions*.

The total partition of the dynamical Lie algebra of the system is thus defined by the following subspaces:

- Subspace of fast directions $\mathcal{F}$: defined by the vector space of directions determined by the control operator $i\hat{H}_1$.

- Subspace of slow directions $\mathcal{S}$: given by the linear span of elements $e^{-i\hat{H}_1 t_1}(-i\hat{H}_0)e^{+i\hat{H}_1 t_1}$.

- Subspace of very slow directions $\mathcal{V}$: defined as $\mathcal{V} := \mathfrak{su}(n)\backslash(\mathcal{F} \oplus \mathcal{S})$.

If an effective Hamiltonian cannot be expressed as a linear combination of elements of the fast and slow directions, then there is no straightforward method to estimate a quantum speed limit, as the ratio $t_r$ from Equation (3.5) no longer provides a physically meaningful result. It is for this reason that given an evolution $\exp(-i\,\hat{H}^{(\mathcal{V})})$ with $\hat{H}^{(\mathcal{V})} \in \mathcal{V}$, it is more practical to approximate it as a product

$$e^{-i\,\hat{H}^{(\mathcal{V})}} \simeq \prod_{j=0}^{k} e^{-i\,\hat{A}_j^{(\mathcal{S})}}, \tag{3.9}$$

with $i\,\hat{A}_j^{(\mathcal{S})} \in \mathcal{S}$ for every $0 \leq j \leq k$. We call this a decomposition of the gate. Note that this is a mere approximation which can be arbitrarily precise depending on the number of gates included in the sequence. Given a decomposition of a unitary evolution $\hat{U} = e^{-i\hat{B}_0}e^{-i\hat{B}_1}\cdots e^{-i\hat{B}_k}$ with $-i\hat{B}_j \in \mathcal{F} + \mathcal{S}$ for every $0 \leq j \leq k$, the sum of all the quantum speed limits of $e^{-i\hat{B}_k}$ serves as an upper bound to the quantum speed limit of $\hat{U}$. This is the core idea of the study for the cases where $\mathcal{V} \neq \mathbf{0}$.

### 3.2.2 The available velocity polytope

In Equation (3.3) we saw the curve $\gamma_{\hat{H}_1}(\alpha)$ of unitary gates that can be approximated arbitrarily fast. With this in mind, given an arbitrary state $|\psi(t)\rangle$ evolving under Equation (3.1), we define the state

$$|\tilde{\psi}(t)\rangle := e^{i\int_0^t u(\tau)\hat{H}_1\,d\tau}\,|\psi(t)\rangle\,. \tag{3.10}$$

Note that the states $|\tilde{\psi}(t)\rangle$ and $|\psi(t)\rangle$ are connected through a gate in the instantaneous curve $\gamma_{\hat{H}_1}(\alpha)$, i.e. we can evolve from one to another with the implementation of a gate that can be achieved arbitrarily fast. Assuming that the state $|\psi(t)\rangle$ evolves according to Equation (3.1), we can derive the dynamic equation of $|\tilde{\psi}(t)\rangle$ as

$$\frac{d}{dt}\,|\tilde{\psi}(t)\rangle = e^{i\int_0^t u(\tau)\hat{H}_1\,d\tau}\left(-i\hat{H}_0\right)e^{-i\int_0^t u(\tau)\hat{H}_1\,d\tau}\,|\tilde{\psi}(t)\rangle\,. \tag{3.11}$$

where $u(t)$ is the control function defined in Equation (3.1). Assuming that the control operator $\hat{H}_1$ is time independent, it can be taken out of the integral of Equation (3.11). The remaining integral $v = \int_0^{t_f} u(t)\,dt$ can take any value $v \in \mathbb{R}$ by varying shape of the control $u(t)$ and the final time $t_f$. Comparing Equation (3.11) with the

Schrödinger equation, the term preceding the ket on the right-hand side represents an effective Hamiltonian $\exp(i\,v\hat{H}_1)\hat{H}_0\exp(-i\,v\hat{H}_1)$. From a physical point of view, this simply represents the state $|\tilde{\psi}(t)\rangle$ evolving under the drift $\hat{H}_0$ between two (arbitrarily fast) rotations around the control operator $\hat{H}_1$. The effective Hamiltonian $\hat{H}_v$ of the evolution can be written as

$$\hat{H}_v := i\mathrm{Ad}_{e^{iv\hat{H}_1}}(-i\hat{H}_0) \tag{3.12}$$

with the adjoint map [52]

$$\begin{array}{rccc} \mathrm{Ad}_{\hat{U}}: & \mathfrak{gl}(n,\mathbb{C}) & \to & \mathfrak{gl}(n,\mathbb{C}) \\ & \hat{A} & \mapsto & \hat{U}\hat{A}\hat{U}^{-1}, \end{array} \tag{3.13}$$

where $\hat{U} \in U(n)$. It is immediate to see that if $\hat{A}$ is a (skew-)Hermitian operator, then $\mathrm{Ad}_{\hat{U}}(\hat{A})$ is also a (skew-)Hermitian operator. If $[\hat{H}_0, \exp(i\,v\hat{H}_1)] \neq 0$, the skew-Hermitian operators $-i\hat{H}_0$ and $-i\hat{H}_v$ are different vectors in the dynamical Lie algebra $\mathcal{L} \subseteq \mathfrak{su}(n)$ of the system. By definition, all $-i\hat{H}_v$ are classified as slow directions in the Lie algebra partition presented in the previous subsection.

By varying all the different values that the parameter $v$ can take in Equation (3.12), we can create a set of possible directions in the dynamical Lie algebra. This expands the number of possible vectors that are used to determine the quantum speed limit using the estimation shown in Equation (3.5). Given a unitary evolution $\hat{U} = \exp(-i\hat{H}_{eff})$, if the implicitly defined effective Hamiltonian $i\hat{H}_{eff}$ is parallel to a vector in the set $\{i\hat{H}_v\}_{v\in\mathbb{R}}$, the quantum speed limit of said evolution has an upper bound in $\|\hat{H}_{eff}\|/\|\hat{H}_v\|$.

However, the uncountable set $\{i\hat{H}_v\}_{v\in\mathbb{R}}$ cannot be computed in the general case. Note that this set is not a vector space and therefore it is not possible to compute a basis to define it, as it is done for Hilbert spaces or Lie algebras. Its approximation is given by the inclusion of a sufficiently large set of vectors $-i\hat{H}_v$. To atone for this, we can find an approximation of $\{i\hat{H}_v\}_{v\in\mathbb{R}}$ by considering linear combinations of these elements. Indeed, the Trotter product formula (also called the Lie product formula) states that

$$\lim_{l\to\infty}\left(e^{-i\frac{\tau}{l}\hat{P}}e^{-i\frac{\tau}{l}\hat{Q}}\right)^l = e^{-i\,\tau(\hat{P}+\hat{Q})}. \tag{3.14}$$

for any pair of complex $n \times n$ matrices $P$, $Q$ [117]. In other words, if the operators $i\hat{P}$ and $i\hat{Q}$ belong to the dynamical Lie algebra of the system, then so does $i\hat{P} + i\hat{Q}$. This is not surprising, as the vector space structure of the dynamical Lie algebra mathematically ensures the same property. An important question, however, is how fast the unitary evolutions displayed in the Trotter product formula can be implemented. Let us assume that $\hat{P}$ and $\hat{Q}$ represent two different $\hat{H}_v$ Hamiltonians as defined in Equation (3.12). An operation $\exp(-i\frac{\tau}{l}\hat{P})$ can be performed in an approximated time

$t = \tau/l$. The total time required to implement the $l$ operations in the left-hand side of Equation (3.12) is

$$t = \lim_{l\to\infty} \sum_{j=1}^{l} \left( \frac{\tau}{l} + \frac{\tau}{l} \right) = 2\tau. \tag{3.15}$$

Therefore the time required to implement $\exp(-i\,\tau(\hat{P}+\hat{Q}))$ is also $2\tau$. For the purpose of estimating the required time for a quantum gate, it makes sense to rewrite the Trotter product formula as

$$\lim_{l\to\infty} \left( e^{-i\,\frac{\lambda_1\tau_1}{l}\hat{P}} e^{-i\,\frac{\lambda_2\tau_2}{l}\hat{Q}} \right)^l = e^{-i\,(\lambda_1\tau_1\hat{P}+\lambda_2\tau_2\hat{Q})}, \qquad \forall\lambda_1,\lambda_2 \geq 0 \text{ and } \lambda_1+\lambda_2 = 1. \tag{3.16}$$

Note that $\lambda_1\hat{P} + \lambda_2\hat{Q}$ is by definition the convex combination of the algebra elements $\hat{P}$ and $\hat{Q}$. Equation (3.16) shows that, if there are two rotations $e^{-i\,\tau_1\hat{P}}$ and $e^{-i\,\tau_2\hat{Q}}$ that can be implemented in times $t = \tau_1$ and $t = \tau_2$ respectively, then the rotation $e^{-i\,(\lambda_1\tau_1\hat{P}+\lambda_2\tau_2\hat{Q})}$ around the direction given by the operator $\lambda_1\hat{P} + \lambda_2\hat{Q}$ can be implemented in time $t = \lambda_1\tau_1 + \lambda_2\tau_2$. If $\tau_1 = \tau_2 =: \tau$ , then any convex combination $\lambda_1\hat{P} + \lambda_2\hat{Q}$ has the same associated expected time $\tau$. Note that in certain cases it could be true that the operation $e^{-i\,(\lambda_1\tau\hat{P}+\lambda_2\tau\hat{Q})}$ may be implemented in a time shorter than $\tau$. However, $\tau$ stills remain as an upper bound for the quantum speed limit of said unitary evolution, thus being a useful data point for its estimation.

We define the available velocity polytope as the set including all elements of $\{\hat{H}_v\}_{v\in\mathbb{R}}$ and their convex combinations, i.e.

$$AvVel\left(\hat{H}_0, \hat{H}_1\right) := \text{conv}\left\{ \text{Ad}_{\exp(v\hat{H}_1)}(-i\hat{H}_0) \,|\, \forall v \in \mathbb{R} \right\}. \tag{3.17}$$

Note that the conv$(A)$ operation represents the convex hull of a set $A$. The convex hull and its computation method will be explained in depth in Section 3.2.3. Since we have chosen $\hat{H}_0$ and $\hat{H}_1$ to be orthogonal, every element $-i\hat{H}_v \in AvVel(\hat{H}_0, \hat{H}_1)$ is also orthogonal to $-i\hat{H}_1$. This can be easily proven using the fact that $Tr(e^{v\hat{H}_1}\hat{H}_0 e^{-v\hat{H}_1}\hat{H}_1) = Tr(\hat{H}_0\hat{H}_1)$.

It is still necessary to determine which vector from $AvVel(\hat{H}_0, \hat{H}_1)$ is the right one to compute the quantum speed limit of an effective Hamiltonian $\hat{H}_{eff}$. To do so, we define the geometric ray

$$r_{\hat{H}_{eff}} := \{-\alpha\, i\hat{H}_{eff} \,|\, \alpha \geq 0\} \tag{3.18}$$

that contains all operators that are in the same single direction in the vector space of the associated Lie algebra. Then the right operator to estimate the quantum speed limit is defined as the intersection

$$\hat{H}_{\cap} := r_{\hat{H}_{eff}} \cap \partial AvVel\left(\hat{H}_0, \hat{H}_1\right) \tag{3.19}$$

where $\partial AvVel(\hat{H}_0, \hat{H}_1)$ represents the boundary of the available velocity polytope. If the intersection $\hat{H}_{\cap}$ exists (see more in Section 3.2.1), then it is unique, as $r_{\hat{H}_{eff}}$ is a ray starting at the coordinate origin, which is contained in the convex set $AvVel(\hat{H}_0, \hat{H}_1)$. Therefore, given a quantum system evolving under a Hamiltonian (3.1) and a unitary evolution $\hat{U}$ with an effective Hamiltonian $\hat{H}_{eff} = i\,\log(\hat{U})$, the quantum speed limit of $\hat{U}$ in the system can be estimated as

$$\tau_{QSL} = \frac{\|\hat{H}_{eff}\|}{\|\hat{H}_{\cap}\|}, \tag{3.20}$$

where $\|\cdot\|$ represents the norm of the operators in the vector space of the Lie algebra. Section 3.2.3 explains more in detail how to compute the intersection point $\hat{H}_{\cap}$ needed for this estimation. The exact value of $\tau_{QSL}$ serves as a (possibly tight) upper bound to the quantum speed limit that is imposed by Heisenberg's uncertainty principle. There are some cases where this estimation can be significantly improved as shown in Section 3.3.3.

### 3.2.3 Geometry and computation of convex sets

Previously we have used convex combinations $\lambda_1 P + \lambda_2 Q$ of two points $P$ and $Q$ with positive coefficients $\lambda_1 + \lambda_2 = 1$ for elements in a Lie algebra. Given a set $\mathcal{A}$ of points contained in an affine space, the convex hull conv($\mathcal{A}$) is the minimal set that contains $\mathcal{A}$ and all its convex combinations. It includes every combination $\sum_{i=1}^{N_p} \lambda_i P_i$ of any finite number $N_p$ of points $P_i \in \mathcal{A}$ with positive weights $\lambda_i$, such that $\sum_{i=1}^{N_p} \lambda_i = 1$. As a visual example, Figure 3.2 shows the convex hull of an arbitrary set of points in a plane.

Finding the exact $AvVel(\hat{H}_0, \hat{H}_1)$ required for the quantum speed limit estimation is a difficult task. However, one can find an approximation to the available velocity polytope by generating a sufficiently large set of points $\mathrm{Ad}_{\exp(v\hat{H}_1)}(\hat{H}_0)$ and then computing its convex hull. This method essentially creates a polygon mesh of the exact $AvVel(\hat{H}_0, \hat{H}_1)$ whose resolution depends on the number of initial points and their distribution along the polytope. If the resolution is high enough, the intersection $\hat{H}_{\cap}$ from Equation (3.19) should be close to the original value. In turn, $\tau_{QSL}$ should also be a good approximation. Let $\hat{H}_{\cap}^{approx}$ be an intersection point found via an approximation of the available velocity polytope and $\hat{H}_{\cap}^{ex}$ the exact intersection point. The polygon mesh is by definition contained in the exact $AvVel(\hat{H}_0, \hat{H}_1)$, which

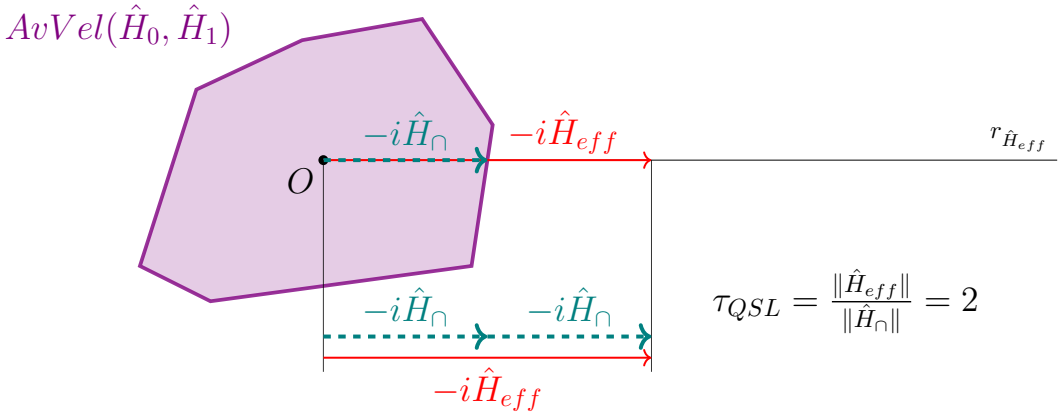


**Figure 3.1:** Two-dimensional visualization of the quantum speed limit estimation given by Equation (3.20) for a system with Hamiltonian (3.1) and a unitary operator $\hat{U} := \exp(-i\hat{H}_{eff})$. The geometrical representation shows the affine space defined by the Lie algebra vector space. The effective Hamiltonian $-i\hat{H}_{eff}$ represents the velocity at which the system has to evolve for $t = 1$ units of time (in arbitrary units) in order to achieve the evolution $\hat{U}$. The violet polygon represents the available velocity $AvVel(\hat{H}_0, \hat{H}_1)$ of the system. The points in the border of $AvVel(\hat{H}_0, \hat{H}_1)$ represent the different velocities under which the system can evolve under the Hamiltonian (3.1). The ray $r_{\hat{H}_{eff}}$ is given by the vector $-i\hat{H}_{eff}$ starting at the origin $O$. The vector $-i\hat{H}_\cap$ is defined as the vector extending from $O$ to the intersection between the ray $r_{\hat{H}_{eff}}$ and the border of $AvVel(\hat{H}_0, \hat{H}_1)$. In this visual example, $-i\hat{H}_{eff}$ is twice as long as $-i\hat{H}_\cap$. As the system can evolve under $-i\hat{H}_\cap$, it evolves with half the speed dictated by $-i\hat{H}_{eff}$. In other words, it takes double the time to produce the evolution $\hat{U}$, i.e. the quantum speed limit estimation is $\tau_{QSL} = 2$.

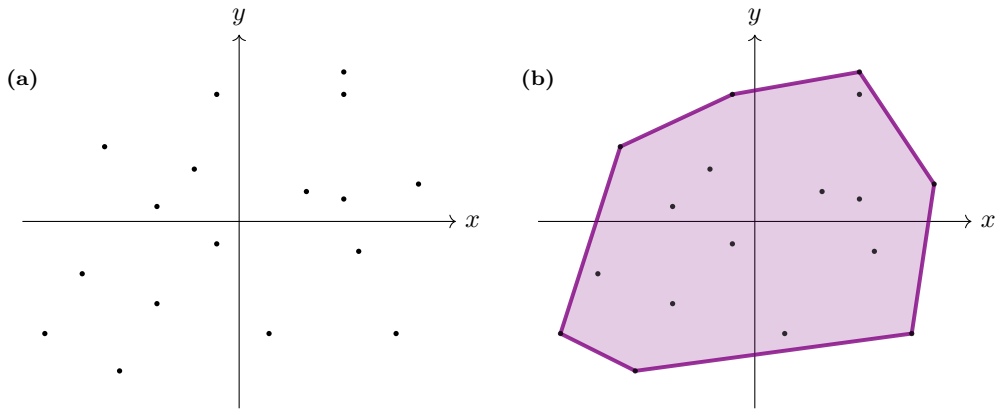


**Figure 3.2:** Visual representation of a convex hull. (a) Set of points $\mathcal{A}$ in the two-dimensional plane. (b) Convex hull of the previous set conv($\mathcal{A}$), represented by the coloured area and outline. The border $\partial$conv($\mathcal{A}$) is given by the set of outer points and the hyperplanes (lines for the current two-dimensional case) that define the facets or simplices of the polytope (i.e. sides of a polygon here).

implies that $\|\hat{H}_{\cap}^{ex}\| \geq \|\hat{H}_{\cap}^{approx}\|$. Thus the associated quantum speed limit estimations fulfill $\tau_{QSL}^{ex} \leq \tau_{QSL}^{approx}$, meaning that the approximated estimation is a valid albeit perhaps looser upper bound to the exact limit.

Computing the convex hull of a set of points in an $k$-dimensional affine space requires heavy calculations. Fortunately, there are specialized tools for this purpose. *Quickhull* is one of the algorithms written to tackle such problem [118]. It takes a set of points in an $k$-dimensional space and returns a list of the different facets that form the border of the convex hull. Each $(k-1)$-dimensional facet is defined by a list of its $k$ vertices, which are points from the initial set. According to this definition, the facets are simplices, i.e. the simplest convex $(k-1)$-dimensional shape that can be described using $k$ points. This includes segments in one dimension, triangles for two dimensions, irregular tetrahedrons for three dimensions, etc.

There exist multiple open-source implementations of this algorithm like the *Qhull* implementation on C++ [119] and its Python wrapper *pyhull* [120]. The latter was used to perform every calculation requiring a convex hull in this project. The Qhull library was later included in the scipy.spatial package under the name ConvexHull [114], making it more accessible to some Python installations.

Calculating the intersection Hamiltonian $\hat{H}_{\cap}$ defined in Equation (3.19) is a priori a simple numerical task that can nevertheless take up some computational time, depending on the resolution of the available velocity polytope (i.e. number of simplices). Algorithm 3.1 presents, in simple pseudocode, the necessary steps to determine $\hat{H}_{\cap}$ when using an available velocity polytope computed via Qhull. Note that this method becomes increasingly more demanding depending on the dimension of the vector

**Algorithm 3.1:** Compute the intersection between the available velocity polytope and a ray pointing in a given direction.

Input:
- **AvVel(**$\hat{H}_0$**,** $\hat{H}_1$**)**: available velocity polytope as a list containing all the simplices defined by their vertices.
- $\hat{\mathbf{H}}_\mathbf{0}, \hat{\mathbf{H}}_\mathbf{1}$: drift and control operators.
- $\hat{\mathbf{H}}_{\mathbf{eff}}$: effective Hamiltonian that generates some unitary evolution.

**for** *every simplex_j in AvVel(*$\hat{H}_0$*,* $\hat{H}_1$*)* **do**
  Get equations that define the hyperplane $\pi_j$ containing *simplex_j*.
  **if** *the hyperplane* $\pi_j$ *has an intersection* $-i\hat{H}_\cap$ *with the ray* $\{-\alpha i \hat{H}_{eff} \,|\, (\alpha \geq 0)\}$ **then**
    **if** $-i\hat{H}_\cap$ *is contained in simplex_j* **then**
      Exit outer **for** loop and return $\hat{H}_\cap$
    **end if**
  **end if**
**end for**

Output:
- $\hat{\mathbf{H}}_\cap$: operator related to the the intersection point between the direction given by the effective Hamiltonian and the border of the available velocity polytope.

space (i.e. the group $\mathfrak{su}(n)$). In turn, the vector space dimension increases exponentially with the number of qubits, making this process a challenging one for large systems.

While the goal of this study was to study elements in Lie algebras, the Qhull algorithm poses a significant challenge: Its original implementation is in principle only intended for spaces with dimension up to 8. Computations in higher-dimensional spaces are possible although they are not guaranteed to succeed due to memory requirements. Data was calculated exceeding this eight-dimensional mark, but it significantly hindered the capability of the study here presented. As a possible solution, there exists an alternative that bypasses the use of a convex hull algorithm by including certain hypotheses over the system. The alternative method is presented and explained in Section 3.2.4.

### 3.2.4 Alternative approximations of the available velocity polytope

Section 3.2.3 covered the topic of how to compute the available velocity polytope using *quickhull*. This method stops being useful at a very low number of qubits. Indeed, since the dimension of the Lie algebra scales exponentially with the number of qubits, this tool already faces problems even with arrays of only three qubits, where $\dim(\mathfrak{su}(2^3)) = 63$. There are alternatives that can be used to provide a slightly worse albeit more applicable approximation. The core idea is to approximate the available velocity polytope by an analytical hypersurface contained in $AvVel(\hat{H}_0, \hat{H}_1)$ that can

be used to calculate the intersection $-i\hat{H}_{\cap}$ needed for the estimation of the quantum speed limit described in Equation (3.20). Ideally, this hypersurface should be as close as possible to the border of $AvVel(\hat{H}_0, \hat{H}_1)$ so that the approximated intersection $-i\hat{H}_{\cap}$ is as close as possible to the exact one. This can be achieved under certain assumptions that are presented below.

To this end, we introduce the concept of rationally independent real values. A set of real values $\{a_1, a_2, \ldots, a_N\}$ is said to be *rationally independent* if for any rational coefficients $k_1, k_2, \cdots, k_N$ the following condition holds true:

$$k_1 a_1 + k_1 a_1 + \cdots + k_N a_N \qquad \Rightarrow \qquad k_j = 0, \quad 1 \leq j \leq N. \tag{3.21}$$

This ensures that every ratio $a_j/a_k$ is an irrational number. Now let $\{\lambda_j\}_{j=0}^{(n-1)} \subset \mathbb{R}$ be the spectrum of the control operator $\hat{H}_1$. Let us assume that every pair of elements in the set $\{\frac{\lambda_j}{2\pi}\}_{j=0}^{(n-1)} \subset \mathbb{R}$ is rationally independent. In this case, the Lie group of all arbitrarily fast operators $e^{\mathcal{F}}$ is

$$e^{\mathcal{F}} = \left\{ \text{diag}\left(e^{-i\lambda_0 w}, e^{-i\lambda_1 w}, \cdots, e^{-i\lambda_{n_1} w}\right) \mid w \in \mathbb{R} \right\}, \tag{3.22}$$

where $\text{diag}(\vec{v})$ represents a diagonal matrix with the nonzero coefficients given by $\vec{v}$. Given that the eigenvalues $\lambda_j$ modulo $2\pi$ are pairwise rationally independent, the exponentials $e^{i\lambda_j w}$ do not have any common period for $w$. In other words, their phases only synchronise when $w = 0$. This irrational vector represents a line along the compact $n$-dimensional torus $\mathbb{T}^n$ (isomorphic to the space of diagonal unitary matrices). This line can approximate any point up to arbitrary precision. From a physical point of view, this means that if the eigenvalues of the control Hamiltonian modulo $2\pi$ are pairwise rationally independent, then we can approximate any diagonal unitary operator up to arbitrary precision at an arbitrary short time, i.e.

$$e^{\mathcal{F}} \approx \mathbb{T}^n. \tag{3.23}$$

Note that the symbol $\approx$ is here used to represent numerical approximation and not a homeomorphism. For every diagonal unitary operator $\hat{D}$ and error $\epsilon > 0$ there exists a coefficient $w \in \mathbb{R}^+$ such that $\|\hat{D}^\dagger e^{-i\hat{H}_1 w} - \mathbb{1}\| < \epsilon$. Furthermore, Equation (3.23) implies that all local phases of the states in the eigenbasis can be adjusted arbitrarily fast.

Since the drift is assumed to be off-diagonal, we can write its matrix representation as

$$\hat{H}_0 = \begin{pmatrix} 0 & a_{01} & a_{02} & \cdots \\ \overline{a}_{01} & 0 & a_{12} & \cdots \\ \overline{a}_{02} & \overline{a}_{12} & 0 & \cdots \\ \vdots & \vdots & \vdots & \ddots \end{pmatrix} = \sum_{\substack{j,k=0 \\ j<k}}^{n-1} (a_{j,k}\hat{e}_{j,k} + \overline{a}_{j,k}\hat{e}_{k,j}) \tag{3.24}$$

where $\hat{e}_{j,k}$ is the null matrix except for a 1 in the entry $(j,k)$. If Equation (3.23) holds, then for every nonzero entry $a_{j,k}$, one can prove that $e^{i\theta}|a_{j,k}|\hat{e}_{j,k} - e^{-i\theta}|a_{j,k}|\hat{e}_{k,j} \in AvVel(\hat{H}_0, \hat{H}_1)$ for every phase $\theta \in [0, 2\pi)$. Note that this element of the available velocity polytope may not belong to the border, but be an inner point instead. In other words, it is a lower bound for the value that the available velocity can take in the direction that the vector represents. Using Equation (3.20), this lower bound of the available velocity can be used as a substitute to $\hat{H}_\cap$ to find an upper bound to the quantum speed limit for unitary operators $\hat{U}$ whose effective Hamiltonians $-i\hat{H}_{eff} = \log(\hat{U})$ are parallel to the direction given by $e^{i\theta}|a_{j,k}|\hat{e}_{j,k} - e^{-i\theta}|a_{j,k}|\hat{e}_{k,j}$. Including only these elements, we define a subset of the available velocity,

$$AvVel_{approx}\left(\hat{H}_0, \hat{H}_1\right) \subset AvVel\left(\hat{H}_0, \hat{H}_1\right), \tag{3.25}$$

where

$$\begin{aligned} AvVel_{approx}\left(\hat{H}_0, \hat{H}_1\right) := conv\Big(\{e^{i\theta}|a_{j,k}|\hat{e}_{j,k} - e^{-i\theta}|a_{j,k}|\hat{e}_{k,j} \quad \Big| \\ \theta \in [0, 2\pi),\, 0 \leq j < k \leq n-1\}\Big). \end{aligned} \tag{3.26}$$

The purpose of $AvVel_{approx}\left(\hat{H}_0, \hat{H}_1\right)$ as an approximation is to circumvent the use of quickhull or any similar algorithm to compute the convex hull of the available velocity. This approximation holds for any finite dimensional Hilbert space, which is the main limitation of quickhull. The second limitation is the number of vectors $-i\hat{H}_v$ needed to approximate $AvVel(\hat{H}_0, \hat{H}_1)$. A large set of vectors $-i\hat{H}_v$ is needed to accurately generate the available velocity polytope. But this significantly increases the number of faces that define the polytope, making Algorithm 3.1 much slower when computing the intersection $-i\hat{H}_\cap$ between the available velocity polytope and the ray defined by an effective Hamiltonian. The alternative approximation shown in Equation (3.25) avoids Algorithm 3.1 altogether, as shown below. Indeed, every point $i\hat{P}$ belonging to the border of $AvVel_{approx}\left(\hat{H}_0, \hat{H}_1\right)$ can be written as

$$i\hat{P}(\vec{\beta}, \vec{\theta}) := \sum_{\substack{j,k=0 \\ j<k}}^{n-1} \beta_{j,k}\left(e^{i\theta_{j,k}}\|a_{j,k}\|\hat{e}_{j,k} + e^{i\theta_{j,k}}\|a_{j,k}\|\hat{e}_{k,j}\right) \tag{3.27}$$

with the constraints

$$\begin{cases} \sum_{\substack{j,k=0 \\ j<k}}^{n-1} \beta_{j,k} = 1, \\ \beta_{j,k} \geq 0 \quad 0 \leq j < k \leq n-1, \\ \theta_{j,k} \in [0,\, 2\pi) \quad 0 \leq j < k \leq n-1. \end{cases} \tag{3.28}$$

Given a ray defined by an effective Hamiltonian $-i\gamma \hat{H}_{eff}$, the intersection $i\hat{P}(\vec{\beta}, \vec{\theta})$ between the ray and the outer border of the available speed polytope is given by

$$-i\gamma H_{eff,\, j,k}\hat{e}_{j,k} - i\gamma \overline{H}_{eff,\, j,k}\hat{e}_{k,j} \;=\; \beta_{j,k}\left(e^{i\theta_{j,k}}\|a_{j,k}\|\hat{e}_{j,k} + e^{i\theta_{j,k}}\|a_{j,k}\|\hat{e}_{k,j}\right), \tag{3.29}$$

whose solutions are

$$\begin{cases} \gamma \;=\; \sum_{\substack{j,k=0 \\ j<k}}^{n-1} \frac{\|H_{eff,\, j,k}\|}{\|a_{j,k}\|} \\ \beta_{j,k} \;=\; \frac{1}{\gamma}\frac{\|H_{eff,\, j,k}\|}{\|a_{j,k}\|} \qquad 0 \leq j < k \leq n-1, \\ \theta_{j,k} \;=\; \arg(-iH_{eff,\, j,k}) \qquad 0 \leq j < k \leq n-1. \end{cases} \tag{3.30}$$

Following Equation (3.20), an upper bound for the quantum speed limit is given by $\tau_{QSL} = 1/\gamma$. Note that this estimation was found without any numerical computations for the convex hull, simply using the definition of the approximation $AvVel_{approx}\left(\hat{H}_0,\, \hat{H}_1\right)$. This bound will not be tight in most cases. Overcoming the numerical complexity of quickhull comes with this additional cost.

On the other hand, the assumption about the rational independence of the spectrum of the control operator $\hat{H}_1$ does not seem to have a physical meaning behind it. Indeed, mathematically speaking the independence happens with a probability of 1. Physically, the eigenvalues can very well be related by rational ratios. Furthermore, in numerical computations, every float number must be approximated by a rational binary decimal. Therefore there exist physical and computational arguments to not employ the aforementioned approximation as is. However, an alternative approach may be used to arrive to the same destination.

Let us assume now that the spectrum $\sigma(\hat{H}_1)/2\pi$ is not pairwise rationally independent. Suppose that the ratios $\lambda_j/\lambda_k$ of every pair of eigenvalues $\lambda_j, \lambda_k \in \sigma(\hat{H}_1)$ are always rational numbers (for every $\lambda_k \neq 0$). If we further assume nonzero eigenvalues, for every pair $\lambda_j, \lambda_k$ there exist two integers $n_1^{(j,k)}, n_2^{(j,k)} \in \mathbb{Z}$ such that $n_1^{(j,k)}\lambda_j + n_2^{(j,k)}\lambda_k = 0$. If we choose the two coefficients $n_1^{(j,k)}$ and $n_2^{(j,k)}$ with the lowest absolute value, they represent the number of periods that the time-dependent

functions $e^{i\,\lambda_j\,t}$ and $e^{i\,\lambda_k\,t}$ have to traverse to be back in phase. Unlike the rationally independent case given in Equation (3.22), the set

$$e^{-i\hat{H}_1\,\omega} = \left\{ \text{diag}\left( e^{-i\lambda_0\,w},\, e^{-i\lambda_1\,w},\, \cdots,\, e^{-i\lambda_{n_1}\,w} \right) \;|\, w \in \mathbb{R} \right\} \tag{3.31}$$

represents a closed curve that is not dense in the subspace of diagonal unitary matrices. In other words, it is technically not possible to approximate every point in $\mathfrak{u}(n)$ with arbitrary precision. Nevertheless, the larger the minimal absolute values for the coefficients $n_1^{(j,k)}$ and $n_2^{(j,k)}$ are for every pair of indices $j \neq k$, the more coverage the closed curve (3.31) will have on the torus $\mathbb{T}^n$. In other words, the more loops the curve does around the different circumferences in the torus, the better we can approximate any point in the torus by a point from the curve. If $n_1^{(j,k)},\, n_2^{(j,k)} \gg 1$ for every pair $j, k$, then the approximation of the available velocity polytope displayed in Equation (3.25) also holds.

The hypothesis of a large number of independent periods $n_1^{(j,k)},\, n_2^{(j,k)}$ implicitly includes the requirement of a non-degenerate spectrum of $\hat{H}_1$. This is not a new condition, as it was also needed for the case of the set of rationally independent eigenvalues of $\hat{H}_1$. It is, however, a strong requirement that should be checked in both cases. Furthermore, it also implies that all eigenvalues of $\hat{H}_1$ are nonzero. This is in reality a special mathematical case that does not bear any physical meaning. Indeed this can be achieved by fixing a different origin of energies or by shifting the global phase of the unitary operators generated by the Hamiltonian.

As a final note on the approximation of the available velocity polytope, both cases can be combined into a single one: The case where some pairs of eigenvalues are rationally independent and some are rationally dependent. For the approximation in Equation (3.31) to be applicable, one simply must ensure that for every pair of rationally dependent eigenvalues $\lambda_j$ and $\lambda_k$, the coefficients $n_1^{(j,k)}$ and $n_2^{(j,k)}$ with minimal absolute value that make $n_1^{(j,k)}\lambda_j + n_2^{(j,k)}\lambda_k = 0$ fulfill the condition $n_1^{(j,k)},\, n_2^{(j,k)} \gg 1$. If $\lambda_j$ and $\lambda_k$ are rationally independent, then there is no additional condition to be fulfilled. This vastly expands the number of physical examples where this approximation is valid.

### 3.2.5 Parametrization of unitary operators that meet the target conditions

To estimate the quantum speed limit in the case of one target gate $\hat{U}_{tgt}$, we only take into account a single element of $SU(n)$ with $n = \dim(\mathcal{H})$. If we have $n_s < n$ state-to-state transfers instead (or a quantum gate in a subspace for the case of fixed local phases), then the set containing all unitary evolutions that meet the target conditions increases. Here we describe a way of parameterizing the set of all gates that meet some target conditions.

Let us begin with the case of a quantum gate acting on a subspace of the total Hilbert space. Assume that we have a set of target conditions with fixed local phases $\{|\psi_0^{(j)}\rangle \to |\psi_f^{(j)}\rangle\}_{j=0}^{n_s-1}$. Then we can expand the two sets $\{|\psi_0^{(j)}\rangle\}_{j=0}^{n_s-1}$ and $\{|\psi_f^{(j)}\rangle\}_{j=0}^{n_s-1}$ into two complete orthonormal bases $\{|\psi_0^{(j)}\rangle\}_{j=0}^{n-1}$ and $\{|\psi_f^{(j)}\rangle\}_{j=0}^{n-1}$. Since we have $n$ $n$-dimensional vectors we can arrange them as the operators

$$\hat{X}_0 := \left(|\psi_0^{(0)}\rangle \mid |\psi_0^{(1)}\rangle \mid \ldots \mid |\psi_0^{(n-1)}\rangle\right) \tag{3.32}$$

and

$$\hat{X}_f := \left(|\psi_f^{(0)}\rangle \mid |\psi_f^{(1)}\rangle \mid \ldots \mid |\psi_f^{(n-1)}\rangle\right). \tag{3.33}$$

By definition, it is easy to prove that both operators are unitary. In the case where $n_s < n$ we can assume without loss of generality that the matrix representation of $\hat{X}_0$ in the canonical basis of the Hilbert space has determinant $\det(\hat{X}_0) = 1$, i.e. $\hat{X}_0 \in SU(n)$. If not, then $\det(\hat{X}_0) = e^{i\delta} \neq 1$. By changing the last column of $\hat{X}_0$ from the state $|\psi_0^{(n-1)}\rangle$ to $e^{-i\delta}|\psi_0^{(n-1)}\rangle$ we ensure that the determinant of the newly defined matrix $\hat{\tilde{X}}_0$ fulfills $\det(\hat{\tilde{X}}_0) = 1$, i.e. $\hat{\tilde{X}}_0 \in SU(n)$, which physically represents the same states. Likewise we can assume $\hat{X}_f \in SU(n)$. While the first $n_s$ columns of $\hat{X}_{0/f}$ are fixed, the remaining $n - n_s$ remain as a free choice.

So, overall, how many different operators can we define that still meet the target conditions? The unitary operator

$$\hat{U}_{\hat{X}_0 \to \hat{X}_f} := \hat{X}_f \hat{X}_0^\dagger = \sum_{j=0}^{n-1} |\psi_f^{(j)}\rangle \langle\psi_0^{(j)}| \tag{3.34}$$

is included in $SU(n)$ and naturally represents the basis change from $\hat{X}_0$ to $\hat{X}_f$. In Equation (3.34), the elements $|\psi_f^{(j)}\rangle \langle\psi_0^{(k)}|$ with indices $0 \leq j, k \leq n_s - 1$ are fixed by the target conditions. On the other hand, the ones with indices $j \geq n_s$ have been chosen arbitrarily by extending the sets of states in the target conditions into two orthonormal bases $\hat{X}_0$ and $\hat{X}_f$. Different choices for the initial and final bases $\hat{X}_0$ and $\hat{X}_f$ lead to different operators $\hat{U}_{\hat{X}_0 \to \hat{X}_f}$. To encapsulate all possible unitary evolutions that meet the target conditions we define the parameterized unitary operator

$$\hat{U}(\vec{\alpha}) := \hat{U}(\hat{W}) := e^{i\theta} \left( \sum_{p=0}^{n_s-1} |\psi_f^{(p)}\rangle \langle\psi_0^{(p)}| + \sum_{j,k=n_s}^{n-1} W_{j-n_s,k-n_s} |\psi_f^{(j)}\rangle \langle\psi_0^{(k)}| \right) \tag{3.35}$$

where $\hat{W}$ is a complex matrix of size $(n - n_s) \times (n - n_s)$ with entries $W_{j,k}$ and $\theta \in \mathbb{R}$. If we define a parametrization $\hat{W}(\vec{\alpha})$ of the unitary group $U(n - n_s)$, then we can rewrite the previous equation as

$$\hat{U}(\vec{\alpha}) := \hat{U}\left(\hat{W}(\vec{\alpha})\right) \tag{3.36}$$

This parameterization will be relevant to search the group $U(n-n_s)$ and the set of all possible target evolutions by varying the coordinates $\vec{\alpha}$. From the definition in Equation (3.35) one can immediately see that the operator meets the target conditions for any choice of $\hat{W}$, up to a physically irrelevant phase $e^{i\theta}$. Nevertheless, we want to ensure that $\hat{U}(\hat{W}) \in SU(n)$. First, we check the condition for unitarity, which leads to

$$\begin{aligned}\hat{U}(\hat{W})^\dagger \hat{U}(\hat{W}) &= \sum_{p=0}^{n_s-1} |\psi_0^{(p)}\rangle \langle\psi_0^{(p)}| + \sum_{j,k=n_s}^{n-1} \left( \sum_{l=0}^{n_s-1} W^*_{j-n_s,l}\, W_{l,k-n_s} \right) |\psi_0^{(j)}\rangle \langle\psi_0^{(k)}| \\ &\stackrel{!}{=} \mathbb{1}_n. \end{aligned} \tag{3.37}$$

Writing the previous condition in the $\{|\psi_0^{(i)}\rangle\}_i$ basis we come to the equality

$$\left(\begin{array}{c|c} \mathbb{1}_{n_s} & 0 \\ \hline 0 & \hat{W}^\dagger \hat{W} \end{array}\right) \stackrel{!}{=} \mathbb{1}_n, \tag{3.38}$$

which implies that

$$\hat{U}(\hat{W}) \in U(n) \quad \Longleftrightarrow \quad \hat{W} \in U(n-n_s). \tag{3.39}$$

Secondly, imposing the required condition on the determinant leads to

$$\begin{aligned} 1 \stackrel{!}{=} & \det\left(\hat{U}(\hat{W})\right) \\ =& \det\left(\hat{X}_0 \hat{X}_f^\dagger \hat{U}(\hat{W})\right) \\ =& e^{i\,n\theta} \det\left( \sum_{p=0}^{n_s-1} |\psi_0^{(p)}\rangle \langle\psi_0^{(p)}| + \sum_{j,k=n_s}^{n-1} W_{j-n_s,k-n_s}\, |\psi_0^{(j)}\rangle \langle\psi_0^{(k)}| \right) \\ =& e^{i\,n\theta} \det\left(\hat{W}\right), \end{aligned} \tag{3.40}$$

where we have used the fact that $\hat{X}_0,\ \hat{X}_f \in SU(n)$. Therefore, combining both results we arrive to the conclusion

$$\hat{U}(\hat{W}) \in SU(n) \quad \Longleftrightarrow \quad \hat{W} \in U(n-n_s) \quad \text{and} \quad \theta = -\frac{\arg\left(\det(\hat{W})\right)}{n}. \tag{3.41}$$

The dependence on $\theta$ can be lifted once the matrix $\hat{W}$ is defined. This makes $\vec{\alpha} \in \mathbb{R}^{(n-n_s)^2}$ the only variable needed to define $\hat{W}(\vec{\alpha}) \in U(n-n_s)$ and $\hat{U}(\hat{W}(\vec{\alpha}))$. The set

$$\mathcal{G}_{TC} := \left\{ \hat{U} \,|\, \hat{U} \in SU(n),\, \hat{U}\,|\psi_0^{(j)}\rangle = e^{i\varphi}\,|\psi_f^{(j)}\rangle\,,\ \varphi \in \mathbb{R},\, j = 0, 1, ..., n_s - 1 \right\} \tag{3.42}$$

contains all the special unitary matrices that are phase equivalent to unitary operators that meet the target conditions. Note that $G_{TC}$ can also be given the structure of a Lie group albeit not with the standard matrix multiplication. In physical terms, $G_{TC}$

simply represents all the unitary operators that meet the target conditions up to an arbitrary global phase[2].

To estimate the quantum speed limit $\tau_{QSL}$ of a quantum gate acting on a subspace defined as $\{|\psi_0^{(j)}\rangle \to |\psi_f^{(j)}\rangle\}_{j=0}^{n_s-1}$ we can determine the shortest time at which any gate $\hat{U}(\hat{W}) \in \mathcal{G}_{TC}$ can be implemented in our system.

For the case of a set of state transfers without fixed local phases $\{|\psi_0^{(j)}\rangle \to e^{i\varphi_j}|\psi_f^{(j)}\rangle\}_{j=0}^{n_s-1}$, we can repeat the same argumentation, turning Equation (3.35) into

$$\hat{U}(\vec{\alpha}) := \hat{U}(\hat{W},\vec{\varphi}) = e^{-i\frac{\arg\left(\det(\hat{W})\right)}{n}} e^{-i\sum_{l=0}^{n_s}\varphi_l}\left(\sum_{p=0}^{n_s-1} e^{i\varphi_p}|\psi_f^{(p)}\rangle\langle\psi_0^{(p)}| + \sum_{j,k=n_s}^{n-1} W_{j-n_s,k-n_s}|\psi_f^{(j)}\rangle\langle\psi_0^{(k)}|\right) \tag{3.43}$$

with $\vec{\varphi} \in \mathbb{R}^{n_s}$. Here, the vector $\vec{\alpha}$ encompasses a parametrization of both the Lie group $U(n-n_s)$ and the phase space $\mathbb{R}^{n_s}$, which contains all parameters of both $\hat{W}$ and $\vec{\varphi}$ respectively. The exponential $e^{-i\sum_{l=0}^{n_s}\varphi_l}$ comes from imposing the condition $\det(\hat{U}(\vec{\alpha})) = 1$. The new restrictions for the parameters are compiled as

$$\hat{U}(\hat{W},\vec{\varphi}) \in SU(n) \iff \begin{cases} \hat{W} \in U(n-n_s)\,, \\ (\varphi_0,...,\varphi_{n_s-1}) \in [0,2\pi]^{n_s}\,. \end{cases} \tag{3.44}$$

Lifting any restriction on the local phases we get $n_s$ more real variables, which represent the subspace of diagonal operators in $U(n_s)$, $\mathcal{T}^{(n_s)}$. This space represents diagonal complex matrices, whose diagonal entries have absolute value equal to 1. I.e., $\mathcal{T}^{(n_s)} \simeq \mathbb{T}^{(n_s)}$ [3]. The total space of unitaries in the special group that meet the target conditions ${\mathcal{G}_{\mathcal{TC}}}^{loc\,ph}$ is defined as ${\mathcal{G}_{\mathcal{TC}}}^{loc\,ph} := \mathcal{G}_{\mathcal{TC}} \otimes \mathcal{T}^{(n_s)}$.

The quantum speed limit $\tau_{QSL}$ for a set of simultaneous state transfers has to be estimated by evaluating the minimal time at which we can perform an operator in ${\mathcal{G}_{\mathcal{TC}}}^{loc\,ph}$.

[2]The map $f: U(n-n_s) \to \mathcal{G}_{TC}$ defined as $\hat{W} \mapsto \hat{U}(\hat{W})$ is a well defined group isomorphism, i.e. it is a bijective homomorphism between $U(n-n_s)$ and $\mathcal{G}_{TC}$. Indeed the inverse function $f^{-1}$ is also well defined and for every element $\hat{V} \in \mathcal{G}_{TC}$ we can define a unitary operator $f^{-1}(\hat{V}) \in U(n-n_s)$. By exploring all the matrices in $U(n-n_s)$ we can account for all the elements in $\mathcal{G}_{TC}$. From the dimension of the $U(n-n_s)$ group, this results in a total of $(n-n_s)^2$ real variables needed to define $\hat{U}(\hat{W})$, i.e. $\mathcal{G}_{TC}$ is an $(n-n_s)^2$-dimensional manifold.

[3]This notation is used to represent $\mathbb{T}^{(n_s)} := S^{1\,\otimes(n_s)}$, i.e. the $(n_s)$-dimensional torus.

### 3.2.6 Algorithm outline

Now that all the required tools have been presented, it is possible to write down an algorithm that is able to compute the quantum speed limit associated with a unitary operator, a quantum gate acting on a subspace or a set of simultaneous state transfers. First, we present a core subroutine that computes the quantum speed limit of any unitary evolution. This subroutine is presented as Algorithm 3.2. Then, the protocol is extended to the latter two cases, finding the minimal quantum speed limit among all the unitary operators that implement the target state-to-state transfers or a gate in a logical subspace. This global routine is later introduced as Algorithm 3.3, which contains Algorithm 3.2 in its description.

We start by defining a function $\tau(\cdot)$ that, given any unitary operator $\hat{V}$, returns the quantum speed limit estimation of said evolution in the studied system

$$\begin{array}{rccc} \tau\ : & U(n) & \longrightarrow & \mathbb{R}^+ \\ & \hat{V} & \longmapsto & \tau\left(\hat{V}\right). \end{array} \tag{3.45}$$

The broad idea is to have the $\tau(\cdot)$ function use the available velocity to determine the quantum speed limit via the estimation show in Equation (3.20) and Figure 3.1. When the effective Hamiltonian $-i\hat{H}_{eff}$ of a gate $\hat{U} = \exp(-i\hat{H}_{eff})$ does not belong to $\mathcal{S}$, i.e. when Equation (3.20) is not directly applicable, then the function $\tau(\cdot)$ adapts the calculation by finding a decomposition of $\hat{U}$ into a sequence $\hat{U} = \hat{U}_1\hat{U}_2\cdots$ of gates whose quantum speed limit can be directly determined with the previous estimation. The quantum speed limit $\tau\hat{U}$ is then be approximated by $\tau\hat{U} = \sum_j \tau\hat{U}_j$. The main structure of $\tau(\cdot)$ is shown step by step in Algorithm 3.2, which is explained in detail below.

While $\tau(\cdot)$ depends on the desired unitary $\hat{U} \in U(n)$ as a variable, the function also implicitly depends on the information of the quantum system, which is passed as an input in the form of the available velocity polytope $AvVel(\hat{H}_0, \hat{H}_1)$ and the control operator $\hat{H}_1$. Therefore, systems with different Hamiltonians lead to different definitions of the function $\tau(\cdot)$, although the same internal structure is maintained. To avoid repeating calculations, we also include as an input a basis $\{-i\hat{A}_j^{(\mathcal{S})}\}_{j=0}^{dim(\mathcal{S})-1}$ of the space of slow directions $\mathcal{S}$, i.e. the space spanned by $AvVel(\hat{H}_0, \hat{H}_1)$. Additionally, there is one last parameter involved, $\epsilon_{gate}$, which is the minimum tolerance that we use to claim that two gates are approximately the same if and only if $\|\hat{U}^\dagger\hat{V}(\vec{\beta}) - \mathbb{1}\| \leq \epsilon_{gate}$.

Algorithm 3.2 starts by computing the direction in the Lie algebra of the effective Hamiltonian $-i\hat{H}_{eff}$ via the logarithm of the given unitary evolution. Then, it checks whether $-i\hat{H}_{eff}$ belongs to the subspace of fast and slow directions $\mathcal{F} + \mathcal{S}$. If it

**Algorithm 3.2:** Quantum speed limit estimation for fixed unitary gate

Input:
- $\hat{H}_1$: control operator of the studied system.
- AvVel($\hat{H}_0$, $\hat{H}_1$): available velocity polytope.
- $\hat{U}$: unitary operator to decompose
- $\epsilon_{gate}$: maximum error tolerance for the approximation of unitary matrices.

Compute $-i\hat{H}_{eff} := \log\left(\hat{U}\right)$.
**if** $-i\hat{H}_{eff} \in \mathcal{F} + \mathcal{S}$ **then**
    Define $-i\hat{H}_{eff}^{(\mathcal{S})}$ as the projection of $-i\hat{H}_{eff}$ onto $\mathcal{S}$.
    Find the intersection $-i\hat{H}_{\cap}$ between the ray defined by $-i\hat{H}_{eff}^{(\mathcal{S})}$ and the polytope AvVel($\hat{H}_0$, $\hat{H}_1$) (see Algorithm 3.1 or Equation (3.29) for the quickhull or the torus approximation cases, respectively).
    $\tau_{QSL} = \|\hat{H}_{eff}^{(\mathcal{S})}\|/\|\hat{H}_{\cap}\|$
**end if**
**else**
    Find a decomposition $\hat{V}(\vec{\beta}) := \prod_{j=0}^{dim(\mathcal{S})-1} e^{-i\beta_j \hat{A}_j}$ that minimizes the error $\|\hat{U}^\dagger \hat{V}(\vec{\beta}) - \mathbb{1}\|$.
    **if** $\|\hat{U}^\dagger \hat{V}(\vec{\beta}) - \mathbb{1}\| > \epsilon_{gate}$ **then**
        Concatenate sequences of gates of slow directions $\hat{V}(\vec{\beta}_{ite=0}, ..., \vec{\beta}_{ite=k}) := \hat{V}(\vec{\beta}_{ite=0})\hat{V}(\vec{\beta}_{ite=1}) \cdots \hat{V}(\vec{\beta}_{ite=k})$ until $\|\hat{U}^\dagger \hat{V}(\vec{\beta}_{ite=0}, ..., \vec{\beta}_{ite=k}) - \mathbb{1}\| \leq \epsilon_{gate}$
        Define the vector $\vec{\beta} = (\vec{\beta}_{ite=0}|\, \vec{\beta}_{ite=1}|\, \cdots\, |\vec{\beta}_{ite=k})$ of dimension $k \cdot \dim(\mathcal{S})$ as the concatenation of all $\vec{\beta}_{ite=j}$.
        **for** $\dim(\mathcal{S}) \leq l \leq k \cdot \dim(\mathcal{S}) - 1$ **do**
            Define $\hat{A}_l \leftarrow \hat{A}_{(l \mod \dim(\mathcal{S}))+1}$
        **end for**
    **end if**
    **for** $0 \leq m \leq size(\vec{\beta})$ **do**
        Find the intersection $-i\hat{H}_{\cap}^{(m)}$ between the ray defined by $-i\hat{A}_m$ and the polytope AvVel($\hat{H}_0$, $\hat{H}_1$) (see Algorithm 3.1 or Equation (3.29) for the quickhull or the torus approximation cases, respectively).
        $\tau_{partial}^{(m)} = \|\hat{A}_m\|/\|\hat{H}_{\cap}^{(m)}\|$
    **end for**
    $\tau(\hat{U}) = \sum_j \tau_{partial}^{(j)}$
**end if**
Output:
- $\tau(\hat{U})$: quantum speed limit estimation for a fixed unitary operator $\hat{U}$ with the available velocity polytope AvVel($\hat{H}_0$, $\hat{H}_1$) and control operator $\hat{H}_1$.

does, then the estimation is quite immediate, as it is a direct application of the estimation $\tau_{QSL}$ previously presented in Equation (3.20). First, it takes the projection of $-i\hat{H}_{eff}$ onto the subspace of slow directions $\mathcal{S}$, denoted as $-i\hat{H}_{eff}^{(\mathcal{S})}$. Then, it finds the intersection between the ray defined by the vector $-i\hat{H}_{eff}^{(\mathcal{S})}$ in the Lie algebra and the border of $AvVel(\hat{H}_0, \hat{H}_1)$. Depending on the method used to compute the available velocity polytope, this intersection is determined in one of two different ways. If $AvVel(\hat{H}_0, \hat{H}_1)$ was constructed using quickhull then it is a polytope that can be embedded in an affine space of dimension $\tilde{d} := \dim(\text{span}(AvVel(\hat{H}_0, \hat{H}_1)))$. It is defined by a set of $(\tilde{d}-1)$-dimensional simplices, each defined by $\tilde{d}$ points in the affine space of the Lie algebra. In this case, the intersection $-i\hat{H}_{\cap}$ is computed with the aid of Algorithm 3.1. Alternatively, if the torus approximation from the previous subsection has been used, then the intersection point $-i\hat{H}_{\cap}$ is determined via Equation (3.29). Once $-i\hat{H}_{\cap}$ has been found, the estimation for the quantum speed limit is given by $\tau_{QSL} = \|\hat{H}_{eff}^{(\mathcal{S})}\|/\|\hat{H}_{\cap}\|$.

On the other hand, if $-i\hat{H}_{eff} \notin \mathcal{F} + \mathcal{S}$, a direct estimation is not possible. Using the basis $\{-i\hat{A}_j^{(\mathcal{S})}\}_{j=0}^{dim(\mathcal{S})-1}$ of $\mathcal{S}$, the goal is then to find a decomposition of the gate $\hat{U}$ in the form of

$$\hat{U} = \left(\prod_{j_1=0}^{dim(\mathcal{S})-1} \exp(-i\,\beta_{j_1}^{(1)}\hat{A}_{j_1}^{(\mathcal{S})})\right)\left(\prod_{j_2=0}^{dim(\mathcal{S})-1} \exp(-i\,\beta_{j_2}^{(2)}\hat{A}_{j_2}^{(\mathcal{S})})\right)... \tag{3.46}$$

If we allow for a certain error in the approximation, it is sufficient to take a finite sequence in Equation (3.46). Algorithm 3.2 initializes this step with only one layer of gates $\prod_{j_1=0}^{dim(\mathcal{S})-1} \exp(-i\,\beta_{j_1}^{(1)}\hat{A}_{j_1}^{(\mathcal{S})})$, trying to minimize the error

$$\epsilon(\vec{\beta}^{(1)}) := \|\hat{U}^\dagger \hat{V}(\vec{\beta}^{(1)}) - \mathbb{1}\| \tag{3.47}$$

where $\hat{V}(\vec{\beta}^{(1)})$ is defined as

$$\hat{V}(\vec{\beta}^{(1)}) := \left(\prod_{j_1=0}^{dim(\mathcal{S})-1} \exp(-i\,\beta_{j_1}^{(1)}\hat{A}_{j_1}^{(\mathcal{S})})\right). \tag{3.48}$$

In this instance, the optimization is implemented with the principal axis algorithm [121] included in the NLopt python package [122]. If $\epsilon(\vec{\beta})$ is larger than the error tolerance $\epsilon_{gate}$ defined as an input in Algorithm 3.2, then the algorithm increases the number of layers in the sequence by 1. To do so, we can define the new error

$$\epsilon(\vec{\beta}^{(1)}, \vec{\beta}^{(2)}) := \|\hat{U}^\dagger \hat{V}(\vec{\beta}^{(1)})\hat{V}(\vec{\beta}^{(2)}) - \mathbb{1}\| \tag{3.49}$$

with the analogously defined $\hat{V}(\vec{\beta}^{(1)})$

$$\hat{V}(\vec{\beta}^{(2)}) := \left( \prod_{j_2=0}^{dim(\mathcal{S})-1} \exp(-i\,\beta_{j_2}^{(2)} \hat{A}_{j_2}^{(\mathcal{S})}) \right). \tag{3.50}$$

Note that in iteration $i$, only the parameters in $\vec{\beta}^{(i)}$ will be optimized until there is a finite sequence at $i = N_\beta$ such that $\epsilon(\vec{\beta}^{(1)}, \vec{\beta}^{(2)}, \ldots, \vec{\beta}^{(N_\beta)}) \leq \epsilon_{gate}$. By definition, the effective Hamiltonian related to each gate $\exp(-i\,\beta_j^{(k)} \hat{A}_j^{(\mathcal{S})})$ is contained in $\mathcal{S}$, which means we can compute the quantum speed limit estimation for each of them as shown before. Thus, the estimation for the quantum speed limit of the original gate is the sum of all the quantum speed limits, i.e.

$$\tau(\hat{U}) \simeq \sum_{j=0}^{dim(\mathcal{S})-1} \sum_{k=1}^{N_\beta} \tau \left( \exp(-i\,\beta_j^{(k)} \hat{A}_j^{(\mathcal{S})}) \right). \tag{3.51}$$

This concludes the algorithm for the estimation of the quantum speed limit of a fixed unitary gate, which provides the foundation for other cases. Now the method can be extended to compute the quantum speed limit of state-to-state transfers and gates acting on subspaces of the Hilbert space.

To implement the extension to other targets we simply need to explore the set of all the gates that meet the target conditions and find the minimum quantum speed limit among them. For this search, we define a parameterization

$$\begin{array}{rccc} \hat{U} : & \mathbb{R}^M & \longrightarrow & \mathcal{U}^{tgt} \\ & \vec{\alpha} & \longmapsto & \hat{U}(\vec{\alpha}) \end{array} \tag{3.52}$$

where $\mathcal{U}^{tgt}$ represents the set of all the unitary operators in $SU(n)$ that meet the target conditions. The exact parameterization depends on whether the target conditions include fixed local gates (cf. Equation (3.36)) or can vary any local phases (cf. Equation (3.43)). In any case, the aforementioned vector $\vec{\alpha}$ includes a parameterization of the previously defined unitary operator $\hat{W}$ that shuffles the evolutions of the states not included in the set of initial and final vectors. The parameterization of $\hat{W}$ adds up to a total of $(n - n_s)^2$ parameters. In the case of arbitrary local phases, $\vec{\alpha}$ also includes the parameters of $\vec{\phi}$ described in Equation (3.43), adding possibly $n_s$ new parameters. The exact dimension $M$ of the parameter space thus depends on the chosen case. The final piece of the puzzle is the inclusion of this parameterization into an algorithm.

The parameterization from Equation (3.52) can be composed with the previous estimator $\tau(\cdot)$ for fixed unitary gates to obtain an estimator for other targets

$$\begin{array}{rccc} \tau \circ \hat{U} : & \mathbb{R}^M & \longrightarrow & \mathbb{R}^+ \\ & \vec{\alpha} & \longmapsto & \tau \left( \hat{U}(\vec{\alpha}) \right). \end{array} \tag{3.53}$$

**Algorithm 3.3:** Quantum speed limit estimation for simultaneous state transfers

1 Input:
- $[\hat{H}_0, \hat{H}_1]$: list including the drift $\hat{H}_0$ and control operator $\hat{H}_1$ of the studied system.
- *state_transfers*: target conditions defined as sets of state transfers $\{|\psi_0^{(j)}\rangle \to |\psi_f^{(j)}\rangle\}_j$ or $\{|\psi_0^{(j)}\rangle \to e^{i\varphi_j}|\psi_f^{(j)}\rangle\}_{j=0}^{n_s-1}$. They may have specific or arbitrary local phases, respectively. A given unitary evolution $\hat{U}$ can be given by the state transfers of two complete orthonormal bases, i.e. $n_s = \dim(\mathcal{H})$

2 Compute AvVel($\hat{H}_0$, $\hat{H}_1$) via *quickhull* (Section 3.2.3) or the torus approximation (cf. Equation (3.26)).

3 Find a basis $\{-i\hat{A}_j^{(\mathcal{S})}\}_{j=0}^{dim(\mathcal{S})-1}$ for the subspace of slow directions $\mathcal{S}$.

4 According to *state_transfers*, parameterize all $\hat{U}(\vec{\alpha})$ that meet the target conditions (cf. Equation (3.44))).

5 Define the figure of merit $\tau_{QSL}(\hat{U}(\vec{\alpha}))$ according to Algorithm 3.2.

6 Optimize $\tau_{QSL} := \min_{\vec{\alpha}} \ \tau_{QSL}(\hat{U}(\vec{\alpha}))$ with $\alpha_j \geq 0$ for every $j$.

7 Output:
- $\tau_{QSL}(U(\vec{\alpha})))$: quantum speed limit estimation for the system with Hamiltonian $\hat{H}_0, +u(t)\hat{H}_1$ and target conditions *state_transfers*.

The function in Equation (3.53) can be used as the figure of merit in a minimization problem over the whole parameter space $\mathbb{R}^M$. Note that, in doing this, we find the minimum value for the quantum speed limit among all the different unitary evolutions that meet the target conditions. The parametrization shown in Equation (3.52) ensures that the figure of merit can be used in one of the many available optimization algorithms. In our case, the subplex algorithm was chosen as a non-linear optimization method that could scout the parameter space efficiently [123, 122]. Once the optimization algorithm has converged, the resulting optimal value $\tau_{QSL}$ gives the estimation for the quantum speed limit for a fixed set of simultaneous state transfers in the chosen quantum system. This value is an approximation that will be more or less tight depending on the approximations used, but will always be an upper bound to the actual quantum speed limit.

The main steps of the quantum speed estimator for state-to-state transfers and gates on subspaces are shown in Algorithm 3.3, which is visually represented in the form of a flowchart in Figure 3.3. There are two different types of inputs needed for the procedure. First, the Hamiltonian of an operator controllable system following Equation (3.1) must be provided, where the drift $\hat{H}_0$ is an operator with null diagonal in the matrix representation that uses the eigenbasis of the control operator $\hat{H}_1$. Second, the data of the target state transfers is passed as a list of tuples $\{(|\psi_0^{(j)}\rangle, |\psi_f^{(j)}\rangle)\}_j$ with the additional information of whether or not local phases should be maintained or not (i.e. whether we want a gate $\{|\psi_0^{(j)}\rangle \to |\psi_f^{(j)}\rangle\}_j$ or a set of targets $\{|\psi_0^{(j)}\rangle \to e^{i\theta_j}|\psi_f^{(j)}\rangle\}_j$ with arbitrary phases $\theta_j$).

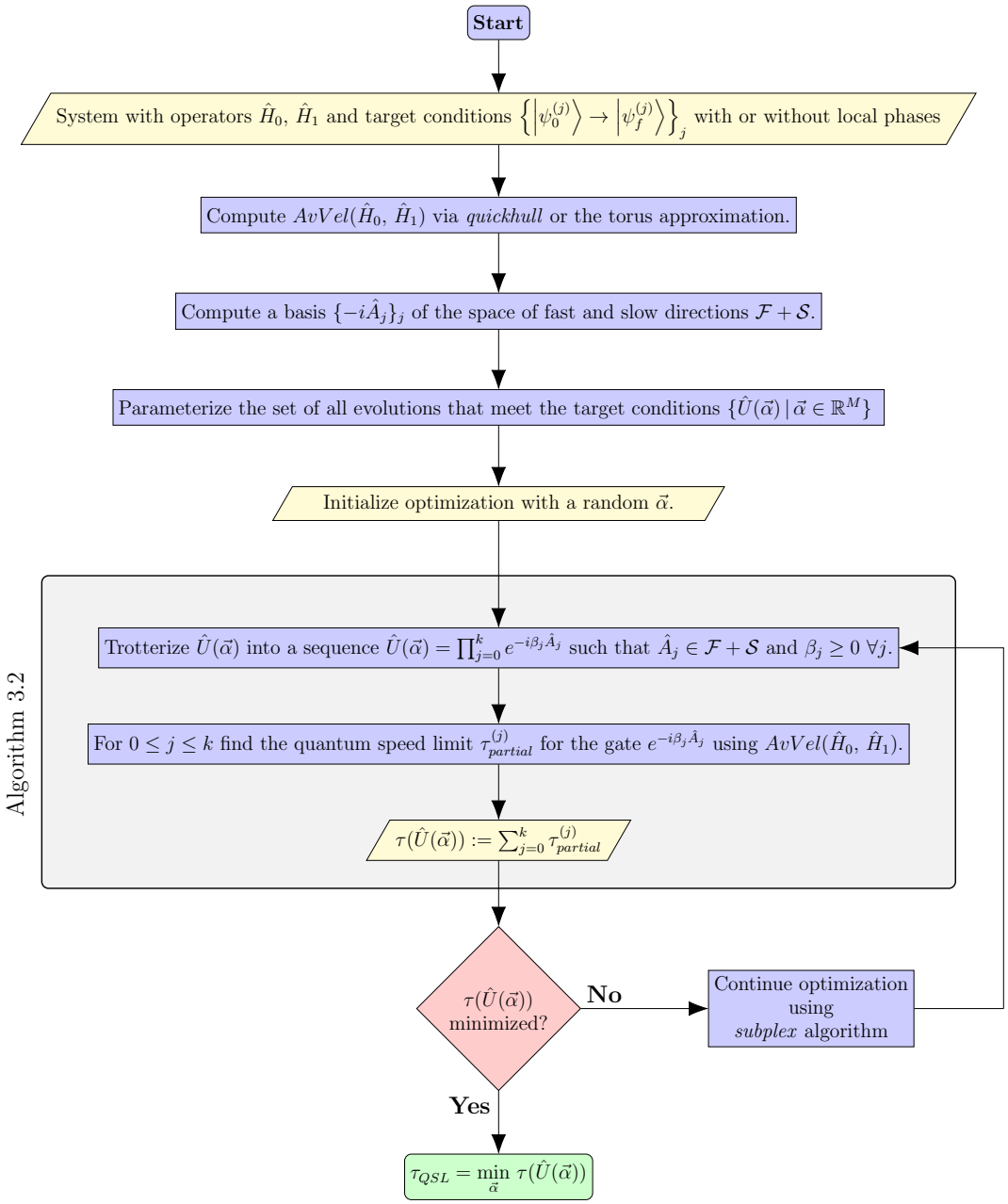


**Figure 3.3:** Flowchart showcasing the main subroutines in Algorithm 3.3. More information on how to calculate $AvVel(\hat{H}_0), \hat{H}_1)$ using quickhull or the torus approximation can be found in Sections 3.2.3 and 3.2.4 respectively. The parametrization of $\hat{U}(\vec{\alpha})$ is linked to the parametrization $\hat{U}(\hat{W}, \vec{\varphi})$ given in Equation (3.44). Algorithm 3.2 provides a figure of merit for the quantum speed limit that can be optimized, e.g. using subplex algorithm [123, 122].

The next step is to construct the available speed polytope. This can be achieved either by generating a sufficiently large number of points in the external hull of the polytope (see Section 3.2.3) or by assuming that the group of arbitrarily fast unitary directions generated by the control can be approximated by a torus (see Section 3.2.4). These two alternatives are shortened as quickhull and the torus approximation in the description of Algorithm 3.3 and in the flowchart of Figure 3.3. This allows us to obtain a basis $\{-i\hat{A}_j^{(\mathcal{S})}\}_{j=0}^{dim(\mathcal{S})-1}$ of the space of slow directions $\mathcal{S}$ and similarly for the space of fast directions $\mathcal{F}$.

Finally, once the available velocity and the spaces $\mathcal{S}$ and $\mathcal{F}$ have been computed, we define an optimization problem that allows us to explore the quantum speed limit estimation of all the different possible unitary evolutions that meet the target conditions. This follows the parameterization presented in Equation (3.53), using $\vec{\alpha}$ as the optimization variables. Note that this optimization includes in its description Algorithm 3.2 as the $\tau(\cdot)$ function. As a possible parameterization of the Lie group $U(n-n_s)$ we use an orthonormal basis $\{i\hat{B}_j\}_{j=0}^{(n-n_s)^2-1}$ of the Lie algebra $\mathfrak{u}(n-n_s)$ (with $\hat{B}_j$ Hermitian for every $j$) such that

$$\hat{W}(\vec{c}) = \exp\left(\sum_{j=0}^{(n-n_s)^2-1} i\, c_j\, \hat{B}_j\right). \tag{3.54}$$

At the end of the optimization, the algorithm provides a single value as a minimum of the figure of merit $\tau \circ \hat{U}(\vec{\alpha})$. This concludes the description of the quantum speed limit estimator for state-to-state transfers and gates acting on subspaces presented in Algorithm 3.3.

## 3.3 Results

To benchmark the quantum speed limit estimator, the method was used in different examples based on a theoretical example where the quantum speed limit for any operator was known to be in a certain interval. This section contains some of the positive and negative results found during the use of the algorithm. Likewise, it also includes the relevant insights obtained during the result analysis, with possible fixes or alternative paths.

To showcase the different types of information we can gather using the quantum speed limit estimator, we take one single quantum system and change the target conditions to study different cases. In order to use the quickhull algorithm we also choose a low-dimensional system. Both conditions make the example presented in [99] a perfect candidate to study the quantum speed limit estimator in a three-dimensional Hilbert space. This example does not directly connect to any particularly

relevant physical case, but it is still an interesting case to test the developed algorithms. Such a system can be described by the Hamiltonian

$$\hat{H}^{(a_1,a_2,a_3)}(t) := \hat{H}_0^{(a_1,a_2,a_3)} + \hat{H}_1(t) := \begin{pmatrix} 0 & a_1 & a_3 \\ \bar{a_1} & 0 & a_2 \\ \bar{a_3} & \bar{a_2} & 0 \end{pmatrix} + u(t) \begin{pmatrix} d_1 & 0 & 0 \\ 0 & d_2 & 0 \\ 0 & 0 & d_3 \end{pmatrix}, \quad (3.55)$$

where the coefficients $a_j$, $i = 1, 2, 3$ are nonzero complex numbers and $d_j$, $j = 1, 2, 3$ are nonzero real numbers. As always, $u(t)$ represents a real control function that can be varied over time at will. On top of that, we also add the restrictions of $d_1 + d_2 + d_3 = 0$ (i.e. choosing the origin of energies for a traceless $\hat{H}_1$) and the two magnitudes $d_1 - d_2$ and $d_2 - d_3$ being rationally independent. The last conditions are necessary to obtain some analytical bounds for the quantum speed limit of any unitary evolution in $SU(3)$, $\tau_{QSL}^{SU(3)}$. A system evolving under Equation (3.55) has a lower and upper bound to this quantum speed limit

$$\tau_{lb} := \frac{2\pi}{3\left(|a_1|^2 + |a_2|^2 + |a_3|^2\right)} \leq \max_{\hat{U} \in SU(3)} \left(\tau_{QSL}(\hat{U})\right) \leq \frac{2\sqrt{6}\pi}{3 \min |a_k|} =: \tau_{ub}. \quad (3.56)$$

Note that the bounds $\tau_{lb}$ and $\tau_{ub}$ have been obtained following the results in example presented in Section 6.3 from [99] and are not an original part of this thesis. This system can be studied with the quantum speed limit estimator from Section 3.2. We can then compare the numerical estimations with the analytical predictions of Equation (3.56). First, we compare the analytical bounds to a set of unitary evolutions in Section 3.3.1. Second, we analyse the case of a single state-to-state transfer in Section 3.3.2. Finally, we compare the case of simultaneous state transfers in Section 3.3.3.

In the end, the numerical method proved to be very demanding and it was deemed inefficient for the purposes of analysing real physical systems. Indeed, the required use of nested optimizations together with the numerical restrictions of quickhull or the harsh approximations needed to apply the torus approximation made it impossible to obtain meaningful positive results in examples based on real physical systems. The method was eventually deprecated for this very reason. While all of the results are valid as an upper bound to the real quantum speed limit of the system, the bounds proved to be not as tight as one would have initially hoped. A deeper discussion on this matter is included in Section 3.3.4.

### 3.3.1 Example A: Unitary gates

As a first step, we test the estimator for the case where the target is a fixed unitary evolution in $SU(3)$. This can be done e.g. by defining an initial and a final orthonormal basis. In the three-dimensional case with Hamiltonian (3.55), this equates to three

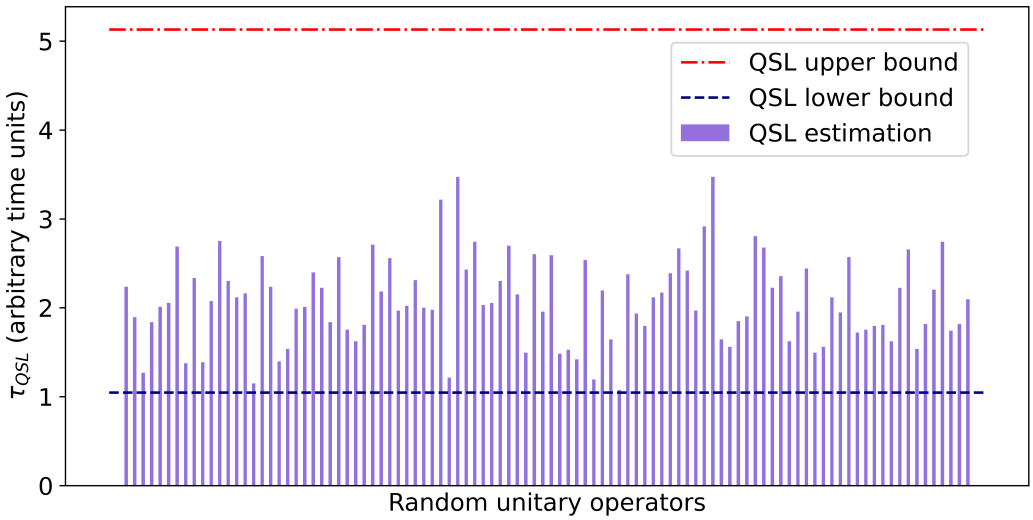


**Figure 3.4:** Bar chart including the quantum speed limit estimation for a hundred random unitary evolutions in $SU(3)$ for the system with Hamiltonian (3.55) with coefficients $a_1 = 1$, $a_2 = -1$, $a_3 = 2i$. Each bar represents the $\tau_{QSL}$ estimation for a different random unitary. Included in the graph are the two analytical bounds given by Equation (3.56).

target conditions with fixed local phases. We provide a target unitary operator $\hat{U}$ and find the minimum quantum speed limit $\tau(e^{i\theta}\hat{U})$ from all the possible operators that just differ on a global phase $e^{i\theta}$ with $\theta \in [0, 2\pi]$. In other words, the phase angle $\theta$ is the only parameter to take into account for the optimization. However, since the Hamiltonian of the system is traceless, the global phase is also fixed and can be chosen to be equal to 1.

For the case of a unitary evolution $\hat{U}$, the estimator is reduced to Algorithm 3.2. This case serves as a preliminary test to check the performance of this subroutine, a core tool that is needed in any other case. After checking the correct behaviour for some isolated cases, we tested the estimator for multiple random unitary matrices in $SU(3)$. To generate these matrices we simply take one of the possible coordinate maps of $SU(3)$, e.g.

$$SU(3) = \left\{ \exp\left( \sum_{\substack{j,k=0 \\ j<k}}^{2} (\alpha_{j,k}\hat{e}_{j,k} - \overline{\alpha}_{j,k}\hat{e}_{k,j}) + \sum_{l=0,1} \beta_l\, i\, (\hat{e}_{l,l} - \hat{e}_{l+1,l+1}) \right) \right| \left| \alpha_{0,1}, \alpha_{0,2}, \alpha_{1,2} \in \mathbb{C},\ \beta_0, \beta_1 \in \mathbb{R} \right\}. \tag{3.57}$$

As an exact value for the Hamiltonian of the system had to be chosen, we arbitrarily used $a_1 = 1$, $a_2 = -1$, $a_3 = 2i$.

The quantum speed limits are shown in Figure 3.4. The bounds from Equation (3.56) are depicted as horizontal lines. Algorithm 3.2 has been used to compute the quantum speed limit of every unitary gate. Coincidentally, the values of all the estimated $\tau_{QSL}$ lie between both of these bounds.

Note that this would not need to be true, in principle. Indeed, the bounds give the interval $[\tau_{lb}, \tau_{ub}] \approx [0.52,\ 5.13]$ (in arbitrary time units) for the shortest time in which every unitary operator in $SU(3)$ can be implemented. In other words, the bounds $[\tau_{lb}, \tau_{ub}]$ give a rough interval for the time in which the slowest unitary evolution can be implemented. It is possible for gates to be faster than this lower bound, i.e. fulfill $\tau(\hat{U}) < \tau_{lb}$. A simple example to demonstrate this is any gate close to the identity. As $\hat{U} \to \mathbb{1}$, the effective Hamiltonian decreases as $\hat{H}_{eff} = i\log(\hat{U}) \to \hat{0}$, where $\hat{0}$ is the null operator. Following Equation (3.19), this implies that $\tau_{QSL} \to 0$.

The results from Figure 3.4 are nevertheless significant from a statistical point of view. The highest estimated quantum speed limit out of all of the randomly chosen unitary gates should be in the interval $[\tau_{lb}, \tau_{ub}]$. This is indeed what can be seen in the random search, where the maximum result yields $\max(\tau) \approx 3.5 \in [\tau_{lb}, \tau_{ub}]$

### 3.3.2 Example B: State-to-state transfer

As a second example we keep the same system described by the Hamiltonian in Equation (3.55) with only one state transfer,

$$|\psi_0\rangle = \hat{U}\,|\psi_f\rangle \quad \text{with} \quad |\psi_0\rangle = \begin{pmatrix}1\\0\\0\end{pmatrix},\ |\psi_f\rangle = \begin{pmatrix}0\\1\\0\end{pmatrix}, \tag{3.58}$$

where the states are represented in the same basis as Hamiltonian ((3.55)), with the control operator $\hat{H}_1$ being diagonal. In this example, we are interested in finding the quantum speed limit of the fastest unitary evolution that can be implemented on the system that fulfills Equation (3.58), up to a global phase, which is also fixed as $\hat{U} \in SU(3)$. As a single transfer, there are no other local relative phases that can be checked between state transfers. Thus according to the parameterization $\hat{U}(\vec{\alpha})$ described in Equation (3.43) all the possible evolutions can be parameterized via a unitary operator $\hat{W} \in U(2)$, i.e. with 4 real parameters.

Once again the Hamiltonian coefficients have been chosen such that $a_2 = -1$ and $a_3 = 2i$. To study multiple cases based on the same example, however, the coefficient $a_1$ has been chosen as a real positive number varying between $3 \cdot 10^{-4}$ and $3 \cdot 10^{1}$. This coefficient was selected in particular, as it links the initial and final state, $a_1 = \langle\psi_0|\,\hat{H}^{(a_1,a_2,a_3)}(t)\,|\psi_f\rangle$. A priori, the quantum speed limit of the transfer defined

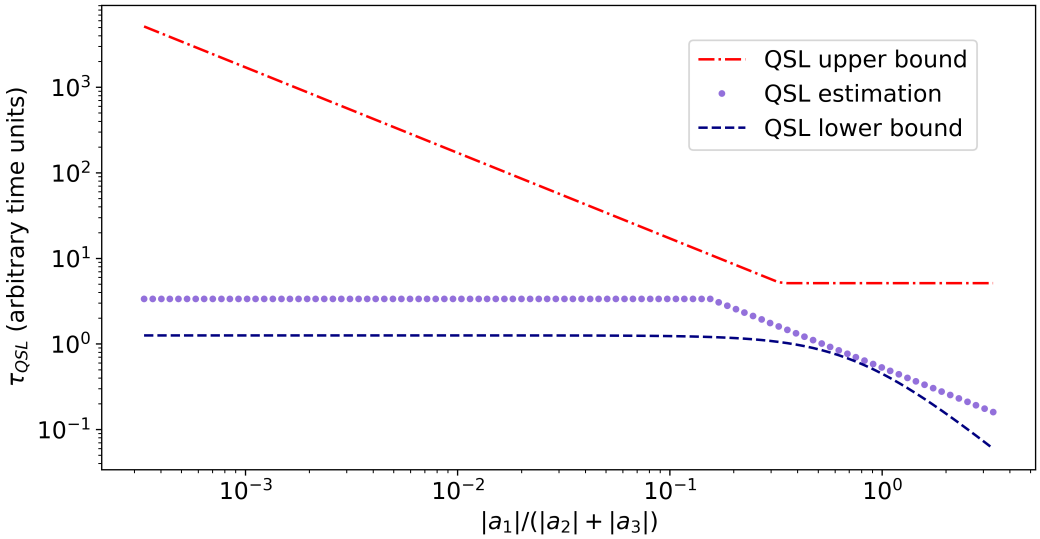


**Figure 3.5:** Quantum speed limit estimation for the system with Hamiltonian (3.55) with coefficients $a_2 = -1$, $a_3 = 2i$ and the state transfer $(1,0,0)^T \rightarrow (0,1,0)^T$. The value of the coefficient $a_1$ is always real and positive. The bounds for the total quantum speed limit are given by Equation (3.56).

by Equation (3.58) should be dependent on this coefficient. The larger the coefficient, the shorter the quantum speed limit should be.

The results can be found in Figure 3.58. As we change the coefficient $a_1$ in Equation (3.55) so does the interval with the analytical bounds for the quantum speed limit from Equation (3.56). Every time the Hamiltonian changes, the available velocity polytope has to be calculated once again. The figure displays the bounds as well as the quantum speed limit of the target state transfer for the different values of $a_1$. As a remark, the upper bound $\tau_{ub}$ is inversely proportional to $a_1$ (i.e. linear with a slope of -1 in the log-log graph) until the interval where $a_1 \geq \min(|a_2|, |a_3|)$, where it remains constant. Conversely, the lower bound $\tau_{lb}$ starts from an asymptotically constant behaviour and tends to decrease as $a_1$ increases.

For $a_1 > 0.17(|a_2| + |a_3|)$, the quantum speed limit of the state transfer decreases: The coefficient $a_1$ represents indeed the exchange factor between the two states and makes the evolution possible. As an interesting note, however, the quantum speed limit $\tau_{QSL}(\hat{U})$ is not always inversely proportional to $a_1$. Indeed, for the case where $a_1 < 0.17(|a_2| + |a_3|)$ we find a surprising behaviour, as the quantum speed limit remains approximately constant. This means that to the left of that value, the parameter $a_1$ no longer remains relevant for the state to state transition.

What happens here from a physical point of view is that for the cases where $a_1$ is relatively small compared to the other coefficients, the norm of the drift in the Lie algebra, $-i\hat{H}_0^{(a_1,a_2,a_3)}$ is mostly given by the $a_2$ and $a_3$ contributions. When we

mix the remaining states in the initial and the final orthonormal bases, the effective Hamiltonians resulting from the evolutions, $-i\hat{H}_{eff} = \log(\hat{U})$, use directions in the available velocity polytope that are mainly given by the other coefficients, ignoring any contribution of $a_1$. In other words, after $a_1$ has decreased enough, there are other directions in the Lie algebra that are more beneficial to trigger the same transition without caring about the $\langle\psi_0|\,\hat{H}^{(a_1,a_2,a_3)}(t)\,|\psi_f\rangle$ coefficient.

### 3.3.3 Example C: Simultaneous state transfers

As a last example, we look at the last possible case in our three-dimensional Hilbert space: Two simultaneous state transfers. Once again we take the system from Equation (3.55) and search for the quantum speed limit of any evolution such that $|\psi_0^{(j)}\rangle = \hat{U}\,|\psi_f^{(j)}\rangle$, where

$$|\psi_0^{(0)}\rangle = \begin{pmatrix}1\\0\\0\end{pmatrix},\ |\psi_0^{(1)}\rangle = \begin{pmatrix}0\\1\\0\end{pmatrix},\ |\psi_f^{(0)}\rangle = \begin{pmatrix}0\\1\\0\end{pmatrix},\ |\psi_f^{(1)}\rangle = \begin{pmatrix}1\\0\\0\end{pmatrix}. \tag{3.59}$$

As there remains only one free state in the basis, the last state-to-state evolution would also be fixed up to a local phase, i.e.

$$|\psi_0^{(2)}\rangle = \begin{pmatrix}0\\0\\1\end{pmatrix} \quad \text{and} \quad |\psi_f^{(2)}\rangle = e^{i\theta}\begin{pmatrix}0\\0\\1\end{pmatrix}. \tag{3.60}$$

Thus the gates that meet the target conditions are equivalent to $\hat{\sigma}_x \oplus e^{i\theta}\mathbb{1}_1$ up to a global phase. Once again we repeat the procedure followed in the previous example, where $a_2 = -1$, $a_3 = 2i$ and $a_1$ is varied along the positive real axis.

The results are shown in Figure 3.6. At first glance, one could believe that the estimated quantum speed limit indeed represents a close approximation. The estimation always remains within the analytical bounds and it seems to be inversely proportional to $a_1$. As the coefficient $a_1$ is the infinitesimal generator of rotation gates between the two first states in the basis, it makes sense that here we obtain a significantly different behaviour than in the previous example. Perhaps one extra target condition reduces the possibilities that we can have in order to generate unitary gates.

This interpretation, however, exposes a flaw in the algorithm. To show this, we define the states in the canonical basis $|e_0\rangle = (1,0,0)^T$, $|e_1\rangle = (0,1,0)^T$ and $|e_2\rangle = (0,0,1)^T$ and we introduce the swap operators

$$\hat{U}_{j,k}\,|e_j\rangle = |e_k\rangle\,, \quad \hat{U}_{j,k}\,|e_k\rangle = |e_j\rangle\,, \quad \hat{U}_{j,k}\,|e_l\rangle = |e_l\rangle \tag{3.61}$$

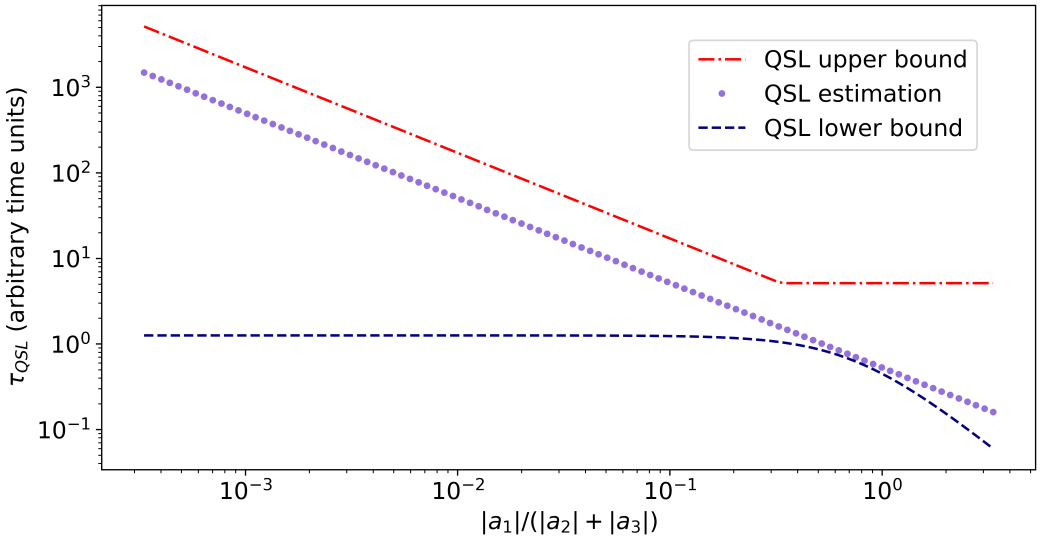


**Figure 3.6:** Quantum speed limit estimation for the system with Hamiltonian (3.55) with coefficients $a_2 = -1$, $a_3 = 2i$ and the evolution $\hat{\sigma}_x \oplus e^{i\theta}\mathbb{1}_1$. The value of the coefficient $a_1$ is always real and positive. The bounds for the total quantum speed limit are given by Equation (3.56).

for $k, j, l \in \{0, 1, 2\}$ and $j \neq k \neq l \neq j$. If we try to analyse the quantum speed limit of the operators $\hat{U}_{j,k}$ we are left with data similar to Figure 3.6, where $\tau(\hat{U}_{0,1}) \propto |a_1|^{-1}$, $\tau(\hat{U}_{1,2}) \propto |a_2|^{-1}$ and $\tau(\hat{U}_{0,2}) \propto |a_3|^{-1}$. However, we know that for an exact quantum speed limit and any two unitary operators $\hat{V}$ and $\hat{W}$ we must abide by the inequality

$$\tau^{ex}\left(\hat{V}\hat{W}\right) \leq \tau^{ex}\left(\hat{V}\right) + \tau^{ex}\left(\hat{W}\right), \tag{3.62}$$

where in this case $\tau^{ex}(\hat{V})$ represents the exact quantum speed limit of the operator $\hat{V}$. Nonetheless, for the case at hand we can find a decomposition of the swap operator such that $\hat{U}_{0,1} = \hat{U}_{0,2}\hat{U}_{1,2}\hat{U}_{0,2}$. Using the quantum speed limit estimator we see that if $|a_1| \ll |a_2|, |a_3|$ then

$$\tau_{QSL}\left(\hat{U}_{0,1}\right) \gg 2\tau_{QSL}\left(\hat{U}_{0,2}\right) + \tau_{QSL}\left(\hat{U}_{1,2}\right). \tag{3.63}$$

While the value of $\tau(\hat{U}_{0,1}) \propto |a_1|^{-1}$ is still valid as an upper bound to the exact quantum speed limit, we know that it is far from the desired value and thus not really that useful as an estimator. In particular, these extremely loose bounds will tend to appear whenever we use coefficients that are orders of magnitude different from one another.

As a workaround, we can make the method more efficient with a simple fix that gets rid of the problems that arise when some coefficients $a_{j,k}$ are orders of magnitude different. Assume a system with a drift Hamiltonian as described in Equation (3.24).

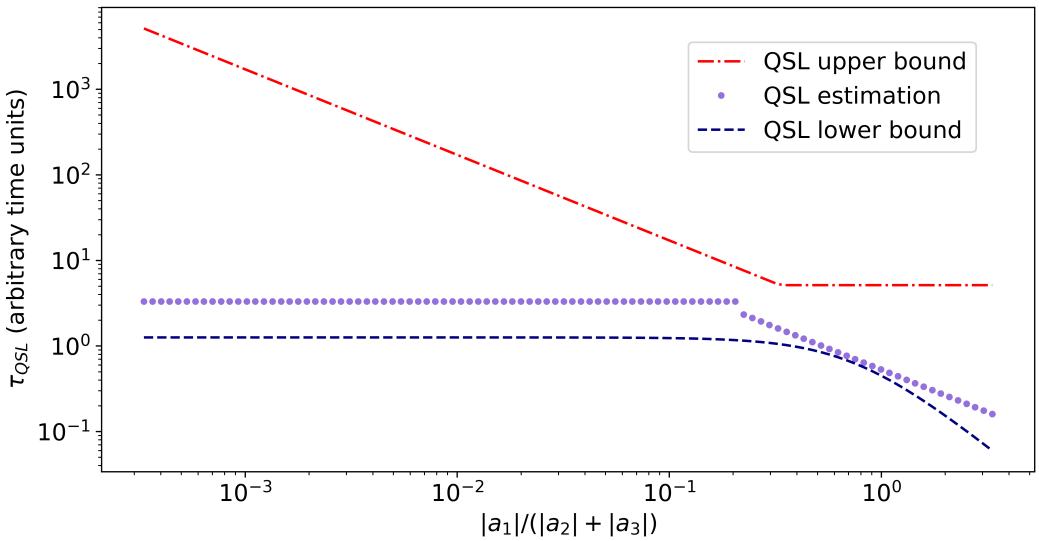


**Figure 3.7:** Quantum speed limit estimation following the case in Figure 3.6 forcing the inclusion $a_1\hat{e}_{0,1} - \overline{a}_1\hat{e}_{1,0} \in \mathcal{V}$ (cf. Equation (3.63)).

Suppose that there exist a coefficient $a_{j,k} \neq 0$ and a sequence $\{a_{c_0,c_1}, a_{c_1,c_2}, ...a_{c_M,c_N}\}$ such that $j = c_0$, $k = c_N$ and

$$\frac{1}{|a_{j,k}|} > \frac{1}{|a_{c_0,c_1}|} + \frac{1}{|a_{c_1,c_2}|} + \cdots + \frac{1}{|a_{c_M,c_N}|}. \tag{3.64}$$

Then we can manually override the use of the coefficient $a_{j,k}$ by declaring that the directions $\hat{e}_{j,k} - \hat{e}_{k,j}$ and $i\hat{e}_{j,k} + i\hat{e}_{k,j}$ should be considered as part of the subspace of very slow directions $\mathcal{V}$. Computationally, this forces the algorithm to find a decomposition using effective Hamiltonians in the other directions such that any effective Hamiltonian alongside $a_{j,k}\hat{e}_{j,k} - \overline{a}_{j,k}\hat{e}_{k,j}$ must be decomposed into a sequence of other Hamiltonians included in the slow and fast directions. This is essentially a different spin on the concept of the connectedness chain shown in Section 2.4.3 and in previous works of controllability [15]. Instead of estimating the quantum speed limit of an evolution that couples two eigenstates $|e_j\rangle$ and $|e_j\rangle$ via the tuple $(j,k)$ in the chain of connectedness, we explore the possibility of using an intermediate state $|e_l\rangle$ by searching for a connectedness chain that includes the tuples $(j,l)$ and $(l,k)$. This provides the possibility of doing a sequence of two evolutions $\hat{U}_{|e_l\rangle\to|e_k\rangle}\hat{U}_{|e_j\rangle\to|e_l\rangle} = \hat{U}_{|e_j\rangle\to|e_k\rangle}$. Under the described conditions, the estimation of the quantum speed limit for the sequence $\hat{U}_{|e_l\rangle\to|e_k\rangle}\hat{U}_{|e_j\rangle\to|e_l\rangle}$ can yield a lower result than the one of the direct evolution $\hat{U}_{|e_j\rangle\to|e_k\rangle}$, i.e. $\tau(\hat{U}_{|e_l\rangle\to|e_k\rangle}) + \tau(\hat{U}_{|e_j\rangle\to|e_l\rangle}) < \tau(\hat{U}_{|e_j\rangle\to|e_k\rangle})$.

Using this procedure in the current example and manually overriding the use of $a_1$ when $|a_1|^{-1} < |a_2|^{-1} + |a_3|^{-1}$ we obtain the data plotted in Figure 3.7. In this case we retrieve a behaviour similar to the example with the state transfer $(1,0,0)^T \to (0,1,0)^T$, exactly as we should expect. While we don't claim that the

estimations for the quantum speed limit in Figure 3.7 are exact, they show a clear improvement over the previous results from Figure 3.6.

### 3.3.4 Numerical complexity and applicability

The idea of the algorithm as a quantum speed limit estimator works from a theoretical point of view as an upper bound for all of the described cases. However, there are a couple of issues that should be discussed, which hinder the applicability of the method.

The first topic to discuss is the physical assumptions on the system. The diagonal control operator $\hat{H}_1$ might seem strange, but for a single control this is always a possibility. The first real assumption comes from demanding the drift $\hat{H}_0$ to have a null diagonal. While this requisite has been used many times in theoretical studies of controllability of systems, it is not a general assumption that can be extended to every case. It does, however, occur in some real physical systems. One of the most simple ones would be a single qubit with a $\hat{X}$ control, whose Hamiltonian reads $-\frac{\omega}{2}\hat{\sigma}_z + u(t)\sigma_x$. After a basis change, we can write the Hamiltonian as $-\frac{\omega}{2}\hat{\sigma}_x + u(t)\sigma_z$, following the required condition of null diagonal on the drift. A similar result occurs for more qubits with off-diagonal controls in the basis where the drift is purely diagonal. This requisite has been used to simplify some of the calculations and derivations to obtain the available velocity. In principle the same procedure could be possible, whether using the numerical convexification or using the approximation via rationally independent terms.

One of the main obstacles in the numerical implementation is the calculation of the available velocity polytope. For a sufficiently low dimensional system, it is not a problem, although creating the available velocity polytope and then finding the intersection points $\hat{H}_\cap$ needed for the quantum speed limit estimation take an increasing amount of time as the Hilbert space dimension increases. However, it is still feasible for two qubits. For larger spaces quickhull is no longer valid and the torus approximation must be used. Here is where the assumptions may not extend to the physically realistic examples; in particular, the rational independence of the eigenvalues. As previously explained, this independence occurs for a randomly chosen set of values with a high probability. Nevertheless, it is true that when using classical simulations, all real values are bound to be represented by a floating-point number, i.e. a rational with a certain precision. But even then, the analytical approximation $e^{\mathcal{F}} \approx \mathbb{T}^n$ holds and all computations that make use of it would be still valid. The real question is whether this condition really happens in physical systems. For the case of qubit arrays, this is a very harsh condition. It implies that the eigenvalues of the control that is acting on a multipartite system cannot be degenerate. Therefore, it requires

the control to be entangling over the qubit partition. Indeed, if $\hat{H}_1$ has a full rationally independent spectrum it implies that it acts on all states of its eigenbasis (up to perhaps a single one-dimensional subspace) with different eigenvalues. On the other hand, the spectrum $\sigma(\cdot)$ of a local operator $\hat{A} \otimes \mathbb{1}_N$ follows the rule $\sigma(\hat{A} \otimes \mathbb{1}_N) = \sigma(\hat{A})$ with each value having a multiplicity of $N$. If $N \geq 2$, any local operator $\hat{A} \otimes \mathbb{1}_N$ is degenerate. In other words, local controls are simply excluded from this condition. As local controls are a staple in qubit arrays, this massively impacts the applicability of the algorithm for large qubit arrays: Either the quickhull algorithm does not work or the torus approximation may not be applicable. The method remains valid for other, more exotic systems however.

As a notable mention, we have included the hypothesis that the system should be operator controllable. This hypothesis is very useful to ensure that the system converges towards an answer, as it should. In practice, however, this assumption is strictly not necessary, as one could explore whether a given evolution or sequence of operators is possible with the information of the available velocity polytope. This could be implemented by adding another subspace to the Lie algebra vector space partition that includes all unavailable directions.

On the computational level, one main step is the decomposition of a quantum gate $\hat{U} = \hat{U}_1 \hat{U}_2 \cdots$ into gates $\hat{U}_j$ whose effective Hamiltonian belongs to the subspace of fast and slow directions. This requirement is also increasingly demanding with respect to the Hilbert space dimension. Not only that, but the method currently does not optimize for a sequence that minimizes $\sum_j \tau(\hat{U}_j)$. Such an optimization would in principle be possible, but it would be adding a third nested optimization to the method, the previous two being the minimization of the total quantum speed limit $\tau(\hat{U}(\vec{(}\alpha)))$ when considering all possible gates $\hat{U}(\vec{(}\alpha))$ that meet the target conditions and the minimization of the actual decomposition error $\|\hat{U}^\dagger \prod_j \hat{U}_j - \mathbb{1}\|$. Trials including this extra optimization have been made. They did not show a real significant improvement while making the calculation a bit more unstable, sometimes even failing to provide estimations of $\tau(\hat{U})$.

Another point to be tested in future work is the behaviour displayed in the example of Section 3.3.3. It shows that to obtain a close estimation for the quantum speed limit (i.e. an upper bound as tight as possible) more work has to be done if the matrix elements $a_{j,k}$ of the drift $\hat{H}_0$ are of significantly different magnitudes. This adds another layer of complexity to the algorithm, requiring an initial study of the available velocity polytope. With this information it is possible to redefine the subspaces $\mathcal{S}$ and $\mathcal{V}$, shifting the directions associated with extremely small coefficients $a_{j,k}$ from $\mathcal{S}$ to $\mathcal{V}$. For a low dimensional space (perhaps one where the convexification methods still

work) this is doable and it would give more accurate speed limits, which is in the end the main goal of this quantum speed limit estimator.

## 3.4 Summary

This chapter has introduced a new method to give an estimation for the quantum speed limit of a quantum system using classical computations that obtain information from the Lie algebra associated to the Hamiltonian of the system. In a way, this is related to the dynamical Lie algebra of the system, but it uses the information of the norm of the various operators that can be implemented on the system to obtain a guess on the speed of said dynamics. This time limit can be computed for either the case of a given unitary operator or for multiple simultaneous state transfers within the same Hilbert space. While we only claim the result of the numerical calculation to be an approximate estimation, the value is always a valid upper bound to the real quantum speed limit of the system. The accuracy of the estimation depends on multiple factors, including among others the precision with which the available velocity polytope was approximated.

The main idea of the method resides in the very definition of the available velocity polytope. There have been some approaches to the quantum speed limit that also make use of this concept from a geometrical definition in the form of adjoint orbits of state evolutions [101]. The concept of the available velocity bypasses the definition of geodesic curves in the analytical geometrical description and uses instead a numerical implementation that can decompose a given evolution into a sequence of multiple ones. The numerical approach was meant to extend the applicability of the method, as the computation of the geodesic curves becomes exponentially more complex with the number of qubits. In this work, however, it was shown that the computation of the available velocity proved to be very challenging as well. The torus approximation was introduced for systems that meet certain conditions, expanding the range of systems that can be studied.

The fact that simultaneous state transfers can be studied vastly extends the capacity of other methods that specialize in single state evolutions due to the Mandelstam-Tamm and Margolus-Levitin quantum speed limits [23, 124, 125]. Similarly, it also exceeds the capabilities of tests that estimate the quantum speed limit of unitary evolutions exclusively [126, 94, 127]. This method provides more flexibility when describing the target conditions, including fixing or varying local phases. This is a resourceful tool for exploring the quantum speed limit of operators working on a subspace of a larger Hilbert space, e.g. the implementation of a quantum logic gate operating on a smaller logical space. Meanwhile it can also be exploited to study the

slowest unitary evolutions to understand what the most demanding dynamics in the system are.

More research is needed to analyse the information that the quantum speed limit estimator gives about the optimal pulses that could generate the target evolution on a system with minimal time. As previously mentioned, sequences of gates $e^{-i\hat{H}_0 t_1}$ and $e^{-i\hat{H}_0 t}e^{-i\hat{H}_1 v}$ can be directly related to sequences of bang-bang pulses. Every evolution with an effective Hamiltonian in the space of slow directions can be decomposed into a sequence of those gates. In other words, the decomposition that the quantum speed limit estimator has incorporated in its algorithm can be also used to describe an optimal pulse to produce the evolution by choosing the right basis of the space of slow directions. This could be used to study why bang-bang pulses appear naturally as solutions in the case of many time-optimal dynamics (see e.g. [128]).

In the future, there are some aspects of the algorithm that could be polished. The most important one is to find alternatives to the numerical computation of the available velocity polytope. The torus approximation, while valid in its own domain, presumes some hypotheses that are physically hard to come by and may also provide a subpar approximation to the exact polytope. Alternatives to this approximation would be a massive improvement towards the usability of the method and the accuracy of the obtained results. This also extends to the point of the use of the connectedness chain shown in Section 3.3.3 to obtain a tighter bound on certain cases. It remains to be seen whether this behaviour is prominent in multiple examples or an artifice that is particularly important in cases with very different coefficient values or for sets of $n-1$ target conditions in an $n$-dimensional Hilbert space.

As an algorithm with multiple nested optmizations, further benchmarking is needed to test its stability and reliability. First, the optmization algorithms subplex and principal axis could be swapped for others to check if there is any improvement in the overall performance. It could be possible that there are other optimization protocols more suitable for the problem at hand. Secondly, we have tried to include a third optimization to find the decomposition of a gate that minimizes the quantum speed limit while also providing a small enough approximation error. This, however, results in longer computation times and sometimes the lack of a final result. The optimizations were prone to get stuck on barren plateaus, a common issue in optimization problems [129]. This is exacerbated when multiple nested optimizations are involved. More work is needed in this area to obtain a better understanding of how these problems are connected.

A straightforward extension to be implemented is the inclusion of multiple controls. In the current work it was assumed that there was only one control, but it would

be possible to define an available velocity for two or more controls. The main caveat would be that the elements in the outer shell of the polytope could be now preceded and followed by sequences of operators generated by the multiple controls $e^{iv_1\hat{H}_1}e^{iv_2\hat{H}_2}e^{iv_3\hat{H}_1}e^{iv_4\hat{H}_2}\cdots$, which could be arbitrarily long. If the operators do not commute, the range of operators that these controls can generate can be significantly large. The case where the control operators $\hat{H}_1$ and $\hat{H}_2$ commute can nevertheless be easily studied. For commuting operators, we only need to exchange the usual terms $-ie^{iv\hat{H}_1}\hat{H}_0e^{-iv\hat{H}_1}$ for the slightly more complex $-ie^{iv_1\hat{H}_1}e^{iv_2\hat{H}_2}\hat{H}_0e^{-iv_1\hat{H}_1}e^{-iv_2\hat{H}_2}$. The rest of the procedure would essentially remain analogous.

Finally, an interesting potential application for the quantum speed estimator would be the study of parametric quantum circuits, the foundation of variational quantum algorithms [64]. Many quantum circuits are defined as a sequence of local and two-qubit gates. With the current setup it is possible to analyze the quantum speed limit of the operators that are reduced to said single-qubit and two-qubit subspaces, even using the convexification algorithm quickhull. If we can write out the control Hamiltonian available for every pair of qubits, we can compute the quantum speed limit of the whole quantum circuit as the sum of quantum speed limit estimations of every layer in the circuit. This is also true if the different controls in the system are local in separate qubits, as we can implement the extended available velocity polytope previously described for commuting controls. This result could determine the coherence times that a system must have to be able to perform a certain quantum circuit or, conversely, the maximum layer depth that a quantum algorithm may have to be successfully implemented on a given qubit array with a known Hamiltonian.

# 4 Graph test for controllability of qubit arrays

## 4.1 Introduction

Universal quantum computing requires operator controllability on the quantum processing units in order to perform every possible quantum logic gate. One way to achieve this, pursued for example in most superconducting qubit architectures, is to couple each qubit to at least one other qubit and drive all qubits locally. This approach becomes impractical for larger qubit arrays due to increasing requirements on physical space for control lines and on calibration time for control pulses. One may wonder whether a number of local drives smaller than the number of qubits would already be sufficient. If so, this would suggest the possibility of more resource-efficient architectures than currently in use.

Here, we show that controllability analysis provides a systematic approach to determine the minimum number of local controls for which any desired quantum logic gate can be implemented. We find that indeed the number of local controls can be smaller than the number of qubits. The minimum number of local controls, for a given size of the qubit array, depends on the type of qubit-qubit couplings. To facilitate analysis of medium-sized qubit arrays, we leverage a graph theory-based approach to controllability analysis and investigate five-qubit arrays starting from the *ibmq_quito* architecture.

Controllability analysis answers the question, in a yes-no fashion, which states can be reached by time evolution from a set of initial states [12, 130]. The standard approach consists in determining the rank of the dynamical Lie algebra of the system and comparing it to the dimension of the algebra that generates the unitary group of all time evolutions [14]. This approach has been extensively used to prove controllability for finite-dimensional systems with sufficiently small Hilbert space dimension [13, 131, 132] and can also be employed in subspaces of infinite-dimensional systems, when combined with Galerkin-type approximations [16, 133, 15, 17]. The focus of these studies has been on single quantum systems. For multi-partite systems, where the

Hilbert space dimension scales exponentially in the number of subsystems, evaluating the Lie rank condition quickly becomes challenging. It has thus mainly been used to identify controllable subspaces in systems which as a whole are not controllable [134, 135, 136, 137]. Positive controllability results for qubit arrays, as needed for universal quantum computing, require an alternative approach.

The exponential scaling of Hilbert space dimension with the number of qubits is evidently inherent to gate-based quantum computing and represents a fundamental obstacle to controllability analysis that cannot be overcome with classical computers. But even for qubit arrays which are classically simulable, use of the Lie rank condition is hampered by numerical instabilities which are common when constructing orthogonal bases in large operator spaces. This latter obstacle can be avoided by resorting to graph theory-based methods for controllability analysis [138, 15, 139] which have successfully been applied to quantum walks [140], quantum networks [141], and quantum rotors [17, 142]. The latter are characterized by a highly degenerate spectrum which results in multiple resonant transitions, i.e., transitions with the same resonance frequency that are driven by the same external control. Controllability can then not simply be read off from the connectivity of the graph. This problem is also present for arrays of locally driven coupled qubits but the different spectral structure requires different graphical methods to prove controllability, as we will discuss below.

The chapter is organized as follows. The basic concepts of controllability analysis are briefly reviewed in section 4.2. The methodology we suggest to use for controllability analysis of coupled qubit arrays is presented in section 4.3 with section 4.3.1 explaining how to deal with resonant transitions, section 4.3.2 presenting the actual graph test in the form of a flow chart and three algorithms and section 4.3.3 illustrating the use of the algorithms on simple two-qubit examples. Our results on five-qubit arrays inspired by the *ibmq_quito* architecture are presented in section 4.4, and section 4.5 concludes.

## 4.2 Controllability analysis

We study quantum systems that couple linearly to controls, such that their Hamiltonian can be expressed as linear contributions of a time-independent drift $\hat{H}_0$ and some drives $u_j(t)\hat{J}_j$ (cf. Equation (2.8)). The controls $u_j(t)$ are real-valued functions and $\hat{H}_j$ are the control operators. A state that evolves under Equation (2.8), is given by $|\psi(t)\rangle = \hat{U}(t; u_1, ...u_m)\,|\psi(0)\rangle$. We consider coherent evolutions since they are the relevant foundation for gate-based quantum information.

For qubit arrays, the drift $\hat{H}_0$ is split into $\hat{H}_0 = \sum_{l=1}^{N_Q} \hat{H}_{0,l} + \hat{H}_c$, representing the independent local Hamiltonians $\hat{H}_{0,l}$ of the $N_Q$ free qubits and the time-independent couplings $\hat{H}_c$ between them. Typically, local controls $\hat{H}_j$ act on single qubits, for example in the form of laser pulses in ion arrays [143] or varying microwave fields for certain superconducting qubits [144]. Regardless of the physical implementation of the qubits, we would like to answer the question whether a system with a set of controls is capable of performing any unitary operation.

The answer can be found by analysing the controllability; in particular, the operator controllability of the system [14]. Here operator controllability follows the definition given in Section 2.4. As a brief summary, a system is operator controllable if and only if we can always choose controls and a final time to carry out any unitary operation, up to a global phase. For simplicity, we refer to this property as 'controllable'. A widely used method for studying the controllability of a quantum system is to analyze the **dynamical Lie algebra** [14, 140, 145]. It is generated by the drift and the $m$ control operators of the system, $\mathcal{L} := Lie(i\hat{H}_0, i\hat{H}_1, ..., i\hat{H}_m)$, i.e., it contains the skew-Hermitian operators $i\hat{H}_0, i\hat{H}_1, ..., i\hat{H}_m$, and their (nested) commutators. A system with Hilbert space dimension $n$ is controllable if the dimension of the dynamical Lie algebra is $n^2$ or $n^2 - 1$. In other words, it is controllable if the dimension of the Lie algebra matches either that of $\mathfrak{su}(n)$ (which generates the special unitary group $SU(n)$) or $\mathfrak{u}(n)$ (which generates the unitary group $U(n)$). This is sometimes referred to as the Lie algebra rank condition [14]. The main difference between generating $U(n)$ or $SU(n)$ is that the former allows the system to perform any unitary evolution including all global phases. Conversely, the latter encompasses all unitary evolutions up to a non-controllable global phase.

Alternatively to constructing the dynamical Lie algebra, a graph test can be used to analyze controllability [139, 17, 146]. The graph encodes the information of the Hamiltonian.

**Definition 1.** *Given a quantum system evolving under Equation* (2.8)*, we can construct an undirected graph according to the rules:*

1. *For every eigenstate $|e_k\rangle$ of $\hat{H}_0$, add a vertex to the graph with a corresponding label.*

2. *For every control $\hat{H}_j$ and every nonzero element $\langle e_i| \hat{H}_j |e_k\rangle$, add an edge between the vertices labelled $|e_i\rangle$ and $|e_k\rangle$. Additionally, add a label to every edge stating which control drives that transition.*

*We call this the **graph of a quantum system**[1].*

Since the nodes of the graph are labelled by the eigenstates $|e_k\rangle$, we use these labels also to name the edges that represent the transitions generated by the controls. The edge joining the vertices $|e_a\rangle$ and $|e_b\rangle$ is denoted by $(a, b)$. For Hermitian controls, the transitions will necessarily happen in both directions, implying an undirected graph. This means, in particular, that both $(a, b)$ and $(b, a)$ refer to the same edge.

An important aspect of the graph are the energy gaps related to the graph edges $\Delta E_{a,b} := \left| E_{|e_a\rangle} - E_{|e_b\rangle} \right|$. If two transitions have the same energy gap $\Delta E_{a,b}$, they are called 'resonant'. Resonant transitions may pose a challenge to controllability since, depending on the local controls, it may be impossible to address them independently.

**Definition 2.** *Let $\mathcal{G}$ be the graph of a system. If two edges $(a, b), (c, d) \in E(\mathcal{G})$ belong to the same control $\hat{H}_j$ and have degenerate energy gaps $\Delta E_{a,b} = \Delta E_{c,d}$, then the two transitions represented by the edges are **coupled** to one another. Alternatively, if an edge $(a, b) \in E(\mathcal{G})$ is not coupled to any other transition belonging to its own control $\hat{H}_j$, the transition is said to be **decoupled**.*

The graph of a system contains the adjacency information for all the possible chains of connectedness on the system (see Section 2.4.3) extended to the case of multiple controls. Decoupled transitions are essentially all the tuples that can be added to any chain of connectedness and still make it non-resonant. On the other hand, coupled transitions may make the chain resonant, hence breaking the sufficient condition for controllability. These combined notions lead to the following theorem, whose proof can be found in Ref. [16]:

**Theorem 4.2.1.** *Let $\mathcal{S}$ be a quantum system following Equation* (2.8) *and let $\mathcal{G}$ be its associated graph. The system $\mathcal{S}$ is **controllable** if there exists a **connected subgraph** of $\mathcal{G}$ that contains **all vertices** of $\mathcal{G}$ and **only decoupled transitions**.*

An undirected graph is said to be connected if for every two vertices there exists a chain of adjacent edges that creates a path between the two selected vertices. A subgraph of a graph $\mathcal{G}$ is a graph defined by a subset of the vertices $V(\mathcal{G})$ and a subset of the edges $E(\mathcal{G})$ that only link vertices in the subset. This means that a subgraph is a graph that we obtain by removing any number of the edges and vertices from the original graph.

[1] Note that given two vertices there can be more than one edge between the two of them (belonging to different controls). Technically, this makes the graph of a system a multigraph.

The main benefit of the graph test in Theorem 4.2.1 is that it allows us to avoid calculating the full dynamical Lie algebra. The graph of a quantum system with Hilbert space dimension $n$ has $n$ vertices. To have a connected subgraph we need to find $n-1$ decoupled transitions such that they create a single connected component. This works quite efficiently if there are no resonant transitions in the system.

In the following, we expand this graph test such that it also works with resonant transitions. To this end, we adapt graphical methods for controllability analysis in degenerate systems [142] to systems with degenerate energy gaps driven by multiple controls. Since resonant transitions are very common in qubit arrays due to the multi-partite structure of the system, this modification opens the route to efficient analysis of controllability of qubit arrays.

## 4.3 Graph test of controllability for coupled subsystems

In this section we outline the algorithm for a graph test for coupled subsystems with resonant transitions. In section 4.3.1 we present methods to determine the graphical commutators already used in rotor systems [17] and we introduce the concept of subalgebras to treat resonant transitions driven by multiple controls. We show in section 4.3.2 that the graphical commutators can be calculated in a systematic way, avoiding the construction of the entire dynamical Lie algebra of a system. We illustrate the use of these methods in section 4.3.3 with simple two-qubit examples.

### 4.3.1 Resonant transitions and graphical commutators

We first present two concepts to decouple resonant transitions without calculating the complete Lie algebra of the system. To this end, we introduce the generalized skew-Hermitian Pauli matrices

$$\begin{aligned} \hat{G}_{j,k} &= \hat{e}_{j,k} - \hat{e}_{k,j}\,, \\ \hat{F}_{j,k} &= i\hat{e}_{j,k} + i\hat{e}_{k,j}\,, \\ \hat{D}_{j,k} &= i\hat{e}_{j,j} - i\hat{e}_{k,k}\,, \end{aligned} \tag{4.1}$$

where $\hat{e}_{j,k}$ is the null matrix except for a 1 in the entry $(j,k)$. The commutators of these matrices with the skew-Hermitian drift are given by [146, 142]

$$\begin{aligned} [i\hat{H}_0, \hat{G}_{j,k}] &= (E_j - E_k)\ \hat{F}_{j,k}\,, \\ [i\hat{H}_0, \hat{F}_{j,k}] &= -\,(E_j - E_k)\ \hat{G}_{j,k}\,. \end{aligned} \tag{4.2}$$

Consider a transition $(i,k)$ with transition matrix element

$$\langle e_i|\hat{H}_j|e_k\rangle = \alpha - i\beta\,, \tag{4.3}$$

where $|e_i\rangle$, $|e_k\rangle$ with $i \neq k$ are eigenstates of the drift Hamiltonian, $\hat{H}_0$, $\alpha, \beta \in \mathbb{R}$ and at least one of them is nonzero. If $(i,k)$ is a decoupled transition, the Lie algebra of the system contains the element

$$\hat{T} = \alpha\hat{F}_{i,k} + \beta\hat{G}_{i,k}\,, \tag{4.4}$$

and the generalized skew-Hermitian Pauli matrices $\hat{G}_{i,k}$, $\hat{F}_{i,k}$ and $\hat{D}_{i,k}$ are also elements of the Lie algebra $Lie(i\hat{H}_0, \hat{T})$, i.e., $dim[Lie(i\hat{H}_0, \hat{T})] = 4$.

If a system contains the two decoupled transitions $\{(i,k),(i,l)\}$ with $\hat{T}_1 = \alpha_1\hat{F}_{i,k} + \beta_1\hat{G}_{i,k}$ and $\hat{T}_2 = \alpha_2\hat{F}_{i,l} + \beta_2\hat{G}_{i,l}$, respectively, and $i \neq l \neq k$, their commutator is of the form $\hat{T}_3 := [\hat{T}_1, \hat{T}_2] = \alpha_3\hat{F}_{k,l} + \beta_3\hat{G}_{k,l}$. The graph of the system thus has an additional edge $(k,l)$, as depicted in Figure 4.1(a) for $i = 0$, $k = 1$ and $l = 2$. For testing controllability, it is often sufficient to know that there exists a transition $(k,l)$, without calculating the coefficients $\alpha_3, \beta_3$. Since the existence of the transition $(k,l)$ can be deduced from the graph with edges $(i,k)$ and $(i,l)$, we refer to this operation as graphical commutator and denote it as $(k,l) = [(i,k),(i,l)]$.

Graphical commutators can be used as an efficient tool to decouple resonant transitions. This is shown in the example depicted in Figure 4.1(b). Consider transitions $\hat{T}_1 = \alpha_1\hat{G}_{1,2} + \beta_1\hat{F}_{1,2}$ (dash-dotted green arrow in Figure 4.1(b)) and $\hat{T}_2 = \alpha_2\hat{F}_{0,3} + \beta_2\hat{G}_{0,3} + \gamma_2\hat{F}_{1,4} + \delta_2\hat{G}_{1,4}$ (dashed blue arrows) with $\hat{T}_1$ decoupled (i.e. the transition $(1,2)$ is not coupled to any other one) and $\hat{T}_2$ consisting of the pair of coupled transitions $\{(0,3),(1,4)\}$, which are not coupled to any other transition. The graphical commutator between $\hat{T}_1$ and $\hat{T}_2$ has then only contributions corresponding to the transition $(2,4)$, depicted by the red arrow. The graph has thus the additional decoupled transition $(2,4)$. Furthermore, the graphical commutator between the decoupled transitions $(1,2)$ and $(2,4)$ is the decoupled transition $(1,4)$. In this example, the resonant transitions $\{(0,3),(1,4)\}$ can thus be decoupled by taking graphical commutators.

In certain instances, the graphical commutators might not give enough information to decouple resonant transitions and determine the controllability of the system. Examples are shown in Figure 4.1(c) and (d). In Figure 4.1(c), the graphical commutator between the coupled transitions $\{(0,1),(2,3)\}$ (dashed blue arrows) and the decoupled transition $(1,2)$ (dash-dotted green arrows) results in the coupled transitions $\{(0,2),(1,3)\}$ (red arrows). This does not allow for decoupling any of the coupled transitions. In Figure 4.1(d), two pairs of coupled transitions are considered, namely

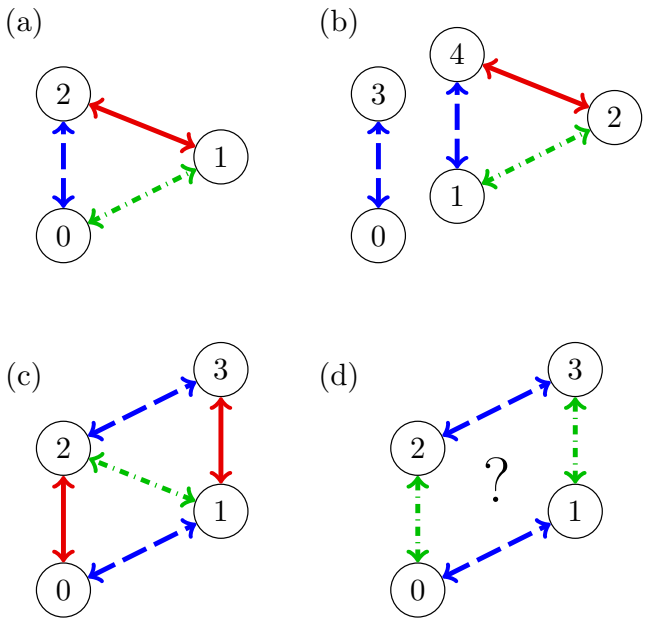


**Figure 4.1:** Examples for graphical commutators. The circles represent the vertices of the graph and the edges (transitions) are depicted by the arrows. Same-colour arrows represent coupled transitions. In all cases, the commutator between the transitions depicted by dashed blue and dash-dotted green arrows result in transitions depicted by solid red arrows. The four panels present the following cases: **(a)** Graphical commutator between two uncoupled transitions $[(0,1),(0,2)] = (1,2)$ **(b)** Graphical commutator between the coupled transitions $\{(0,3),(1,4)\}$ and the uncoupled transition $(1,2)$ results in the uncoupled transition $(2,4)$ **(c)** Graphical commutator between the coupled transitions $\{(0,1),(2,3)\}$ and the uncoupled transition $(1,2)$ results in the coupled transition $\{(0,2),(1,3)\}$. **(d)** The commutator between the coupled transitions $\{(0,2),(1,3)\}$ and $\{(0,1),(2,3)\}$ cannot be determined graphically.

$\{(0,1),(2,3)\}$ (dashed blue arrows) and $\{(0,2),(1,3)\}$ (dash-dotted green arrows). The graphical commutators $[(0,1),(0,2)]$ and $[(1,3),(2,3)]$ both result in the transition $(1,2)$. Without further knowledge of the coefficients of the corresponding Lie algebra elements, it is not possible to determine whether the two terms result in a non-zero transition $(1,2)$, or whether they cancel each other.

In such cases, we make use of an alternative procedure to decouple resonant transitions, which takes into account that in qubit systems, the same (coupled) transitions are often driven by different controls. Consider a system with drift $\hat{H}_0$ and two controls that both drive the two resonant transitions $\{(1,2),(3,4)\}$. The Lie algebra of the system thus contains the terms

$$\begin{aligned}\hat{T}_4 &= \alpha_4\hat{F}_{1,2} + \beta_4\hat{G}_{1,2} + \gamma_4\hat{G}_{3,4} + \delta_4\hat{G}_{3,4}\,,\\ \hat{T}_5 &= \alpha_5\hat{F}_{1,2} + \beta_5\hat{G}_{1,2} + \gamma_5\hat{G}_{3,4} + \delta_5\hat{G}_{3,4}\,.\end{aligned} \tag{4.5}$$

The two transitions $(1,2)$ and $(3,4)$ are decoupled if $\hat{T}_6 := \alpha_6\hat{F}_{1,2}+\beta_6\hat{G}_{1,2}$ is an element of the Lie algebra $Lie(i\hat{H}_0,\hat{T}_4,\hat{T}_5)$ for any real $\alpha_6,\beta_6$ (at least one of them nonzero). This is true if and only if $dim\left[Lie(i\hat{H}_0,\hat{T}_4,\hat{T}_5)\right] = dim\left[Lie(i\hat{H}_0,\hat{G}_{1,2},\hat{G}_{3,4})\right] = 7$, i.e., when the generated sub-algebra has maximum dimension (for a given number of transitions). Note that we have deliberately chosen transitions $\{(1,2),(3,4)\}$, which have no vertex in common, i.e., they are disjoint. Restricting ourselves to disjoint transitions, the maximum dimension of the generated sub-algebra is $3n_t+1$, where $n_t$ is the number of transitions that are coupled. In order to determine, if a set of $n_t$ transitions driven by $n_t$ different controls is decoupled, it is thus sufficient to calculate the dimension of the sub-algebra with maximal dimension $3n_t+1$. This is typically much smaller than the dimension of the Lie algebra of the complete system. If the transitions are not disjoint, the dimension of the relevant subalgebra scales quadratically with the number of transitions $n_t$. This, although feasible for a small number of transitions, would make the construction of the subalgebras more demanding

In the following we use both methods, i.e., graphical commutators and the calculation of the dimension of small sub-algebras, in order to decouple resonant transitions. This allows us to extend the graph test for controllability to coupled susbystems with resonant transitions.

### 4.3.2 Algorithms for graph test of controllability for coupled subsystems with resonant transitions

Our graph test for controllability of a quantum system with resonant transitions is divided into several steps, depicted in Figure 4.2. The main output of the complete

algorithm is a variable conveying whether the system is controllable, not controllable or whether the test remains inconclusive.

As can be seen in Figure 4.2, the first stage is creating the initial graph of the quantum system (A1). The step-by-step definition is found in algorithm 4.1. To compute this graph, we diagonalize the drift $\hat{H}_0$, taking its eigenstates as the vertices of the graph. Then, we determine the nonzero transitions $\langle e_a| \hat{H}_j |e_b\rangle$ for all $m$ controls and take these to be the edges $(a, b)$ of the graph. Numerically, we take into account all transitions that are larger or equal than a certain tolerance, $\delta_H > 0$, i.e.,

$$\left|\langle e_a| \hat{H}_j |e_b\rangle\right| \geq \delta_H \quad \longrightarrow \quad (a, b)\,. \tag{4.6}$$

The next step is to determine which transitions are coupled. As defined in section 4.2, two or more transitions are coupled if and only if they have the same energy gap and are generated by the same control. Any transition not coupled to any other one is by definition a decoupled transition. Note that two transitions generated by different controls can never be coupled to one another. To numerically compare the energy gaps, we define a minimal tolerance $\delta_E > 0$ such that two transitions driven by the same control, $(a, b)$ and $(c, d)$, are considered coupled if $|\Delta E_{a,b} - \Delta E_{c,d}| \leq \delta_E$.

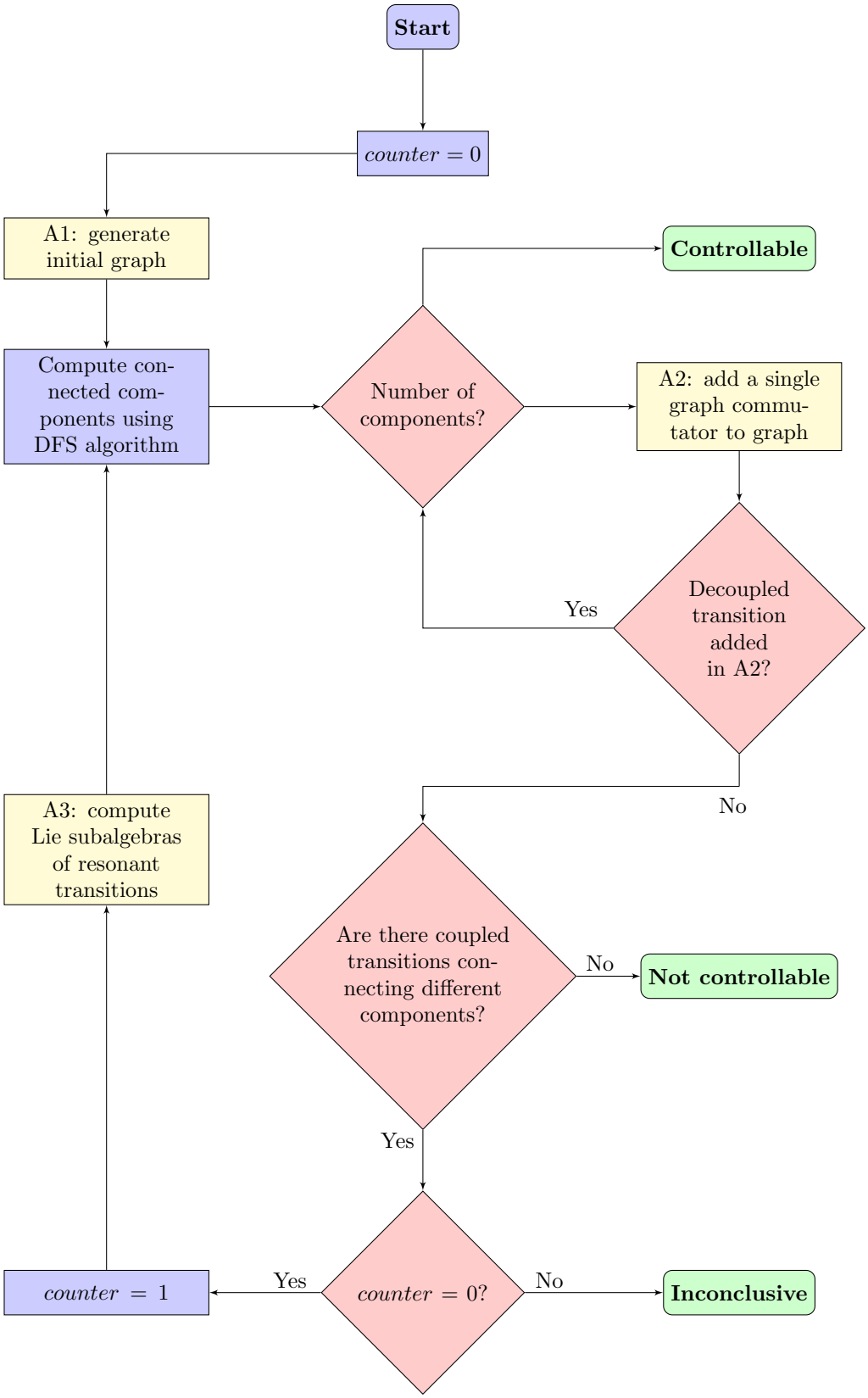


**Figure 4.2:** Flowchart representing the necessary steps and order in which the three main subroutines (A1-3) are used. The three possible results for this test are displayed in the three green round cells.

**Algorithm 4.1:** Compute the initial graph of the system

Input:

- ***H_op***: list including the drift $\hat{H}_0$ and all control operators $\hat{H}_j$ in the logical basis.
- $\delta_{\mathbf{H}}$: minimum tolerance for a nonzero transition coefficient.
- $\delta_{\mathbf{E}}$: minimum tolerance for two energy gaps to be identical.

Diagonalize $\hat{H}_0$ and represent all control operators $\hat{H}_j$ in the eigenbasis of $\hat{H}_0$.
Initialize *decoupled-graph*, representing every eigenstante $|e_a\rangle$ of $\hat{H}_0$ as a vertex in the graph.
**for** *every control* $\hat{H}_j$ *in H_op* **do**
    **for** $0 \leq a < b <$ *Hilbert space dimension* **do**
        **if** $\left|\langle e_a| \hat{H}_j |e_b\rangle\right| > \delta_H$ **then**
            Add $(a, b)$ to *transition-list*.
        **end if**
    **end for**
    Sort *transition-list* by the energy gaps $\Delta E_{a,b} := |E_a - E_b|$
    **for** *every* $(a, b)$ *in transition-list* **do**
        Add all transitions $(c, d)$ resonant to $(a, b)$ (i.e. $|\Delta E_{a,b} - \Delta E_{c,d}| < \delta_E$) to a new, separate list *resonant-trans-ab* (including $(a, b)$).
        Add coefficients $\langle e_c| \hat{H}_j |e_d\rangle$ of all resonant transitions $(c, d)$ into a new list *resonant-coef-ab* (including $(a, b)$).
        **if** *resonant-trans-ab has more than one element* **then**
            Add *resonant-trans-ab* as a new entry in the list *coupled-transitions*.
            Add *resonant-coef-ab* as a new entry in the list *coupled-coefficients*.
        **else**
            Add *resonant-trans-ab* as a decoupled transition in *decoupled-graph*.
        **end if**
        Remove all resonant transitions $(c, d)$ and $(a, b)$ from *transition-list*.
    **end for**
**end for**
Output:

- ***decoupled-graph***: a dictionary containing all vertices of the graph (eigenstates of $\hat{H}_0$) and all decoupled transitions as edges.
- ***coupled-transitions***: a list of lists containing all coupled transitions stored as dictionaries and sorted by their respective energy gap $\Delta E_{a,b}$. Resonant transitions from the same control with the same $\Delta E_{a,b}$ are stored in the same inner list since they are coupled.
- ***coupled-coefficients***: a list of lists of the transition coefficients, matching the order of *coupled-transitions*.

**Algorithm 4.2:** Add a single decoupled transition using graphical commutators

Input:
- ***decoupled-graph***: from algorithm 4.1.
- ***graph-components***: list containing the sets representing the connected components of *decoupled-graph*.
- ***coupled-transitions***: from algorithm 4.1.

*transition-added* = False
*connecting-transitions-found* = False
$i = 0$
**while** *($i$ < length of coupled-transitions)* ***and*** *(transition-added = False)* **do**
    $i = i + 1$
    *element_i = coupled-transitions*[$i$]
      # element_i is a set of coupled transitions of the form $\{(a_0, a_1), (a_2, a_3), ...\}$
    $j = 0$
    **while** *($j$ < length of element_i)* ***and*** *(transition-added = False)* **do**
        $j = j + 1$
        $(b_0, b_1)$ = *element_i*[$j$]
        **if** $b_0$ *and* $b_1$ *belong to different components in graph-components* **then**
            *connecting-transitions-found* = True
            *component_0* = component in *graph-components* containing $b_0$
            *component_1* = component in *graph-components* containing $b_1$
            $k = 0$
            **while** *($k$ < number of transitions in decoupled-graph)* ***and*** *(transition-added = False)* **do**
                $k = k + 1$
                $(c_0, c_1)$ = $k$-th transition in *decoupled-graph*
                **if** *($\{c_0, c_1\} \subset$ component_0)* ***or*** *($\{c_0, c_1\} \subset$ component_1)* **then**
                    *graphical-commutator* = [*element_i*, $(b_0, b_1)$]
                    **if** *graphical-commutator is a single transition* **then**
                        *transition-added* = True
                        Add *graphical-commutator* to *decoupled-graph*
                        Merge *component_0* and *component_1* in *graph-components*
                    **end if**
                **end if**
            **end while**
        **end if**
    **end while**
**end while**

Output:
- ***decoupled-graph***: updated after the routine.
- ***graph-components***: updated after the routine.
- ***transition-added***: True if a transition was added during this subroutine to *decoupled-graph*; False otherwise.
- ***connecting-transitions-found***: True if at least one transition in *coupled-transitions* connects different components; False otherwise.

**Algorithm 4.3:** Subroutine to compute subalgebras of repeated resonant transitions

Input:
- ***decoupled-graph***: from algorithm 4.2.
- ***graph-components***: from algorithm 4.2.
- ***coupled-transitions***: from algorithm 4.1.
- ***coupled-coefficients***: from algorithm 4.1.

**for** *every set of resonant transitions* $\{(a_0, a_1), (a_2, a_3), ...\}$ *in coupled-transitions* **do**
  *resonant-set* $= \{(a_0, a_1), (a_2, a_3), ...\}$
  **if** *resonant-set contains only disjoint transitions* **then**
    **if** *resonant-set connects different components in graph-components* **then**
      **if** *resonant-set appears multiple times in coupled-transitions* **then**
        Set $m$ as the number of times *resonant-set* is generated by different controls.
        Set $n_t$ as the number of coupled transitions in *resonant-set*
        **for** $0 \leq j < m$ **do**
          Using the coefficients in *coupled-coefficients* related to the $j$-th instance of *resonant-set*, generate an array *T-array-j* to represent the transition.
          #
          $\hat{T}_j = \alpha^{(j)}_{a_0,a_1}\hat{F}_{a_0,a_1} + \beta^{(j)}_{a_0,a_1}\hat{G}_{a_0,a_1} + \alpha^{(j)}_{a_2,a_3}\hat{F}_{a_2,a_3} + \beta^{(j)}_{a_2,a_3}\hat{G}_{a_2,a_3} + ...$
          # *T-array-j* $= \left(\alpha^{(j)}_{a_0,a_1}, \beta^{(j)}_{a_0,a_1}, 0, \alpha^{(j)}_{a_2,a_3}, \beta^{(j)}_{a_2,a_3}, 0, ...\right)$
        **end for**
        **if** $dim\left(Lie\left\{i\hat{H}_0, \textit{T-array-0}, ..., \textit{T-array-m}\right\}\right) = 3n_t + 1$ **then**
          Add every transition in *resonant-set* to *decoupled-graph*
        **end if**
      **end if**
    **end if**
  **end if**
**end for**

Output:
- ***decoupled-graph***: updated after the routine.

We sort all the transitions of each control according to the energy gaps $\Delta E_{a,b}$ and separate them depending on whether they are coupled or not. If a coupled transition $(a,b)^{(j)}$ is generated by multiple controls $\hat{H}_j$, we also calculate and store the corresponding transition coefficients $\langle e_a| \hat{H}_j |e_b\rangle = \alpha_{a,b}^{(j)} + \beta_{a,b}^{(j)} i$. Note that here, we have introduced the notation $(a,b)^{(j)}$ to indicate that the transition $(a,b)$ is driven by the control $\hat{H}_j$.

The output of algorithm 4.1 encompasses the *decoupled-graph*, the *coupled-transitions* and the *coupled-coefficients*. The first output, *decoupled-graph*, is a dictionary that contains all vertices (eigenstates) and all decoupled edges (decoupled transitions) of the systems graph. These are the elements that we can use directly to test the controllability of the system using Theorem 4.2.1. In the second output, *coupled-transitions*, every set of coupled transitions is stored as a list of tuples $(a,b)$. Coupled transitions cannot be immediately used for the test in Theorem 4.2.1, but are necessary for generating additional decoupled transitions, by using graphical commutators or subalgebras of resonant transitions. The last output variable *coupled-coefficients* consists of the entries $\langle e_a| \hat{H}_j |e_b\rangle = \alpha_{a,b}^{(j)} + \beta_{a,b}^{(j)} i$ for every coupled transition $(a,b)^{(j)}$ which are required for calculating the dimension of the subalgebras.

Once the initial graph of the system has been computed, we check if the graph containing only decoupled transitions (*decoupled-graph*) is connected. To do so, we determine the number of connected components in the graph. In terms of graph theory, a component is a connected subgraph that it is not contained in any larger connected subgraph. In other words, each of the connected parts into which we can divide a graph is called a component of the graph. Therefore, the graph is connected if and only if it has exactly one component. One of the many possible ways to count the number of components is to use the depth-first search (DFS) algorithm[2]. If the *decoupled-graph* is already connected, we can stop the routine and state that the system is indeed controllable.

If the graph is not connected, then algorithm 4.2 is called. The aim of this algorithm is to search for an additional edge of the graph by using graphical commutators. As explained in section 4.2, the graphical commutators of a coupled transition and a decoupled transition may generate a new decoupled transition. Note that, instead of identifying and adding every possible combination of commutators between a decoupled transition and a set of coupled transitions, we are only interested in commutators that result in a decoupled transition which connects different components of the graph and therefore potentially creates a connected graph. That is, in algorithm 4.2 we compute the commutator of a coupled transition that connects two separate components

[2]The DFS algorithm is a common recursive algorithm to explore systematically all vertices in a graph. It uses an exhaustive search by traversing down a chain of edges, or by backtracking when not possible.

of *decoupled-graph* with a decoupled transition in one of the two components. If the result of this commutator is a decoupled transition, then this new edge will connect the two components in *decoupled-graph*, merging them into a single component. If a new decoupled transition is added to the *decoupled-graph* during this step, the number of connected components is counted again to determine if the graph is now connected.

If the number of components is still larger than one, i.e. if the *decoupled-graph* is not connected after algorithm 4.2, and no new transition was added during its last call, then we check if there is any transition in *coupled-transitions* that connects different components of *decoupled-graph*. If this is not the case, the routine is stopped. If all transitions, coupled and decoupled, only connect vertices within the same components, then all possible commutators result in transitions within the same components. The number of components will stay constant and the graph will never be connected. This implies that the system is not controllable.

However, if there exists at least one coupled transition connecting different components, then this argument is no longer valid and the controllability of the system is not yet decided. For these cases, we use the *coupled-coefficients* that are related to the *coupled-transitions* to obtain a more conclusive answer.

This step is carried out by algorithm 4.3. It builds upon the updated *decoupled-graph* from algorithm 4.2 and tries to add new decoupled transitions by computing the low-dimensional subalgebras of resonant transitions driven by different controls. First, the algorithm selects the transitions from *coupled-transitions* that connect different components. In particular, we are exclusively interested in sets of disjoint transitions, such that the dimension of the associated subalgebras remains low. Next, the algorithm finds out if those transitions have a multiplicity equal to or higher than 2, that is, if the same sets of coupled transitions $\{(a_0, a_1), (a_2, a_3), ...\}^{(j)}$ are generated multiple times by different controls $\hat{H}_j$. Following the reasoning presented in section 4.3.1, we try to generate the full associated subalgebra of the *coupled-transitions*, $\{(a_0, a_1), (a_2, a_3), ...\}$, by using their respective *coupled-coefficients*. If a subalgebra with maximal dimension is generated, we take all transitions $\{(a_0, a_1), (a_2, a_3), ...\}$ as effectively decoupled. This allows us to add every transition $(a_k, a_l)$ as a decoupled edge to *decoupled-graph*. Note that in algorithm 4.3, we compute the Lie subalgebras of the resonant transitions including $i\hat{H}_0$, where we deduce the commutators $\left[i\hat{H}_0, \{(0,1),(2,3)\}^{(j)}\right]$ using Equation (4.2). This makes these calculations simple and encompassed within a vector space of dimension $3n_t$, with $n_t$ being the number of transitions in $\{(a_0, a_1), (a_2, a_3), ...\}$.

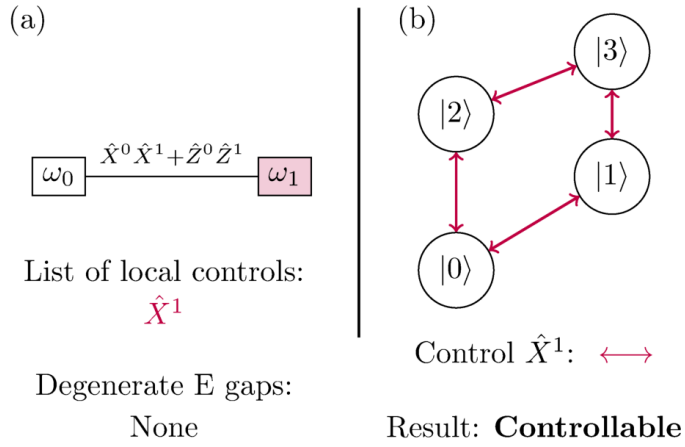


**Figure 4.3:** **(a)** Two-qubit system with Hamiltonian (4.7), where $\omega_0 = 5$ GHz, $\omega_1 = 5.5$ GHz, $J = 150$ MHz. **(b)** Graph of the system. All transitions are decoupled, making the system controllable by Theorem 4.2.1.

Finally, we compute the new number of components in *decoupled-graph* using DFS once again. If the graph is still not connected, we use algorithm 4.2 to add as many graphical commutators as possible to connect the remaining components. If the graph ends up with one single component, the system is controllable. If there are more components and there are no transitions in *coupled-transitions* that connect any of them, then the system is proven to be not controllable. If none of these two hold to be true, then the controllability test remains inconclusive. Indeed, unlike the dynamical Lie algebra method, the test might yield no definitive answer. If a graph is not connected, we cannot ensure that the system is not controllable, generally speaking. It might be that the graph can be connected after computing a large number of commutators or that it will remain forever not connected. Calculating this quantity of commutators is tantamount to computing the dynamical Lie algebra and would therefore be unfeasible for relatively large systems.

### 4.3.3 Illustrative examples

Here we present two examples constructed to showcase how the algorithms described in section 4.3.2 work. We start by considering the two-qubit system shown in Figure 4.3(a), described by the Hamiltonian

$$\hat{H}_{2A}(t) = \hat{H}_0 + u_1(t)\hat{H}_1 \tag{4.7}$$

with the drift

$$\hat{H}_0 = \sum_{i=0}^{1} -\frac{\omega_i}{2}\hat{Z}^{(i)} + J\left(\hat{X}^{(0)}\hat{X}^{(1)} + \hat{Z}^{(0)}\hat{Z}^{(1)}\right), \tag{4.8}$$

and a single local control $\hat{H}_1 = \hat{X}^{(1)}$ acting on qubit 1. Here, $\omega_i$ are the natural frequencies of the qubits and $J$ is the coupling strength. For simplicity, we use the

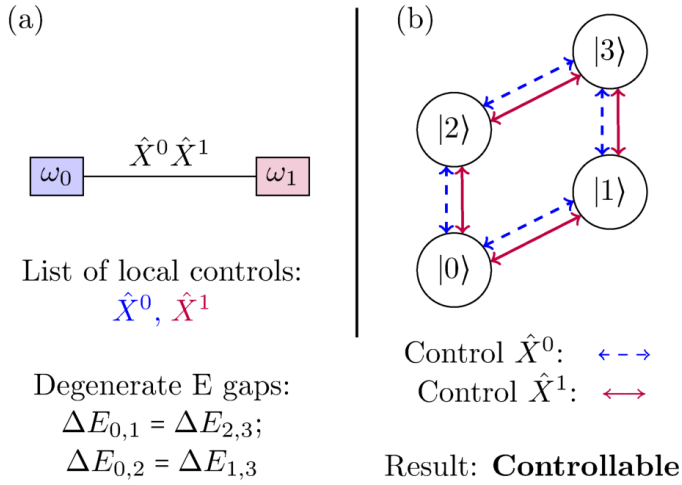


**Figure 4.4:** **(a)** Two-qubit system with Hamiltonian (4.9) where $\omega_0 = 5$GHz, $\omega_1 = 5.5$ GHz, $J = 150$ MHz. Both local controls are necessary for the system to be controllable. **(b)** Graph of the system. Theorem 4.2.1 is not directly applicable due to the coupled transitions. A study of the coefficients reveals that it is possible to decouple all transitions.

notation $\hat{X}^{(j)} = \hat{\sigma}_x^j$ for the Pauli matrices. Algorithm 4.1 results in the graph shown in Figure 4.3(b) with the circular vertices representing the eigenstates of $\hat{H}_0$. The local control $\hat{H}_1$ gives rise to four non-zero transitions, which form the edges of the graph, denoted by the arrows in Figure 4.3(b). The different lengths of the arrows indicate that all four transitions have different energy gaps and are thus decoupled. The actual controllability test for this example consists simply of algorithm 4.1 and the DFS algorithm, which proves that the graph is connected and the system is controllable. In other words, from every vertex $i = 0, ...3$, every other vertex of the graph can be reached by following the edges belonging to decoupled transition, as seen in Figure 4.3(b).

A second example is illustrated in Figure 4.4(a). Here, the Hamiltonian is given by

$$\hat{H}_{2B}(t) = \hat{H}_0 + \sum_{j=1}^{2} u_j(t)\hat{H}_j \tag{4.9}$$

with the drift

$$\hat{H}_0 = \sum_{i=0}^{1} -\frac{\omega_i}{2}\hat{Z}^{(i)} + J\hat{X}^{(0)}\hat{X}^{(1)}\,, \tag{4.10}$$

and two local controls

$$\hat{H}_1 = \hat{X}^{(1)} \qquad \text{and} \qquad \hat{H}_2 = \hat{X}^{(0)} \tag{4.11}$$

acting on the qubits 1 and 0, respectively. The main difference between Equation (4.9) and Equation (4.7) is the omission of $\hat{Z}^{(0)}\hat{Z}^{(1)}$ in the drift Hamiltonian. This

| | Transition parameters | | | |
|---|---|---|---|---|
| | $(0,1)$ | $(2,3)$ | $(0,2)$ | $(1,3)$ |
| $\hat{X}^{(0)}$ | $0.967$ | $0.967$ | $-0.253$ | $0.253$ |
| $\hat{X}^{(1)}$ | $-0.281$ | $0.281$ | $-0.960$ | $-0.960$ |

**Table 4.1:** Control coefficients $\langle e_a| \hat{H}_j |e_b\rangle$ for the system (4.9). The coupled transitions are $\{(0,1),(2,3)\}$ and $\{(0,2),(1,3)\}$. They appear with double multiplicity, once for each control.

severely impacts the graph, as seen in Figure 4.4. The symmetries that had previously been broken by including $\hat{Z}^{(0)}\hat{Z}^{(1)}$ appear in the energy gap degeneracies, $\Delta E_{0,1} = \Delta E_{2,3}$ and $\Delta E_{0,2} = \Delta E_{1,3}$. There are no decoupled transitions and the number of components in the initial graph is equal to four. A second difference is the second local control. The transitions driven by the controls $\hat{X}^{(1)}$ (which is the same local control as in Equation (4.7)) and $\hat{X}^{(0)}$ consist of two pairs of coupled transitions $\{(0,1),(2,3)\}$ and $\{(0,2),(1,3)\}$ shown by purple solid and dashed blue arrows respectively in Figure 4.4(b).

In this example, graphical commutators do not yield any new transition that we could add to the graph. In fact, we can only take commutators of pairs of coupled transitions, analogously to the case depicted in Figure 4.1(d). Since there is no definitive answer, graphical commutators are not useful in this particular instance. However, since there exist coupled transitions which connect different components of the graph, algorithm 4.3 can be applied. The coefficients $\langle e_a| \hat{H}_j |e_b\rangle = \alpha^{(j)}_{a,b} + \beta^{(j)}_{a,b} i$ of the coupled transitions are shown in Table 4.1. Note that in this example, the coefficients are real, $\beta^{(j)}_{a,b} = 0$. The Lie algebra thus contains the terms

$$\begin{aligned} \hat{T}_0 &= \alpha^{(0)}_{0,1}\hat{F}_{0,1} + \alpha^{(0)}_{2,3}\hat{F}_{2,3}\,, \\ \hat{T}_1 &= \alpha^{(1)}_{0,1}\hat{F}_{0,1} + \alpha^{(1)}_{2,3}\hat{F}_{2,3}\,. \end{aligned} \tag{4.12}$$

It is immediate to see that we can isolate the term $\hat{F}_{2,3}$ by a linear combination of $\hat{T}_0$ and $\hat{T}_1$. This means that all operators $\hat{F}_{2,3}, \hat{G}_{2,3}, \hat{D}_{2,3}$ are elements of the subalgebra. Similarly, the opposite linear combination can isolate the element $\hat{F}_{0,1}$, adding $\hat{F}_{0,1}, \hat{G}_{0,1}, \hat{D}_{0,1}$ to the generated subalgebra. This means that the dimension of $Lie\left(i\hat{H}_0, \hat{T}_0, \hat{T}_1\right) = 7$ (including the contribution of $i\hat{H}_0$) is maximal and thus the transitions $(0,1)$ and $(2,3)$ can be decoupled. Analogously, $(0,2)$ and $(1,3)$ may be decoupled as well. This means that all the edges are decoupled in the graph of Figure 4.4. By virtue of Theorem 4.2.1, this implies controllability of the system.

| Coupling strengths (MHz) | | | |
|---|---|---|---|
| $J_{0,1}$ | $J_{1,2}$ | $J_{1,3}$ | $J_{3,4}$ |
| 100 | 250 | 170 | 300 |
| **Qubit frequencies (GHz)** | | | |
| $\omega_0$ | $\omega_1$ | $\omega_2$ | $\omega_3$ | $\omega_4$ |
| 5.301 | 5.081 | 5.322 | 5.164 | 5.052 |

**Table 4.2:** Parameters for the system (4.13). The qubit frequencies are those of [21]. The coupling strengths have been chosen to be in the range of hundreds of MHz, common for this type of qubits.

## 4.4 Results

In this section, we examine qubit systems which are used for quantum computing. With the algorithm presented in section 4.3, we can efficiently prove if a given qubit array is controllable. We present three different examples based on the IBM five-qubit array *ibmq_quito* [21]. We do not use the exact parameters of this system, but simply its configuration and realistic parameters (except for the natural frequencies which correspond to the real data [21]).

The Hamiltonian of an array similar in structure to *ibmq_quito* can be expressed as:

$$\hat{H}^{quito}(t) = -\sum_{j=0}^{4} \frac{\omega_j}{2} \hat{Z}^{(j)} + \hat{H}_c^{quito} + \sum_{k=1}^{m} u_k(t) \hat{H}_k \,, \tag{4.13}$$

where $u_k(t)$ represent local controls and the couplings $\hat{H}_c^{quito}$ are of the form

$$\hat{H}_c^{quito} = J_{0,1}\hat{H}_{0,1} + J_{1,2}\hat{H}_{1,2} + J_{1,3}\hat{H}_{1,3} + J_{3,4}\hat{H}_{3,4} \tag{4.14}$$

with each $\hat{H}_{j,k}$ representing an entangling (time-independent) coupling between the qubits $j$ and $k$. The following three examples are based on Equation (4.13) for different types of couplings and local controls. We will prove that while the original IBM design is indeed controllable there exist options that require fewer resources for controllability.

The set of parameters, including the natural frequencies $\omega_j$ and the coupling strengths $J_{i,j}$ are found in Table 4.2. We use these parameters for all examples presented in this section.

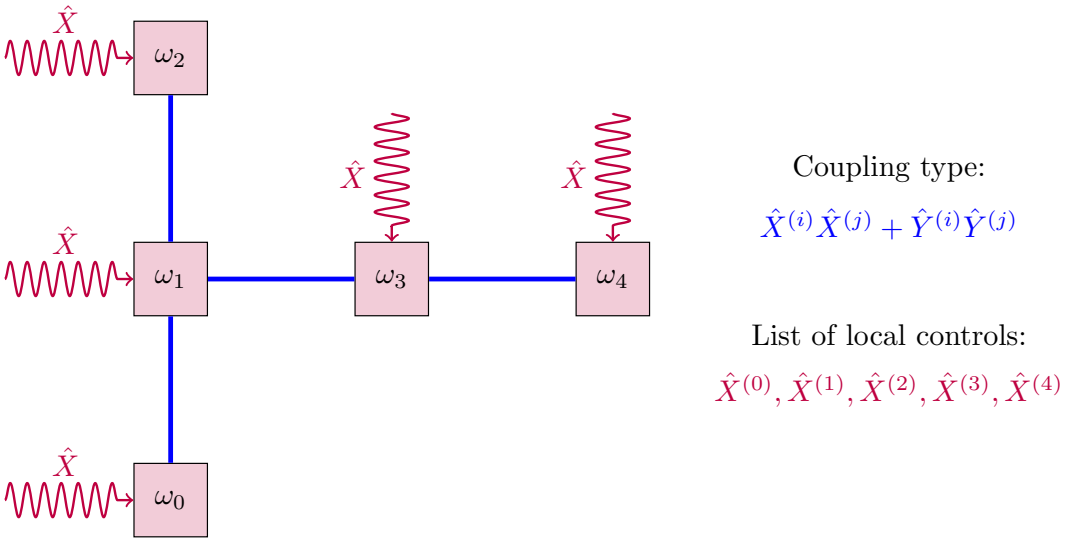


**Figure 4.5:** Five-qubit system inspired by IBM's *ibmq_quito* with Hamiltonian found in Equation (4.13). The rectangles present the qubits with natural frequencies $\omega_j$, $j = 1 - 5$, and the lines indicate the couplings between the qubits. Local controls are to be assumed in every qubit in the form of $\hat{X}^{(j)}$.

### 4.4.1 Example A: five-qubit system similar to *ibmq_quito*

This example mimics the qubit arrangement of *ibmq_quito*. The static couplings in Equation (4.14) are [147]

$$\hat{H}_{ij} = J_{i,j}\left(\hat{X}^{(i)}\hat{X}^{(j)} + \hat{Y}^{(i)}\hat{Y}^{(j)}\right). \tag{4.15}$$

A local control $\hat{H}_j = \hat{X}^{(j)}$ is added to every qubit. The system diagram is shown in Figure 4.5.

For a five-qubit system, there is a total of 32 vertices. After running algorithm 4.2 for this example with an energy gap tolerance of $\delta_E = 0.01$GHz, we obtain an initial graph with only 7 decoupled edges, resulting in a total of 25 different connected components. Use of algorithm 4.2 alone is not enough in this case, since the graphical commutators do not yield any new results. Executing algorithm 4.3, a total of 192 new edges are added to the graph. These turn out to be more than sufficient to connect all the components and achieve a connected graph.

We can thus conclude that the system presented in Figure 4.5 is controllable and therefore suitable to perform any unitary operation. In the following examples we investigate whether the five-qubit array is also controllable if the number of local controls is reduced.

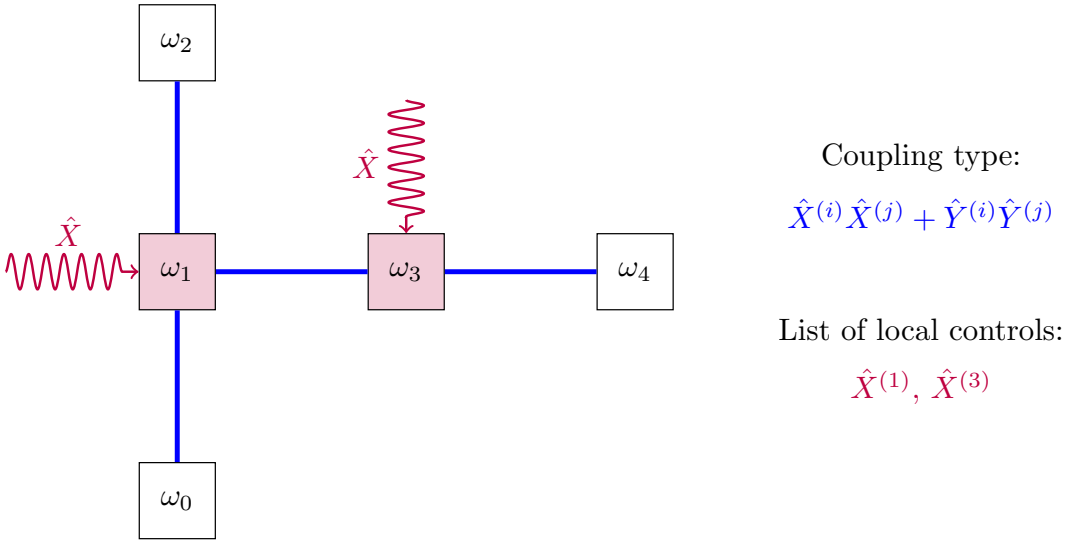


**Figure 4.6:** Same as Figure 4.5 with fewer controls, located on qubits 1 and 3 (pink rectangles).

### 4.4.2 Example B: five-qubit system with reduced number of controls

Next, we investigate the controllability of a five-qubit system with a reduced number of local controls. For the drift Hamiltonian, we consider the same five-qubit system as before with all parameters as listed in Table 4.2 but decrease the number of local controls to two. This is depicted in Figure 4.6, which represents one of the ten different scenarios with two local controls $\hat{H}_j = \hat{X}^{(j)}$.

Running algorithm 4.1 we obtain identical results to those in section 4.4.1: a graph with only 7 decoupled transitions and 25 different connected components. Again, it is crucial to use algorithm 4.3 to make the graph connected. It may come as a surprise that the number of new edges that we can add is again 192. In other words, the number of new decoupled edges has not been reduced by removing three of the local controls. With the new decoupled edges included, the system is indeed controllable.

We could attempt to take this study further to single local control. However, with a single local control $\hat{X}^{(j)}$, we always obtain an inconclusive result, no matter on which qubit we apply it. Although this hints to the possibility of the system not being controllable, the algorithm cannot conclusively determine it, similarly to the case shown in Figure 4.4. In that two-qubit example we can prove using the Lie algebra method that a single local control $\hat{X}^{(j)}$ is never sufficient. We therefore conjecture that the least number of local controls required for the system to be controllable is two. One may wonder whether independent $\hat{X}^{(j)}$- and $\hat{Y}^{(j)}$-controls acting on the same qubit change the controllability. Assuming the local, field-free Hamiltonians to be proportional to $\hat{Z}^{(j)}$, there is no additional benefit from a second control, since a

| Distance | Controllability | # cases |
|---|---|---|
| 1 | Controllable | 4 |
| 2 | Inconclusive | 4 |
| 3 | Controllable | 2 |

**Table 4.3:** Study of controllability for a five-qubit system similar to *ibmq_quito* but with only two local controls.

single local control $\hat{X}^{(j)}$ that does not commute with $\hat{H}_0$ is sufficient to also generate a $\hat{Y}^{(j)}$ contribution and viceversa.

Since two local controls is the minimum number to obtain a controllable system, we now study how the position of the control affects controllability. We categorize all possible arrangements of two local controls $\hat{X}^{(j)}$ by their distance. For example, the local controls for qubits 1 and 3, shown in Figure 4.6, have distance equal to 1 since they are direct neighbors connected by a single coupling. Analogously, we can set local controls separated by two couplings (e.g. on qubit 2 and 3) that have distance 2, or local controls for qubits separated by three couplings (e.g qubits 0 and 4) that have distance 3. The results of the controllability tests for all these possible arrangements of two local controls are shown in Table 4.3.

Accordingly, the five-qubit system is controllable with two local controls if they have either distance one or three, independent of the position of the controls themselves. On the other hand, if the controls are at distance 2, the algorithm returns an inconclusive answer. This implies that algorithm 4.3 cannot decouple enough transitions for the graph to be connected. In fact, it turns out that no new transitions could be added at all. This is because the coefficients $\langle e_a| \hat{H}_j |e_b\rangle$ of the different transitions depend on the position of the local control that drives them. By shifting a local control to a neighboring qubit, it is common to see a change in some of the coefficients. The transition coefficients of same-type controls for a set of coupled transitions tend to be linearly independent when the controls are shifted by an odd number of qubits and dependent in the even case. This allows us to generate maximal subalgebras only for controls that are at an odd qubit-distance, turning the coupled transitions into decoupled transitions that can eventually make the graph connected.

### 4.4.3 Example C: five-qubit system with single local control

To conclude the list of examples, we demonstrate that the number of local controls that is required for the system to be controllable also depends on the type for couplings connecting the qubits. We showcase a system that is controllable with a minimal number of local controls, i.e., a single local control. The main difference between this

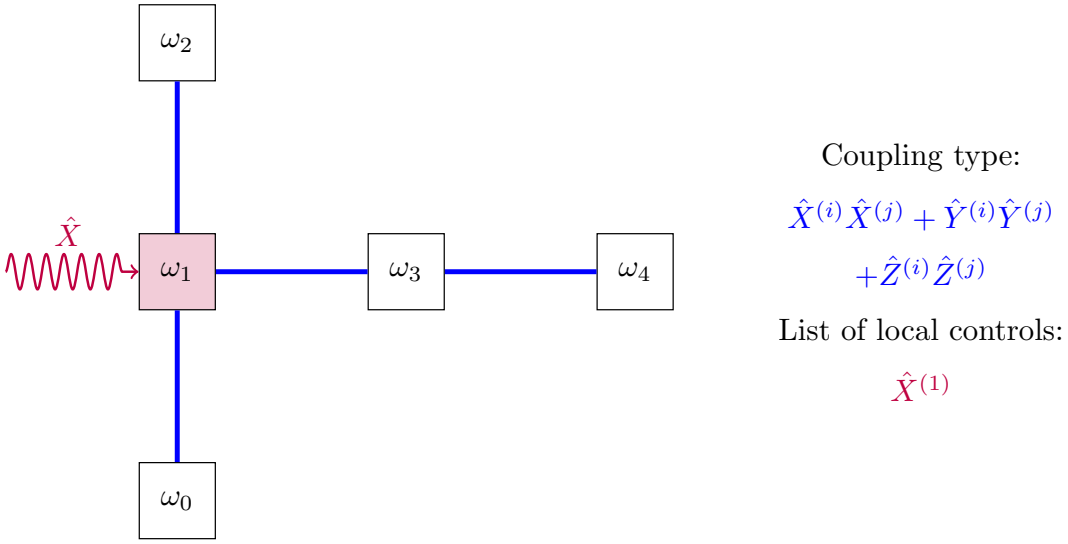


**Figure 4.7:** Diagram introducing a modified version of IBM's *ibmq_quito* with $\hat{Z}\hat{Z}$ contributions added to every coupling and all local controls removed except for $\hat{X}^{(1)}$.

example (shown in Figure 4.7) and the previous ones (displayed in Figure 4.5 and 4.6) is that the couplings are of the form

$$\hat{H}_{ij} = J_{i,j}\left(\hat{X}^{(i)}\hat{X}^{(j)} + \hat{Y}^{(i)}\hat{Y}^{(j)} + \hat{Z}^{(i)}\hat{Z}^{(j)}\right), \tag{4.16}$$

i.e., they have an extra term $\hat{Z}^{(i)}\hat{Z}^{(j)}$ compared to the couplings considered in the examples before. These kinds of couplings can be achieved in systems of superconducting qubits by harnessing both capacitive and inductive interactions between the qubits. Executing algorithm 4.1 with $\delta_E = 0.1$GHz, we obtain a total of 24 initially decoupled edges and a total of 14 connected components. This is already more promising than the examples in section 4.4.1 and section 4.4.2. Furthermore, use of graphical commutators results in the system being controllable, ending up with 37 decoupled edges that are sufficient to make the graph connected. The controllability analysis thus shows that with the $\hat{Z}^{(i)}\hat{Z}^{(j)}$ addition, the system is controllable with only one local control. In Figure 4.7, we have added a local control on qubit 1, but additional tests show that the same statement is true for any single local control $\hat{X}^{(j)}$, independent of its position at qubit 0 to 4. Therefore, this controllable system has a minimal number of local controls at the cost of using a more complex type of two-qubit couplings.

The effect of couplings of the form $\hat{Z}^{(i)}\hat{Z}^{(j)}$ on the graph of the system had been shown in [1]. They can be understood by considering the simple two-qubit systems shown in Figure 4.3 and Figure 4.4. In Figure 4.4, couplings of the form $\hat{X}^{(i)}\hat{X}^{(j)}$ result in two pairs of resonant (coupled) transitions for each local control. Therefore, two local controls are required to decouple the transitions and ensure controllability. In Figure 4.3, a single control $\hat{X}$ is sufficient due to the $\hat{Z}^{(0)}\hat{Z}^{(1)}$ term in its coupling.

This term is already diagonal in the eigenbasis of the free qubits, which means that it does not mix the eigenstates of the free qubits. However, it shifts their eigenenergies, such that all four vertices of the graph correspond to different transition frequencies and thus a single local control corresponds to four decoupled transitions, making the system controllable. A similar effect happens in the present five-qubit example, where the couplings have an off-diagonal contribution $\hat{X}^{(i)}\hat{X}^{(j)} + \hat{Y}^{(i)}\hat{Y}^{(j)}$ and a diagonal part $\hat{Z}^{(i)}\hat{Z}^{(j)}$. The former mixes the free-qubit eigenstates and in turn creates more edges in the graph with the inclusion of a local control like $\hat{X}^{(j)}$. The latter changes some resonant energy gaps and decouples the transitions associated to them. The combination of these two effects achieves controllability with a minimal number of local controls, as seen in Figure 4.7. The special role of this coupling has already been observed for spin systems, where spin chains have been proven to be controllable with a number of local controls smaller than the number of spins [134].

## 4.5 Summary

We have presented a practical way to test for operator controllability in order to numerically verify the ability of a given qubit array to implement universal quantum computing. The graph theory-based approach allows for analyzing comparatively large qubit systems for which the evaluation of the Lie rank condition for controllability would be difficult or impossible. Indeed, the computationally expensive calculation of nested commutators of the drift and control Hamiltonians, which is required to construct the system's dynamical Lie algebra, is avoided in graphical methods. On the other hand, in some cases, a graphical controllability test remains inconclusive. We believe that the disadvantage is small in view of the positive results that can be obtained for systems not amenable to the Lie rank condition.

The key challenge in controllability tests for systems of coupled qubits using graph theory-based methods is due to the tensor product structure of Hilbert space. This leads to graphs that often consist of sets of coupled (resonant) transitions. A similar problem was encountered in the controllability analysis of driven quantum rotors [17] which are highly degenerate systems with multiple resonant transitions. In that case, the specific spectral structure allowed for an inductive evaluation of the graphical commutators [142]. Here, we have made no assumptions on the spectral structure of the system. Instead, we have found and implemented numerically efficient ways to decouple the resonant transitions such as to make them exploitable for the graph test. In particular, our algorithm only determines those graphical commutators which are relevant because they add to the connectivity of the graph. Moreover, we have made use of fact that in qubit arrays, coupled transitions are typically driven by several controls: These coupled transitions become decoupled if the dimension of the

subalgebra that they generate when driven by different controls is maximal. Since the sub-algebras are very small compared to the Hilbert space of the complete system, their numerical construction does not pose a challenge. The remaining limitation to the number of qubits $N_Q$, for which a controllability test can be carried out, is the exponential scaling of the Hilbert space dimension with $N_Q$ because the drift Hamiltonian (including the qubit-qubit couplings) needs to be diagonalized. Typically, the drift is sparse in the logical basis. For the graph test presented here, only a single diagonalization of the (sparse) drift Hamiltonian is necessary to obtain the initial graph.

We have illustrated the utility of our approach by showing how controllability analysis can be used to determine the minimum number of local controls required for universal quantum computing in existing quantum processing units. To this end, we have chosen the five-qubit array *ibmq_quito* [21] as specific example, treating the qubit-qubit couplings as fixed. This is justified since, whenever a system with time-independent couplings is controllable, the corresponding system with tunable couplings is controllable as well. The actual *ibmq_quito* system contains a local control for each of the five qubits. Our analysis has shown that by modifying the couplings between the qubits, the number of local controls necessary for universal quantum computing can be reduced to a single local control. For standard qubit-qubit couplings the minimal number of local controls is two. Analyzing the controllability for different positions of the two local controls reveals that the distance between the local controls is essential for the system to be controllable: The two local controls must be separated by an odd number (one or three) of qubit-qubit couplings in order to provide controllability and allow for universal quantum computing. These results showcase the utility of our graph test for improving the design and scalability of qubit arrays.

In future work, it will be interesting to gather a deeper understanding of the required control distance, as this might allow for generalizing our findings to larger qubit arrays. One natural next step will be extending our approach from local to non-local controls, as obtained when using e.g. tunable couplers. Our graph test is limited by the exponential scaling of the Hilbert space, a common issue among algorithms run on a classical computer, which can only be overcome by mapping the controllability analysis to a quantum device. Another important open question is the relationship between the minimal number of local controls and the quantum speed limit for universal quantum computing. The quantum speed limit [92] refers to the minimum time in which a quantum process, such as a quantum gate, can be executed. For a complete universal set of gates, the quantum speed limit can be obtained using quantum optimal control [75]. Given a quantum system and a set of controls, the time required for any particular operation will always be equal or longer than the

time required for the same operation in the same system with more controls added. Conversely, reducing the number of local controls is likely to increase the time needed to carry out a gate. Thus, reducing the number of local controls has to be balanced with the requirement of sufficiently fast logical operations. The minimal sets of local controls from controllability analysis as suggested here offers a good starting point to find the best balanced set of controls with quantum optimal control. Finally, a further important perspective for future work is the question of controllability of systems coupled to the environment. It will be interesting to see whether graph methods can be utilized in this context.

# 5 Controllability of qubit arrays using parametric quantum circuits

## 5.1 Introduction

Universal quantum computing [32] requires controllability on the quantum processing unit, so that every quantum logic gate can be implemented. A common layout in hardware platforms such as those based on superconducting circuits achieves this by combining two-qubit couplings with local drives for each qubit of the array [144, 11]. While effective, this approach becomes demanding for larger arrays, due to both the physical space needed for each control as well as the associated calibration. Controllability tests can help identify less resource-intensive architectures that are still capable of performing the same quantum gates [148].

Controllability in general studies the dynamics that can be implemented in a quantum system driven by a set of controls [14, 130, 12]. In particular, a system is pure-state controllable if it can reach all final states. Alternatively, an (evolution) operator controllable system is capable of implementing every unitary gate, a necessary feature for universal quantum computing. Tests for these two different types of controllability rely on computing the rank of the dynamical Lie algebra of the Hamiltonian [14] or utilize methods based graph theory [138, 15, 139, 148]. For small system sizes, the tests can be carried out analytically [13, 131, 132, 142]. For some high- and infinite-dimensional systems, controllability can be determined using induction arguments [16, 133, 15, 17]. Beyond these special cases, a numerical approach is possible in principle [148], but is limited by the exponential scaling of the Hilbert space dimension with respect to the number of qubits. In other words, the accuracy and feasibility of controllability tests for increasing system size suffer from the curse of dimensionality.

Here, we present a hybrid quantum-classical controllability test, for both pure-state and operator controllability of qubit arrays. The hybrid method we propose evaluates the controllability of the qubit array by measurements on a quantum device, either the system to be studied with an extra auxiliary qubit or one that mimics the dynamics

of the original system. This opens up a new way of designing controllable qubit arrays with fewer resources, helping to address the issue of scalability. To do so, we harness the computational power of quantum circuits to extract information directly from the qubit array under study. While this method relies on the same mathematical foundations behind the dynamical Lie algebra of the system, its design circumvents the issues that arise from finding a basis of the Lie algebra and all the orthonormalization calculations that it entails. Furthermore, mapping these operations to parametric quantum circuits may imply that some systems can be explored even when the Lie rank condition can no longer be evaluated analytically or on a classical computer.

Parametric quantum circuits constitute the basis of many algorithms, for example variational algorithms for solving computationally hard optimization problems [18, 149]. The circuits consist of a set of parametric gates that can be used to measure a cost function. After a classical optimization, the parameters are updated to give a new cost value, continuing the feedback loop of the algorithm. It is necessary to include enough independent optimization parameters to reach the best possible solution. However, minimizing the number of parametric gates and circuit depth is also key in the era of noisy quantum devices [63]. In order to reduce the noise of the circuit while maintaining its optimization capability, every redundant parameter should be identified and removed from the circuit. This goal is related to the dimensional expressivity of the circuit and can be achieved with dimensional expressivity analysis [19, 20], a hybrid quantum-classical algorithm to systematically find redundant parameters.

In order to leverage dimensional expressivity analysis to test for controllability, we define a parametric quantum circuit based on the architecture of a given qubit array with local controls and qubit couplings. We then use dimensional expressivity analysis to quantify the number of independent parameters which is related to the controllability of the original qubit array. We provide a complete description of how to carry out the hybrid controllability test on a quantum circuit, opening the possibility of obtaining information of the controllability of a quantum device before it is built.

The chapter is organized as follows. The basic concepts of controllability analysis and parametric quantum circuits are briefly reviewed in section 5.2. The pure-state controllability test is presented in section 5.3, including its derivation, definition and showcase examples. Section 5.4 extends the test to operator controllability, making use of the Choi-Jamiołkowski isomorphism. Section 5.5 concludes.

## 5.2 Theoretical background

To define controllability tests for qubit arrays, we combine the notions of system controllability and circuit expressivity. For the sake of a self-contained chapter, we briefly recap the basic ideas in this section.

### 5.2.1 Controllability

Previously we have mentioned that pure-state controllability is the relevant type of controllability when we are interested in are state transfers, i.e., evolving the system from an initial state to a certain target state. It is equivalent to proving that all state transfers are possible in a system. This, however, is not the strongest type of controllability that can be defined. Pure-state controllability is sufficient to guarantee that there will always be evolution operators $\hat{U}_{|\psi_0\rangle,|\psi_f\rangle}$ to connect any two states $|\psi_0\rangle$ and $|\psi_f\rangle$, yet not enough to ensure that it is possible to generate every operation $\hat{U}$ in the special unitary group $SU\,(d)$, where $d = \dim(\mathcal{H})$. Pure-state controllability does not guarantee that simultaneous state-to-state transfers are always possible. This property is instead related to the operator controllability of the system. A system with linearly coupled controls (cf. Equation (2.8)) and Hilbert space dimension $d$ is operator controllable if for every unitary evolution $\hat{U}_{target} \in SU(d)$ there exist a final time $T \geq 0$, a phase angle $\varphi \in [0, 2\pi)$ and a set of controls $\{u_j\}_{j=1}^{m}$ such that $\hat{U}_{target} = e^{i\varphi}\hat{U}(T; u_1, ...u_m)$.

Note that for both types of controllability there are no restrictions on the final time $T \leq \infty$ at which state transfers, respectively unitary operations, are implemented. Consequently, this time $T$, while always finite, can be arbitrarily large. The question of controllability only inquires whether it is possible at all to perform the desired dynamics. Similarly, it does not impose any restrictions on the maximum amplitude that the controls $u_j(t)$ from (2.8) can take. Finite amplitude is a physical restriction that impacts the final time required to perform the different operations, but does not mathematically change the controllability of the system.

If the Hamiltonian of the system is known, there exist algebraic and numerical tests tailored for both types of controllability [107, 150, 145, 14, 148].

### 5.2.2 Dimensional expressivity

Parametric quantum circuits have multiple applications, as they constitute the base for variational quantum algorithms [64]. Their design and study are pivotal factors in the efficiency of the algorithms. In particular, parameter dependence and the set of final states that can be produced are two key topics that determine the capability

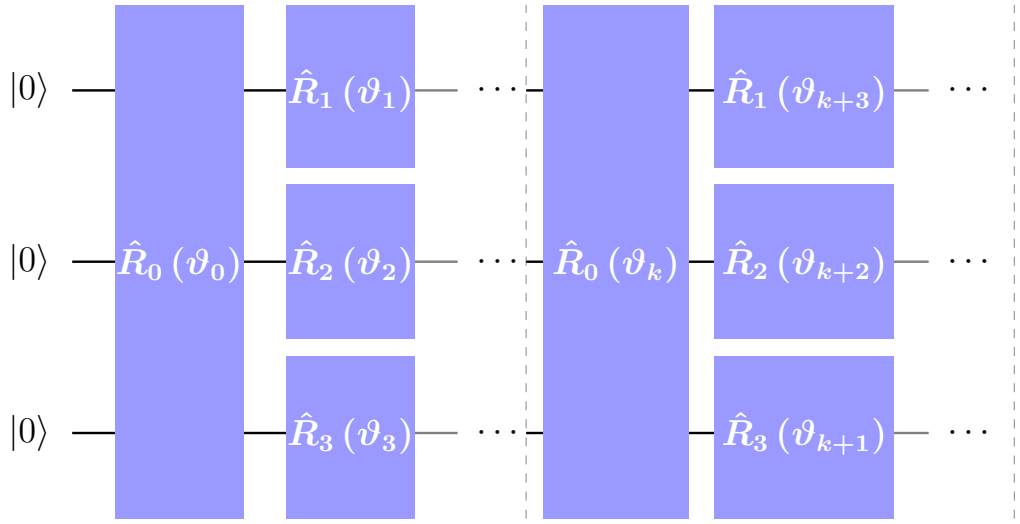


**Figure 5.1:** Three-qubit example of the parametric circuit $C_{PSC}(\vec{\vartheta})$ (5.7) for testing pure-state controllability with initial state $|000\rangle$ in the qubits' logical basis. Each layer (only two displayed in the diagram) includes an entangling gate $\hat{R}_0$ and a sequence of local gates $\hat{R}_j$ (with $j \geq 1$), one for every control present in the qubit array.

of the algorithms. Lacking some necessary parametric gates leads to unsuccessful algorithms, whereas including too many dependent parameters is detrimental for the purpose of optimization. We introduce here notions and definitions related to these issues that are relevant for the controllability tests. This subsection follows the theory presented in Section 2.5

Minimizing the number of redundant parameters is therefore a relevant matter in the design of parametric quantum circuits. Fewer redundant parameters may result in more resource-efficient circuits that can produce the same manifold of states. We describe

As a reminder, the dimensional expressivity $expr_{dim}$ of a circuit $C(\vec{\vartheta})$ with parameters $\vartheta \in \mathcal{P}$ is a measure of the amount of states that can be produced at the end of the circuit by varying the parameters. The exact value of the dimensional expressivity represents both , i.e. the dimension of $C\left(\mathcal{P}\right)$ as a real differentiable manifold [19].

We have previously presented the dimensional expressivity analysis as a sequential hybrid quantum-classical algorithm. This approach provides an efficient method to find a maximal set of independent parameters on a quantum circuit [19, 20]. The number of independent parameters serves as a measure for the dimensional expressivity of the studied circuit.

## 5.3 Pure-state controllability test using dimensional expressivity

This section introduces the novel connection between the dimensional expressivity of quantum circuits and the pure-state controllability of quantum systems. We present the design of a circuit associated to a controlled system that allows us to check its pure-state controllability. We include two examples to showcase its functionality.

### 5.3.1 Circuit expressivity and pure-state controllability

We consider a qubit array with Hamiltonian (2.8). We identify the drift $\hat{H}_0$ as the time-independent part, which includes the local free-qubit Hamiltonians and some time-independent couplings between them. Similarly, the operators $\hat{H}_j$ with $1 \leq j \leq m$ are coupled to the $m$ different external controls acting on the system. In order to use dimensional expressivity analysis to determine controllability of a qubit array, it is necessary to define a parametric quantum circuit that can be run on the system, according to the different controls at disposal. If we can show that all normalized states in the Hilbert space are reachable from a certain initial state using only gates generated by the system's controls, we have proven pure-state controllability.

A straightforward choice for the possible parametric gates in the circuit is

$$\hat{R}_j(\alpha) := \exp\left(-i\,\frac{\alpha}{2}\hat{H}_j\right), \qquad 0 \leq j \leq m, \tag{5.1}$$

i.e. rotations around either the drift $\hat{H}_0$ or the control operators $\hat{H}_j$ (2.8). The gates $\hat{R}_0(\alpha)$ can be implemented by letting the system evolve under its time-independent drift Hamiltonian $\hat{H}_0$ for a certain time $t = \frac{\alpha}{2}$. For the other gates, $\hat{R}_j(\alpha)$ with $j \geq 1$, we make use of the local controls. In these gates the $\hat{H}_0$ contribution can be neglected by assuming that the controls can be chosen such that $\|u_j(t)\hat{H}_j\| \gg \|\hat{H}_0\|$. A realistic approach to the $\hat{R}_j(\alpha)$ implementation is to consider short rotations with intense controls $u_j(t)$, so that the $\hat{H}_0$ contribution is insignificant in comparison. The amplitude of $u_j(t)$ is usually adjusted externally and it has no imposed restriction.

We want to design a parametric quantum circuit $C_{PSC}(\vec{\vartheta})$, starting with an arbitrary initial state $|\psi_0\rangle \in \mathcal{H}$ and exclusively composed of the rotation gates $\hat{R}_j(\vartheta_k)$. We then use dimensional expressivity analysis to measure the dimensional expressivity of the system. If it is maximal, i.e. $expr_{dim} = 2d - 1$ for $\dim(\mathcal{H}) = d$, we have a manifold of reachable states with local real dimension $2d - 1$. This manifold is a subset of $\mathcal{H}$. We now prove that it is in fact the whole unit sphere of $\mathcal{H}$. If we assume that the gates $\hat{R}_j(\alpha)$ are cyclic and that every parameter $\vartheta_k$ is used in a single rotation gate in the

circuit, we can treat each $\vartheta_k$ as if it had periodic boundaries, i.e. $\vartheta_k \in \mathbb{S}^1$. For an array of $n$ parameters $\vec{\vartheta}$ the parameter space verifies

$$\mathcal{P} \cong \underbrace{\mathbb{S}^1 \times \cdots \times \mathbb{S}^1}_{n} \cong \mathbb{T}^n. \tag{5.2}$$

This implies that $\mathcal{P}$ is a connected, compact set without boundary. Assume a circuit $C_{PSC}(\vec{\vartheta})$ that has maximal dimensional expressivity. Then, the manifold of reachable states $C_{PSC}(\mathcal{P}) \subseteq \mathcal{H}$ is a connected, compact manifold without boundary and with maximal local real dimension. Consequently $C_{PSC}(\mathcal{P}) = \mathcal{S}^{\mathcal{H}} \subset \mathcal{H}$. Thus, the system is pure-state controllable.

So far, we have found a sufficient condition for pure-state controllability. We now want to identify a condition for non-controllable systems. To this end, we need to prove that there are some states that are not reachable by any of the possible dynamics that we can implement with the different operators $\hat{H}_j$ and their nested commutators. Hypothetically, we could do a sequence of the rotation gates (5.1) around the drift, the control operators and their nested commutators and test if all of them are linearly independent. However, generating the exponential of the commutator of two control operators (or one control operator and the drift) $\exp i\,\beta[\hat{H}_j, \hat{H}_k]$ is no trivial task. It may require optimal control to generate a specific rotation for the exact angle $\beta$ and the chosen commutator $[\hat{H}_j, \hat{H}_k]$. Instead, we access the different commutators by concatenating a series of multiplications, as in the Baker-Campbell-Hausdorff formula:

$$\begin{aligned}\exp\left(i\,\alpha\hat{A}\right)\exp\left(i\,\beta\hat{B}\right) = \exp\Bigg(&i\alpha\hat{A} + i\beta\hat{B} - \frac{1}{2}\alpha\beta[\hat{A},\hat{B}] \\ &- \frac{i\,\alpha^2\beta}{12}[\hat{A},[\hat{A},\hat{B}]] \\ &+ \frac{i\,\alpha\beta^2}{12}[\hat{B},[\hat{A},\hat{B}]]\cdots\Bigg).\end{aligned} \tag{5.3}$$

Assume that we have a parametric quantum circuit consisting of a sequence of $n$ rotations,

$$C^n_{seq}(\vec{\vartheta}) := \exp\left(-i\,\vartheta_n\hat{A}_n\right)\cdots\exp\left(-i\,\vartheta_1\hat{A}_1\right)|\psi_0\rangle \tag{5.4}$$

with $\hat{A}_j \in \{\hat{H}_k\}_{k=0}^m \forall 1 \leq j \leq n$. We can use Eq. (5.3) multiple times on the exponential sequence on the right-hand side of Eq. (5.4) to express it as a single exponential dependent on $\vec{\vartheta}$, the different operators $A_j$ and their nested commutators. Assume as well that the dimensional expressivity in the circuit $expr_{\dim}(C^n_{seq}(\vec{\vartheta})) = d_n$ is less than the maximum possible. We define a new parametric circuit by adding one more rotation to the chain of operations,

$$C^{n+1}_{seq}(\vec{\vartheta}, \vartheta_{n+1}) := \exp\left(-i\,\vartheta_{n+1}\hat{A}_{n+1}\right) C^n_{seq}(\vec{\vartheta}). \tag{5.5}$$

If the dimensional expressivity of $C_{seq}^{n+1}$ and $C_{seq}^{n}$ are the same for every $\vartheta_{n+1} \in \mathbb{R}$ and every $\hat{A}_{n+1} \in \{\hat{H}_k\}_{k=0}^{m}$, then the number of linearly independent $\partial_j C(\vec{\vartheta})$ remains the same. In other words, we are not able to find more linearly independent operators and thus, the dimensional expressivity of the system cannot be increased. This means that the manifold of reachable states does not have a maximal local dimension and hence there will be some states to which our initial state cannot evolve. Therefore the system is not pure-state controllable.

There may be cases where, for given $C_{seq}^{n}(\vec{\vartheta})$ and $\hat{A}_{n+1}$, there exist two different parameters $\vartheta_{n+1}$ and $\tilde{\vartheta}_{n+1}$ such that

$$expr_{\dim}\left(C_{seq}^{n+1}(\vec{\vartheta}, \vartheta_{n+1})\right) > expr_{\dim}\left(C_{seq}^{n+1}(\vec{\vartheta}, \tilde{\vartheta}_{n+1})\right). \tag{5.6}$$

This is common in cases where $\tilde{\vartheta}_j = 0$ for every $1 \leq j \leq n+1$. Looking at Eq. (5.3), note that using repeated parameters (e.g. $\alpha = \beta$) will make the coefficients preceding the commutators have the same absolute value (e.g. $\alpha^2\beta = \alpha\beta^2$). This is evidently unfavorable to generate more linearly independent $\partial_j C(\vec{\vartheta})$ due to the symmetries created.

In principle, it would be necessary to prove that the expressivity of $C_{seq}^{n+1}$ does not increase for any $\vartheta_{n+1} \in \mathbb{R}$. However, as long as there exists one $\vartheta_{n+1}$ that increases the dimensional expressivity for an operator $\hat{A}_n$, the set of $\{\tilde{\vartheta}_{n+1}\} \subset \mathbb{R}$ that would not raise the expressivity will have measure zero. This can be justified as follows. Assume that the first $n$ parameters are independent (i.e. $\det(S_n) \neq 0$), with $n$ less than the maximal dimensional expressivity, and that there exist some parameters that can increase the expressivity. This implies that the analytic function $f(\vec{\vartheta}) := \det(S_{n+1})$ is not constant 0. The set of parameters that would not increase the expressivity belong to $f^{-1}(0)$. With the regular level set theorem [151], $f^{-1}(0)$ is an $n$-dimensional manifold in the $(n+1)$-dimensional parameter space $\mathcal{P}$. Thus, the set of parameters that would not increase the expressivity has Lebesgue measure zero in $\mathcal{P}$. In other words, by choosing $\vartheta_{n+1}$ randomly we increase the dimensional expressivity with probability 1.

The next section uses these ideas to systematically design quantum circuits that can be used to determine for a controlled quantum system whether it is pure-state controllable or not.

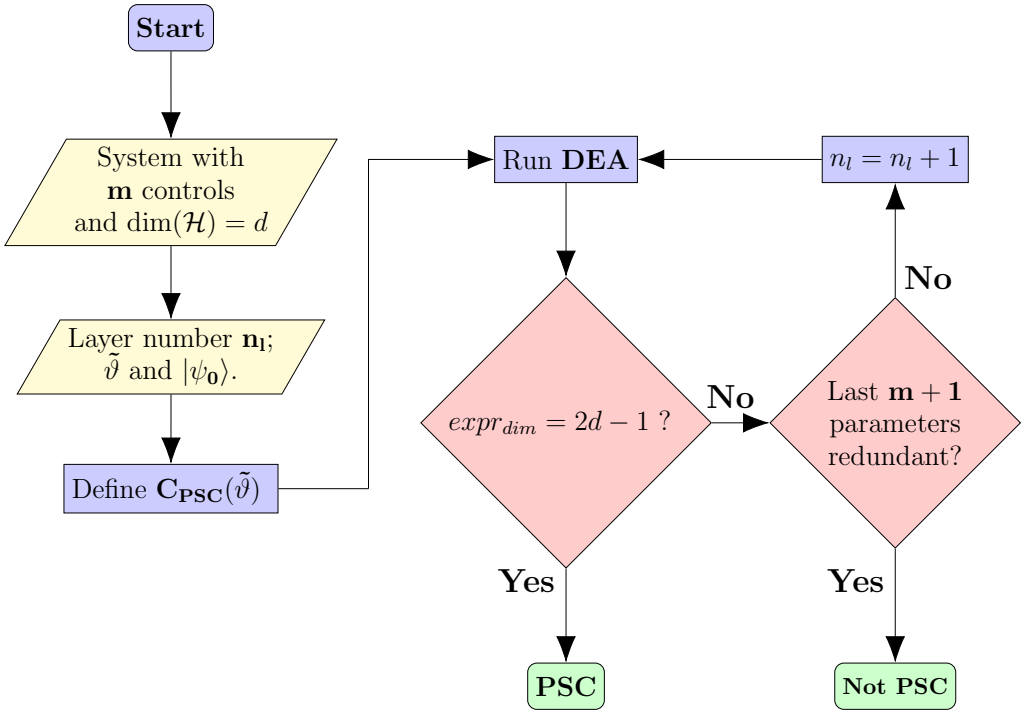


**Figure 5.2:** Flowchart for the pure-state controllability algorithm. The yellow rhomboids show the initial inputs necessary to define the circuit $C_{PSC}(\vec{\vartheta})$.

### 5.3.2 Controllability test

Given a system with operators $\hat{H}_j$ with $0 \leq j \leq m$ (cf. Eq. (2.8)), we define the parametric quantum circuit

$$C_{PSC}(\vec{\vartheta}) = \left( \prod_{j=0}^{n_l-1} \hat{R}_m(\vartheta_{j(m+1)+m}) \cdots \right. \\ \left. \hat{R}_1(\vartheta_{j(m+1)+1}) \hat{R}_0(\vartheta_{j(m+1)}) \right) |\psi_0\rangle \,, \tag{5.7}$$

where $|\psi_0\rangle$ is the initial state of the circuit, $m$ the total number of controls in the system and $n_l$ the number of layers in the circuit. A diagram of this circuit is shown in Figure 5.1 for a three-qubit example. The initial state $|\psi_0\rangle$, chosen and fixed at the start of the circuit, can be any pure state. The number of layers $n_l$ should be decided at the start of the algorithm. All gates in $C_{PSC}(\vec{\vartheta})$ are parametric with different parameters $\vartheta_k$, ranging from $\vartheta_0$ to $\vartheta_{n_l m-1}$. Each of the $n_l$ layers in the circuit has a similar architecture: It starts with the rotation $\hat{R}_0$ around the drift Hamiltonian, an entangling gate if it includes time-independent qubit couplings, and then a sequence of local gates, from $\hat{R}_1$ to $\hat{R}_m$, that use all the different controls sorted by a chosen order.

The pure-state controllability test for a system evolving under the Hamiltonian (2.8) is then defined as follows: If the circuit (5.7) reaches maximal expressivity, the system is controllable. A schematic flowchart of the pure-state controllability test is shown in Figure 5.2. If the maximum expressivity of $2d-1$ for a Hilbert space with $\dim(\mathcal{H}) = d$ has not been met with $n_l$ layers, another layer can be added (encompassing a full set of rotation gates with their respective new parameters) and the test can be repeated for the new circuit with $n_l + 1$ layers. By definition, the dimensional expressivity can only augment at the rate of one per parameter $\vartheta_j$ at maximum. For a system with $m$ controls, there are a total of $m + 1$ parameters per layer. Therefore, the minimum number of layers needed to reach maximum expressivity for $m$ controls is

$$n_{l,\,\text{min}} = \left\lceil \frac{2d-1}{m+1} \right\rceil . \tag{5.8}$$

Since layers may have some redundant parameters, the dimensional expressivity may not necessarily rise at the maximum rate and more layers may have to be included. Consequently, the algorithm is best started with the minimum number of layers required to achieve maximum expressivity and additional layers shall be concatenated as needed.

It may as well happen that the dimensional expressivity remains the same even with the inclusion of a new layer. In this case the test stops, as the dimensional expressivity will not further increase. In instances where the dimensional expressivity reaches a plateau, it is necessary to double-check using a different array of random parameters $\vec{\vartheta}$ and repeat this comparison with the $n_l$- and $n_l + 1$-layered circuits, following the reasoning explained in section 5.3.1. Using a random set of parameters will yield an answer on whether the expressivity can be increased or not with probability 1. If the dimensional expressivity remains at a value less than $2d - 1$ for a sufficiently large set of different random parameters, then the system is labelled not pure-state controllable and the test concludes.

The algorithm will always end with an affirmative or negative result regarding pure-state controllability. The loop in Figure 5.2 will be exited under one of the following conditions: Either maximal dimensional expressivity is reached or a last layer exclusively composed of redundant parameters is found. In other words, the method ends when the finite upper bound of the dimensional expressivity has been reached or when the expressivity before and after the addition of a new layer remains the same. Since the dimensional expressivity is always an integer, the loop must conclude in a finite number of iterations.

Parameters with repeated values in the same rotation gates (e.g. $\vartheta_p = \vartheta_q$ on gates $\hat{R}_j(\vartheta_p)$ and $\hat{R}_j(\vartheta_q)$ for a certain $j$) are usually detrimental to reach maximum

| Coupling strengths (MHz) | | |
|---|---|---|
| $J_{0,1}$ | $J_{1,2}$ | $J_{2,3}$ |
| 170 | 220 | 150 |
| **Qubit frequencies (GHz)** | | |
| $\omega_0$ | $\omega_1$ | $\omega_2$ | $\omega_3$ |
| 5.40 | 5.30 | 5.42 | 5.37 |

**Table 5.1:** Parameters for the Hamiltonian (5.9). The frequencies and the coupling strengths have been chosen in a range that is common for superconducting circuits.

expressivity. A trivial example is the case of $\vec{\vartheta} = \vec{0}$, where the maximum possible dimensional expressivity of $C_{PSC}(\vec{0})$ is always $m + 1$, with $m$ the number of local controls.

A more detailed description of the algorithm can be found in Section 5.4.3. This includes step-by-step pseudo code and the exact parts of the method that can be performed classically and with quantum computations.

### 5.3.3 Examples

To illustrate the described algorithm, we consider a four-qubit array with the following Hamiltonian:

$$\hat{H}_{4q}(t) = \sum_{j=0}^{3} -\frac{\omega_j}{2}\hat{\sigma}_z^{(j)} + \sum_{k=0}^{2} J_{k,k+1}\hat{\sigma}_x^{(k)}\hat{\sigma}_x^{(k+1)} + \hat{H}_{ctrl}(t) \tag{5.9}$$

The first term encompasses the free-qubit Hamiltonians and the second one contains the time-independent couplings. The qubit frequencies $\omega_j$ and the coupling strengths $J_{k,k+1}$ have been chosen to fit the ones normally used in superconducting circuits [152] and their exact value can be found in Table 5.1. The last operator, $\hat{H}_{ctrl}(t)$, contains all the relevant information about the controls, including their number and type. We choose two configurations of controls to study two separate systems with Hamiltonian (5.9), one that is pure-state controllable and one that is not.

First, we assume the controls from Eq. (5.9) to be

$$\hat{H}_{ctrl}(t) = u_1(t)\hat{\sigma}_x^{(1)} + u_2(t)\hat{\sigma}_x^{(2)}. \tag{5.10}$$

This system is operator controllable, as proven by the Lie algebra rank condition [14] and the graph method [148]. This in particular implies that it is also pure-state controllable. A diagram of the system may be found in Figure 5.3.

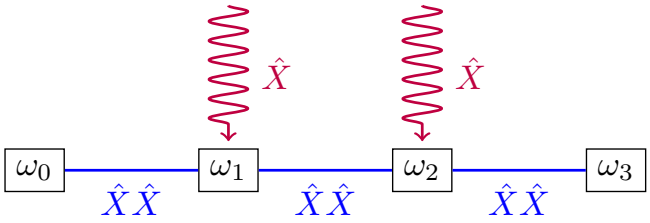


**Figure 5.3:** Four-qubit system that is pure-state controllable, cf. Eqs. (5.9) and (5.10).

Since the system only has two controls, each layer of the circuit will have exactly 3 gates—the entangling gate involving the drift and the two related to the local controls coupling to $\hat{\sigma}_x^1$ and $\hat{\sigma}_x^2$, respectively. We have chosen $|\psi_0\rangle = |0000\rangle$ (in the logical basis of the free qubits) as the initial state of the circuit and $n_l = 11$, matching the minimal number of layers to obtain maximum dimensional expressivity (cf. Eq. (5.8)). For a circuit acting on a four-qubit array, it has a value of $expr_{dim} = 31$. We have generated a random set of parameters $\vec{\vartheta} \in [0, 2\pi]^{33}$ (since in this case $(m+1) \cdot n_l = 33$). We have classically simulated the parametric quantum circuit and calculated the $S_{C_{PSC},n}(\vec{\vartheta})$ matrices from Eq. (2.33). We have both determined the redundant parameters in the circuit and estimated the dimensional expressivity.

In these simulations, the maximum dimensional expressivity is steadily reached, with every layer raising it by 3. The maximum value of $expr_{dim} = 31$ is achieved with the first parameter of the last layer, proving that the system is pure-state controllable. In this example the minimum number of layers that we had chosen was enough to reach maximum expressivity. The same behaviour has been observed for all the different random sets of parameters $\vec{\vartheta}$ tested. The same configuration of gates was further tested using different random initial states $|\psi_0\rangle$, yielding similar results.

Second, we present a system that is not pure-state controllable, whose control operators are

$$\hat{H}_{ctrl}(t) = u_1(t)\hat{\sigma}_x^{(0)} + u_2(t)\hat{\sigma}_y^{(2)} + u_3(t)\hat{\sigma}_z^{(3)}, \tag{5.11}$$

cf. Figure 5.4.

The exact dimension of the Lie algebra $\mathcal{L}$ of the system described by Equations (5.9) and (5.11) can be found following the method the method described in [14]. To do this, we must generate a basis of $\mathcal{L}$, whose cardinality will be equal to the dimension of the dimension of the Lie algebra. Given a system following Equation (2.8), we can compute a basis by starting with a linearly independent set of the elements of zeroth order: The drift $\hat{H}_0$ and the control operators $\hat{H}_j$ (for $1 \leq j \leq m$). We complete the basis by including the nested commutators of the elements of zeroth order that are

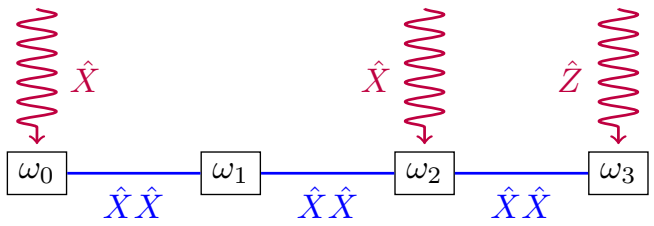


**Figure 5.4:** Four-qubit system that is not pure-state controllable, cf. equations (5.9) and (5.11).

linearly independent, i.e. $[\hat{H}_{j_1}, [\hat{H}_{j_2}, ...[\hat{H}_{j_k}, \hat{H}_{j_{k+1}}]...]]$. Since the dimension has an upper bound, this method must converge in a finite number of iterations.

In the case of Equations (5.9) and (5.11), we reach a dimension of $\dim(\mathcal{L}) = 120 < \dim(\mathfrak{su}(16)) = 255$, which only proves that the system is not operator controllable. The system would be pure-state controllable if and only if

$$\dim\left(Lie\left([\rho_0, \mathcal{L}]\right)\right) = 2\dim(\mathcal{H}) - 2 \tag{5.12}$$

with $\rho_0 = |0000\rangle\langle 0000|$ [14]. We confirm that the system is not pure-state controllable since $\dim\left(Lie\left([\rho_0, \mathcal{L}]\right)\right) = 28 < 30$ for the current system. Even though there are more local controls than in the first example, the system is not controllable due to their positions. Similarly as before, we create a circuit with four gates (related to the drift and the three local controls) per layer. We choose a minimum number of layers $n_l = 8$ (different to the one before due to the different number of controls), $|\psi_0\rangle = |0000\rangle$ and a set of random parameters $\vec{\vartheta} \in [0, 2\pi]^{32}$.

At the end of the last layer the dimensional expressivity yields a total of 29 out of the 31 that would imply pure-state controllability. Following the flowchart depicted in Figure 5.2 we have added a new layer ($n_l = 9$) with a new set of random parameters and repeated the dimensional expressivity analysis. According to our simulation, the new layer contains only redundant parameters (i.e. the expressivity remains at 29), which stops the algorithm and means that the system is not pure-state controllable. To verify the validity of this outcome, we have repeated the test for multiple different random sets of parameters. In every instance the same result is reached, which leads to the conclusion that the system is indeed not pure-state controllable, as discussed in section 5.3.1.

## 5.4 Operator controllability test using dimensional expressivity analysis

Operator controllability is the relevant type of controllability for a qubit array in order to perform all quantum logic gates. Its connection to the dimensional expressivity of a circuit is less evident, since dimensional expressivity is related to the different states that can be reached. The Choi-Jamiołkowski isomorphism [153, 154] allows to bridge the gap with a map between operators on a Hilbert space $\mathcal{H}$ and states in $\mathcal{H} \otimes \mathcal{H}$. It is used, for example, in quantum process tomography, allowing to employ techniques from state tomography to operators [155]. Similarly, by doubling the number of qubits, we can exploit the channel-state duality between operators in the original system and states in the bipartite extended system for controllability analysis.

### 5.4.1 Lifting pure-state to operator controllability via the Choi-Jamiołkowski isomorphism

Let us assume a qubit array with Hamiltonian (2.8) for which we seek to determine operator controllability. This system with Hilbert space $\mathcal{H}$ and dimension $dim(\mathcal{H}) = d$ will henceforth be referred to as the original system. We then define a bipartite extended system in $\mathcal{H} \otimes \mathcal{H}$ composed of the original system and the same number of auxiliary qubits. To simplify the argument, we first assume no dynamics over the auxiliary qubits. Later we extend our discussion to include some local Hamiltonians on the auxiliary qubits. Given any operator $\hat{O} \in L(\mathcal{H} \otimes \mathcal{H})$, we write $\hat{O}^A$ to indicate that the operator only acts non-trivially on the partition of the original system ($A$), i.e.

$$\hat{O}^A = \hat{Q} \otimes \mathbb{1}_d \tag{5.13}$$

for some operator $\hat{Q}$. Analogously, we write $\hat{O}^{AB}$ for operators that act non-trivially on both partitions (the original system and the auxiliary qubits). Neglecting the local contributions of the auxiliary qubits, the Hamiltonian of the extended system is given by

$$\hat{H}^A(t) = \hat{H}(t; u_1, ...u_m) \otimes \mathbb{1}_2^{\otimes q} \tag{5.14}$$

where $q$ is the number of qubits in the original system.

We assume that the extended system can be prepared in a maximally entangled state,

$$|\psi_{ME}\rangle = \sum_{i=0}^{d-1} \frac{1}{\sqrt{d}} |e_i\rangle \otimes |e_i\rangle \,, \tag{5.15}$$

where $\{|e_i\rangle\}_0^{d-1}$ is an orthonormal basis of $\mathcal{H}$.

We define the circuit on the extended system

$$C_{OC}^{A}(\vec{\vartheta}) := \prod_{j=0}^{k} \Big( \hat{R}_m^A(\vartheta_{j(m+1)+m}) \cdots \\ \hat{R}_1^A(\vartheta_{j(m+1)+1}) \hat{R}_0^A(\vartheta_{j(m+1)}) \Big) |\psi_{ME}\rangle \,. \tag{5.16}$$

The rotations $\hat{R}_k^A(\alpha)$ are given by the drift ($k = 0$) and the control operators ($1 \leq k \leq m$) of the original subsystem:

$$\hat{R}_k^A(\alpha) := \exp\left( -i \frac{\alpha}{2} \hat{H}_k \otimes \mathbb{1}_2^{\otimes q} \right), \qquad 0 \leq k \leq m, \tag{5.17}$$

with $\hat{H}_k$ given in Eq. (2.8).

A visual representation of the circuit is found in Figure 5.5. The parameter space $\mathcal{P} \ni \vec{\vartheta}$ is assumed to be connected and compact without boundary (e.g. with every coordinate $\vartheta_i$ being cyclic). The final state of the circuit will always be of the form

$$C_{OC}^{A}(\vec{\vartheta}) = \frac{1}{\sqrt{d}} \sum_{i=0}^{d-1} |e_i\rangle \otimes \left( \hat{U}(\vec{\vartheta}) |e_i\rangle \right), \tag{5.18}$$

with $\hat{U}(\vec{\vartheta})$ a unitary operator depending on the circuit's parameters.

Our goal is to prove that dimensional expressivity of the extended system is enough to determine operator controllability of the original system. To this end, we make use of the Choi-Jamiołkowski isomorphism [153, 154, 156]. The map it describes is written as

$$\begin{aligned} \Lambda(\hat{A}) &:= \left( \mathbb{1}_{\mathcal{L}_{\mathcal{H}}} \otimes \hat{A} \right) (|\phi\rangle \langle\phi|) \\ &= \sum_{i,j} |\psi_i\rangle \langle\psi_j| \otimes \hat{A}\Big( |\psi_i\rangle \langle\psi_j| \Big) \end{aligned} \tag{5.19}$$

for any operator $\hat{A}$ in the Hilbert space of linear operators on the Liouville space and the unnormalized state $|\phi\rangle = \sum_i |\psi_i\rangle \otimes |\psi_i\rangle$, with $\{|\psi_i\rangle\}_{i=0}^{d-1}$ an orthonormal basis of $\mathcal{H}$.

Identifying $\hat{A}$ in Eq. (5.19) with $\hat{U}(\vec{\vartheta})$ in Eq. (5.18), we know that

$$\begin{aligned} \hat{U}(\mathcal{P}) &\cong \Lambda(\hat{A}) \\ &= \sum_{i,j=0}^{d-1} |e_i\rangle \langle e_j| \otimes \left( \hat{U}(\mathcal{P}) |e_i\rangle \langle e_i| \hat{U}(\mathcal{P})^\dagger \right). \end{aligned} \tag{5.20}$$

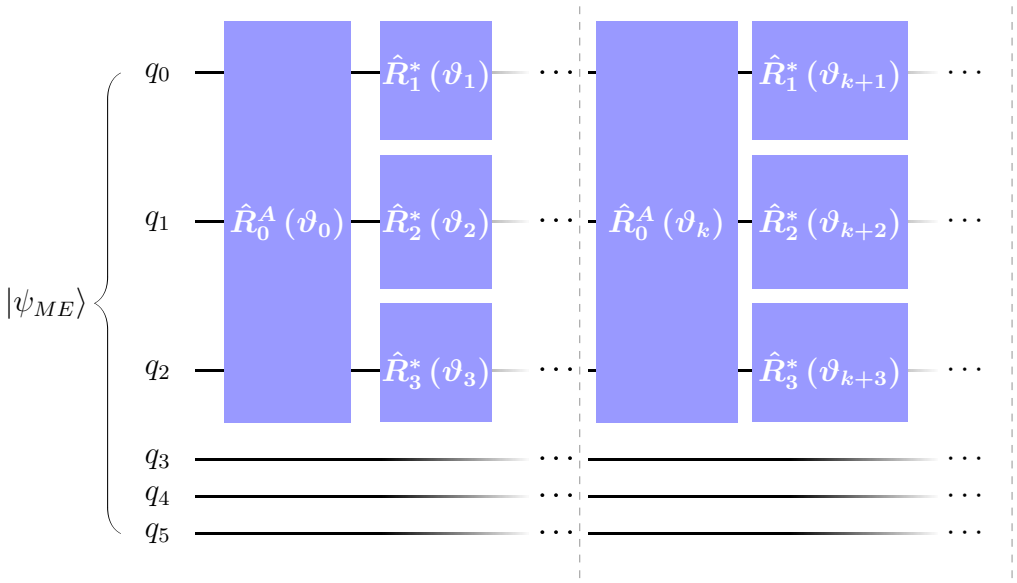


**Figure 5.5:** Parametric circuit for the extended system required to perform the operator controllability test (5.16) for a three-qubit system. The qubits $q_i$ with $i = 0, 1, 2$ constitute the original system, whereas $q_j$ with $j = 3, 4, 5$ are the auxiliary qubits.

The operators $\hat{U}(\vec{\vartheta})$ are unitary for every $\vec{\vartheta} \in \mathcal{P}$, hence purity-preserving. We transform the density matrix representation from Eq. (5.20) into a pure-state representation, resulting in

$$\hat{U}(\mathcal{P}) \cong \sum_{i=0}^{d-1} |e_i\rangle \otimes \hat{U}(\mathcal{P}) |e_i\rangle \cong C_{OC}^A(\mathcal{P}). \tag{5.21}$$

Therefore, there exists an embedding between the evolutions $\hat{U}(\mathcal{P})$ that are generated using a combination of rotations given by the controls and the final states of the circuit $C_{OC}^A(\mathcal{P})$. A system with traceless operators as in Eq. (2.8) and $\dim(\mathcal{H}) = d$ is operator-controllable if and only if the manifold of the unitary evolutions that can be generated $\hat{U}_{\hat{H}}$ is isomorphic to $SU(d)$. Evidently, $\hat{U}(\mathcal{P}) \subseteq \hat{U}_{\hat{H}} \subseteq SU(d)$. Since the parameter space $\mathcal{P}$ is connected and compact without boundary, $\hat{U}(\mathcal{P}) = SU(d)$ if and only if $\dim(\hat{U}(\mathcal{P})) = \dim(SU(d))$. Thus, using Eq. (5.21), the system will be operator-controllable if $\dim(C_{OC}^A(\mathcal{P})) = \dim(SU(d))$, i.e., if the dimensional expressivity of the circuit $C_{OC}^A(\vec{\vartheta})$ is $d^2 - 1$.

From here we proceed analogously as the pure-state controllability test from section 5.3.1. We present the outline of the operator controllability test in Figure 5.7. If the dimensional expressivity is less than $d^2 - 1$, we inspect the parameters in the last circuit layer. If they all are redundant, the test ends and the system is deemed not controllable. Indeed, if all parameters in the last layer are redundant, we are unable to find more linearly independent operators in the dynamical Lie algebra of the system. If the number of linearly independent elements of the algebra (i.e. number of independent parameters) is less than $\dim(SU(d))$, there exist some unitary operations that cannot be implemented. Therefore, the system is not operator controllable. This

step must be checked with multiple arrays of random parameters $\vec{\vartheta}$, as there may be a set of arrays of parameters with measure zero over $\mathcal{P}$ that yield a lower value for the dimensional expressivity. The same arguments we used in section 5.3.1 apply here, as $C^A_{OC}(\mathcal{P})$ is a manifold of states in $\mathcal{H} \otimes \mathcal{H}$.

If at least one parameter in the last circuit layer is independent, the test continues. We iterate by adding a new layer and calculating the circuit's expressivity. The algorithm will eventually come to an end, either with maximal value for the dimensional expressivity or with a layer of redundant parameters at the end of the circuit.

We now move to a more realistic setting that incorporates dynamics in the auxiliary qubits. We undertake this by including the drift of the auxiliary partition. The new Hamiltonian of the bipartite system is then

$$\hat{H}^{AB}(t) = \hat{H}(t; u_1, ...u_m) \otimes \mathbb{1}_2^{\otimes q} + \sum_{j=0}^{q-1} -\frac{\omega_j}{2} \hat{\sigma}_z^{(j+q)}, \tag{5.22}$$

with

$$\hat{\sigma}_z^k := \mathbb{1} \otimes ... \otimes \mathbb{1} \otimes \underbrace{\hat{\sigma}_z}_{k \text{ position}} \otimes \mathbb{1} \otimes ... \mathbb{1}. \tag{5.23}$$

It results in the following circuit to test operator controllability

$$\begin{aligned} C^{AB}_{OC}(\vec{\vartheta}) := \prod_{j=0}^{k} \Big( & \hat{R}^A_m(\vartheta_{j(m+1)+m}) ... \hat{R}^A_1(\vartheta_{j(m+1)+1}) \\ & \hat{R}^B_0(\vartheta_{j(m+1)}) \hat{R}^A_0(\vartheta_{j(m+1)}) \Big) \left| \psi_{ME} \right\rangle, \end{aligned} \tag{5.24}$$

where

$$\hat{R}^B_0(\alpha) := \exp\left( i \frac{\alpha}{2} \sum_{j=0}^{q-1} \frac{\omega_j}{2} \hat{\sigma}_z^{(j+q)} \right). \tag{5.25}$$

Note that the parameters $\vartheta_{j(m+1)}$ of the gates $\hat{R}^A_0$ and $\hat{R}^B_0$ in the same layer $j$ are always the same because there is no active control over these operators—they are due to the time-independent part of the Hamiltonian. In other words, these gates are implemented by letting the system evolve a certain amount of time $t = \vartheta_{j(m+1)}/2$. The number of parameters per layer for a system with $m$ controls remains equal to $m + 1$, despite having an extra rotation gate per layer. A diagram of the new circuit is found in Figure 5.6.

If we choose an orthonormal basis for the $B$ partition consisting of the eigenstates of the auxiliary qubits, then

$$C^{AB}_{OC}(\mathcal{P}) \cong \sum_{i=0}^{d-1} \left( \hat{U}(\mathcal{P}) e^{\varphi_i(\vec{\vartheta})} \left| e_i \right\rangle \right) \otimes \left| e_i \right\rangle .. \tag{5.26}$$

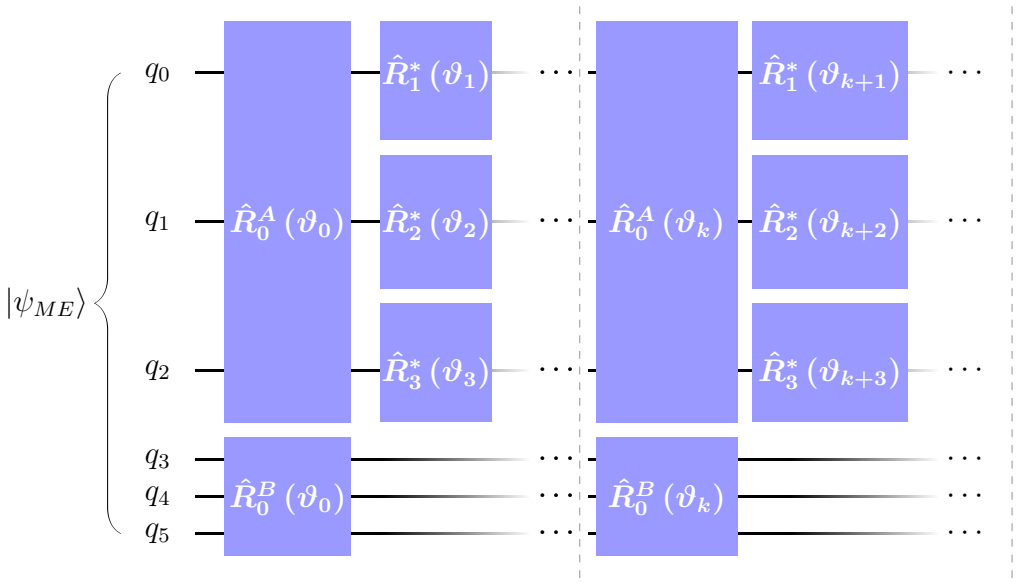


**Figure 5.6:** Circuit on the extended system required to perform the operator controllability test (5.24) for a three-qubit system. The qubits $q_i$ with $i = 0, 1, 2$ constitute the original system, whereas $q_j$ with $j = 3, 4, 5$ are the auxiliary qubits. The rotations $\hat{R}_0^B$ (cf. Eq. (5.25)) include the free-qubit dynamics of the auxiliary qubits.

The only difference between equations (5.21) and (5.26) is the local phases $\varphi_i(\vec{\vartheta})$, which are uniquely determined for any array of parameters $\vec{\vartheta}$. These do not change the value of the dimensional expressivity since for any array $\vec{\vartheta}$ there exists a neighborhood in which

$$C_{OC}^{A}(\vec{\vartheta}) \cong C_{OC}^{AB}(\vec{\vartheta}). \tag{5.27}$$

This implies the local dimension of the manifold of reachable states to be identical, i.e., the dimensional expressivity to be the same. Therefore, we can include the local Hamiltonians of the auxiliary qubits in our calculations to describe a more realistic model and still use the Choi-Jamiołkovski isomorphism to design the parametric quantum circuit (5.24).

### 5.4.2 Controllability test

Once again we consider a qubit array with traceless Hamiltonian (2.8) and the corresponding extended system, composed of the original $q$-qubit array and $q$ more auxiliary qubits. We assume the extra qubits to have arbitrary natural frequencies $\omega_j$, such that the Hamiltonian of the extended system is given by Eq. (5.22) and the parametric quantum circuit by Eq. (5.24). As shown in Figure 5.6 for a three-qubit example, for a system with $m$ controls the circuit has exactly $m + 1$ parameters per layer. As for pure-state controllability, it is encouraged to choose a number of layers $n_l$ that would a priori be sufficient to reach the maximum dimensional expressivity. In

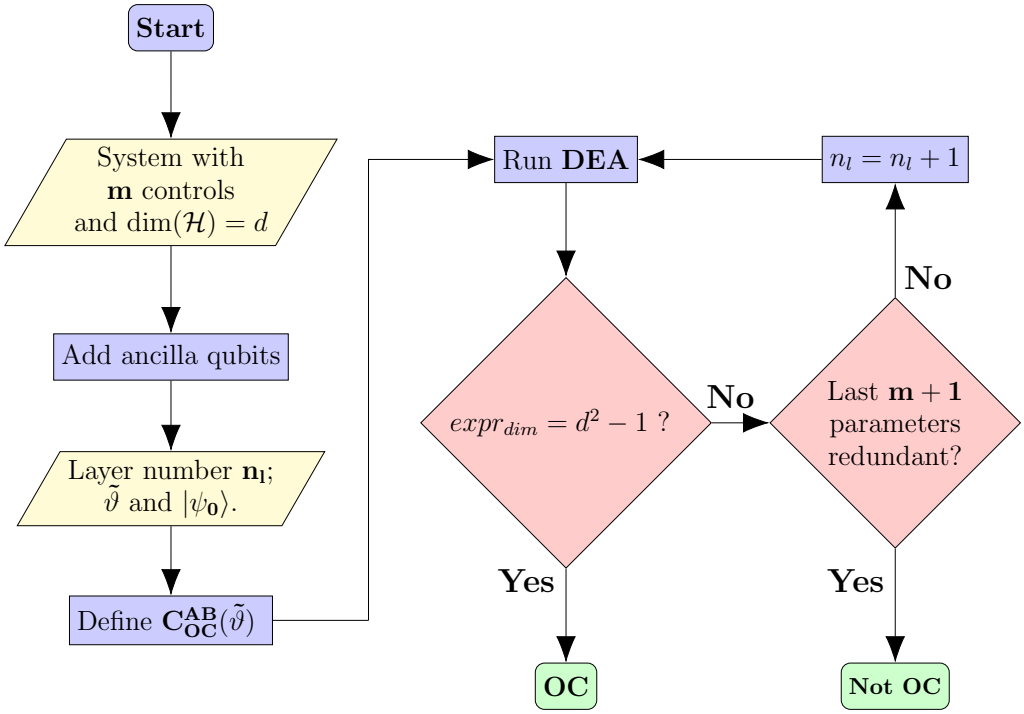


**Figure 5.7:** Flowchart for the algorithm testing operator controllability. The yellow rhomboids show the initial inputs necessary to define the circuit $C_{OC}^{AB}(\vec{\vartheta})$.

the case of operator controllability, it is $\dim(\mathfrak{su}(d)) = d^2 - 1$, with $d$ the Hilbert space dimension of the original system, $d = 2^q$ [1]. Thus, the condition for the minimum number of layers to obtain the maximal dimensional expressivity is

$$n_{l,\,\text{min}} = \left\lceil \frac{d^2 - 1}{m + 1} \right\rceil . \tag{5.28}$$

With the dimensional expressivity we find the maximum number of linearly independent states in $\mathcal{H} \otimes \mathcal{H}$ that can be generated in a neighborhood of $C_{OC}^{AB}(\vec{\vartheta})$. This in turn yields information about the maximum number of linearly independent operators on $\mathcal{H}$ that can be generated by the original system around the identity. Since we know that these operators belong to the Lie algebra $\mathfrak{su}(d)$ we simply want to determine if we can span all the $d^2 - 1$ dimensions in the algebra, i.e. having operator controllability, or not.

The operator controllability of a system evolving under the Hamiltonian (2.8) is determined as follows: If the circuit (5.24) has dimensional expressivity equal to $d^2 - 1$, then the system is operator controllable. Analogously to the pure-state controllability test, if this value for the dimensional expressivity is not reached, another layer should

[1] We only claim that the value for the maximal dimensional expressivity is $d^2 - 1$ (with $d = 2^q$) for the circuits $C_{OC}^{AB}$ (5.24). Other parametric quantum circuits acting on $\mathcal{H} \otimes \mathcal{H}$ could in principle reach higher values of expressivity, up to $2^{2q+1} - 1$

be concatenated at the end of the circuit. If all the new parameters in the last layer are redundant, then the system is not operator controllable (with a probability of measure 1); otherwise, the process of concatenating layers shall be repeated. The main steps of the algorithm is displayed in Figure 5.7. Similarly to section 5.3.1, it is important to to ensure the validity of a result of "not operator controllable" by repeating the test for different arrays of random parameters.

Similarly as before, the pseudo code of the algorithm can be found in Section 5.4.3.

### 5.4.3 Algorithm outline

Here we present an outline for the methods described in Figures 5.2 and 5.7 in the form of pseudo code. Algorithm 5.1 displays the main steps for applying the dimensional expressivity analysis to a circuit for the pure-state controllability test as defined in Equation (5.7) and operator controllability test given in Equation (5.24). There are two main differences between the two cases: The circuit definition (including the rotation gates $\hat{R}_j(\alpha)$ and the initial state $|\psi_0\rangle$) and the maximum dimensional expressivity $expr_{dim}$ that the circuit has to reach to determine whether the system is controllable or not.

For a pure-state controllability test, one must set $test\_type = 'PSC'$. The circuit description is passed in terms of a list of parameters *para* ($\vec{\vartheta}$ from Equation (2.28)), a list of operators for the rotation gates $\hat{G}_{list}$ (given by the drift and the control operators, cf. Equation (5.1)), the initial state $|\psi_0\rangle$ (which can be chosen freely) and the parameter index *last_lay* at which the last circuit layer starts. A numerical tolerance *tol* is also required for computing the rank of the matrices $S_{C,n}$ (cf. Equation (2.33).

For the operator controllability test, $test\_type$ should be $'OC'$. The circuit should be defined including the auxiliary qubits, as depicted in Figure 5.6. This encompasses the definition of the generators of rotations which are passed as $\hat{G}_{list}$. In this case, the initial state $|\psi_0\rangle$ must be the maximally entangled state $|\psi_{ME}\rangle$ shown in Equation (5.15). The rest of the inputs are treated analogously to the previous case.

Finally, for either type of controllability, the computation of the $S_{C,n}$ matrices can be done with classical numerical calculations (as shown in Algorithm 5.2) or it may be achieved using real quantum circuits, as seen in [19]. This chapter showcases examples using the former one, although the latter is the intended version for the devised hybrid quantum-classical controllability test.

**Algorithm 5.1:** Controllability test using dimensional expressivity analysis

\\This method is defined for a circuit $C(\vec{\vartheta})$ only containing parametric rotation gates $\hat{R}_j(\vartheta_j)$
\\$\hat{R}_j(\vartheta_j) := \exp\left(-i\,\frac{\vartheta_j}{2}\hat{G}_j\right)$
\\$C(\vec{\vartheta}) := \hat{R}_{len(\vec{\vartheta})}(\vartheta_{len(\vec{\vartheta})}) \cdots \hat{R}_0(\vartheta_0)\,|\psi_0\rangle$
Input:
• ***test_type***: it can be 'PSC' or 'OC' depending on which controllability test should be run.
• ***para***: array $\vec{\vartheta}$ with all parameters $\vartheta_j$.
• $\hat{\mathbf{G}}_{\mathbf{list}}$: list including all the operators $\hat{G}_j$ in matrix form.
• $|\psi_\mathbf{0}\rangle$: initial state of the circuit.
• ***last_lay***: parameter index at which the last layer starts
\\I.e. the last layer starts with $\hat{R}_{last\_lay}(\vartheta_{last\_lay})$
• ***tol***: tolerance for computing the matrix rank function.

*hildim* ← len($|\psi_0\rangle$)
\\Expressivity right before the last layer
*expr_bll* ← Algorithm_5.2(*para*, $\hat{G}_{list}$, $|\psi_0\rangle$, *last_lay -1*, *tol*
\\Expressivity of the total circuit C
*expr_tot* ← Algorithm_5.2(*para*, $\hat{G}_{list}$, $|\psi_0\rangle$, len(*para*), *tol*
**if** *test_type is 'PSC'* **then**
  *max_exp* ← $2hildim - 1$
**else**
  *max_exp* ← $hildim^2 - 1$
**end if**
**if** $expr\_tot \geq max\_exp$ **then**
  *test_result* ← 1
    \\System is controllable
**else**
  **if** $expr\_tot > expr\_bll$ **then**
    *test_result* ← 2
      \\Test is inconclusive. Repeat test for a circuit containing an additional layer
  **else**
    *test_result* ← 0
      \\System is not controllable
  **end if**
**end if**
Output:
• ***expr_tot***: circuit dimensional expressivity
• ***test_result***: 0, 1 or 2 depending on whether the system is not controllable, controllable or the test is inconclusive. For inconclusive tests, one can repeat the algorithm adding a new layer to the circuit.

**Algorithm 5.2:** Classical calculation of $rank(S_{C,n})$ (cf. Eq. (2.33)).
This classical algorithm can be replaced by measurements on a quantum device as defined in [19].

\\This method is defined for a circuit $C(\vec{\vartheta})$ only containing parametric rotation gates $\hat{R}_j(\vartheta_j)$
\\$\hat{R}_j(\vartheta_j) := \exp\left(-i\,\frac{\vartheta_j}{2}\hat{G}_j\right)$
\\$C(\vec{\vartheta}) := \hat{R}_{len(\vec{\vartheta})}(\vartheta_{len(\vec{\vartheta})}) \cdots \hat{R}_0(\vartheta_0)\,|\psi_0\rangle$
Input:
- ***para***: array $\vec{\vartheta}$ with all parameters $\vartheta_j$.
- $\hat{\mathbf{G}}_{\mathbf{list}}$: list including all the operators $\hat{G}_j$ in matrix form.
- $|\psi_{\mathbf{0}}\rangle$: initial state of the circuit.
- ***n***: Dimension of the square matrix $S_n$ to be calculated (cf. Eq. (2.33)).
- ***tol***: tolerance used for computing matrix rank function.

*hildim* $\leftarrow$ len($|\psi_0\rangle$)
$J_n \leftarrow$ zero_array[2*hildim*,*n*]
**for** $j$ *in* $1, ..., n$ **do**
    $\partial C_j \leftarrow \frac{\partial C}{\partial \vartheta_j}(\vec{\vartheta})$
    $J_n[0 : hildim, j-1] \leftarrow Re\,(\partial C_j)$
    $J_n[hildim : 2hildim, j-1] \leftarrow Im\,(\partial C_j)$
**end for**
*Sn* $\leftarrow J_n^T J_n$
*rank_Sn* $\leftarrow rank(Sn, tol)$ \\compute rank of matrix *Sn* with tolerance *tol*
Output:
- ***rank_Sn***: rank of the matrix $S_{C,n}$

| Coupling strengths (MHz) | | | | | |
|---|---|---|---|---|---|
| $J_{0,1}$ | $J_{1,2}$ | | | | |
| 170 | 220 | | | | |
| **Qubit frequencies (GHz)** | | | | | |
| Original | | | Auxiliary | | |
| $\omega_0$ | $\omega_1$ | $\omega_2$ | $\omega_3$ | $\omega_4$ | $\omega_5$ |
| 5.40 | 5.30 | 5.42 | 5.37 | 5.29 | 5.34 |

**Table 5.2:** Parameters for the Hamiltonian (5.29) and the auxiliary qubits necessary for the circuit (5.24).

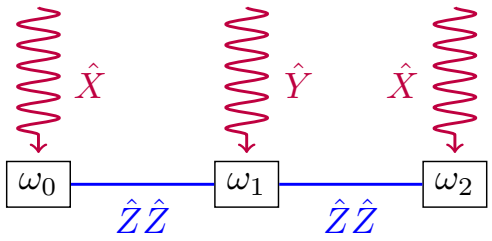


**Figure 5.8:** Example of a three-qubit system that is operator-controllable, cf. Eq. (5.30)

### 5.4.4 Examples

In the following we consider a three-qubit array with Hamiltonian

$$\hat{H}_{3q}(t) = \sum_{j=0}^{2} -\frac{\omega_j}{2}\hat{\sigma}_z^{(j)} + \sum_{k=0}^{1} J_{k,k+1}\hat{\sigma}_z^{(k)}\hat{\sigma}_z^{(k+1)} + \hat{H}_{ctrl}(t). \tag{5.29}$$

The second term, containing the time-independent two-qubit couplings, has been modified to $\hat{\sigma}_z^k\hat{\sigma}_z^{k+1}$ simply to showcase a qubit interaction different from the one in the previous examples. The qubit frequencies $\omega_j$ and the coupling strengths $J_{k,k+1}$ are listed in Table 5.2. We take two different $\hat{H}_{ctrl}(t)$ to study an example that is operator controllable and one that is not.

The first one is given by

$$\hat{H}_{ctrl}(t) = u_1(t)\hat{\sigma}_x^{(0)} + u_2(t)\hat{\sigma}_y^{(1)} + u_3(t)\hat{\sigma}_x^{(2)}, \tag{5.30}$$

see Figure 5.8. It is operator controllable as can easily be proven by the Lie algebra rank condition [14] and the graph method [148].

Since we have 3 controls in the original three-qubit system, the minimum number of layers needed to reach the maximum value of dimensional expressivity for the bipartite system, $expr_{dim} = 63$, is $n_l = 16$ according to Eq. (5.28). The orthonormal basis used to define the maximally entangled state $|\psi_{ME}\rangle$ is the logical basis of the free qubits.

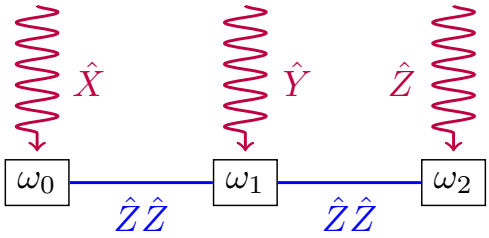


**Figure 5.9:** Example of a three-qubit system that is not operator-controllable, cf. Eq. (5.31).

Last, we generate a random set of parameters $\vec{\vartheta} \in [0, 2\pi]^{64}$. Maximum dimensional expressivity of 63 is found for the last parameter of the last layer, confirming that the system is operator controllable.

For the second example, we choose a different set of controls,

$$\hat{H}_{ctrl}(t) = u_1(t)\hat{\sigma}_x^{(0)} + u_2(t)\hat{\sigma}_y^{(1)} + u_3(t)\hat{\sigma}_z^{(2)}, \tag{5.31}$$

see Figure 5.9, making the system not controllable. We repeat the same procedure as before, since the number of controls is again $m = 3$. At the end of 16 layers the circuit only reaches $expr_{dim} = 31$, which is less than the 63 needed for operator controllability. We could add another layer to verify that every new rotation gate will have a redundant parameter. However, in this case it is sufficient to inspect the rank of the matrices $S_n$ from Eq. (2.33) in the last layers. We find that the last independent parameter appears at the end of the tenth layer, with all the remaining ones being exclusively formed by redundant parameters. This is a sufficient condition to determine that the system is not operator controllable (as long as it is verified with multiple sets of random parameters).

We emphasize that it is important to corroborate every "not controllable" result with different arrays $\vec{\vartheta}$ chosen at random. Selecting $\vec{\vartheta}$ in a non-randomized fashion may lead to cases where the dimensional expressivity is lower than the maximum value reached with other different parameters. This would yield wrong results in terms of controllability. It is easily rationalized in terms of symmetries of the commutators $[\hat{H}_i, \hat{R}_k^A(\vartheta_j)]$. These are linked to the partial derivatives of the circuit $\partial_i C_{OC}^{AB}(\vec{\vartheta})$ and to the dimensional expressivity of the circuit. Performing further numerical tests on the previously discussed examples, we have experimented with selecting parameters instead of choosing them at random. Wrong results with lower dimensional expressivity arose when all the parameters were chosen to be the same, e.g. $\vartheta_j = 1$ for every $j$. In every instance, these problems vanished as soon as we generated a new set of random parameters.

Another important issue concerns the minimum tolerance $\tau$ used to determine the rank of the $S_n$ matrices. More precisely, $\tau$ represents the threshold at which the

values of the singular value decomposition of $S_n$ are considered zero. $\tau$ is crucial to determine the different redundant parameters and the expressivity of the circuit. If $\tau$ is too high, then some linearly independent vectors might be deemed dependent by mistake, which would revert on a wrong lower value of the circuit expressivity, potentially turning a controllable system into a fake non-controllable one. Conversely, if $\tau$ is too small some errors might start to add up to make linearly dependent vectors look as if they were independent, falsely showing some parameters as independent. This would in turn raise the dimensional expressivity, usually above the $d^2-1$ threshold that we know to be valid for the case of the operator controllability test. To avoid these cases, it is advisable to use operators with similar orders of magnitude and try different ranges for $\tau$ depending on the order of magnitude of the operators $\hat{H}_j$ from Eq. (2.8). If the dimensional expressivity analysis is performed on quantum hardware, the tolerance $\tau$ will also depend on the device noise. Indeed, the accuracy of the measurements and the circuit dynamics will take a toll on the accuracy of the rank of the matrices $S_n$. Inevitably, noisier devices will require higher tolerances to determine whether there are redundant parameters (i.e. whether $\det(S_n) = 0$) or not.

## 5.5 Summary

We have introduced two hybrid quantum-classical algorithms to test pure-state and operator controllability of qubit arrays. As opposed to usual Lie rank and graph methods, the presented algorithms are run directly on a quantum circuit designed to mimic the dynamics of the quantum system to be studied. The method is also devised as an alternative to the cases where the dynamical Lie algebra can no longer be evaluated analytically or numerically on a classical computer. We have showcased the capabilities of the procedure with four paradigmatic examples that cover all scenarios for pure-state and operator controllability.

A useful application of these tests is the resource-efficient design of quantum chips. Our algorithm provides a systematic way to deduce the minimal number of local controls and qubit couplings required to maintain controllability, as a prerequisite of universal quantum computation. In other words, it allows one to identify redundant controls and thus to ease scaling up the quantum chip size. Importantly, the tests allow to obtain this information before the devices are built, as long as the associated quantum circuit can be implemented on a different device. Note that while the rank analysis of the $S_n$ matrices scales with the size of the system Hilbert space, this does not pose a fundamental limitation. It can be overcome by mapping the rank computation to a quantum device. More precisely, the quantum device would then be used to find the lowest eigenvalue of $S_n$ in order to determine whether a parameter is redundant or not. This permits the efficient identification of redundant

parameters and the removal of their parametric gates in the circuit. Noise in the device running our hybrid algorithm will limit the accuracy of the lowest eigenvalue and thus determine the minimum threshold for an eigenvalue to be considered zero.

In addition to its practical aspects, at the conceptual level, our work has revealed the close connection between the controllability of quantum systems and the dimensional expressivity of quantum circuits. In particular, this insight arises from the relation between the states that can be reached in a controllable system and the final states that can be produced in a parametric quantum circuit. The dimensional expressivity analysis allowed us to efficiently quantify the circuit expressivity. Its search for redundant parameters was essential in determining which controls contributed to reach more states in the Hilbert space. The link between the pure-state and operator controllability test is the inclusion of the Choi-Jamiołkovski isomorphism that creates a map between operators in a Hilbert space and the states of the extended bipartite space.

Variational quantum algorithms have previously been used to improve the design of optimal pulses in quantum systems [157]. Quantum optimal control theory in general [12, 130] encompassses both the design of the pulse shapes, i.e., control synthesis, and controllability analysis. The controllability tests described here thus extend the use of parametric quantum circuits to the second pillar of quantum optimal control. Quantum optimal control is also closely related to system characterization where controls can be interleaved with free evolutions [158, 159] or applied continuously [160].

In future work, it will be interesting to study systems with non-local controls, e.g. tunable two-qubit couplings. Moreover, it may be possible to expand our approach to systems other than qubit arrays. To this end, the key task will be to find a mapping from the non-qubit system to the associated quantum circuit that runs on a qubit array. The problem of mapping certain dynamics to a quantum circuit has already been a subject of extensive research, for example, when using parametric variational algorithms for calculating the electronic structure of molecules [161, 41] or their quantum dynamics [162]. An interesting future perspective is to explore the extension of our approach to the controllability of subgroups. This is sometimes referred to as $G$-controllability, where $G$ is a subgroup of the unitary group $U(n)$. This would be relevant both to open quantum system control and machine learning. While this is not a trivial task for the general case, the method here presented could be extended to analyse certain cases of $G$-controllability. More work in this direction is needed to give a more definitive answer. Finally, an intriguing question is how the removal of redundant controls affects the minimum time at which certain dynamics can be implemented, i.e., the quantum speed limit of the system. A controllable system with a

new control added can have the same or a lower minimum time for a state transfer or unitary gate. Conversely, removing redundant controls might incur a higher minimum time. Most likely, quantum device design will have to balance the requirements for controllability and operation speed.

# 6 Controllability condition for modular qubit arrays

## 6.1 Introduction

One of the main goals of quantum computing is to design an efficient configuration of qubits on which we can apply any arbitrary quantum gate. One of the goals of the previously introduced controllability tests [14, 148, 163] is to determine whether a given qubit array is suitable for universal quantum computing regarding the different unitary operations that can be implemented on the system[7]. To achieve this, it is necessary to find a trade-off between universality and the complexity of the system's architecture. This complexity is in great part determined by the resources that are added to connect and alter the qubits, i.e. the qubit couplings that allow for entanglement in the system and the controls that can be modified over time. Reducing the amount of built-in resources while maintaining the computational capability of the quantum device is a critical point in the successful design of quantum processors.

Previously, we have discussed some of the limitations of every mentioned controllability test. For a numerical calculation of the Lie rank condition, a relatively small number of qubits might start to add up numerical errors due to the curse of dimensionality. The proposed graph method (see Chapter 4) circumvents the calculation of the full algebra, vastly expanding the number of cases that can be studied. Nevertheless, the method will eventually fail for similar reasons, as the dimension of the graph (i.e. the Hilbert space dimension) also scales exponentially with the number of qubit. Similarly, the dimensional expressivity test (see Chapter 5) depends on the noise of the quantum processor on which the parametric quantum circuit is supposed to run. Larger systems will require the addition of more layers in the circuit, which in turn might reach the maximal depth at which circuits can be accurately implemented in the device. Thus, both classical and hybrid tests that rely on numerical computations are inevitably doomed to fail for a certain number of qubits. These are hard facts to face in a technological landscape where the ultimate goal is a quantum computer consisting of thousands of qubits.

There is, however, a way to salvage the previous controllability analysis without a limitation of an upper bound in the qubit array size. The current chapter sheds some light on further applications of the controllability studies. It constructs possible configurations of operator controllable qubit arrays for an arbitrarily large number of qubits. We present an algebraic result that allows allows for the design of larger devices by using smaller quantum processing units that are linked via entangling controls.

The current landscape for quantum computing focuses on a gate-based approach [164], but the topic of controllability needs a well defined Hamiltonian to perform the necessary calculations. Understanding the full Hamiltonian of a qubit array is a crucial point to obtain trustworthy controllability results that may lead to the design of quantum processors that allow for a modular architecture. But for quantum systems that are open to the public for performing quantum circuits, the information required for controllability might not be directly available. However, if two-qubit gate connections are listed for a quantum processor, we can make an educated guess about the two-qubit entangling term of the system Hamiltonian. For example, diagonal two-qubit gates may be engineered via a $\hat{Z}^i \otimes \hat{Z}^j$ interaction and other local phase gates. Following the current design of some quantum systems based on superconducting qubits like IBM [21], Google [43] or Rigetti [165], we have focused on two-qubit couplings. To determine the coupling strength $J_{i,j}$, i.e. the coefficient that precedes the entangling term, one can use the gate's duration as if it was a half Rabi oscillation. The coupling strength $J_{i,j}$ is therefore inversely proportional to the listed duration. Finally, it is customary to add local controls in every qubit that allow for fast single-qubit operations.

In the preceding examples we have used static couplings. This meant that no control was coupled to these interactions and, as such, they belonged to the time-independent drift of the system Hamiltonian. However it is possible to treat couplings as controls in the form of tunable couplings whose intensity can be changed over time [35, 36, 37]. Evidently, tunable couplings are preferable for controllability purposes: They allow for entanglement generation and count as an additional control in the Hamiltonian, which may lead to more linearly independent commutators and a larger dimension of the dynamical Lie algebra. Treating one coupling as static, however, lifts the necessity to calibrate the associated control or to include it among the variables that have to be optimized to perform a certain unitary evolution. In the following, we will count the number of couplings in a qubit array, making a distinction between time-independent couplings and tunable couplings. These tunable couplings will be the perfect tool to generate entangling controls between controllable quantum processing units.

The structure of this chapter is as follows. Section 6.2 spells out the main result of controllability, that extends the usability of previous controllability tests to larger qubit arrays. Section 6.3 contains all the necessary tools to derive the proof of the given theorem. Section 6.4 contains some possible designs for arbitrarily large arrays that are in theory capable of universal quantum computing. Finally, Section 6.5 presents a summary and the outlook.

## 6.2 Controllability of bipartite systems with an entangling control

Looking at the broader picture, the idea that we pose in this section is very simple. Assume we have two (possibly different) qubit arrays with some configurations of qubit couplings and controls that are proven to be operator controllable. This verification can be achieved by means of any of the available tests. If we connect both arrays with a control that is capable of generating some entanglement between them, the resulting multipartite system (composed of both original arrays and the new tunable coupling) is also operator controllable. If we label each of the arrays as a module, we can keep connecting modules to the original system with one entangling operation per new module and design an arbitrarily large system that is operator controllable.

This allows us to rephrase the concept as follows:

*If $\mathcal{A}$ and $\mathcal{B}$ are two separate qubit arrays that are operator controllable, then the system composed by*

- *The subsystem $\mathcal{A}$*
- *The subsystem $\mathcal{B}$*
- *An additional control $w_{ent}(t)\hat{H}_{ent}$ that is entangling between the $\mathcal{A}$ and $\mathcal{B}$ partitions*

*is also operator controllable.*

The generality of the statement might be surprising at first glance. It does not take into account any of the properties of the original qubit arrays other than operator controllability. As will be proven in Section 6.3, this result is independent of the number of qubits on each subsystem, the type and placement of qubit couplings or even the position and kind of controls. But, in fact, this shares similarities to some well-known properties in the area of quantum computing.

If we have a look at the most trivial example from a gate-oriented perspective, we get to a more familiar statement. In the case of two qubits, the set of local operations plus any entangling two-qubit gate forms a universal set. In other words, by applying a series of single-qubit gates and the chosen entangling gate we can approximate any two-qubit quantum gate. Here, having access to all local gates implies that the original systems, two separate qubits, are operator controllable. The entangling gate has the same effect as the entangling control that we use to connect both systems. To link this example back to the original statement, one simply has to include a minor modification: Substitute the qubits for *qudits* (perhaps of different dimensions $d_1$ and $d_2$). Indeed, by definition, any system can be viewed as a qudit with its dimension $d$ equal to the Hilbert space dimension of the system. The set of local unitary operators in two qubits $SU(2) \otimes SU(2)$ is substituted by $SU(d_1) \otimes SU(d_2)$. Every local gate in $SU(d_1) \otimes SU(d_2)$ can be implemented given the assumption of controllability on the separate partitions. In these terms, we can say that given two qudits with dimensions $d_1$ and $d_2$ and an entangling Hermitian operator $\hat{G}$ the set composed of local operations on the two qudits and the entangling rotation gates $\hat{R}_{\hat{G}}(\phi)$ forms a universal set[1]. Once two controllable systems are connected by an entangling control (e.g. a tunable coupler), they can be understood as a controllable system in itself. Which implies that we can connect it to a different controllable system using a new entangling control to make a controllable system. Note that the type of entangling operation between partitions is not relevant to prove controllability, as we will see in Section 6.3. In particular, the result is also true for any two-qubit tunable coupling as long as each of the qubits belongs to a different partition.

Naturally, having only one entangling operation between two partitions may hinder the speed at which information (and in particular entanglement) can travel through the system. Nevertheless, one possible goal is to use partitions that are large enough to run a certain kind of quantum algorithm or operation. In said case, this type of architecture is ideal to use each partition as a quantum processing unit capable of parallelising a more complex quantum algorithm. After performing simultaneous calculations the information of each processing unit can be merged to make use of the full computational power. While this is the most efficient use for such design, the universality of the system would still allows us to use it for any kind of quantum circuit.

As an example, we can use one of the T-shaped five-qubit systems presented in Chapter 4, inspired by the former *ibmq_quito* quantum processor [21]. We had already proven its controllability using the adapted graph method for qubit arrays and saw

[1]Note that here we have extended the term "rotation gates" to any gate in the form of $\hat{R}_{\hat{G}}(\phi) := \exp(-i\frac{\phi}{2}\hat{G})$, following the notation already introduced in Chapter 5.

that, when properly placed, the 5-qubit system is operator controllable with only two $\hat{X}$ local controls and the displayed two-qubit couplings in the form of $\hat{X}\hat{X} + \hat{Y}\hat{Y}$.

The two five-qubit arrays have been connected by a tunable coupling. The control operator of this entangling control is assumed to be in the form of $\hat{X}^{(4)}\hat{X}^{(7)}$, acting on the fourth and seventh qubit. Evidently, the two qubits belong to the first and second partition respectively. Note that this choice is fully arbitrary, and that any other entangling control between both subsystems would have done the trick.

The Hamiltonian of the system is defined as

$$\hat{H}(t)^{2T_5} = \hat{H}^{quito,\,A}(t) \otimes \mathbb{1} + \mathbb{1} \otimes \hat{H}^{quito,\,B}(t) + w_{ent}(t)\hat{X}^{(4)}\hat{X}^{(7)} \tag{6.1}$$

where the partial Hamiltonians $\hat{H}^{quito,\,(A/B)}(t)$ are given by Equation (4.13) with the sole difference that the qubit frequencies $\omega_j$ and coupling strengths $J_{i,j}$ may differ. The controls for both partitions are also meant to be taken as independent.

Once we have a system that is operator controllable, like the one displayed on Figure 6.1, we can add more controls without affecting controllability. On the contrary, this can have beneficial consequences on the system, like allowing faster unitary gates or generating the same Lie algebra using commutators of lower depth. For example, imagine that we wanted to implement some entangling two-qubit operation on the zeroth and ninth qubit displayed in Figure 6.1. Then, intuitively we would have faster options if we also had a tunable coupling between those two qubits. With the current setup, these two qubits are at a distance of seven couplings (six static plus the tunable coupling following the chain 0-1-3-4-7-6-8-9). While we have continuously spoken about minimizing resources, we have to be realistic: The quantum speed limit for large qubit arrays with minimal number of controls and couplings may grossly surpass the decoherence limit of the system.

These concepts will be developed in Section 6.4. There we will venture to sketch some possible designs for large arrays that use fewer resources than those available on the market, knowing that the question of quantum speed limit will still be relevant and open.

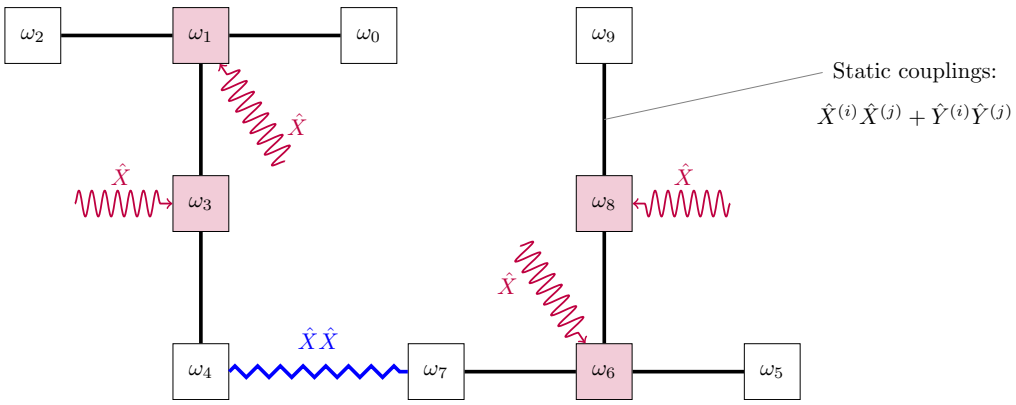


**Figure 6.1:** Example of an operator controllable system based on the connection of two five-qubit systems. The local controls and static qubit couplings follow the descriptions of Figure 4.6. The blue zigzag line between the fourth and seventh qubit represent a tunable coupling in the shape of $\hat{X}^{(4)}\hat{X}^{(7)}$.

## 6.3 Mathematical derivation

To obtain the aforementioned result, we use an analytical approach to prove controllability of the multipartite system using the Lie rank condition. This section proves that by adding any two-qubit tunable coupling between the subsystems $\mathcal{A}$ and $\mathcal{B}$ we can make the whole system $\mathcal{A} \otimes \mathcal{B}$ controllable.

### 6.3.1 Notation and problem statement

Let $\mathfrak{A} \cong \mathfrak{su}(2^M)$ and $\mathfrak{B} \cong \mathfrak{su}(2^N)$ be the dynamical Lie algebras of two separate controllable qubit arrays $\mathcal{A}$ and $\mathcal{B}$, with $M$ and $N$ qubits respectively. The elements of the algebra $\mathfrak{A}$ of the first subsystem can be represented as linear combinations of tensor products of Pauli matrices $\hat{\sigma}_\alpha$ (with $\alpha \in \{0,1,2,3\}$). Following the notation introduced in Equation (2.13), we represent single Pauli matrices in $\mathfrak{A}$ by

$$\hat{\sigma}_\alpha^{(\mu)} := \mathbb{1}_2 \otimes \ldots \otimes \mathbb{1}_2 \otimes \underbrace{\hat{\sigma}_\alpha}_{\mu\text{-th position}} \otimes \mathbb{1}_2 \otimes \ldots \mathbb{1}_2, \tag{6.2}$$

with $\alpha \in [0,1,2,3]$. Similarly, we represent the elements of $\mathfrak{B}$ following the same notation

$$\hat{\sigma}_j^{(n)} := \mathbb{1}_2 \otimes \ldots \otimes \mathbb{1}_2 \otimes \underbrace{\hat{\sigma}_j}_{n\text{-th position}} \otimes \mathbb{1}_2 \otimes \ldots \mathbb{1}_2, \tag{6.3}$$

with $j \in [0,1,2,3]$. To avoid confusion we use Greek letters for the indices of elements belonging to $\mathfrak{A}$ and Latin ones for those in $\mathfrak{B}$.

Let us assume that the system $\mathcal{A}$ is described by the traceless Hamiltonian:

$$\hat{H}^{\mathcal{A}}(t) = \hat{A}_0 + \sum_{\rho=1}^{C_A} u_\rho(t)\hat{A}_\rho, \tag{6.4}$$

where $\hat{A}_0$ is the time-independent drift, $u_\rho(t)$ are the real-valued controls, $\hat{A}_\rho$ the operators to which the controls are coupled and $C_A$ the number of controls in the system. The dynamical Lie algebra of the system is given by

$$\mathfrak{A} := Lie\left[\{i\hat{A}_\rho\}_{\rho=0}^{C_A}\right] \simeq \mathfrak{su}(2^M). \tag{6.5}$$

Analogously, we assume the system $\mathcal{B}$ to be described by

$$\hat{H}^{\mathcal{B}}(t) = \hat{B}_0 + \sum_{j=1}^{C_B} v_j(t)\hat{B}_j, \tag{6.6}$$

with a dynamical Lie algebra

$$\mathfrak{B} := Lie\left[\{i\hat{B}_j\}_{j=0}^{C_B}\right] \simeq \mathfrak{su}(2^N). \tag{6.7}$$

Ignoring local contributions, a two-qubit coupling between the $\mu$-th qubit in $\mathcal{A}$ and the $n$-th qubit in $\mathcal{B}$ can be in general written as

$$\hat{H}_c^{\mu,n} = \sum_{\alpha,j=1}^{3} c_{\alpha,j}\hat{\sigma}_\alpha^{(\mu)} \otimes \hat{\sigma}_j^{(n)}, \tag{6.8}$$

where the coefficients $c_{\alpha,j}$ are real-valued, with at least one of them nonzero. Thus, if we connect two qubits from $\mathcal{A}$ and $\mathcal{B}$ by an entangling two-qubit coupling $w(t)\hat{H}_c^{\mu,n}$ that we can treat as an independent control, then the Hamiltonian of the $\mathcal{A}\otimes\mathcal{B}$ system is

$$\begin{aligned}\hat{H}^{\mathcal{AB}}(t) =& \hat{H}^{\mathcal{A}}(t) \otimes \mathbb{1}_{2^N} + \mathbb{1}_{2^M} \otimes \hat{H}^{\mathcal{B}}(t) + w(t)\,\hat{H}_c^{\mu,n} \\ =& \hat{A}_0 \otimes \mathbb{1}_{2^N} + \mathbb{1}_{2^M} \otimes \hat{B}_0 + \qquad (6.9)\\ &+ \sum_{\rho=1}^{C_A} u_\rho(t)\hat{A}_\rho \otimes \mathbb{1}_{2^N} + \sum_{j=1}^{C_B} v_j(t)\mathbb{1}_{2^M} \otimes \hat{B}_j + w(t)\hat{H}_c^{\mu,n}. \qquad (6.10)\end{aligned}$$

Note that the drift of $\hat{H}^{\mathcal{AB}}$ is given by

$$\hat{H}_0^{\mathcal{AB}} = \hat{A}_0 \otimes \mathbb{1}_{2^N} + \mathbb{1}_{2^M} \otimes \hat{B}_0, \tag{6.11}$$

which encompasses the contributions of the drifts of $\mathcal{A}$ and $\mathcal{B}$. The dynamical Lie algebra of the bipartite system is given by

$$\mathcal{L}_{\mathcal{A}\otimes\mathcal{B}} := Lie\left[i\hat{H}_0^{\mathcal{AB}},\ \{i\hat{A}_\rho\otimes\mathbb{1}_{2^N}\}_{\rho=1}^{C_A},\ \{i\mathbb{1}_{2^M}\otimes\hat{B}_j\}_{j=1}^{C_B},\ i\hat{H}_c^{\mu,n}\right], \tag{6.12}$$

which is contained in $\mathcal{L}_{\mathcal{A}\otimes\mathcal{B}}\subseteq\mathfrak{su}(2^{M+N})$. The different operators in the previous equation include, in order of appearance, the drift of the total system, the local controls on the partition $\mathcal{A}$, the local controls on the partition $\mathcal{B}$ and the entangling control. In the following, we will prove that for two operator controllable systems $\mathcal{A}$ and $\mathcal{B}$ following Equation (6.4) and Equation (6.6) respectively, the bipartite system $\mathcal{A}\otimes\mathcal{B}$ with the two-qubit control $w(t)\hat{H}_c^{\mu,n}(t)$ is also operator controllable. Mathematically, this is equivalent to

$$\begin{cases}\mathfrak{A}=\mathfrak{su}(2^M)\\ \mathfrak{B}=\mathfrak{su}(2^N)\end{cases}\quad\Rightarrow\quad\mathcal{L}_{\mathcal{A}\otimes\mathcal{B}}=\mathfrak{su}(2^{M+N}) \tag{6.13}$$

for every $\hat{H}_c^{\mu,n}$ following Equation (6.8).

### 6.3.2 Operations with tensor products of Pauli matrices

Most of the needed calculations to generate the dynamical Lie algebra of the total system from Equation (6.12), involve commutators of the entangling control $\hat{H}_c^{\mu,n}$ with local operators of either subsystem. It is therefore important to understand what elements can be generated using only linear combinations of commutators of local operators. To obtain controllability in the complete system means to obtain every element in the total Lie algebra. To ensure this it is enough to show that a basis of the Lie algebra is achievable. For the case of the maximal algebra of $\mathcal{A}\otimes\mathcal{B}$, $\mathfrak{su}(2^{N+M})$, a possible basis is

$$\mathfrak{su}(2^{N+M})=\text{span}\ \{i\,\hat{\sigma}_{\alpha_1}\otimes\hat{\sigma}_{\alpha_2}\otimes\cdots\otimes\hat{\sigma}_{\alpha_M}\otimes\hat{\sigma}_{j_1}\otimes\hat{\sigma}_{j_2}\otimes\cdots\otimes\hat{\sigma}_{j_N}\}_{j_k,\alpha_\beta=0}^{3} \tag{6.14}$$

with at least one nonzero subindex $j_k$ or $\alpha_\beta$ in every element. All of the elements from the basis shown in Equation (6.14) present the same structure with different subindices. If we start from an element in the basis and define operations to change the Pauli indices to other possible values, we can generate a basis of $\mathfrak{su}(2^{N+M})$ and prove controllability. There are three qualitatively different possible index changes: Changing a nonzero index to a nonzero index, turning a nonzero index to zero or setting a zero index to a nonzero index. Here we introduce the associated three operations using local commutators on the $\mathfrak{B}$ subsystem. From here on, all subscripts $b$ of the Pauli operators $\hat{\sigma}_b^a$ are assumed to be nonzero unless explicitly stated otherwise. For simplicity, we also use a cyclic notation in the Pauli indices $\{1,2,3\}$, e.g. $\hat{\sigma}_{3+1}=\hat{\sigma}_4:=\hat{\sigma}_1$.

We start with an operation that allows us to change an index $j \in \{1,2,3\}$ of a Pauli matrix $\hat{\sigma}_j^{(n)}$ to $j+1$ for tensor products of Pauli matrices in the subsystem $\mathcal{B}$:

$$f_{cyc}^{(n)}\left(i\hat{\sigma}_j^{(n)}\right) := -\frac{1}{2}[i\hat{\sigma}_{j+2}^{(n)},\ i\hat{\sigma}_j^{(n)}] = i\hat{\sigma}_{j+1}^{(n)}. \tag{6.15}$$

Note that $f_{cyc}^{(n)}(\cdot)$ is defined using only commutators of elements in the Lie algebra $\mathfrak{B}$. Analogous operations can be defined for other values of $1 \leq n \leq N$. Since $\mathcal{B}$ is assumed to be controllable, $i\hat{\sigma}_{j+2}^{(n)} \in \mathfrak{B}$ for every $1 \leq n \leq N$. With the function $f_{cyc}^{(n)}(\cdot)$ we can cycle through all the nonzero indices of a Pauli matrix. This operation has some interesting properties. First, if we have a skew-Hermitian operator $i\hat{\sigma}_j^{(n)}\hat{\sigma}_j^{(m)}$ with $m \neq n$, then $f_{cyc}^{(n)}(i\hat{\sigma}_j^{(n)}\hat{\sigma}_k^{(m)}) := f_{cyc}^{(n)}(i\hat{\sigma}_j^{(n)})\hat{\sigma}_k^{(m)}$. In other words, if we have a tensor product of Pauli matrices, $f_{cyc}^{(n)}$ does not change the indices of Pauli matrices in a position $m \neq n$. Second, for Hermitian operators $\hat{A}$ acting on the first system $\mathcal{A}$, the definition can be naturally extended to $f_{cyc}^{(n)}(i\hat{A}\otimes\hat{\sigma}_j^{(n)}) := \hat{A}\otimes f_{cyc}^{(n)}(i\hat{\sigma}_j^{(n)})$. This operation will be relevant to compute the Lie algebra of the multipartite system. If $i\hat{A}\otimes\hat{\sigma}_j^{(n)} \in \mathcal{L}_{\mathcal{A}\otimes\mathcal{B}}$ and for the local operator $i\mathbb{1}_{2^M}\otimes\hat{\sigma}_{j+2}^{(n)} \in \mathcal{L}_{\mathcal{A}\otimes\mathcal{B}}$, then $\hat{A}\otimes f_{cyc}^{(n)}(i\hat{\sigma}_j^{(n)}) \in \mathcal{L}_{\mathcal{A}\otimes\mathcal{B}}$. The second hypothesis is trivially fulfilled if $\mathbb{1}_{2^M}\otimes\mathfrak{su}(N) \in \mathcal{L}_{\mathcal{A}\otimes\mathcal{B}}$, which is something that still has to be formally proven.

For the second operation we define a function using commutators of operators in $\mathcal{B}$ to turn a Pauli index from zero to $j>0$ at a position $n$. To achieve this it is imperative to have at least another Pauli matrix $\hat{\sigma}_k^{(m)}$ at a position $m \neq n$. The operation is given by

$$f_{gen\,k}^{(n,m)}\left(i\hat{\sigma}_0^{(n)}\hat{\sigma}_k^{(m)}\right) := -\frac{1}{4}\left[i\hat{\sigma}_0^{(n)}\hat{\sigma}_{k+1}^{(m)},\ \left[i\hat{\sigma}_j^{(n)}\hat{\sigma}_{k+1}^{(m)},\ i\hat{\sigma}_0^{(n)}\hat{\sigma}_k^{(m)}\right]\right] = i\hat{\sigma}_j^{(n)}\hat{\sigma}_k^{(m)}. \tag{6.16}$$

Analogous operations can be defined for other values of $1 \leq n,m \leq N$ and $j \in \{1,2,3\}$. Similarly as before, the function $f_{gen\,k}^{(n,m)}$ can be extended to other operators $i\mathcal{A}\otimes\hat{\sigma}_0^{(n)}\hat{\sigma}_k^{(m)}$ acting on the total Hilbert space. By definition, this operation is not affected by any other Pauli matrices at any position other than $m$ and $n$.

Finally, the third operation removes a Pauli matrix from the tensor product, i.e. it takes an element $\hat{\sigma}_j^{(n)}$ and sets it to $\hat{\sigma}_0^{(n)}$. To do so it is necessary to have another Pauli matrix $\hat{\sigma}_k^{(m)}$ in the tensor product. The operation is defined as

$$f_{rem}^{(n,m)}\left(i\hat{\sigma}_j^{(n)}\hat{\sigma}_k^{(m)}\right) := -\frac{1}{4}\left[i\hat{\sigma}_0^{(n)}\hat{\sigma}_{k+1}^{(m)},\ \left[i\hat{\sigma}_j^{(n)}\hat{\sigma}_{k+1}^{(m)},\ i\hat{\sigma}_j^{(n)}\hat{\sigma}_k^{(m)}\right]\right] = \hat{\sigma}_0^{(n)}\hat{\sigma}_k^{(m)}, \tag{6.17}$$

where similar functions can be defined for other positions $n,m$ and indices $j,k$. The same properties described for the operations $f_{cyc}^{(n)}$ and $f_{gen\,k}^{(n,m)}$ apply to $f_{rem}^{(n,m)}$.

We can define operations $f_{cyc}^{(\rho)}$, $f_{gen\,k}^{(\rho,\tau)}$ and $f_{rem}^{(\rho,\tau)}$ analogous to Equations (6.15-6.17) acting on the subsystem $\mathcal{A}$ instead of the subsystem $\mathcal{B}$. With this set of operations

we can transform any Pauli matrix tensor product (cf. Equation (6.14)) with at least one Pauli matrix acting on $\mathcal{A}$ and one acting on $\mathcal{B}$ and transform it into any other tensor product of Pauli matrices that is entangling between $\mathcal{A}$ and $\mathcal{B}$. In other words, if we have access to all the different local operations then we can transform any non-local tensor product of Pauli matrices into any other non-local tensor product of Pauli matrices. This will be a core idea in turning the entangling tunable coupling into other elements in the total Lie algebra by only using local operations, i.e. extending local controllability of the subsystems to the total system $\mathcal{A} \otimes \mathcal{B}$.

### 6.3.3 Preliminary lemmas

In this subsection we present and prove a collection of lemmas that are necessary for the final theorem. Together, they focus on proving that the dynamical Lie algebras $\mathfrak{A} \simeq \mathfrak{su}(2^M)$, $\mathfrak{su}(2^M) \simeq \mathfrak{B}$ of the initial subsystems belong to the dynamical Lie algebra $\mathcal{L}_{\mathcal{A}\otimes\mathcal{B}}$ of the total system, i.e. that $\mathfrak{A} \otimes \mathbb{1}_{2^N} \subseteq \mathcal{L}_{\mathcal{A}\otimes\mathcal{B}}$, and $\mathbb{1}_{2^M} \otimes \mathfrak{B} \subseteq \mathcal{L}_{\mathcal{A}\otimes\mathcal{B}}$.

Bear in mind that this result is not immediate. Equation (6.5) (respectively Eq. (6.7)) shows that all elements in $\{i\hat{A}_\rho\}_{\rho=0}^{C_A}$ (resp. $\{i\hat{B}_\rho\}_{j=0}^{C_B}$) are necessary to generate the Lie algebra $\mathfrak{A}$ (resp. $\mathfrak{B}$) in the general case. Looking at the elements that generate $\mathcal{L}_{\mathcal{A}\otimes\mathcal{B}}$ in Equation (6.12), one can see that neither $i\hat{A}_0$ nor $i\hat{B}_0$ appear directly among the elements. They appear, however, in the form of $\hat{H}_0^{\mathcal{AB}}$. Indeed they are both time independent elements, which means that a priori we cannot control them independently. Therefore it is necessary to prove that, by using commutators with other elements and their linear combinations, it is possible to generate the algebras $\mathfrak{A} \otimes \mathbb{1}_{2^N}$ and $\mathbb{1}_{2^M} \otimes \mathfrak{B}$.

First, we present two lemmas that combined show that $\mathfrak{A} \otimes \mathbb{1}_{2^N}$ can be generated using the elements in Equation (6.12). Intuitively it should be possible to separate them, as they act on different subspaces. Here that suspicion is formally proven.

**Lemma 6.3.1.** *Let $\{\mathbf{v}_i\}_{i=0}^m$ be a set of vectors in a vector space $V_A$. Let $\mathbf{w} \in V_B$ be another vector on a vector space $V_B$ such that $V_A \cap V_B = \{\mathbf{0}\}$. If the set $\{\mathbf{v}_i\}_{i=1}^m$ is linearly independent, then the set $\{\mathbf{v}_0 + \mathbf{w}\} \cup \{\mathbf{v}_i\}_{i=1}^m$ is also linearly independent.*

*Proof.* To prove that the second set is linearly independent we simply must show that for the following equality to hold,

$$c_0 (\mathbf{v}_0 + \mathbf{w}) + \sum_{i=1}^{m} c_i \mathbf{v}_i = 0,$$

all the coefficients $c_j$ (with $0 \leq j \leq m$) must be zero. Since $\mathbf{w} \perp \mathbf{v}_i \, \forall j \in \{1, 2, ..., m\}$ it is evident that $c_0 = 0$. This leaves us with the equation

$$\sum_{i=1}^{m} c_i \mathbf{v}_i = 0.$$

If the set $\{\mathbf{v}_i\}_{i=1}^{m}$ is linearly independent, then $c_i = 0 \, \forall j \in \{1, 2, ..., m\}$, which means that the elements in the set $\{\mathbf{v}_0 + \mathbf{w}\} \cup \{\mathbf{v}_i\}_{i=1}^{m}$ are also linearly independent. □

**Lemma 6.3.2.** *Let $\{i\hat{A}_\rho\}_{\rho=0}^{C_A} \subset \mathfrak{su}(2^M)$ be a set of linearly independent traceless skew-Hermitian operators that generate the algebra $\mathfrak{A} := Lie\left[\{i\hat{A}_\rho\}_{\rho=0}^{C_A}\right]$. Let $i\hat{B}_0 \in \mathfrak{su}(2^N)$ be a nonzero operator such that $[i\hat{A}_\rho \otimes \mathbb{1}_{2^N} \, i\mathbb{1}_{2^M} \otimes \hat{B}_0] = 0$ for every $0 \leq \rho \leq C_A$. Then the following implication holds true:*

$$\begin{aligned} &\textit{If } \mathfrak{A} \cong \mathfrak{su}(2^M) \textit{ and } \mathfrak{A}' := Lie\left[i\hat{A}_0 \otimes \mathbb{1}_{2^N} + i\mathbb{1}_{2^M} \otimes \hat{B}_0, \{i\hat{A}_\rho \otimes \mathbb{1}_{2^N}\}_{\rho=1}^{C_A}\right] \\ &\qquad \textit{then } \mathfrak{A}' \cong \mathfrak{su}(2^M) \otimes \mathbb{1}_{2^N} \bigoplus i\mathbb{1}_{2^M} \otimes \hat{B}_0. \end{aligned} \tag{6.18}$$

*Proof.* Assume that the hypothesis $\mathfrak{A} \cong \mathfrak{su}(2^M)$ is true. Let $\{\hat{G}_\rho\}_{\rho=0}^{2^{2M}-2}$ be the basis of $\mathfrak{A}$ spanned by $\{i\hat{A}_\rho\}_{\rho=0}^{C_A}$ generated by the procedure described in Section 2.3.4. We are going to show that $\hat{G}'_\rho := \hat{G}_\rho \otimes \mathbb{1}_{2^N} \in \mathfrak{A}'$ for every $1 \leq \rho \leq 2^{2M} - 2$. Since $[i\hat{A}_\rho \otimes \mathbb{1}_{2^N}, i\mathbb{1}_{2^M} \otimes \hat{B}_0] = 0$ for every $\rho$, for every $\hat{G}_\rho \in \mathfrak{A}$ of depth $p \geq 1$ we can generate the associated $\hat{G}'_\rho \in \mathfrak{A}'$. Additionally, for every element $\hat{G}_\rho$ of depth $p = 0$ and index $\rho > 1$, $\hat{G}'_\rho = \hat{A}_\rho \otimes \mathbb{1}_{2^N} \in \mathfrak{A}'$ by definition. By virtue of Lemma 6.3.1, since $\{\hat{G}'_\rho\}_{\rho=0}^{2^{2M}-2}$ is a linearly independent set, the set $\{i\hat{A}_0 \otimes \mathbb{1}_{2^N} + i\mathbb{1}_{2^M} \otimes \hat{B}_0\} \cup \{\hat{G}_\rho\}_{\rho=1}^{2^{2M}-2} \subset \mathfrak{A}'$ must be linearly independent as well.

We have found a $(2^{2M} - 1)$-dimensional set of linearly independent terms in $\mathfrak{A}'$. Given that $\mathfrak{A}' \subseteq \mathfrak{su}(2^M) \otimes \mathbb{1}_{2^N} \bigoplus i\mathbb{1}_{2^M} \otimes \hat{B}_0$, then $2^{2M} - 1 \leq \dim(\mathfrak{A}') \leq 2^{2M}$.

Let us assume that $\dim(\mathfrak{A}') = 2^{2M} - 1$ to see that we reach a contradiction. The algebra

$$\mathfrak{G} := Lie\left[\{\hat{G}_\rho\}_{\rho=1}^{2^{2M}-2}\right] \tag{6.19}$$

has dimension $\dim(\mathfrak{G}) = 2^{2M} - 2$. By definition of $\hat{G}_\rho$, the set $\{i\hat{A}_0, \hat{G}_1, ...\hat{G}_{2^{2M}-2}\}$ is a basis of $\mathfrak{A} \cong \mathfrak{su}(2^M)$. If $\dim(\mathfrak{A}') = 2^{2M} - 1$ then

$$[i\hat{A}_0 \otimes \mathbb{1}_{2^N} + i\mathbb{1}_{2^M} \otimes \hat{B}_0, \mathfrak{G} \otimes \mathbb{1}_{2^N}] = [i\hat{A}_0 \otimes \mathbb{1}_{2^N}, \mathfrak{G} \otimes \mathbb{1}_{2^N}] \subseteq \mathfrak{G} \otimes \mathbb{1}_{2^N}, \tag{6.20}$$

which makes $\mathfrak{G}$ an ideal[2] of $\mathfrak{su}(2^M)$ of dimension $2^{2M}-2$. But this is not possible, since the special unitary algebras $\mathfrak{su}(n)$ are simple (i.e. they do not contain any non-trivial ideal). Thus $\dim(\mathfrak{G}) = 2^{2M}-1$ and $\dim(\mathfrak{A}') = 2^{2M}$, proving the implication of this lemma. □

The last needed lemma shows how to generate the total algebra $\mathcal{L}_{\mathcal{A}\otimes\mathcal{B}}$ using the entangling control $\hat{H}_c^{\mu,n}$ and the two local dynamical Lie algebras. In other words, this lemma presents a method to obtain all the remaining entangling elements in the total algebra using only linear combinations of commutators.

**Lemma 6.3.3.** *Let $\mathfrak{A} \cong \mathfrak{su}(2^M)$ and $\mathfrak{B} \cong \mathfrak{su}(2^N)$. Let*

$$\hat{H}_c^{\mu,n} := \sum_{\alpha,j\in[1,2,3]} c_{\alpha,j}\hat{\sigma}_\alpha^{(\mu)} \otimes \hat{\sigma}_j^{(n)} \quad \in \mathfrak{A}\otimes\mathfrak{B} \tag{6.21}$$

*be a nonzero Hermitian operator with $1 \le \mu \le M$, $1 \le n \le N$, $c_{\alpha,j} \in \mathbb{R}$, $i\hat{\sigma}_\alpha^{(\mu)} \in \mathfrak{A}$ and $i\hat{\sigma}_j^{(n)} \in \mathfrak{B}$. Then*

$$\mathcal{L} := Lie\left[\mathfrak{A}\otimes\mathbb{1}_{2^N},\ \mathbb{1}_{2^M}\otimes\mathfrak{B},\ i\hat{H}_c^{\mu,n}\right] \cong \mathfrak{su}(2^{M+N}) \tag{6.22}$$

*Proof.* We use tensor products of Pauli matrices for the bases of the algebras $\mathfrak{su}(2^M)$, $\mathfrak{su}(2^M)$ and $\mathfrak{su}(2^{M+N})$.

Without loss of generality, we can assume the two qubit coupling to be of the form $\hat{H}_c^{\mu,n} = c_{\alpha,j}\hat{\sigma}_\alpha^{(\mu)} \otimes \hat{\sigma}_j^{(n)}$, with only one nonzero coefficient $c_{\alpha,j}$ for some fixed $\alpha, j \in [1,2,3]$. Indeed, assume that $\hat{H}_c^{\mu,n}$ has a nonzero contribution $\hat{\sigma}_3^{(\mu)} \otimes \hat{\sigma}_3^{(n)}$, i.e., $c_{3,3} \neq 0$. We can prove that $i\hat{\sigma}_3^{(\mu)} \otimes \hat{\sigma}_3^{(n)}$ belongs to the dynamical Lie algebra of the total system by using commutators of $i\hat{H}_c^{\mu,n}$ with elements of $\mathfrak{A}\otimes\mathbb{1}_{2^N}$ and $\mathbb{1}_{2^M}\otimes\mathfrak{B}$. Starting from any general $i\hat{H}_c^{\mu,n}$ as depicted in Equation (6.21), we can isolate a single tensor product of Pauli matrices $i\hat{\sigma}_3^{(\mu)} \otimes \hat{\sigma}_3^{(n)}$ (again, assuming $c_{3,3} \neq 0$). Let us see explicitly how to obtain this term. Given the usual commutation relations we compute the following element:

$$\begin{aligned}
&\left[i\hat{\sigma}_3^{(\mu)}\otimes\mathbb{1}_{2^N},\ \left[i\hat{\sigma}_1^{(\mu)}\otimes\mathbb{1}_{2^N},\ i\sum_{\alpha,j=1}^{3} c_{\alpha,j}\hat{\sigma}_\alpha^{(\mu)}\otimes\hat{\sigma}_j^{(n)}\right]\right] = \\
&\qquad = \left[i\hat{\sigma}_3^{(\mu)}\otimes\mathbb{1}_{2^N},\ 2i\sum_{j=1}^{3} c_{3,j}\hat{\sigma}_2^{(\mu)}\otimes\hat{\sigma}_j^{(n)} - 2i\sum_{k=1}^{3} c_{2,k}\hat{\sigma}_3^{(\mu)}\otimes\hat{\sigma}_k^{(n)}\right] \\
&\qquad = 4i\sum_{j=1}^{3} c_{3,j}\hat{\sigma}_1^{(\mu)}\otimes\hat{\sigma}_j^{(n)} \quad \in \mathcal{L},
\end{aligned} \tag{6.23}$$

[2] An ideal in a Lie algebra $\mathcal{L}$ is a vector subspace $\mathcal{I}$ so that $[\mathcal{L},\mathcal{I}] \subseteq \mathcal{I}$.

where we have eliminated all coefficients with $\alpha \neq 3$. Similarly,

$$\left[ i\hat{\sigma}_3^{(\mu)} \otimes \mathbb{1}_{2^N},\ \left[ i\hat{\sigma}_1^{(\mu)} \otimes \mathbb{1}_{2^N},\ 4i \sum_{j=1}^{3} c_{3,j} c_{3,j} \hat{\sigma}_1^{(\mu)} \hat{\sigma}_j^{(n)} \right] \right] \ =\ 16i\, c_{3,3}\, \hat{\sigma}_1^{(\mu)} \hat{\sigma}_1^{(n)} \quad \in \mathcal{L}. \tag{6.24}$$

Therefore, using commutators we were able to obtain a single tensor product of Pauli matrices between algebras, $\hat{\sigma}_\alpha^{(\mu)} \otimes \hat{\sigma}_j^{(n)}$ (with $\alpha = j = 1$ in the previous example). For any two-qubit operator we can isolate one term and assume it to be in the form $\hat{\sigma}_\alpha^{(\mu)} \otimes \hat{\sigma}_j^{(n)}$. If

$$Lie\left[ \mathfrak{A} \otimes \mathbb{1}_{2^N},\ \mathbb{1}_{2^M} \otimes \mathfrak{B},\ i\hat{\sigma}_\alpha^{(\mu)} \otimes \hat{\sigma}_j^{(n)} \right] \cong \mathfrak{su}(2^{M+N}) \tag{6.25}$$

then Equation (6.22) is true, since

$$Lie\left[ \mathfrak{A} \otimes \mathbb{1}_{2^N},\ \mathbb{1}_{2^M} \otimes \mathfrak{B},\ i\hat{\sigma}_\alpha^{(\mu)} \otimes \hat{\sigma}_j^{(n)} \right] \subseteq Lie\left[ \mathfrak{A} \otimes \mathbb{1}_{2^N},\ \mathbb{1}_{2^M} \otimes \mathfrak{B},\ i\hat{H}_c^{\mu,n} \right]. \tag{6.26}$$

To prove Equation (6.25), we show that we can obtain every element

$$i\left( \hat{\sigma}_{\alpha_1}^{(1)} ... \hat{\sigma}_{\alpha_M}^{(M)} \right) \otimes \left( \hat{\sigma}_j^{(1)} ... \hat{\sigma}_{j^N}^{(N)} \right) \qquad \forall \alpha_\beta, j_k \in [0,1,2,3], \tag{6.27}$$

with at least one $\alpha_\beta$ or $j_k$ nonzero. These elements form a basis of $\mathfrak{su}(2^{M+N})$. Note that the elements where $\alpha_\beta = 0$ with $1 \leq \beta \leq M$ already belong to $\mathbb{1}_{2^M} \otimes \mathfrak{B}$, whereas the terms with $j_k = 0$ for every $0 \leq k \leq N$ belong to $\mathfrak{A} \otimes \mathbb{1}_{2^N}$. Therefore, we only have to prove it for the cases where at least one $\alpha_\beta$ and at least one $j_k$ are nonzero. Starting with the two qubit coupling $\hat{H}_c^{\mu,n} = c_{\alpha,j} \hat{\sigma}_\alpha^{(\mu)} \otimes \hat{\sigma}_j^{(n)}$ and using the operations $f_{cyc}^{(n)}$, $f_{gen\,k}^{(n,m)}$, $f_{rem}^{(n,m)}$, $f_{cyc}^{(\rho)}$, $f_{gen\,k}^{(\rho,\tau)}$ and $f_{rem}^{(\rho,\tau)}$ (for every possible value of $n$, $m$, $\rho$ and $\tau$) defined in Section 6.3.2 we can obtain any non-local tensor product of Pauli matrices using only commutators of $\hat{H}_c^{\mu,n}$ and local operators. Therefore, we can generate a basis of $\mathfrak{su}(2^{M+N})$ and the proof concludes.

□

With these three lemmas we have all the necessary intermediate results to prove the main idea of this chapter, which is properly shown and discussed in the following subsection.

### 6.3.4 Controllability of two controllable qubit arrays coupled via a two-qubit control

We finally can prove that the system formed by two controllable qubit arrays and a two-qubit tunable coupling that connects both is also operator controllable and hence

a suitable candidate for universal quantum computing. The condition that must be satisfied had already been summarized in Equation (6.13).

The whole proof is compacted in the following theorem:

**Theorem 6.3.4.** *Let $\mathcal{A}$ and $\mathcal{B}$ be two operator controllable qubit arrays with $M$ and $N$ qubits and Hamiltonians* (6.4) *and* (6.6)*. Let $\hat{H}_c^{\mu,n}$ be a two-qubit operator given by Equation (6.8). Then, the extended bipartite system with a tunable two-qubit coupling described in Equation (6.9) is operator controllable.*

*Proof.* A simple calculation of the dynamical Lie algebra from Equation (6.12) yields

$$\begin{aligned}
\mathcal{L}_{\mathcal{A}\otimes\mathcal{B}} &= Lie\left[1,\ \{i\hat{A}_\rho\otimes\mathbb{1}_{2^N}\}_{\rho=1}^{C_A},\ \{i\mathbb{1}_{2^M}\otimes\hat{B}_j\}_{j=1}^{C_B},\ i\hat{H}_c^{\mu,n}\right] = \\
&= Lie\left[Lie\left[i\hat{H}_0^{\mathcal{AB}},\ \{i\hat{A}_\rho\otimes\mathbb{1}_{2^N}\}_{\rho=1}^{C_A}\right],\ \{i\mathbb{1}_{2^M}\otimes\hat{B}_j\}_{j=1}^{C_B},\ i\hat{H}_c^{\mu,n}\right] \overset{\text{Lemma 6.3.2}}{=} \\
&= Lie\left[\mathfrak{A}\otimes\mathbb{1}_{2^N}\bigoplus i\mathbb{1}_{2^M}\otimes\hat{B}_0,\ \{i\mathbb{1}_{2^M}\otimes\hat{B}_j\}_{j=1}^{C_B},\ i\hat{H}_c^{\mu,n}\right] = \\
&= Lie\left[\mathfrak{A}\otimes\mathbb{1}_{2^N},\ i\mathbb{1}_{2^M}\otimes\hat{B}_0,\ \{i\mathbb{1}_{2^M}\otimes\hat{B}_j\}_{j=1}^{C_B},\ i\hat{H}_c^{\mu,n}\right] = \\
&= Lie\left[\mathfrak{A}\otimes\mathbb{1}_{2^N},\ Lie\left[i\mathbb{1}_{2^M}\otimes\hat{B}_0,\ \{i\mathbb{1}_{2^M}\otimes\hat{B}_j\}_{j=1}^{C_B}\right],\ i\hat{H}_c^{\mu,n}\right] = \\
&= Lie\left[\mathfrak{A}\otimes\mathbb{1}_{2^N},\ \mathbb{1}_{2^M}\otimes\mathfrak{B},\ i\hat{H}_c^{\mu,n}\right] \overset{\mathcal{A},\mathcal{B}\text{ operator controllable}}{=} \\
&= Lie\left[\mathfrak{su}(2^M)\otimes\mathbb{1}_{2^N},\ \mathbb{1}_{2^M}\otimes\mathfrak{su}(2^N),\ i\hat{H}_c^{\mu,n}\right] \overset{\text{Lemma 6.3.3}}{=} \\
&= \mathfrak{su}\left(2^{M+N}\right).
\end{aligned} \tag{6.28}$$

Therefore the bipartite system is operator controllable for any entangling two-qubit coupling. □

As a final note and without an explicit proof, this result can also be extended to any type of control that is entangling between the partitions $\mathcal{A}$ and $\mathcal{B}$. The main idea behind it is that the same process by which $i\hat{H}_0^{\mathcal{AB}}$ was reduced to a single product $c_{\alpha,j}\hat{\sigma}_\alpha^{(\mu)}\otimes\hat{\sigma}_j^{(n)}$ can be analogously defined for any type of entangling coupling, independently of the number of qubits on which it acts.

At first, this may seem like an unnecessary remark, as two-qubit couplings are often more easily implemented than interactions between three or more qubits. But it opens up a range of possibilities that are not constricted by this hypothesis. For example, it includes global controls that operate simultaneously on every qubit, like electromagnetic fields acting on trapped ions or on NV centers. Furthermore, using entangling controls that affect more than two qubits may increase the ratio at which information is shared between the two subsystems, depending on the architecture of

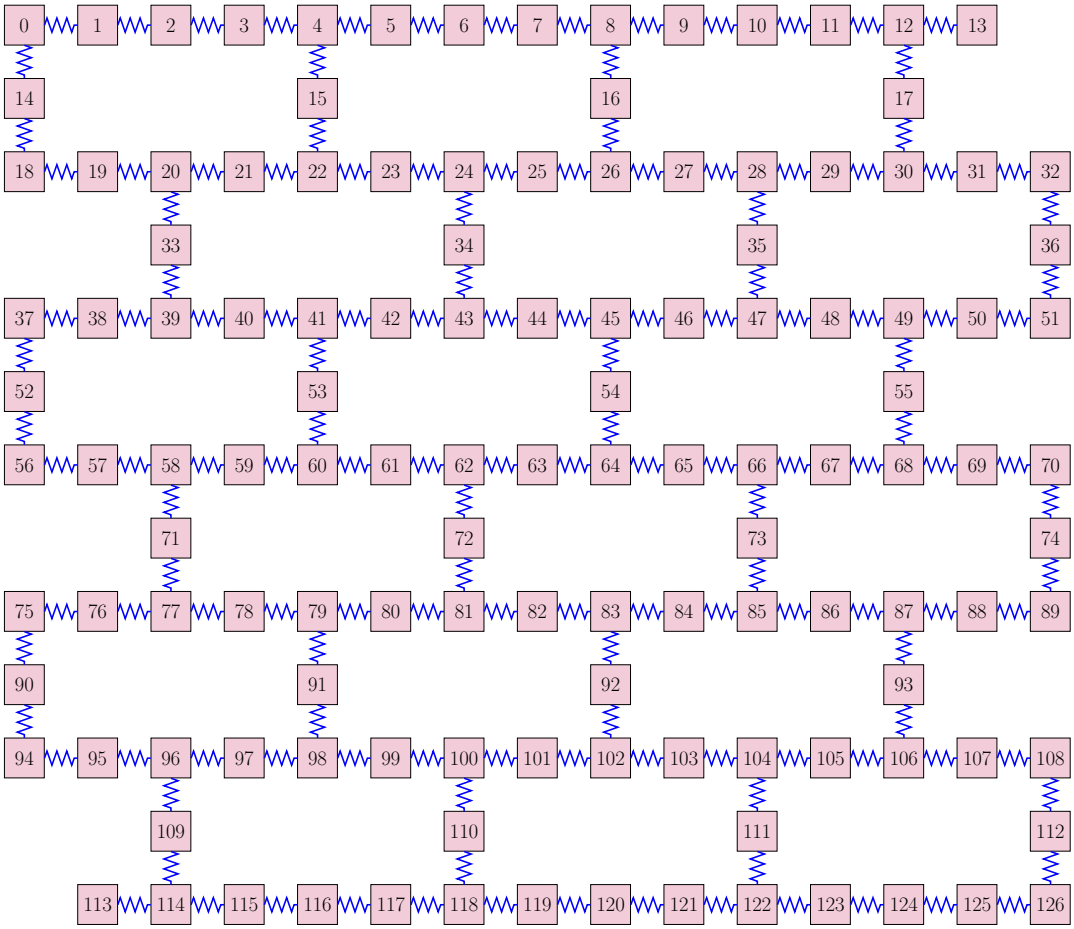


**Figure 6.2:** Qubit array based on available devices from IBM [21]. The blue zigzag lines represent two-qubit tunable couplings that connect the neighbouring qubits in the two-dimensional configuration.

the remaining couplings and controls. This generality offers a great freedom when using controllable subsystems as building blocks of a larger, controllable system.

## 6.4 Design of large qubit arrays

To showcase a possible application of this idea, we take as inspiration one of the quantum processors from IBM [21] that is available to the public. We will then design a similar architecture using smaller quantum processing units that have already been demonstrated to be controllable. This will show how many local controls and couplings can be removed from the system while maintaining operator controllability.

We start with the 127-qubit system shown in Figure 6.2. This two-dimensional array is particularly well suited to this method, as it already has a regular pattern consisting

mainly of three-by-five rectangles. All qubits are equipped with local controls and two-qubit tunable couplings between nearest neighbours. In total it comprises 144 tunable couplings and 127 local controls. Note that proving controllability on this device using the graph test or the dimensional expressivity test is extremely demanding due to the considerably large number of qubits. Finding a decomposition into quantum processing units that form an operator controllable system also implies that the original system is operator controllable. In other words, combining this method with the previous controllability tests also extends the dimension of the systems whose controllability can be determined.

The first building block that we are going to use is a T-shaped five-qubit system. This configuration is based on the *ibmq_quito* system previously discussed. Its Hamiltonian can be written as

$$\begin{aligned}\hat{H}_{5T}(t) \;=\; & \sum_{j=0}^{4} \hat{H}^{(j)}_{1qubit} + \hat{H}^{(1)}_{control}(t) + \hat{H}^{(3)}_{control}(t) \\ & + \hat{H}^{(0,1)}_{coup} + \hat{H}^{(1,2)}_{coup} + \hat{H}^{(1,3)}_{coup} + \hat{H}^{(3,4)}_{coup}\end{aligned} \tag{6.29}$$

where the single-qubit Hamiltonian $\hat{H}^{(j)}_{1qubit}$, the

$$\begin{aligned}\hat{H}^{(j)}_{1qubit} \;=\; & -\frac{\omega_j}{2}\hat{\sigma}^{(j)}_z; \qquad \hat{H}^{(j)}_{control}(t) \;=\; u_j(t)\hat{\sigma}^{(j)}_x; \\ & \hat{H}^{(j,k)}_{coup} \;=\; J_{j,k}\left(\hat{\sigma}^{(j)}_x\hat{\sigma}^{(k)}_x + \hat{\sigma}^{(j)}_y\hat{\sigma}^{(k)}_y\right);\end{aligned} \tag{6.30}$$

for any qubit frequencies $\omega_j$, coupling strengths $J_{j,k}$ and controls $u_j(t)$. In Chapter 4 we had proven that this system is controllable with two single local controls and time-independent or static couplings. The coupling type is inspired on the interactions that can be found in superconducting qubits.

To provide a cover for the qubit array in Figure 6.2 we need to include two more systems. The second one is arbitrarily chosen to be a five-qubit system arranged in a line with Hamiltonian

$$\begin{aligned}\hat{H}_{5L}(t) \;=\; & \sum_{j=0}^{4} \hat{H}^{(j)}_{qubit} + \hat{H}^{(1)}_{control}(t) + \hat{H}^{(2)}_{control}(t) \\ & + \hat{H}^{(0,1)}_{coup} + \hat{H}^{(1,2)}_{coup} + \hat{H}^{(2,3)}_{coup} + \hat{H}^{(3,4)}_{coup},\end{aligned} \tag{6.31}$$

with four static couplings and two local controls.

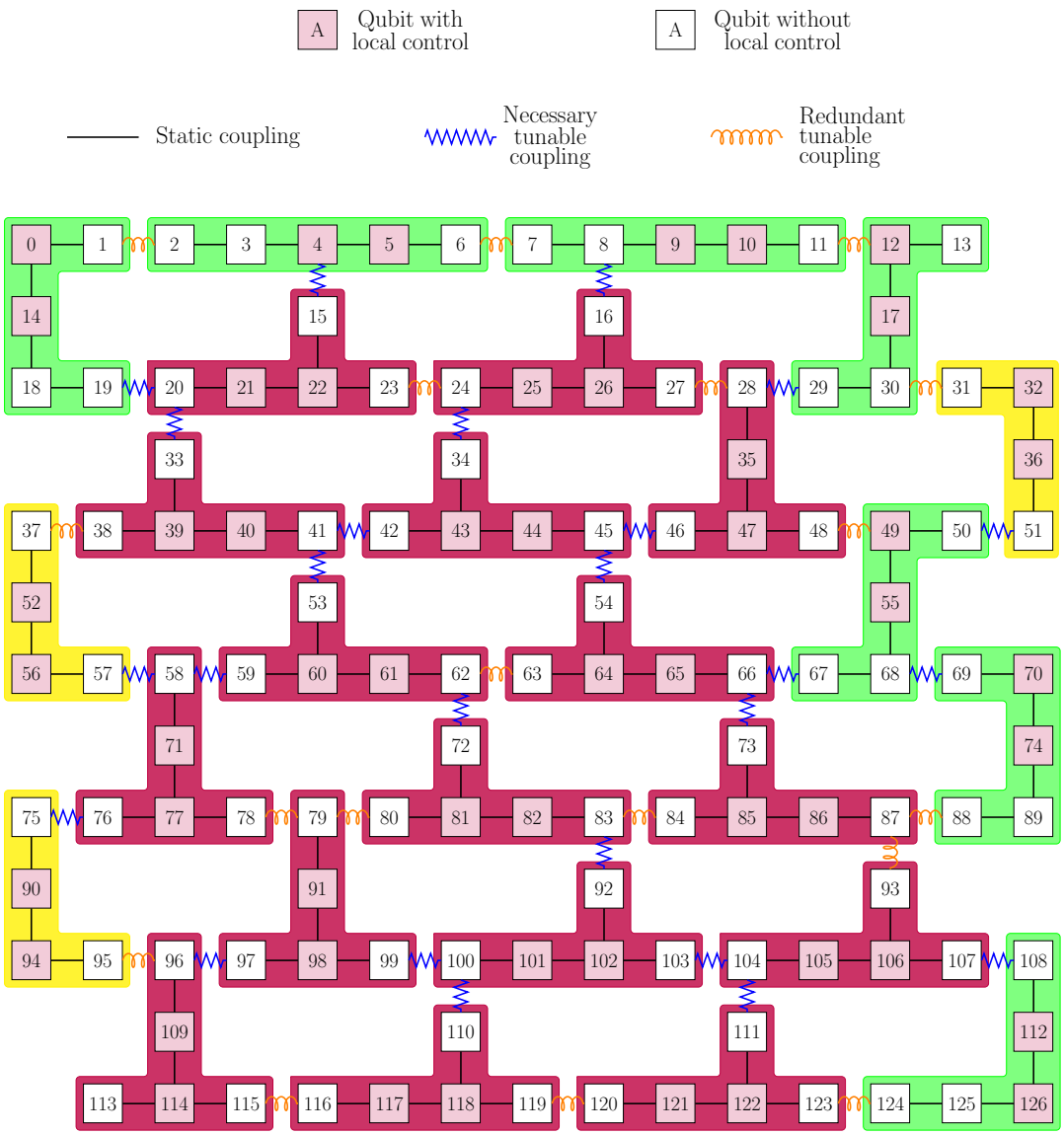


**Figure 6.3:** Controllable qubit array proposed as an alternative to the one in Figure 6.2. The shaded qubits are equipped with local controls, while the blank ones are not. The blue zigzag lines are tunable couplings needed for the system to be controllable. The coiled lines represent tunable couplings that were present in the original system but can be removed without hampering controllability on the system. Each five- or four-qubit coloured area represents one of the three controllable modules defined in Equations (6.29)-(6.32). Each colour represents one of the different configurations. The couplings contained in every module are static couplings as opposed to the other time-dependent ones.

Last, we remove one qubit from the previous system to define a four-qubit line with similare features

$$\begin{aligned}\hat{H}_{4L}(t) \;=\; \sum_{j=0}^{4} \hat{H}^{(j)}_{qubit} + \hat{H}^{(1)}_{control}(t) + \hat{H}^{(2)}_{control}(t) \\ + \hat{H}^{(0,1)}_{coup} + \hat{H}^{(1,2)}_{coup} + \hat{H}^{(2,3)}_{coup} + \hat{H}^{(3,4)}_{coup}.\end{aligned} \tag{6.32}$$

Using copies of the systems defined by $\hat{H}_{5L}(t)$, $\hat{H}_{5L}(t)$ and $\hat{H}_{5L}(t)$ we can build a similar architecture to the 127-qubit system. To make the whole system controllable we simply must connect each subsytem to another one using a tunable coupling. The result is shown in Figure 6.3. This newly defined system downgrades some of the tunable couplings from the previous system to static couplings, effectively reducing the numbers of controls in the system. Similarly, we can remove some of the extra tunable couplings in the system (the ones depicted with coiled orange lines) without losing controllability in the system. Alternatively, the couplings can remain in the design to maintain the connectivity between qubits. The main achievement, however, is the reduction in the number of local controls to roughly two fifths of the original amount. This is obtained simply by reducing the number of controls in each module by finding controllable qubits arrays with any desired controllability test. Comparing exact numbers, IBM's system is composed of 127 local controls and 144 tunable couplings; the alternative system has only 52 local controls, 101 static couplings and 25 tunable couplings. There are a total of 18 tunable couplings, which can be removed to lower the number of resources or left in place to improve quantum information transfer. The modified system is a simplified version of the original one with fewer resources, which may be beneficial for scaling up the architecture, which can easily be done by connecting new modules to the current system.

As a last note, we can also obtain information about the original system thanks to the modified one. In particular, we can prove that the original system is controllable. To do so, we simply need to recall two properties of controlled systems. The first one is that if a quantum system is controllable, the same system with more controls must be controllable too. We know that the system in Figure 6.3 with only the static couplings and the necessary tunable couplings (indicated by blue zigzag lines) is controllable. If we add the removed local controls back on every qubit and the redundant tunable couplings, then the system must be controllable too. The second property is that if a qubit array with static couplings is controllable, then the same system but with tunable couplings is also controllable. This can be proven since the dynamical Lie algebra of the first system must be contained in the algebra of the second one. Therefore the modified system from Figure 6.3 with tunable couplings instead of static couplings is also controllable. So the system with local controls in every qubit and tunable couplings between any neighbouring qubits must be controllable as well. In other words, we have proven that the original system from Figure 6.2 is operator controllable too and thus potentially capable of universal quantum computing. This also shows another possible application of the method to determine controllability on large qubit arrays: If the modified modular system is controllable—perhaps using fewer controls and some static instead of tunable couplings—then the original system on which it is based is operator controllable as well.

## 6.5 Summary

This chapter has presented a method to design arbitrarily large controllable qubit arrays by using smaller controllable systems. It has been mathematically proven that this is a generally valid result for any pair of controllable qubit arrays and any entangling control. This serves as a versatile tool that can be applied to most cases. Furthermore, it can be done inductively, concatenating the subsystem after subsystem to generate larger systems. It serves as a modular design based on subsystems acting as quantum processing units while still maintaining controllability, a requirement for universal quantum computing. An example based on IBM's systems has been studied, where controllability could be guaranteed using far fewer couplings and controls.

This modular approach still requires using subsystems that are proven to be operator controllable. In other words, it makes controllability tests still relevant for larger systems, even when the total dimension of the Hilbert space exceeds the capabilities of the controllability test. In particular, the results from the graph test and the dimensional expressivity test have been key in showing operator controllability in IBM's system. In particular, developing more efficient controllability tests ensures that the subsystems in the partition can be of a considerable size, reducing the total number of tunable couplings that have to be included in the total system.

In future work, it would be interesting to study the quantum speed limit of the total system compared to the one of the two previous subsystems. The rate at which information can be exchanged in the multipartite system may depend on different factors like the maximum amplitude of the entangling control or the coupling distance between two qubits in the total array. To mitigate a possibly higher quantum speed limit, more than one tunable coupling can be added to speed up the implementation of entangling unitary operations.

In any case, even if information transfer between subsystems is slow, the system and its architecture can be tailored to run quantum algorithms that can be parallelized. Using each subsystem as a quantum processing unit, quantum circuits could be designed such that calculations are run in parallel on each subsystem and, at the end, all the information is merged before measuring. The parallelization of quantum algorithms is a discussed topic in the development of quantum computation. It has been hypothesized to bring some benefits like reducing circuit depth for certain cases [166] or helping with the implementation of decision diagrams [167].

A future goal is the extension of the proof to systems that are not based on qubits. Throughout all lemmas, we have assumed that our systems where built on two-dimensional qubits, allowing us to use tensor products of Pauli matrices as the basis

for the dynamical Lie algebras. In the general case, it may not be possible to assume such a basis, which makes the derivations in the lemmas inapplicable. A possible approach would be using a general basis for $\mathfrak{su}(n)$ with well known symmetries and commutator properties. If the same arguments can be made using e.g. the generalized skew-Hermitian Pauli matrices as a basis, then the result of controllability can also be extended to any other type of quantum system. Note that this is a mere hypothesis and not certain valid result. Intuitively it makes sense that Lie algebras of qubit arrays, i.e. $\mathfrak{su}(2^N)$, do not show any merit over other systems with different Hilbert space dimension. Nevertheless, more work is necessary to ensure this statement.

Finally, an interesting problem to be solved is the analysis of two connected subsystems that have operator controllability on some subspace. In particular, it is relevant to know whether the total system with an entangling control shows operator controllability on a larger subspace. The purpose of this study is twofold. First, it serves as an analysis for quantum systems with a smaller logical subspace in which the quantum operations can be performed. For example, this is a typical case in quantum error correction, where some qubits are used for measuring and are not active part of the logical calculations [168]. Secondly, it paves the way for obtaining information about an important physical model: Quantum systems embedded in a larger not controllable space, a typical model for open quantum systems.

# 7 Conclusions and outlook

In this thesis we have covered a wide range of topics related to the analysis of scalable qubit arrays that are capable of universal quantum computing. As it has been proven that certain quantum algorithms require a great number of qubits to be efficient [169], finding architectures of large qubit arrays with fast dynamics that use a low number of controls and couplings is a much sought-after goal in the landscape of quantum technologies. This work has tackled some of the relevant problems that stand in the way of this ambitious objective.

In Chapter 3 we have introduced a new method to estimate the quantum speed limit of a quantum system. It is based on the hypothesis that the time-independent drift of a system's Hamiltonian is the main contribution to the quantum speed limit. The newly defined available velocity polytope contains the associated information needed to quantify the time that a quantum system requires to implement some target dynamics. This produces a natural decomposition of the Lie algebra into fast, slow and very slow directions, depending on their contribution to the quantum speed limit. The method offers a large versatility, as these dynamics can be chosen to be either a given unitary evolution, a set of simultaneous state transfers or a quantum gate acting on a proper subspace of the Hilbert space. The main idea relies on finding the intersection given by the direction of a unitary evolution in the Lie algebra vector space and the available velocity. For the case of state transfers and gates on subspaces, the algorithm is able to find the minimum quantum speed limit among all the different unitary evolutions that implement the target dynamics. While the estimator works for low-dimensional systems, more work is needed to extend it to larger devices. In its current state, the algorithm may not always provide accurate estimations, as seen in the case where the coefficients in the Hamiltonian differ by orders of magnitude. Nevertheless, with the right adjustments, the method could potentially lend itself to some very promising applications in the world of quantum technologies. First, it could be used to study the quantum speed limit of noncontrollable systems, which provide an open door to the analysis of open quantum systems. There have been attempts to define the concept of quantum speed limit for certain open systems [96, 124, 170], but further study is advised to extend the notions to a more general case. Second, the estimator could be directly used to obtain an upper bound to the time required for

a quantum algorithm. As the method can find the speed limit for single-qubit and two-qubit operations, the very base foundations of most quantum algorithms, it can also provide an estimated minimal running time for the quantum algorithm. It would also be interesting to compare this result with other estimations of the quantum speed limits, like those associated with adiabatic quantum algorithms [171].

The various controllability tests are another core topic of the thesis. The control of quantum systems is a thriving field of study in quantum physics [12], and understanding the feasible dynamics in a quantum system is key to unlocking its full potential. Controllability tests are therefore a useful tool to understand what a quantum system is capable of. In Chapter 2 we have presented the fundamental difference between pure-state controllability and operator controllability in a system. The former one ensures that all state transfers are possible, while the latter one — and strictly stronger one — implies that all unitary operations are achievable. Operator controllability is a requirement for a universal computer that can implement every quantum gate. The aim of Chapters 4 and 5is the design of efficient controllability tests. In principle, these tests are suitable for general quantum systems, although they are specifically tailored for qubit arrays. More precisely, the examples used are based on superconducting qubits [152], one of the most predominant platforms for real qubit implementations. Previous controllability tests heavily rely on an analytical calculation of the dynamical Lie algebra of the system [132, 51, 14]. The ones here proposed use numerical computation that avoid a full calculation of the algebra while obtaining the same necessary information.

The graph test from Chapter 4 checks whether a quantum system has a maximal dynamical Lie algebra while avoiding the computation of a complete basis. For every controlled quantum system, it is possible to define a graph that represents the eigenstates and the transitions that the controls generate between them. By analysing the connectivity of the graph, one can determine if the system is operator controllable. This method is based on a pre-existing controllability test [16]. However, the original test fails on systems with degenerate energy gaps. The main original contribution is the extension of the method to surpass these degeneracies, making it suitable for multipartite systems and, in particular, qubit arrays. An important note is that the method may give inconclusive results in some cases, particularly in the case of not controllable systems. To test the algorithm itself, we have studied a five-qubit example based on a previously available IBM quantum device. We conclude that it is possible to obtain controllability of the system with fewer controls and even reduce it to the extreme case of a single local control. A natural next step is to examine the effect of this reduction the number of controls on the quantum speed limit of the system. Finding a suitable balance between the controls and couplings in a system and its quantum speed limit is also left as a future goal.

Chapter 5 presents a completely original controllability test in the form of a quantum-hybrid algorithm. It introduces the novel approach of measuring controllability directly on a quantum device using parametric quantum circuits. Gauging expressivity of parametric quantum circuits is a useful tool for their use in optimization problems, like variational quantum algorithms. Here we have mapped the problem of controllability to the expressivity of a circuit. To estimate the expressivity we use the dimensional expressivity analysis [20, 19], a hybrid algorithm that mixes quantum measurements on a circuit with classical computations. For every quantum system, it is possible to define a parametric quantum circuit whose dimensional expressivity reflects the dimension of the reachable set of the system. This can be done for pure-state and for operator controllability, giving a definitive answer for both a positive and a negative result. The test has been used to study some qubit arrays using classical simulations of the quantum circuits. The next logical step would be to try the method on a real quantum device. It would also be relevant to see if the test can be linked to other works that analyse the Lie algebra associated to a parametric quantum circuit [172].

In future work, it would be interesting to use both controllability tests to study controllability of subspaces, necessary for the case of a higher-dimensional Hilbert space that contains logical space contained in a smaller subspace. This happens in many qubit platforms, where there are more than two energy levels in the Hilbert space. Similarly, the field of open quantum systems could benefit from efficient controllability tests, as they more accurately represent a real controlled quantum system [173]. Furthermore, it may be possible to link the tests to the quantum speed limit of a system. The number of graphical commutators needed on the graph to make it connected may be an indicator on the complexity of the dynamics, thus increasing with the quantum speed limit. Similarly, the quantum circuit used in the expressivity test may be used to determine the number of times the drift must be used in a gate decomposition, serving as an estimation to the quantum speed limit. A last question to answer in this area is knowing when pure-state controllability implies operator controllability on a qubit array. This question arose when failing at finding systems with two-qubit couplings and local controls with more than two qubits that were pure-state controllable but not operator controllable. This may hint to the fact that pure-state controllable systems with these kind of architectures are in general also operator controllable. If this conjecture was correct, it would be very useful in order to use the simpler tests to prove the stronger property.

The latest featured project is the design of large controllable qubit arrays using the modular architecture presented in Chapter 6. We presented mathematical evidence that connecting controllable qubit arrays via tunable couplings results in a larger controllable system, independent of the number, type and location of previous local

controls and couplings. It paves a path toward scalable designs suitable for universal quantum computing. It is still necessary to check controllability on every module that is added as a building block, making the controllability tests a useful tool. We have used this approach to prove controllability on a quantum system whose dimension exceeds the maximum one on which we can check controllability. Once again we have used one of IBM's systems as inspiration for the studied example, significantly reducing the resulting number of controls and couplings. An important piece of information would be the rate at which the modular multipartite system can exchange information between the different subsystems. This may reveal which algorithms can be implemented on the system and which would take too long. To mitigate this, it is always possible to add more tunable couplings that improve the connectivity on the array, which may lead to faster dynamics. The use of controllable subsystems is still useful when considering quantum algorithms that can be parallelized into different quantum processing units. More in-depth research is needed to understand how this architecture compares to other configurations that have been proposed for quantum computing [174, 175].

In essence, this work has brought together a combination of numerical tools and new insights for the theoretical study and design of qubit arrays, in the hope that this modest contribution will bring us a small step closer to the long-held wish of universal quantum computing.

# 8 Bibliography


[1] D. Pohl. “Analyzing Controllability in the 3-Qubit Array with minimal local controls.” Bachelor’s Thesis. 2022.

[2] R. P. Feynman. “Simulating physics with computers”. In: *Int. j. Theor. phys* 21.6 (1982). DOI: 10.1007/BF02650179.

[3] D. Deutsch and R. Jozsa. “Rapid solution of problems by quantum computation”. In: *Proceedings of the Royal Society of London. Series A: Mathematical and Physical Sciences* 439.1907 (1992), pp. 553–558. DOI: 10.1098/rspa.1992.0167.

[4] D. R. Simon. “On the power of quantum computation”. In: *SIAM journal on computing* 26.5 (1997), pp. 1474–1483. DOI: 10.1137/S0097539796298637.

[5] L. K. Grover. “A fast quantum mechanical algorithm for database search”. In: *Proceedings of the twenty-eighth annual ACM symposium on Theory of computing*. 1996, pp. 212–219. DOI: 10.1145/237814.237866.

[6] P. W. Shor. “Polynomial-time algorithms for prime factorization and discrete logarithms on a quantum computer”. In: *SIAM review* 41.2 (1999), pp. 303–332. DOI: 10.1137/S0036144598347011.

[7] D. P. DiVincenzo. “The physical implementation of quantum computation”. In: *Fortschritte der Physik: Progress of Physics* 48.9-11 (2000), pp. 771–783. DOI: 10.1002/1521-3978(200009)48:9/11<771::AID-PROP771>3.0.CO;2-E.

[8] S. Wiesner. “Conjugate coding”. In: *ACM Sigact News* 15.1 (1983), pp. 78–88. DOI: 10.1145/1008908.1008920.

[9] D. J. Wineland, M. Barrett, J. Britton, J. Chiaverini, B. DeMarco, W. M. Itano, B. Jelenković, C. Langer, D. Leibfried, V. Meyer, *et al.* “Quantum information processing with trapped ions”. In: *Philosophical Transactions of the Royal Society of London. Series A: Mathematical, Physical and Engineering Sciences* 361.1808 (2003), pp. 1349–1361. DOI: 10.1098/rsta.2003.1205.

[10] G. Burkard, T. D. Ladd, A. Pan, J. M. Nichol, and J. R. Petta. “Semiconductor spin qubits”. In: *Reviews of Modern Physics* 95.2 (2023), p. 025003. DOI: 10.1103/RevModPhys.95.025003.

[11] J. J. García-Ripoll. *Quantum Information and Quantum Optics with Superconducting Circuits*. Cambridge University Press, 2022. DOI: 10.1017/9781316779460.

[12] S. J. Glaser, U. Boscain, T. Calarco, *et al.* "Training Schrödinger's cat: quantum optimal control. Strategic report on current status, visions and goals for research in Europe". In: *Eur. Phys. J. D* 69 (Dec. 2015), p. 279. DOI: 10.1140/epjd/e2015-60464-1.

[13] S. G. Schirmer, H. Fu, and A. I. Solomon. "Complete controllability of quantum systems". In: *Phys. Rev. A* 63 (6 May 2001), p. 063410. DOI: 10.1103/PhysRevA.63.063410.

[14] D. d'Alessandro. *Introduction to quantum control and dynamics*. CRC press, 2021. DOI: 10.1201/9781003051268.

[15] U. Boscain, M. Caponigro, T. Chambrion, and M. Sigalotti. "A weak spectral condition for the controllability of the bilinear Schrödinger equation with application to the control of a rotating planar molecule". In: *Comm. Math. Phys.* 311.2 (2012), pp. 423–455. DOI: 10.1007/s00220-012-1441-z.

[16] T. Chambrion, P. Mason, M. Sigalotti, and U. Boscain. "Controllability of the discrete-spectrum Schrödinger equation driven by an external field". In: *Annales de l'Institut Henri Poincaré C* 26.1 (2009), pp. 329–349. DOI: 10.1016/j.anihpc.2008.05.001.

[17] M. Leibscher, E. Pozzoli, C. Pérez, M. Schnell, M. Sigalotti, U. Boscain, and C. P. Koch. "Full quantum control of enantiomer-selective state transfer in chiral molecules despite degeneracy". In: *Communications Physics* 5.1 (2022), pp. 1–16. DOI: 10.1038/s42005-022-00883-6.

[18] A. Peruzzo, J. McClean, P. Shadbolt, M.-H. Yung, X.-Q. Zhou, P. J. Love, A. Aspuru-Guzik, and J. L. O'brien. "A variational eigenvalue solver on a photonic quantum processor". In: *Nature communications* 5.1 (2014), p. 4213. DOI: 10.1038/ncomms5213.

[19] L. Funcke, T. Hartung, K. Jansen, S. Kühn, and P. Stornati. "Dimensional expressivity analysis of parametric quantum circuits". In: *Quantum* 5 (2021), p. 422. DOI: 10.22331/q-2021-03-29-422.

[20] L. Funcke, T. Hartung, K. Jansen, S. Kühn, M. Schneider, and P. Stornati. "Dimensional Expressivity Analysis, best-approximation errors, and automated design of parametric quantum circuits". In: *arXiv preprint arXiv:2111.11489* (2021). DOI: 10.48550/arXiv.2111.11489.

[21] *IBM Quantum*. https://quantum-computing.ibm.com/services. Accessed: 2024-08-19.

[22] H.-P. Breuer and F. Petruccione. *The theory of open quantum systems*. OUP Oxford, 2002. DOI: 10.1093/acprof:oso/9780199213900.001.0001.

[23] S. Deffner and S. Campbell. “Quantum speed limits: from Heisenberg’s uncertainty principle to optimal quantum control”. In: *Journal of Physics A: Mathematical and Theoretical* 50.45 (2017), p. 453001. DOI: 10.1088/1751-8121/aa86c6.

[24] L. B. Levitin and T. Toffoli. “Fundamental Limit on the Rate of Quantum Dynamics: The Unified Bound Is Tight”. In: *Phys. Rev. Lett.* 103 (16 Oct. 2009), p. 160502. DOI: 10.1103/PhysRevLett.103.160502.

[25] F. S. Levin. *An introduction to quantum theory*. Cambridge University Press, 2002. DOI: 10.1017/CBO9781139164177.

[26] D. J. Griffiths and D. F. Schroeter. *Introduction to quantum mechanics*. Cambridge university press, 2018. DOI: 10.1017/9781316995433.

[27] C. N. Cohen-Tannoudji. “Nobel Lecture: Manipulating atoms with photons”. In: *Rev. Mod. Phys.* 70 (3 July 1998), pp. 707–719. DOI: 10.1103/RevModPhys.70.707.

[28] L. M. K. Vandersypen and I. L. Chuang. “NMR techniques for quantum control and computation”. In: *Rev. Mod. Phys.* 76 (4 Jan. 2005), pp. 1037–1069. DOI: 10.1103/RevModPhys.76.1037.

[29] D. A. Golter, T. Oo, M. Amezcua, K. A. Stewart, and H. Wang. “Optomechanical quantum control of a nitrogen-vacancy center in diamond”. In: *Physical review letters* 116.14 (2016), p. 143602. DOI: 10.1103/PhysRevLett.116.143602.

[30] M. M. Alqahtani, M. S. Everitt, and B. M. Garraway. “Cavity QED photons for quantum information processing”. In: *Journal of Physics B: Atomic, Molecular and Optical Physics* 55.18 (2022), p. 184004. DOI: 10.1088/1361-6455/ac864f.

[31] A. Chatterjee, P. Stevenson, S. De Franceschi, A. Morello, N. P. de Leon, and F. Kuemmeth. “Semiconductor qubits in practice”. In: *Nature Reviews Physics* 3.3 (2021), pp. 157–177. DOI: 10.1038/s42254-021-00283-9.

[32] M. A. Nielsen and I. L. Chuang. *Quantum computation and quantum information*. Cambridge university press, 2010. DOI: 10.1017/CBO9780511976667.

[33] R. Babbush, C. Gidney, D. W. Berry, N. Wiebe, J. McClean, A. Paler, A. Fowler, and H. Neven. “Encoding electronic spectra in quantum circuits with linear T complexity”. In: *Physical Review X* 8.4 (2018), p. 041015. DOI: 10.1103/PhysRevX.8.041015.

[34] J. M. Martyn, Z. M. Rossi, A. K. Tan, and I. L. Chuang. “Grand unification of quantum algorithms”. In: *PRX Quantum* 2.4 (2021), p. 040203. DOI: 10.1103/PRXQuantum.2.040203.

[35] A. Blais, A. M. van den Brink, and A. M. Zagoskin. “Tunable coupling of superconducting qubits”. In: *Physical review letters* 90.12 (2003), p. 127901. DOI: 10.1103/PhysRevLett.90.127901.

[36] A. Niskanen, K. Harrabi, F. Yoshihara, Y. Nakamura, S. Lloyd, and J. S. Tsai. "Quantum coherent tunable coupling of superconducting qubits". In: *Science* 316.5825 (2007), pp. 723–726. DOI: 10.1126/science.1141324.

[37] Y. Chen, C. Neill, P. Roushan, N. Leung, M. Fang, R. Barends, J. Kelly, B. Campbell, Z. Chen, B. Chiaro, *et al.* "Qubit architecture with high coherence and fast tunable coupling". In: *Physical review letters* 113.22 (2014), p. 220502. DOI: 10.1103/PhysRevLett.113.220502.

[38] P. Benioff. "The computer as a physical system: A microscopic quantum mechanical Hamiltonian model of computers as represented by Turing machines". In: *Journal of statistical physics* 22 (1980), pp. 563–591. DOI: 10.1007/BF01011339.

[39] D. Deutsch. "Quantum theory, the Church–Turing principle and the universal quantum computer". In: *Proceedings of the Royal Society of London. A. Mathematical and Physical Sciences* 400.1818 (1985), pp. 97–117. DOI: 10.1098/rspa.1985.0070.

[40] P. W. Shor. "Algorithms for quantum computation: discrete logarithms and factoring". In: *Proceedings 35th annual symposium on foundations of computer science*. Ieee. 1994, pp. 124–134. DOI: 10.1109/SFCS.1994.365700.

[41] A. Kandala, A. Mezzacapo, K. Temme, M. Takita, M. Brink, J. M. Chow, and J. M. Gambetta. "Hardware-efficient variational quantum eigensolver for small molecules and quantum magnets". In: *Nature* 549.7671 (2017), pp. 242–246. DOI: 10.1038/nature23879.

[42] J. Tilly, H. Chen, S. Cao, D. Picozzi, K. Setia, Y. Li, E. Grant, L. Wossnig, I. Rungger, G. H. Booth, *et al.* "The variational quantum eigensolver: a review of methods and best practices". In: *Physics Reports* 986 (2022), pp. 1–128. DOI: 10.1016/j.physrep.2022.08.003.

[43] F. Arute, K. Arya, R. Babbush, D. Bacon, J. C. Bardin, R. Barends, R. Biswas, S. Boixo, F. G. Brandao, D. A. Buell, *et al.* "Quantum supremacy using a programmable superconducting processor". In: *Nature* 574.7779 (2019), pp. 505–510. DOI: 10.1038/s41586-019-1666-5.

[44] F. Pan, K. Chen, and P. Zhang. "Solving the sampling problem of the sycamore quantum circuits". In: *Physical Review Letters* 129.9 (2022), p. 090502. DOI: 10.1103/PhysRevLett.129.090502.

[45] H.-S. Zhong, H. Wang, Y.-H. Deng, M.-C. Chen, L.-C. Peng, Y.-H. Luo, J. Qin, D. Wu, X. Ding, Y. Hu, *et al.* "Quantum computational advantage using photons". In: *Science* 370.6523 (2020), pp. 1460–1463. DOI: 10.1126/science.abe8770.

[46] H.-S. Zhong, Y.-H. Deng, J. Qin, H. Wang, M.-C. Chen, L.-C. Peng, Y.-H. Luo, D. Wu, S.-Q. Gong, H. Su, *et al.* "Phase-programmable gaussian boson sampling using stimulated squeezed light". In: *Physical review letters* 127.18 (2021), p. 180502. DOI: 10.1103/PhysRevLett.127.180502.

[47] L. S. Madsen, F. Laudenbach, M. F. Askarani, F. Rortais, T. Vincent, J. F. Bulmer, F. M. Miatto, L. Neuhaus, L. G. Helt, M. J. Collins, *et al.* "Quantum computational advantage with a programmable photonic processor". In: *Nature* 606.7912 (2022), pp. 75–81. DOI: 10.1038/s41586-022-04725-x.

[48] A. M. Turing. *Computing machinery and intelligence*. Springer, 2009. DOI: 10.1007/978-1-4020-6710-5_3.

[49] T. L. Nguyen, J.-M. Raimond, C. Sayrin, R. Cortinas, T. Cantat-Moltrecht, F. Assemat, I. Dotsenko, S. Gleyzes, S. Haroche, G. Roux, *et al.* "Towards quantum simulation with circular Rydberg atoms". In: *Physical Review X* 8.1 (2018), p. 011032. DOI: 10.1103/PhysRevX.8.011032.

[50] B. C. Hall. "Lie Groups, Lie Algebras, and Representations". In: *Quantum Theory for Mathematicians*. New York, NY: Springer New York, 2013, pp. 333–366. DOI: 10.1007/978-1-4614-7116-5_16.

[51] G. Dirr and U. Helmke. "Lie theory for quantum control". In: *GAMM-Mitteilungen* 31.1 (2008), pp. 59–93. DOI: 10.1002/gamm.200890003.

[52] J.-P. Serre. *Lie algebras and Lie groups: 1964 lectures given at Harvard University*. Springer, 2009. DOI: 10.1007/978-3-540-70634-2.

[53] B. G. Wybourne. "Classical groups for physicists". In: (1974). DOI: 10.1002/piuz.19750060613.

[54] M. Hagemann, D. Klawitter, and D. Lordick. "Force driven ruled surfaces". In: *J. Geom. Graph* 17.2 (2013), pp. 193–204.

[55] V. Jurdjevic and H. J. Sussmann. "Control systems on Lie groups". In: *Journal of Differential equations* 12.2 (1972), pp. 313–329. DOI: 10.1016/0022-0396(72)90035-6.

[56] D. D'Alessandro. "Uniform finite generation of compact Lie groups". In: *Systems & control letters* 47.1 (2002), pp. 87–90. DOI: 10.1016/S0167-6911(02)00178-0.

[57] Y. L. Sachkov. "Controllability of invariant systems on Lie groups and homogeneous spaces". In: *Journal of Mathematical Sciences* 100.4 (2000), pp. 2355–2427. DOI: 10.1007/s10958-000-0002-8.

[58] M. Leibscher, E. Pozzoli, C. Pérez, M. Schnell, M. Sigalotti, U. Boscain, and C. P. Koch. "Full quantum control of enantiomer-selective state transfer in chiral molecules despite degeneracy". In: *Communications Physics* 5.1 (2022), p. 110. DOI: 10.48550/10.1038/s42005-022-00883-6.

[59] E. Pozzoli. “Some problems of evolution and control in quantum mechanics”. PhD thesis. Sorbonne Unniversité, 2021.

[60] S.-H. Lin, R. Dilip, A. G. Green, A. Smith, and F. Pollmann. “Real- and Imaginary-Time Evolution with Compressed Quantum Circuits”. In: *PRX Quantum* 2 (1 Mar. 2021), p. 010342. DOI: 10.1103/PRXQuantum.2.010342.

[61] A. Barenco, C. H. Bennett, R. Cleve, D. P. DiVincenzo, N. Margolus, P. Shor, T. Sleator, J. A. Smolin, and H. Weinfurter. “Elementary gates for quantum computation”. In: *Physical review A* 52.5 (1995), p. 3457. DOI: 10.1103/PhysRevA.52.3457.

[62] Y. Du, M.-H. Hsieh, T. Liu, and D. Tao. “Expressive power of parametrized quantum circuits”. In: *Physical Review Research* 2.3 (2020), p. 033125. DOI: 10.1103/PhysRevResearch.2.033125.

[63] J. Preskill. “Quantum computing in the NISQ era and beyond”. In: *Quantum* 2 (2018), p. 79. DOI: 10.22331/q-2018-08-06-79.

[64] M. Cerezo, A. Arrasmith, R. Babbush, S. C. Benjamin, S. Endo, K. Fujii, J. R. McClean, K. Mitarai, X. Yuan, L. Cincio, *et al.* “Variational quantum algorithms”. In: *Nature Reviews Physics* 3.9 (2021), pp. 625–644. DOI: 10.1038/s42254-021-00348-9.

[65] M. Lubasch, J. Joo, P. Moinier, M. Kiffner, and D. Jaksch. “Variational quantum algorithms for nonlinear problems”. In: *Phys. Rev. A* 101 (1 Jan. 2020), p. 010301. DOI: 10.1103/PhysRevA.101.010301.

[66] S. Sim, P. D. Johnson, and A. Aspuru-Guzik. “Expressibility and entangling capability of parameterized quantum circuits for hybrid quantum-classical algorithms”. In: *Advanced Quantum Technologies* 2.12 (2019), p. 1900070. DOI: 10.1002/qute.201900070.

[67] L. Friedrich and J. Maziero. “The quantum cost function concentration dependency on the parametrization expressivity”. In: *arXiv preprint arXiv:2301.06883* (2023). DOI: 10.48550/arXiv.2301.06883.

[68] D. M. Greenberger, M. A. Horne, and A. Zeilinger. “Going beyond Bell’s theorem”. In: *Bell’s theorem, quantum theory and conceptions of the universe*. Springer, 1989, pp. 69–72. DOI: 10.1103/PhysRevA.52.3457.

[69] M. Larocca, N. Ju, D. García-Martín, P. J. Coles, and M. Cerezo. “Theory of overparametrization in quantum neural networks”. In: *Nature Computational Science* 3.6 (2023), pp. 542–551. DOI: 10.1038/s43588-023-00467-6.

[70] E. Fontana, N. Fitzpatrick, D. M. Ramo, R. Duncan, and I. Rungger. “Evaluating the noise resilience of variational quantum algorithms”. In: *Physical Review A* 104.2 (2021), p. 022403. DOI: 10.1103/PhysRevA.104.022403.

[71] J. Kim, J. Kim, and D. Rosa. “Universal effectiveness of high-depth circuits in variational eigenproblems”. In: *Physical Review Research* 3.2 (2021), p. 023203. DOI: 10.1103/PhysRevResearch.3.023203.

[72] J. D. Bekenstein. “Energy Cost of Information Transfer”. In: *Phys. Rev. Lett.* 46 (10 Mar. 1981), pp. 623–626. DOI: 10.1103/PhysRevLett.46.623.

[73] S. Lloyd. “Ultimate physical limits to computation”. In: *Nature* 406.6799 (2000), pp. 1047–1054. DOI: 10.1038/35023282.

[74] S. Patsch, D. M. Reich, J.-M. Raimond, M. Brune, S. Gleyzes, and C. P. Koch. “Fast and accurate circularization of a Rydberg atom”. In: *Physical Review A* 97.5 (2018), p. 053418. DOI: 10.1103/PhysRevA.97.053418.

[75] M. H. Goerz, F. Motzoi, K. B. Whaley, and C. P. Koch. “Charting the circuit-QED Design Landscape Using Optimal Control Theory”. In: *npj Quantum Inf.* 3 (Sept. 2017), p. 37. DOI: 10.1038/s41534-017-0036-0.

[76] P. Pfeifer and J. Fröhlich. “Generalized time-energy uncertainty relations and bounds on lifetimes of resonances”. In: *Reviews of Modern Physics* 67.4 (1995), p. 759. DOI: 10.1103/RevModPhys.67.759.

[77] A. Ruschhaupt, J. G. Muga, and G. C. Hegerfeldt. “Detector models for the quantum time of arrival”. In: *Time in Quantum Mechanics-Vol. 2*. Springer, 2009, pp. 65–96. DOI: 10.1007/978-3-642-03174-8_4.

[78] V. V. Dodonov and A. V. Dodonov. “Energy–time and frequency–time uncertainty relations: Exact inequalities”. In: *Physica Scripta* 90.7 (2015), p. 074049. DOI: 10.1088/0031-8949/90/7/074049.

[79] M. R. Frey. “Quantum speed limits—primer, perspectives, and potential future directions”. In: *Quantum Information Processing* 15 (2016), pp. 3919–3950. DOI: 10.1007/s11128-016-1405-x.

[80] W. Heisenberg. “Über den anschaulichen Inhalt der quantentheoretischen Kinematik und Mechanik”. In: *Zeitschrift für Physik* 43.3 (1927), pp. 172–198. DOI: 10.1007/BF01397280.

[81] H. P. Robertson. “The uncertainty principle”. In: *Physical Review* 34.1 (1929), p. 163. DOI: 10.1103/PhysRev.34.163.

[82] W. Pauli. *Die allgemeinen prinzipien der wellenmechanik*. Ed. by H. Bethe, F. Hund, N. F. Mott, W. Pauli, A. Rubinowicz, G. Wentzel, and A. Smekal. Springer, 1933, pp. 83–272. DOI: 10.1007/978-3-642-52619-0_2.

[83] L. Mandelstam and I. Tamm. “The Uncertainty Relation Between Energy and Time in Non-relativistic Quantum Mechanics”. In: *Selected Papers*. Ed. by B. M. Bolotovskii, V. Y. Frenkel, and R. Peierls. Berlin, Heidelberg: Springer Berlin Heidelberg, 1991, pp. 115–123. DOI: 10.1007/978-3-642-74626-0_8.

[84] N. Margolus and L. B. Levitin. “The maximum speed of dynamical evolution”. In: *Physica D: Nonlinear Phenomena* 120.1-2 (1998), pp. 188–195. DOI: 10.1016/S0167-2789(98)00054-2.

[85] V. Giovannetti, S. Lloyd, and L. Maccone. “Quantum limits to dynamical evolution”. In: *Phys. Rev. A* 67 (5 May 2003), p. 052109. DOI: 10.1103/PhysRevA.67.052109.

[86] K. Svozil, L. B. Levitin, T. Toffoli, and Z. Walton. “Maximum speed of quantum gate operation”. In: *International Journal of Theoretical Physics* 44.7 (2005), pp. 965–970. DOI: 10.1007/s10773-005-7073-8.

[87] P. M. Poggi. “Geometric quantum speed limits and short-time accessibility to unitary operations”. In: *Physical Review A* 99.4 (2019), p. 042116. DOI: 10.1103/PhysRevA.99.042116.

[88] A. Rivas and S. F. Huelga. *Open quantum systems*. Vol. 10. Springer, 2012. DOI: 10.1007/978-3-642-23354-8.

[89] P. W. Milonni. *The quantum vacuum: an introduction to quantum electrodynamics*. Academic press, 2013. DOI: 10.1016/C2009-0-21295-5.

[90] I. Siddiqi. “Engineering high-coherence superconducting qubits”. In: *Nature Reviews Materials* 6.10 (2021), pp. 875–891. DOI: 10.1038/s41578-021-00370-4.

[91] T. Caneva, M. Murphy, T. Calarco, R. Fazio, S. Montangero, V. Giovannetti, and G. E. Santoro. “Optimal control at the quantum speed limit”. In: *Physical review letters* 103.24 (2009), p. 240501. DOI: 10.1103/PhysRevLett.103.240501.

[92] S. Deffner and S. Campbell. “Quantum speed limits: from Heisenberg’s uncertainty principle to optimal quantum control”. In: *Journal of Physics A: Mathematical and Theoretical* 50.45 (2017), p. 453001. DOI: 10.1088/1751-8121/aa86c6.

[93] M. H. Goerz, T. Calarco, and C. P. Koch. “The quantum speed limit of optimal controlled phasegates for trapped neutral atoms”. In: *Journal of Physics B: Atomic, Molecular and Optical Physics* 44.15 (2011), p. 154011. DOI: 10.1088/0953-4075/44/15/154011.

[94] S. Ashhab, P. De Groot, and F. Nori. “Speed limits for quantum gates in multiqubit systems”. In: *Physical Review A—Atomic, Molecular, and Optical Physics* 85.5 (2012), p. 052327. DOI: 10.1103/PhysRevA.85.052327.

[95] M. Aifer and S. Deffner. “From quantum speed limits to energy-efficient quantum gates”. In: *New Journal of Physics* 24.5 (2022), p. 055002. DOI: 10.1088/1367-2630/ac6821.

[96] A. del Campo, I. L. Egusquiza, M. B. Plenio, and S. F. Huelga. “Quantum speed limits in open system dynamics”. In: *Physical review letters* 110.5 (2013), p. 050403. DOI: 10.1103/PhysRevLett.110.050403.

[97] C. Liu, Z.-Y. Xu, and S. Zhu. “Quantum-speed-limit time for multiqubit open systems”. In: *Physical Review A* 91.2 (2015), p. 022102. DOI: 10.1103/PhysRevA.91.022102.

[98] R. Uzdin and R. Kosloff. “Speed limits in Liouville space for open quantum systems”. In: *Europhysics Letters* 115.4 (2016), p. 40003. DOI: 10.1209/0295-5075/115/40003.

[99] A. Agrachev and T. Chambrion. “An estimation of the controllability time for single-input systems on compact Lie groups”. In: *ESAIM: Control, Optimisation and Calculus of Variations* 12.3 (2006), pp. 409–441. DOI: 10.1051/cocv:2006007.

[100] P. J. Jones and P. Kok. “Geometric derivation of the quantum speed limit”. In: *Phys. Rev. A* 82 (2 Aug. 2010), p. 022107. DOI: 10.1103/PhysRevA.82.022107.

[101] M. T. Johnsson, L. Van Luijk, and D. Burgarth. “Exact and lower bounds for the quantum speed limit in finite-dimensional systems”. In: *Physical Review A* 108.5 (2023), p. 052403. DOI: 10.1103/PhysRevA.108.052403.

[102] M. Murphy, S. Montangero, V. Giovannetti, and T. Calarco. “Communication at the quantum speed limit along a spin chain”. In: *Physical Review A—Atomic, Molecular, and Optical Physics* 82.2 (2010), p. 022318. DOI: 10.1103/PhysRevA.82.022318.

[103] D. Lucarelli. “Quantum optimal control via gradient ascent in function space and the time-bandwidth quantum speed limit”. In: *Physical Review A* 97.6 (2018), p. 062346. DOI: 10.1103/PhysRevA.97.062346.

[104] J. Lee, C. Arenz, H. Rabitz, and B. Russell. “Dependence of the quantum speed limit on system size and control complexity”. In: *New Journal of Physics* 20.6 (2018), p. 063002. DOI: 10.1088/1367-2630/aac6f3.

[105] J. Liu, D. Segal, and G. Hanna. “Hybrid quantum-classical simulation of quantum speed limits in open quantum systems”. In: *Journal of Physics A: Mathematical and Theoretical* 52.21 (2019), p. 215301. DOI: 10.1088/1751-8121/ab15eb.

[106] N. Khaneja, R. Brockett, and S. J. Glaser. “Time optimal control in spin systems”. In: *Phys. Rev. A* 63 (3 Feb. 2001), p. 032308. DOI: 10.1103/PhysRevA.63.032308.

[107] C. Altafini. “Controllability of quantum mechanical systems by root space decomposition of su (N)”. In: *Journal of Mathematical Physics* 43.5 (2002), pp. 2051–2062. DOI: 10.1063/1.1467611.

[108] R. A. Horn and C. R. Johnson. “Norms for vectors and matrices”. In: *Matrix analysis* (1990), pp. 313–386. DOI: 10.1017/CBO9780511810817.

[109] D. M. Reich, M. Ndong, and C. P. Koch. "Monotonically convergent optimization in quantum control using Krotov's method". In: *The Journal of chemical physics* 136.10 (2012). DOI: 10.1103/PhysRevA.66.053619.

[110] M. Goerz, D. Basilewitsch, F. Gago-Encinas, M. G. Krauss, K. P. Horn, D. M. Reich, and C. Koch. "Krotov: A Python implementation of Krotov's method for quantum optimal control". In: *SciPost physics* 7.6 (2019), p. 080. DOI: 10.21468/SciPostPhys.7.6.080.

[111] T. Caneva, T. Calarco, and S. Montangero. "Chopped random-basis quantum optimization". In: *Physical Review A* 84.2 (2011), p. 022326. DOI: 10.1103/PhysRevA.84.022326.

[112] N. Khaneja, T. Reiss, C. Kehlet, T. Schulte-Herbrüggen, and S. J. Glaser. "Optimal control of coupled spin dynamics: design of NMR pulse sequences by gradient ascent algorithms". In: *Journal of magnetic resonance* 172.2 (2005), pp. 296–305. DOI: 10.1016/j.jmr.2004.11.004.

[113] T. A. Loring. "Computing a logarithm of a unitary matrix with general spectrum". In: *Numerical Linear Algebra with Applications* 21.6 (2014), pp. 744–760. DOI: 10.1002/nla.1927.

[114] P. Virtanen, R. Gommers, T. E. Oliphant, *et al.* "SciPy 1.0: Fundamental Algorithms for Scientific Computing in Python". In: *Nature Methods* 17 (2020), pp. 261–272. DOI: 10.1038/s41592-019-0686-2.

[115] G. C. Hegerfeldt. "Driving at the quantum speed limit: optimal control of a two-level system". In: *Physical review letters* 111.26 (2013), p. 260501. DOI: 10.1103/PhysRevLett.111.260501.

[116] G. Bachman and L. Narici. *Functional analysis*. Courier Corporation, 2000.

[117] H. F. Trotter. "On the product of semi-groups of operators". In: *Proceedings of the American Mathematical Society* 10.4 (1959), pp. 545–551. DOI: 10.1090/S0002-9939-1959-0108732-6.

[118] C. B. Barber, D. P. Dobkin, and H. Huhdanpaa. "The quickhull algorithm for convex hulls". In: *ACM Transactions on Mathematical Software (TOMS)* 22.4 (1996), pp. 469–483. DOI: 10.1145/235815.235821.

[119] C. B. Barber, D. P. Dobkin, and H. Huhdanpaa. "Qhull: Quickhull algorithm for computing the convex hull". In: *Astrophysics Source Code Library* (2013), ascl–1304.

[120] S. P. Ong. *Pyhull: a Python wrapper of the Qhull library*.

[121] R. Brent. *Algorithms for Minimization without Derivatives*. Prentice-Hall, 1972.

[122] S. G. Johnson. *The NLopt nonlinear-optimization package*. https://github.com/stevengj/nlopt. 2007.

[123] T. H. Rowan. “Functional stability analysis of numerical algorithms”. PhD thesis. Austin, TX: Department of Computer Science, University of Texas at Austin, 1990.

[124] Y.-J. Zhang, W. Han, Y.-J. Xia, J.-P. Cao, and H. Fan. “Quantum speed limit for arbitrary initial states”. In: *Scientific reports* 4.1 (2014), p. 4890. DOI: 10.1038/srep04890.

[125] N. Hörnedal and O. Sönnerborn. “Margolus-Levitin quantum speed limit for an arbitrary fidelity”. In: *Physical Review Research* 5.4 (2023), p. 043234. DOI: 10.1103/PhysRevResearch.5.043234.

[126] V. Giovannetti, S. Lloyd, and L. Maccone. “The speed limit of quantum unitary evolution”. In: *Journal of Optics B: Quantum and Semiclassical Optics* 6.8 (2004), S807. DOI: 10.1088/1464-4266/6/8/028.

[127] A. Farmanian and V. Karimipour. “Quantum Speed Limits for Implementation of Unitary Transformations”. In: *arXiv preprint arXiv:2406.03964* (2024). DOI: arXiv.2406.03964.

[128] L. Innocenti, G. De Chiara, M. Paternostro, and R. Puebla. “Ultrafast critical ground state preparation via bang–bang protocols”. In: *New Journal of Physics* 22.9 (2020), p. 093050. DOI: 10.1088/1367-2630/abb1df.

[129] A. Arrasmith, M. Cerezo, P. Czarnik, L. Cincio, and P. J. Coles. “Effect of barren plateaus on gradient-free optimization”. In: *Quantum* 5 (2021), p. 558. DOI: 10.22331/q-2021-10-05-558.

[130] C. P. Koch, U. Boscain, T. Calarco, *et al.* “Quantum optimal control in quantum technologies. Strategic report on current status, visions and goals for research in Europe”. In: *EPJ Quantum Technol.* 9 (2022), p. 19. DOI: 10.1140/epjqt/s40507-022-00138-x.

[131] H. Fu, S. G. Schirmer, and A. I. Solomon. “Complete controllability of finite-level quantum systems”. In: *Journal of Physics A: Mathematical and General* 34.8 (Mar. 2001), p. 1679. DOI: 10.1088/0305-4470/34/8/313.

[132] C. Altafini. “Controllability of quantum mechanical systems by root space decomposition of su(N)”. In: *Journal of Mathematical Physics* 43.5 (2002), pp. 2051–2062. DOI: 10.1063/1.1467611.

[133] N. Boussaïd, M. Caponigro, and T. Chambrion. “Weakly coupled systems in quantum control”. In: *IEEE Trans. Automat. Control* 58.9 (2013), pp. 2205–2216. DOI: 10.1109/TAC.2013.2255948.

[134] X. Wang, P. Pemberton-Ross, and S. G. Schirmer. “Symmetry and Subspace Controllability for Spin Networks With a Single-Node Control”. In: *IEEE Transactions on Automatic Control* 57.8 (2012), pp. 1945–1956. DOI: 10.1109/TAC.2012.2202057.

[135] X. Wang, D. Burgarth, and S. Schirmer. "Subspace controllability of spin-$\frac{1}{2}$ chains with symmetries". In: *Phys. Rev. A* 94 (5 Nov. 2016), p. 052319. DOI: 10.1103/PhysRevA.94.052319.

[136] J. Chen, Y. Zhou, J. Bian, J. Li, and X. Peng. "Subspace controllability of symmetric spin networks". In: *Phys. Rev. A* 102 (3 Sept. 2020), p. 032602. DOI: 10.1103/PhysRevA.102.032602.

[137] F. Albertini and D. D'Alessandro. "Subspace controllability of multi-partite spin networks". In: *Systems & Control Letters* 151 (2021), p. 104913. DOI: 10.1016/j.sysconle.2021.104913.

[138] F. Albertini and D. D'Alessandro. "The Lie algebra structure and controllability of spin systems". In: *Linear Algebra and its Applications* 350.1 (2002), pp. 213–235. DOI: 10.1016/S0024-3795(02)00290-2.

[139] U. Boscain, M. Caponigro, and M. Sigalotti. "Multi-input Schrödinger equation: controllability, tracking, and application to the quantum angular momentum". In: *Journal of Differential Equations* 256.11 (2014), pp. 3524–3551. DOI: 10.1016/j.jde.2014.02.004.

[140] C. Godsil and S. Severini. "Control by quantum dynamics on graphs". In: *Physical Review A* 81.5 (2010), p. 052316. DOI: 10.1103/PhysRevA.81.052316.

[141] C. Gokler, S. Lloyd, P. Shor, and K. Thompson. "Efficiently Controllable Graphs". In: *Phys. Rev. Lett.* 118 (26 June 2017), p. 260501. DOI: 10.1103/PhysRevLett.118.260501.

[142] E. Pozzoli, M. Leibscher, M. Sigalotti, U. Boscain, and C. P. Koch. "Lie algebra for rotational subsystems of a driven asymmetric top". In: *J. Phys. A: Math. Theor.* 55 (2022), p. 215301. DOI: 10.1088/1751-8121/ac631d.

[143] C. Figgatt, A. Ostrander, N. M. Linke, K. A. Landsman, D. Zhu, D. Maslov, and C. Monroe. "Parallel entangling operations on a universal ion-trap quantum computer". In: *Nature* 572.7769 (2019), pp. 368–372. DOI: 10.1038/s41586-019-1427-5.

[144] P. Krantz, M. Kjaergaard, F. Yan, T. P. Orlando, S. Gustavsson, and W. D. Oliver. "A quantum engineer's guide to superconducting qubits". In: *Applied Physics Reviews* 6.2 (2019), p. 021318. DOI: 10.1063/1.5089550.

[145] S. Schirmer, I. Pullen, and A. Solomon. "Identification of dynamical Lie algebras for finite-level quantum control systems". In: *Journal of Physics A: Mathematical and General* 35.9 (2002), p. 2327. DOI: 10.1088/0305-4470/35/9/319.

[146] U. Boscain, E. Pozzoli, and M. Sigalotti. "Classical and quantum controllability of a rotating symmetric molecule". In: *SIAM Journal on Control and Optimization* 59.1 (2021), pp. 156–184. DOI: 10.1137/20M1311442.

[147] M. Roth, M. Ganzhorn, N. Moll, S. Filipp, G. Salis, and S. Schmidt. “Analysis of a parametrically driven exchange-type gate and a two-photon excitation gate between superconducting qubits”. In: *Physical Review A* 96.6 (2017), p. 062323. DOI: 10.1103/PhysRevA.96.062323.

[148] F. Gago-Encinas, M. Leibscher, and C. Koch. “Graph test of controllability in qubit arrays: A systematic way to determine the minimum number of external controls”. In: *Quantum Science and Technology* 8.4 (2023), p. 045002. DOI: 10.1088/2058-9565/ace1a4.

[149] J. R. McClean, J. Romero, R. Babbush, and A. Aspuru-Guzik. “The theory of variational hybrid quantum-classical algorithms”. In: *New Journal of Physics* 18.2 (2016), p. 023023. DOI: 10.1088/1367-2630/18/2/023023.

[150] F. Albertini and D. D’Alessandro. “Notions of controllability for bilinear multilevel quantum systems”. In: *IEEE Transactions on Automatic Control* 48.8 (2003), pp. 1399–1403. DOI: 10.1109/TAC.2003.815027.

[151] J. M. Lee and J. M. Lee. *Smooth manifolds*. Springer, 2012. DOI: 10.1007/978-1-4419-9982-5_1.

[152] M. Kjaergaard, M. E. Schwartz, J. Braumüller, P. Krantz, J. I.-J. Wang, S. Gustavsson, and W. D. Oliver. “Superconducting qubits: Current state of play”. In: *Annual Review of Condensed Matter Physics* 11 (2020), pp. 369–395. DOI: 10.1146/annurev-conmatphys-031119-050605.

[153] M.-D. Choi. “Completely positive linear maps on complex matrices”. In: *Linear algebra and its applications* 10.3 (1975), pp. 285–290. DOI: 10.1016/0024-3795(75)90075-0.

[154] A. Jamiołkowski. “Linear transformations which preserve trace and positive semidefiniteness of operators”. In: *Reports on Mathematical Physics* 3.4 (1972), pp. 275–278. DOI: 10.1016/0034-4877(72)90011-0.

[155] S. Lloyd, M. Mohseni, and P. Rebentrost. “Quantum principal component analysis”. In: *Nature Physics* 10.9 (2014), pp. 631–633. DOI: 10.1038/nphys3029.

[156] M. Jiang, S. Luo, and S. Fu. “Channel-state duality”. In: *Physical Review A* 87.2 (2013), p. 022310. DOI: 10.1103/PhysRevA.87.022310.

[157] A. B. Magann, C. Arenz, M. D. Grace, T.-S. Ho, R. L. Kosut, J. R. McClean, H. A. Rabitz, and M. Sarovar. “From pulses to circuits and back again: A quantum optimal control perspective on variational quantum algorithms”. In: *PRX Quantum* 2.1 (2021), p. 010101. DOI: 10.1103/PRXQuantum.2.010101.

[158] N. Wittler, F. Roy, K. Pack, M. Werninghaus, A. S. Roy, D. J. Egger, S. Filipp, F. K. Wilhelm, and S. Machnes. “Integrated Tool Set for Control, Calibration, and Characterization of Quantum Devices Applied to Superconducting Qubits”. In: *Phys. Rev. Appl.* 15 (3 Mar. 2021), p. 034080. DOI: 10.1103/PhysRevApplied.15.034080.

[159] J. Z. Lu, R. A. Bravo, K. Hou, G. A. Dagnew, S. F. Yelin, and K. Najafi. "Learning quantum symmetries with interactive quantum-classical variational algorithms". In: *arXiv preprint arXiv:2206.11970* (2023). DOI: 10.48550/arXiv.2206.11970.

[160] A. Dutkiewicz, T. E. O'Brien, and T. Schuster. "The advantage of quantum control in many-body Hamiltonian learning". In: *arXiv preprint arXiv:2304.07172* (2023). DOI: 10.48550/arXiv.2304.07172.

[161] R. Xia and S. Kais. "Qubit coupled cluster singles and doubles variational quantum eigensolver ansatz for electronic structure calculations". In: *Quantum Science and Technology* 6.1 (2020), p. 015001. DOI: 10.1088/2058-9565/abbc74.

[162] P. J. Ollitrault, A. Miessen, and I. Tavernelli. "Molecular quantum dynamics: A quantum computing perspective". In: *Accounts of Chemical Research* 54.23 (2021), pp. 4229–4238. DOI: 10.1021/acs.accounts.1c00514.

[163] F. Gago-Encinas, T. Hartung, D. M. Reich, K. Jansen, and C. P. Koch. "Determining the ability for universal quantum computing: Testing controllability via dimensional expressivity". In: *Quantum* 7 (2023), p. 1214. DOI: 10.22331/q-2023-12-21-1214.

[164] S. Kwon, A. Tomonaga, G. Lakshmi Bhai, S. J. Devitt, and J.-S. Tsai. "Gate-based superconducting quantum computing". In: *Journal of Applied Physics* 129.4 (2021), p. 041102. DOI: 10.1063/5.0029735.

[165] A. Cervera-Lierta. "Exact Ising model simulation on a quantum computer". In: *Quantum* 2 (2018), p. 114. DOI: 10.22331/q-2018-12-21-114.

[166] A. Broadbent and E. Kashefi. "Parallelizing quantum circuits". In: *Theoretical computer science* 410.26 (2009), pp. 2489–2510. DOI: 10.1016/j.tcs.2008.12.046.

[167] S. Li, Y. Kimura, H. Sato, and M. Fujita. "Parallelizing quantum simulation with decision diagrams". In: *IEEE Transactions on Quantum Engineering* (2024). DOI: 10.1109/TQE.2024.3364546.

[168] S. J. Devitt, W. J. Munro, and K. Nemoto. "Quantum error correction for beginners". In: *Reports on Progress in Physics* 76.7 (2013), p. 076001. DOI: 10.1088/0034-4885/76/7/076001.

[169] G. G. Guerreschi and A. Y. Matsuura. "QAOA for Max-Cut requires hundreds of qubits for quantum speed-up". In: *Scientific reports* 9.1 (2019), p. 6903. DOI: 10.1038/s41598-019-43176-9.

[170] B. Mohan, S. Das, and A. K. Pati. "Quantum speed limits for information and coherence". In: *New Journal of Physics* 24.6 (2022), p. 065003. DOI: 10.1088/1367-2630/ac753c.

[171] J.-H. Chen. “Lower bounds for adiabatic quantum algorithms by quantum speed limits”. In: *Physical Review Research* 5.3 (2023), p. 033175. DOI: 10.1103/PhysRevResearch.5.033175.

[172] R. Wiersema, D. Lewis, D. Wierichs, J. Carrasquilla, and N. Killoran. “Here comes the SU (N): multivariate quantum gates and gradients”. In: *Quantum* 8 (2024), p. 1275. DOI: 10.22331/q-2024-03-07-1275.

[173] C. P. Koch. “Controlling open quantum systems: tools, achievements, and limitations”. In: *Journal of Physics: Condensed Matter* 28.21 (2016), p. 213001. DOI: 10.1088/0953-8984/28/21/213001.

[174] N. M. Linke, D. Maslov, M. Roetteler, S. Debnath, C. Figgatt, K. A. Landsman, K. Wright, and C. Monroe. “Experimental comparison of two quantum computing architectures”. In: *Proceedings of the National Academy of Sciences* 114.13 (2017), pp. 3305–3310. DOI: 10.1073/pnas.1618020114.

[175] T. Metodi and A. I. Faruque. *Quantum computing for computer architects*. Springer Nature, 2022. DOI: 10.1007/978-3-031-01731-5.

# Declaration of authorship

I declare to the Freie Universität Berlin that I have completed the submitted dissertation independently and without the use of sources and aids other than those indicated. The present thesis is free of plagiarism. I have marked as such all statements that are taken literally or in content from other writings. This dissertation has not been submitted in the same or similar form in any previous doctoral procedure.

I agree to have my thesis examined by a plagiarism examination software.

Berlin, 21 August 2024
Fernando Gago Encinas